Western Australia School of Mines
Department of Exploration Geophysics

Feasibility of Using Regional Seismic Reflections Surveys to Discover Iron Oxide Copper-gold (IOCG) Deposits in the Gawler Craton, South Australia.

Okan Evans Onojasun

This thesis is presented for the Degree of

Doctor of Philosophy

Of

Curtin University

July 2018

Declaration

This thesis contains no materials that have been accepted for the award of any other degree or diploma in any university.

To the best of my knowledge and belief, this thesis contains no materials previously published except where due acknowledgement has been made

Every reasonable effort has been made to acknowledge the owners of copyright material. I would be pleased to hear from any copyright owner who has been omitted or incorrectly acknowledged.

Signature……

Date……

To my late Father and my only blood Brother

Okan Vincent and Okan Emmanuel

May your gentle souls continue to rest in the bosom of our Lord Jesus Christ

Abstract

For the past several decades iron oxide copper-gold (IOCG) deposits have been discovered and developed across different parts of Australia and represent a potential target for economic copper production. However, the 'easy' and nearby deposits are already discovered and exploited and current discoveries are under moderate to thick cover with weak geophysical or geochemical signatures; hence, they are hard to quarry and interpret. Historically, discoveries were based upon potential field data (magnetics and gravity) and early successes were proven by drilling a grid of vertical or inclined parallel holes. As stated in Malehmir et al., 2012: "As discovery becomes deeper, the cost and effort to drill through barren cover rocks becomes greater". Thus, the traditional approaches to finding IOCG deposits in the Gawler Craton are becoming less effective and more expensive, so another approach is needed.

The seismic reflection method seems very promising especially for detailed mapping at depth and is routinely used in sedimentary environments. Early applications of the seismic reflection method were considered very costly and the results were not encouraging or simply poorly understood. However, recent research and success in the area of hard-rock seismic provides huge potential for delineating ore-bodies as well as mine planning in complex hard-rock terrains. Most of these recent works are at mine-scale; however, not much has been done at a larger or regional scale (apart from GA and state geological seismic surveys), probably because there has not been a compelling argument to proceed with such work.

This research therefore, is aimed at defining the seismic signature of IOCG deposits from a camp to regional-scale perspective using available geophysical and petrophysical data as well as establishing the cost effectiveness of seismic reflection vs drilling. Past studies tend to focus on the technical viability and have not seriously considered survey geometries that are cost effective enough to be taken up in exploration. The Gawler Craton, South Australia was selected as a region for my investigations, with Hillside, Olympic Dam, Vulcan and Mount Gunson mine sites selected for the case studies. The working hypothesis to be tested is: "is it feasible to

find IOCG deposits with regional (10–50 km lengths and 3–5 km depths) seismic reflection surveys"

The forward modelling experiments at the Hillside, Olympic Dam and Vulcan deposits reveal that the seismic reflection method is contrary to previous beliefs very good for detecting the presence of IOCG-related intrusive structures at many scales. In the Hillside modelling experiment for instance, we can see the various lithological boundaries and contacts from the depth-converted migrated sections. Reflections from various lithological contacts and the lack of reflections from the edges of intrusions are identifiable when compared with the geological model. In general, the depth converted, migrated modelled data images resemble the geological models and this is also the case when examining real 2D and 3D seismic surveys over these IOCG deposits. Even with relatively sparse acquisition parameters (80 m source spacing and 40 m receiver spacing), one can still detect many important lithological boundaries that show local changes indicative of a possible mineralising event.

Results from the Olympic Dam and Vulcan modelling experiments are the clearest in demonstrating that seismic reflection method is capable of providing detailed continuous images of structures while maintaining good resolution at depth. Reflections are identifiable largely due to acoustic impedance changes across contacts between altered fragmentals and intrusive lavas within the hematite-rich breccia. This is inferred from a clear similarity between the idealised noise-free images from the synthetic data and the sparse, 2D, deep crustal seismic data provided by Geoscience Australia in 2003. The Mt Gunson modelling demonstrates how the seismic reflection might enable new discoveries from a new exploration concept.

This work demonstrates that with representative geological models and fairly basic petrophysics, we can simulate the measured data sufficiently well as to identify potentially mineralised IOCG intrusions with economically viable seismic survey geometries.

Acknowledgements

First and foremost, I would like to thank my mother, who makes sure I drink from the well of knowledge. You singlehandedly raised me since I was one month when my father departed this sinful world. Words cannot express how grateful I am to you mum for all of the sacrifices that you've made on my behalf. Your prayer for me was what sustained me thus far.

In a special way I thank my supervisor, Professor Milovan Urosevic, for his motivation and strong criticism which constantly put me on my toes. The amount of time invested by him in this dissertation is unquantifiable. His style of supervision will continue to remain as my greatest source of inspiration in many years to come. I am grateful to the supervisory panel members: Professor Maxim Lebedev, Professor Peter Williams and Dr. Sasha Ziramov for serving as my committee members even at hardship. Many thanks to Professor Boris and entire staff of Exploration Geophysics Department for providing the necessary facilities during my research work. I equally express my profound gratitude Deep Exploration Technology (DET) for sponsoring the research.

I thank my sponsors: Federal Republic of Nigeria through the Tertiary Education Trust Fund (TETFund) for providing the scholarship and management of Federal University of Petroleum Resources, Nigeria for granting me study leave. I am most grateful to Professor John Etu-Efortor, formal Dean College of Science and immediate past vice chancellor FUPRE for his fatherly role. God will remember you in sensitive places sir. I equally thank my colleagues in Physics Department, Federal University of Petroleum Resource, Nigeria. In particular, I am grateful to the Head of Department, Professor Edison Enaibe and Dr Onifade Sikiru for their support and useful advice whenever I was at a cross road. Many thanks to Dr. Mrs Emudianughe Juliet and Mr. Stephen Okonkwo for the valuable role they played in my life during transition from been an applicant to a lecturer in FUPRE

Special thanks to my wonderful children Goodness, Treasure, Immanuela as well as my brothers and extended family for their support while the program lasted. I thank my dear friend and Sister, Ijemigbeyi Favour for her invaluable assistance to me, may the Almighty God Himself reward you beyond your imagination. I equally thank Dr Saaid Peters, Dr Anderson Brooks, Dr Villian Pithok, Engr. and Mrs O, Augus, Dr and Mrs Ade, Miss Vera Ehizua, Miss Clarisse Strode, Dr. Miss Charity Mudava, Dr Eric Takam, Dr Mohammad Hossain and many others too numerous to mention. My heartfelt appreciation also goes to the pastorate and members of the Redeemed Christian Church of God, Foursquare Gospel Church (White House Community Church), Omega Fire Ministries and Central Point Church all in Perth, Western Australia, for their prayers and support.

I would also like to acknowledge the following software vendors. Their software applications were essential in the creation of this thesis: Deco Geophysical (Radex Pro), Geosoft (Oasis Montaj), Halliburton (ProMAX), Schlumberger (GoCAD, OMNI 3D), Tesseral Technologies (Tesseral).

Finally, I thank the Universal Divine Triumvirate, way maker, miracle worker, promise keeper, light in the darkness, ancient of days, lily of the valley, bright and morning star, the Omnipotent, Omnipresent and Omniscient GOD, for seeing me through this academic odyssey despite all the difficulties. In all sincerity, I have experienced your guidance day by day. You are the one who let me finish this program. You made all things beautiful for me in your own time and now this is my season of jubilee; may your name for ever be praised. Thank you, Lord!

Table of Contents

List of Figures

List of Tables

Preface

This thesis presents my investigation into the feasibility of using seismic reflection surveys to detect iron oxide copper-gold (IOCG) deposits in the Gawler Craton. Following the discovery of the giant Olympic Dam deposit in 1975, the entire craton has undergone intensive scrutiny in the search for similar deposits. An ongoing aspect that has generated a lot of interest is determining the best way to economically explore these deposits.

There are many geophysical and traditional methods that can be used to discover such deposits, such as potential field methods and drilling. In particular, potential field methods have been employed in the past to delineate both the major structures that lead to the location of prospective targets, and the direct targeting of the IOCG deposits themselves. Unfortunately, potential field methods are only very good for shallow investigations due to low resolution and ambiguity with depth (Urosevic et al., 2007). For the Gawler Craton, which is our focus, the 'easy' and nearby deposits have been discovered and exploited, and current discoveries are under moderate-to-thick cover with weak geophysical or geochemical signatures.

The current reliance on potential field methods to identify drilling targets limits further exploration due to the inherent ambiguity in their interpretation, particularly where thick regolith cover is present, which is largely the case for the Gawler Craton region. As an example of the limitations of the current reliance on gravity and magnetics, in the recent Hillside discovery, IOCG mineralisation is under thin sediment cover (approximately 10–40 m), and relied more on following up previous copper occurrences (small quarries) in the area rather than on distinctive geophysical anomalies. An inspection of Figure 1 reveals the relatively indistinct, weak gravity and magnetic anomalies. Such responses for a near-surface deposit indicate that these methods may not be able to provide sufficient confidence in vectoring of IOCG mineralisation. Another method is needed to help delineate such targets.

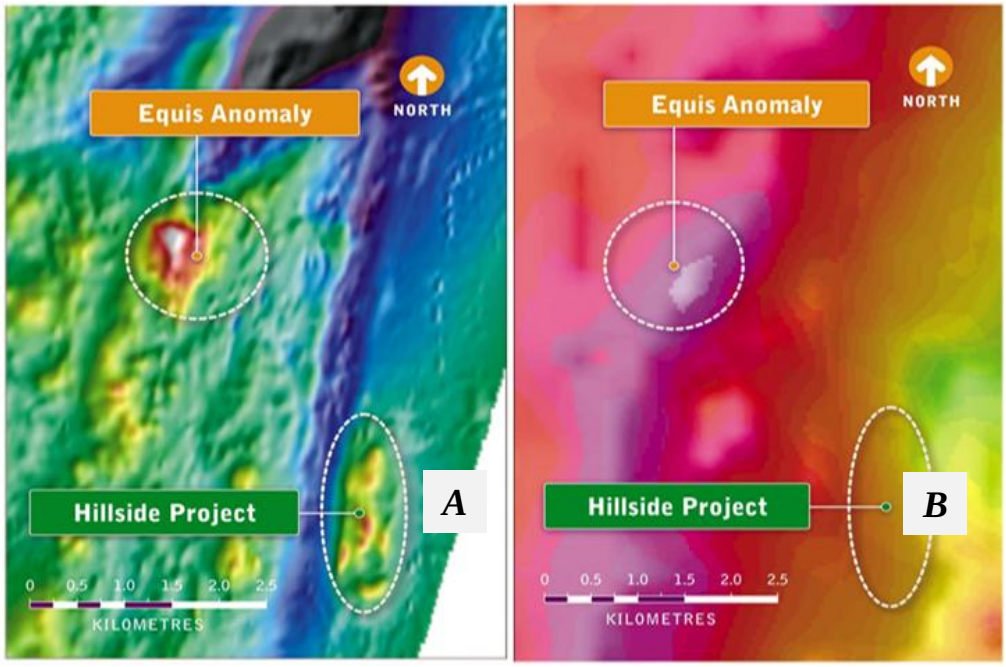

Figure 1.1 Equis anomalies of the Hillside copper project: A) magnetic map and B) gravity map. Both maps reveal weak gravity and magnetic anomalies, which suggest that these methods lack the resolution to provide sufficient information on the possible presence of IOCG mineralisation (Rex Minerals, 2010).

The seismic reflection method represents relatively new technology for mineral exploration. It offers a distinct advantage over most other geophysical techniques because of its superior penetration and spatial resolution at depth. The use of the seismic reflection approach in mineral provinces is relatively expensive compared to traditional geophysical methods and many early trials were not encouraging. However, further investigations in this area provide greater promise in the ability to reliably discover and delineate ore-bodies in complex hard-rock environments (Wright, 1981; Pretorius, et al., 1989, 1997; DeWet, and Hall, 1994; Milkereit, et al., 1992a; Duweke, et al. 2002; Urosevic, et al., 2008).

Despite the many superior attributes, the use of the surface seismic reflection method in a “hard-rock” terrain (igneous and metamorphosed crystalline rocks) has started relatively recently. Mainly due its high cost seismic reflection surveys for mineral exploration are often conducted at mine scale (less than 1–5 km in extent). Little has been done at the camp–regional scale (100’s to 1000’s of square km covered) apart

from Geoscience Australia conducting 2D transects, as well as some state geological seismic surveys. This is probably because there has not been a compelling argument to proceed with such work. The deposits themselves cannot be detected solely by geophysical methods, but geological mapping and drilling is also required. The cost effectiveness of seismic reflection surveys for Cu-Au exploration in the Gawler Craton has never been evaluated and the exact role of the seismic reflection method within the existing "greenfields" exploration methodology is not well defined. The seismic method has much promise, but it is not yet a standard exploration tool like gravity, magnetics, electrical and EM methods.

On commencement of this research work, I embarked on the task of investigating the feasibility of using seismic reflection surveys to detect large-scale IOCG deposits. The principal hypothesis to be tested in my research is whether IOCG deposits can be detected by analysing the seismic signatures of the Fe–rich mineralised rocks in breccias/intrusions, especially along prospective large fault structures (though not many may end up being mineral deposits). The Fe-rich rocks that are part of what defines an IOCG deposit are likely to have greater density and higher P-wave velocities than the host rock; thus, a physical contrast may be exploited.

Previous modelling experiments (Rex Minerals, 2013) indicate that the petrophysics and structural models based on such a proposition are valid as they compare well with available potential field data. It must be emphasised here that prior to commencement of this work, the application of seismic reflection surveys were only considered at the mine scale. Luckily, the application of seismic reflection surveys for a greenfields exploration became one of the research paths within the large research group – Deep Exploration Technologies Corporative Research Centre (DETCRC). That provided my research with the field data and the chance to test my working hypothesis. The forward models were produced and subsequently a comparative analysis involving relevant case studies available at Hillside, Olympic Dam and Vulcan deposits was carried out to investigate seismic signature of IOCG deposits at a range of scales. Details of the modelling experiments and comparisons

with survey data are provided in Chapters 4–7. Each modelling experiment aims to investigate a specific IOCG deposit in terms of its seismic signature specifics and in general its detectability and mapability by reflection seismic methods. The agreement of the modelled and recorded seismic response will be useful to understand the seismic signature of IOCG deposits. Of particular interest is to evaluate the effectiveness of seismic reflection surveys, as part of a greenfields exploration approach, for finding an IOCG deposit.

1. Introduction

Australia has vast mineral resources. Australia is also one of the leading suppliers of bauxite and iron ore, second largest producer of alumina, lead and manganese, and third largest producer of brown coal, gold, nickel, zinc and uranium (MCA, 2012, McKay, et al., 2013). Many mineral deposits are spread across Australia from Indian Ocean to Pacific Ocean and South Ocean to Timor Sea. Despite very rich commodities the rate of new discoveries is not encouraging (AIMR, 2013).

Indeed the effectiveness of mineral exploration is now a major concern worldwide as the industry is starting to emerge from a significant period of low commodity prices (Melehmir et al., 2012). Currently, explorers have shifted their attention from high growth to capital preservation, while producers have changed their focus from "volume at all costs" to "competition cost" in terms of being in the lowest tier on the cost curve. New discoveries are needed but it is clear that at the current cost of the commodities these discoveries have to fit into the new economic model. This can be true for copper exploration where the desire to find large, low cost deposits has become an imperative.

1.1 Location of Study Area

South Australia is host to various mineral resources worth over A$70b, either committed or under construction (Martin, 2012). The state is also host to about 69% of Australia's economically demonstrated or proven resources of copper with a total production of 2.2 million tonnes (Mt) in the last ten years (Geoscience Australia & ABERE, 2010). Apart from the giant Olympic Dam discovered in 1975, it also hosts the three most significant copper discoveries in the last ten years in Australia namely: Carrapateena, Prominent Hill and Hillside. Figure 1.2 shows the major copper and uranium mineral systems found in the Craton.

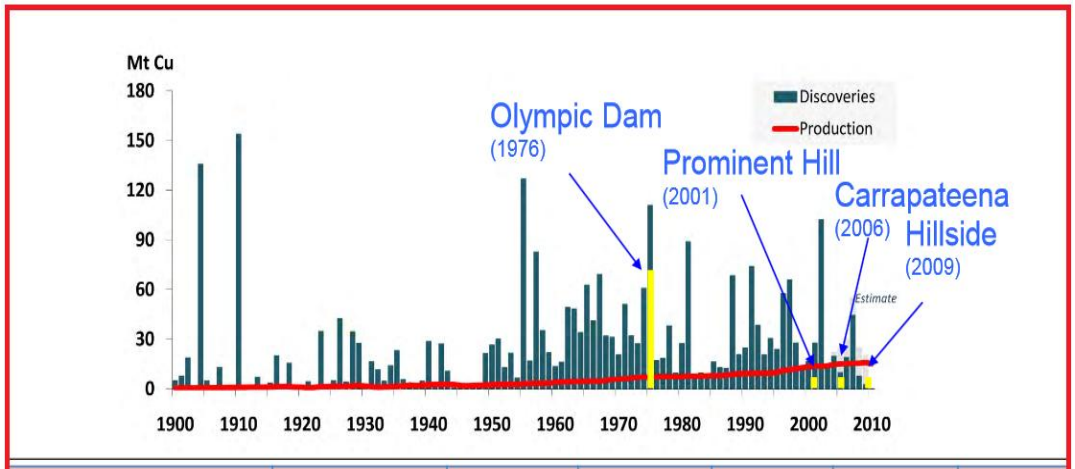

Deposit / Craton	Style	Discovery	Size (Mt)	Cu (%)	Au (g/t)	U (ppm)
Olympic Dam / Gawler	IOCG, Breccia	1976	9576	0.82	0.31	260
Prominent Hill / Gawler	IOCG, Breccia	2001	186	1.10	0.70	
Carrapateena / Gawler	IOCG, Breccia	2006	800	0.80	0.30	155
Hillside / Gawler	IOCG, Skarn	2009	337	0.60	0.30	

Figure 1.2: Copper and Uranium deposit System found in Gawler Craton (from Tyne, 2014). Green bar shows the level of copper discoveries in Metric tonne, red indicate the level of productions and the yellow bar indicates the total estimates copper-gold reserve from the various systems.

The Gawler Craton is a region that has not been substantially metamorphosed, deformed or remobilised, except by minor epeirogenic movements, prior to deposition of Pandurra Formation sediments after 1424 Ma (PIRSA, 2003). The Craton consists of Mesoarchean-to-earliest Paleoproterozoic basement that is overlain by a series of Paleoproterozoic basins (Wade, et al., 2012). The majority of the presently discovered IOCG deposits are from basement rocks. The basement is said to occur around the two belts situated within the north-central and southern axis, and is said to have similar ages and lithologies (Wade, et al., 2012; Parker, et al., 1993; Vassallo and Wilson, 2002). Mineralisations are marked by extensive hematite-magnetite (iron) alteration and brecciation (Barton, and Johnson, 2004; Williams, and Skirrow, 2000).

1.2 Iron-Oxide Copper-gold Deposits

Iron-oxide copper-gold deposits consist of small- to large-size hematite-rich ore-bodies, which form at shallow to mid crustal levels in extensional, continental settings such as intracratonic and intra-arc rifts, continental magmatic arcs and back-arc basins (Corriveau, 2005; Salisbury, and Snyder, 2007; Hitzman, et al., 1992). The deposit occurs around the margins of large igneous bodies, which intrude into sedimentary strata; hence, they usually form a pipe-like sheet around the host strata. The hematite-rich deposit comprises approximately 30 to 70% of the rock and co-exists with copper sulphides, uranium oxides and gold (Salisbury and Snyder, 2007). Some of the characteristic features include: crustal settings, which have exceptionally voluminous, pervasive alkaline metasomatism; abundance of magnetite and/or hematite with very high impedance minerals and low Ti contents (Hitzman, et al., 1992; Partington, and Williams, 2000; Williams, et al., 2005; Corriveau, 2005; Knight, et al., 2002).

In IOCG deposits, the (sulphide) ore is usually hosted within the breccias or veins and also occurs as disseminations. They consist of two or more elements, with copper and gold being the most economically significant. These elements are usually associated with large-scale granitic intrusions and fault zones. IOCG deposits generally occur in a range of tectonic settings, such as along subduction-related continental margins, regions of orogenic basin collapse, or regions of anorogenic magmatism, and have been recognised in many localities around the world. Figure 1.3 shows the distribution of recognised IOCG deposits across the globe.

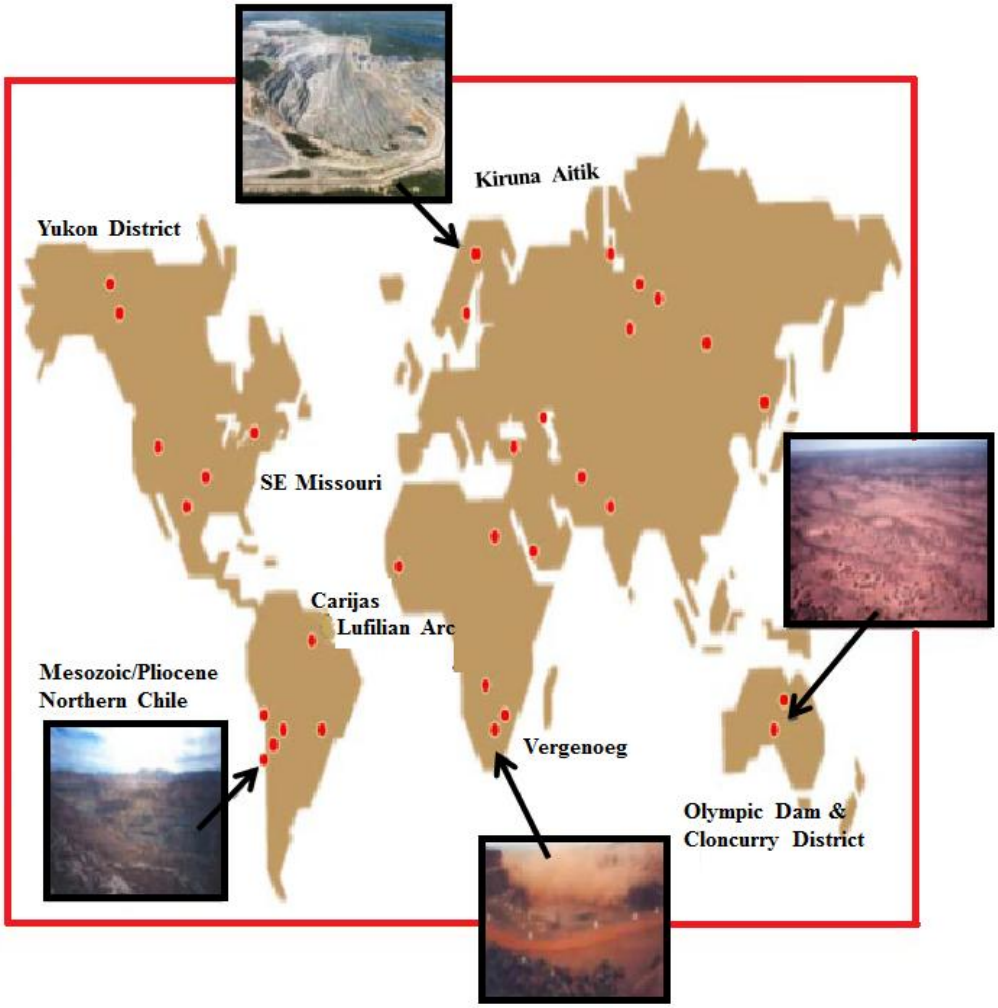

Figure 1.3: Distribution of world recognized IOCG deposits (modified after Hitzman, 2000). The figure above shows the diversity of the class of IOCG deposits as they have been recognised in many localities around the world.

1.3 Origin of IOCG Deposits

The origin and nature of IOCG class of deposits are still highly contentious and debatable as no consensus exists, on the defining characteristic, notably why IOCG are so rich in iron oxides. Answering this question requires a quantitative understanding of hydrothermal redox reactions by the fluids involved in ore formation, which needs to be based on a clear paragenetic understanding of geological evolution in the ore-forming system (Barton and Johnson, 1996; Williams et al. 2005; Bastrakov et al. 2007; Barton 2014). Debate on IOCG genesis initially

focussed on whether these ore systems may be fundamentally magmatic or amagmatic (Fig. 1.5). That is, whether they involved a dominantly magmatic source of ore fluid and metals (Pollard, 2000; 2006; Fig. 1.5a), or had host rock sources of metal and chlorine, and basinal and/or surficial source of fluids (Barton and Johnson, 1996; Haynes, 2000; Fig. 1.5b). The exploration implications of this distinction are profound, given that the former implies that IOCG deposits will be found only in association with suitably specialised intrusions that were emplaced at, or below the depths of mineralisation and able to evolve copper-bearing fluids, whereas the latter implies that the local crust must have contained ample older sources of metals and that either older or contemporary evaporates must have been present as sources of chlorine.

From the genetic point of view, IOCG deposits and their associated polymetallic mineralisation are still not fully understood leading to difficulties in classification. (for example Hillside is listed as an IOCG and a Skarn deposit). There is also a major concern as to whether the magma has a direct link to the mantle or lower crust, especially for the large deposits, or if the deposits themselves can be found in hydrothermal systems within the crust (Williams, et al., 2005). Despite the divergent opinions, IOCG deposits remain highly significant as they represent a source of iron-related copper ore, which forms the basis for industrial development globally. An example is the Olympic Dam as it hosts a voluminous polymetallic suite of Fe-Cu-U-(Au-Ag) (Williams, 1999) and is presently the fifth largest low-grade copper producer in the world. Figure 1.4 shows the IOCG formation is based on magmatic-hydrothermal linkages. The deposit is first transported to the surface through melting and crystallisation. From the primary melt, it crystallises with diamond, feldspar and kimberlites as by-product; it further crystallises after contact with mafic/ultramafic with a Porphyry/IOCG as the product at around 10 km. This crystallisation process continues until it surfaces. Figure 1.5 is an example of a typical flow pathway and hydrothermal properties for alternative models for IOCG deposits. Each has a slightly different source and path of fluid flow (magmatic, surface or basin and metamorphic derived sources). Magmatic derived source suggest distinctive

composition and proximity to source; regional Na(–Ca) is coincidental, surface or basin derived source implies coeval or older brine source, necessary but indifferent to type of heat source, and available upper crustal plumbing. Metamorphic derived source implies metaevaporitic (or conceivably mantle) Cl source with regional plumbing. It should be noted that these approximate to "end member" models and are not mutually exclusive. That is, IOCG deposits may be formed in hybrid systems with coeval or superimposed contributions from different types of deep-seated brine. In the specific case illustrated, economic copper-gold deposits are conceptually restricted to the part of the system with a magmatic fluid component and absent from iron oxide bodies formed in parts of the system dominated by external fluids. The crystalline basement rocks in the Gawler craton are thought to be Cu-rich and any evidence of such fluid conduits means that Cu mineralisation is possible. Table 1.1 shows the summary of alternative geological models for IOCG system systems.

One major distinguishing feature of all IOCG deposit is the abundant occurrence of barren ironstones dominated by magnetite and/or hematite assemblies with small anomalous amounts of economically associated metals (Barton, and Johnson, 2004). The number of relatively barren Fe-oxide-rich occurrences exceeds the Cu (-Au) ones significantly. The absence of metals in these instances further provides the needed understanding into the formative processes necessary to produce large polymetallic deposits. Barton and Johnson (2004) suggest that economic copper-gold mineralisation is a later feature in the regional development of an IOCG. However, it is generally believed that in any IOCG formation an early sulphide-poor magnetite stage precedes a subsequent metal-bearing hematite stage.

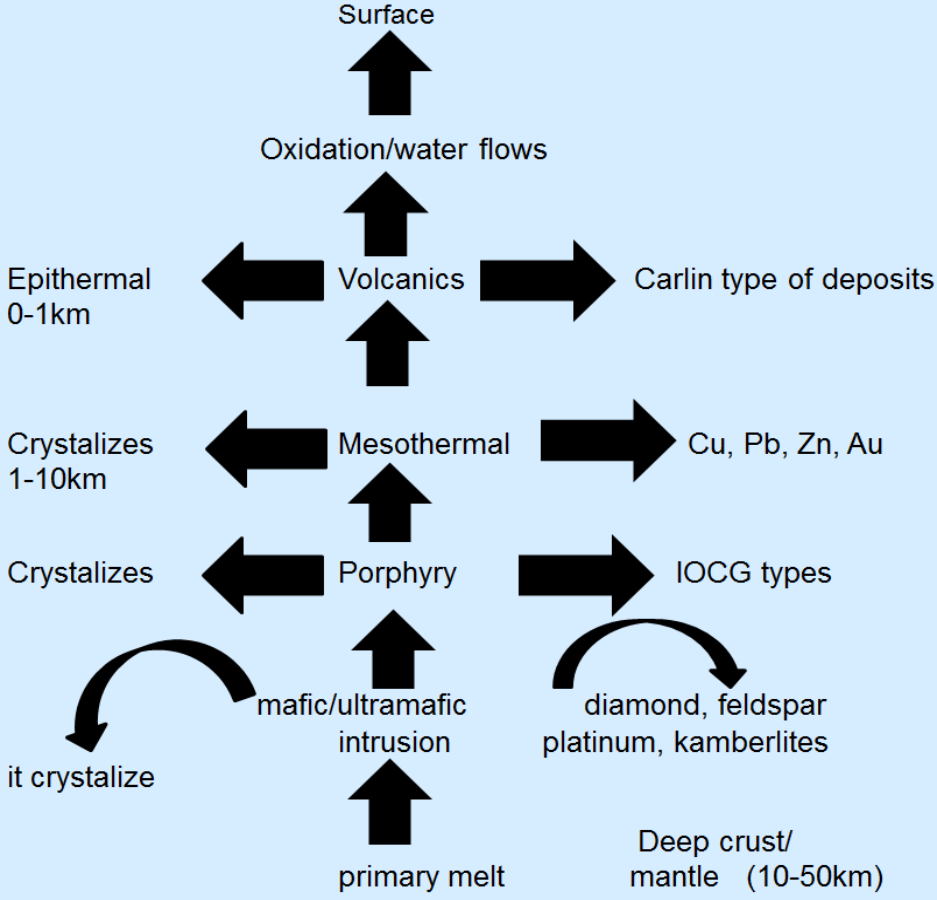

Figure 1.4: IOCG formation based on hydrothermal sources (modified from Jackson, 2012). The deposit is transported to the surface through melting and crystallisation. From the primary melt, it crystallises with diamond, feldspar and kimberlites as by-product; it further crystallises after contact with mafic/ultramafic with a Porphyry/IOCG as the product at around 10 km. This crystallisation process continues until it surfaces.

Alternative models based on principal fluid sources by Barton and Johnson (2004) are provided in Figure 1.5 and detailed in Table 1.1.

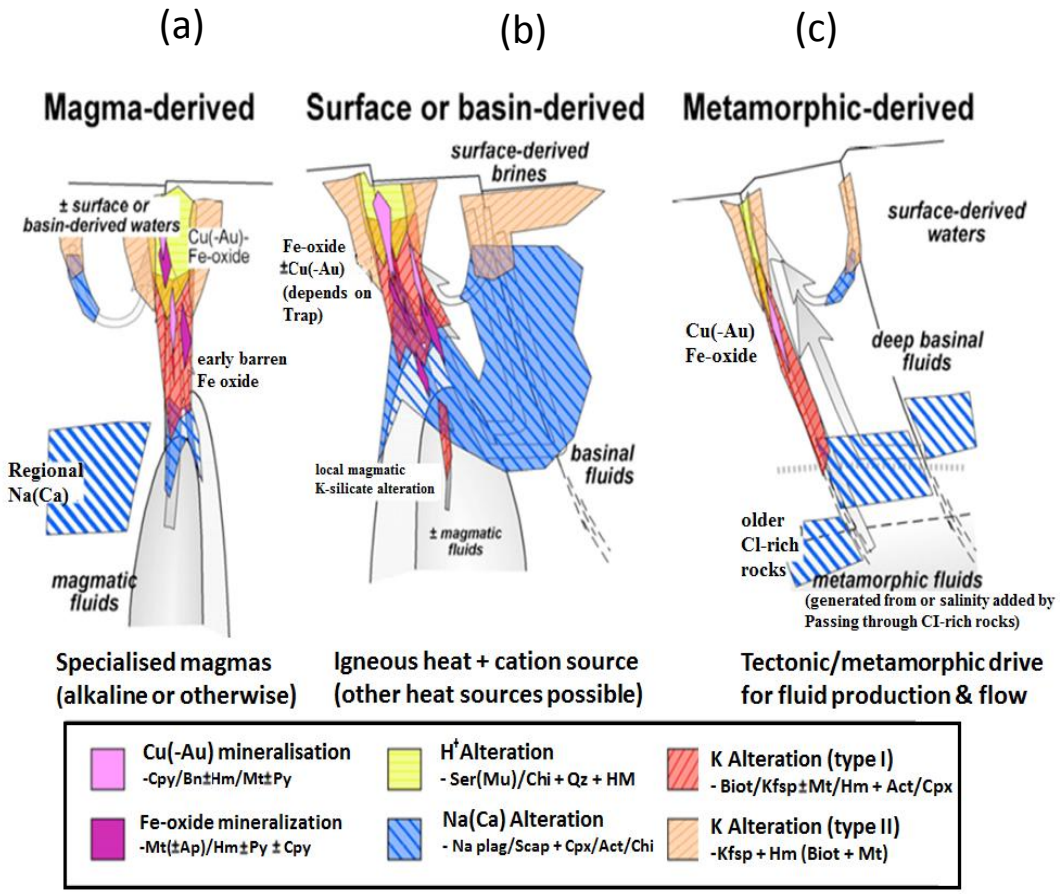

Figure 1.5: Diagrammatic explanation of flow paths and hydrothermal attributes for alternative models (Barton and Johnson, 2004). Each has a slightly different source and path of fluid flow: (a) Magmatic source implies distinctive composition and proximity to source; regional Na(–Ca) is coincidental, (b) Evaporitic source implies coeval or older brine source, necessary but indifferent to type of heat source, and available upper crustal plumbing and (c) Metamorphic source implies metaevaporitic (or conceivably mantle) Cl source with regional plumbing The crystalline basement rocks in the Gawler craton are thought to be Cu-rich and any evidence of such fluid conduits means that Cu mineralisation is possible.

Fluid Source	Magmatic	Non-magmatic	
		Basin/Surface	Metamorphic
Fundamental Process	• Release of $S^{=}$-poor metal-bearing brine from magma; rise of buoyancy • Cooling, wall-rock reaction ± fluid mixing provide trap	• Thermal convection of non-magmatic brines; wall rock reaction provides metals • Cooling, wall-rock reaction or fluid mixing provide trap; second fluid may provide metals	• Metamorphic release of brine components by devolatillisation or reaction with other aqueous fluids; rise by buoyancy • Cooling, wall-rock reaction ± fluid mixing provide trap
Igneous Associations	• High-K, oxidised suites ranging in composition from diorites to granites • Carbonatite and strongly alkaline connections proposed by some	• Igneous rocks diverse (gabbro to granite); non-magmatic examples known • Key heat source in most • Material source, diversity reflected in geochemistry	• No necessary connection, though commonly present • Could be heat source in some settings • Can be material source
Hydrothermal alteration in feldspathic hosts	• Na(Ca) and other types (K, H^+) link to magmas • Regional Na(Ca) coincident but not directly related to Cu(-Au)	• K (type I), H^+ ± Na(Ca) in upwelling zones • Na(Ca) ± K (type II) in recharge zones	• Primarily K and H^+ alteration associated with deposits • Regional Na(Ca) association reflects sources
Relationship of Fe-oxides to Cu(-Au)	• Some Fe-oxides with Cu(-Au), may be deeper or higher-T equivalents • Barren Fe-oxides may form from distinct fluids and commonly older hydrothermal systems in same area	• Mt-rich are deeper, earlier, higher T parts of ore-forming; Mt or Hm also typical with Cu • Barren Fe-oxides represent lack of S trap for Cu or lack of second Cu-bearing fluid	• Fe-oxides present, but relatively minor (Bi or Chl common); Fe-oxides commonly generated by breakdown of mafic minerals rather than Fe introduction
Local setting: depth/ structure	• Shallow to mid-crustal levels; commonly along regional structures but near causative intrusions	• In (mainly) brittle upper crust; plumbing provided by regional or volcano-tectonic structures	• Mid- to shallow crustal levels near or on major structures; surface fluids require shallow levels
Global setting	• Arcs or extensional environments that produce characteristic magmas (oxidised high-K or alkaline)	• Regions with appropriate brine sources (arid settings or older Cl-rich materials), plumbing systems, and thermal drives	• Regions with Cl-rich low- to intermediate-grade source rocks; compressional setting (e.g. basin collapse) or prograde metamorphism
Key references	• Hauck (1989), Pollard (2000), Groves & Vielreicher (2001)	• Barton & Johnson (1996, 2000), Haynes *et al*. (1995), Haynes (2000)	• Williams (1994), De Jong *et al*. (1998), Hitzman (2000)

Table 1.1 Summary of alternative genetic models for IOCG system systems as proposed in Barton and Johnson (2004). Although there is broad agreement on what generally constitutes this family of deposits, there is little consensus on the characteristics of the geological systems and the processes that form them. This summary makes it substantially different predictions about what should be related and hence has direct consequences for the system-scale footprints that one would expect and ultimately how those footprints might be utilized.

1.4 Age and Tectonic Setting:

IOGC deposits vary in age and occur in different tectonic environments, for example, within Australia and some parts of South America. Where the largest of these deposits are found, the deposits tend to be hosted in Mesoproterozoic to Neoproterozoic rocks (1,800 to 850 Ma), while many other deposits are found in the Phanerozoic with the important Chilean iron oxide copper-gold belt hosting the Mesozoic Candelaria deposit (Herrington, 2011). Hitzman et al. (1992) suggested a

class of Proterozoic iron oxide deposits that is spatially and temporally connected with rift-related extensional tectonics based on some of the major iron oxide deposits across the world. However, more recent discoveries show that most IOCG deposit are formed from Archaean to Proterozoic as well as wider range of tectonic environments (Barton and Johnson, 1996).

Three end-member tectonic environments that host the vast majority of IOCGs have been identified as intra-continental orogenic collapse (i.e., Cloncurry District), intra-continental anorogenic magmatism (i.e., districts hosting Olympic Dam and Pea Ridge) and extensional environments along a subduction-related continental margin (i.e., IOCG districts of northern Chile), (Hitzman, 2000). Further studies in the Gawler craton (Hand, et al., 2007) and Cloncurry district (Betts, et al., 2006) have suggested that magmatism and mineralisation at the Olympic Dam and Cloncurry deposits occurred in a compressional (orogenic) regime and intra-continental formation in association with syn-orogenic magmatism. Figure 1.6 shows the age distribution of IOCG deposits in terms of main commodity recovered (Cu or Fe). The Gawler craton IOCG deposits tend to be relatively old (early-mid Proterozoic). Hence there is some opportunity for a deposit to be significantly altered and any mineralisation to be re-mobilised over time.

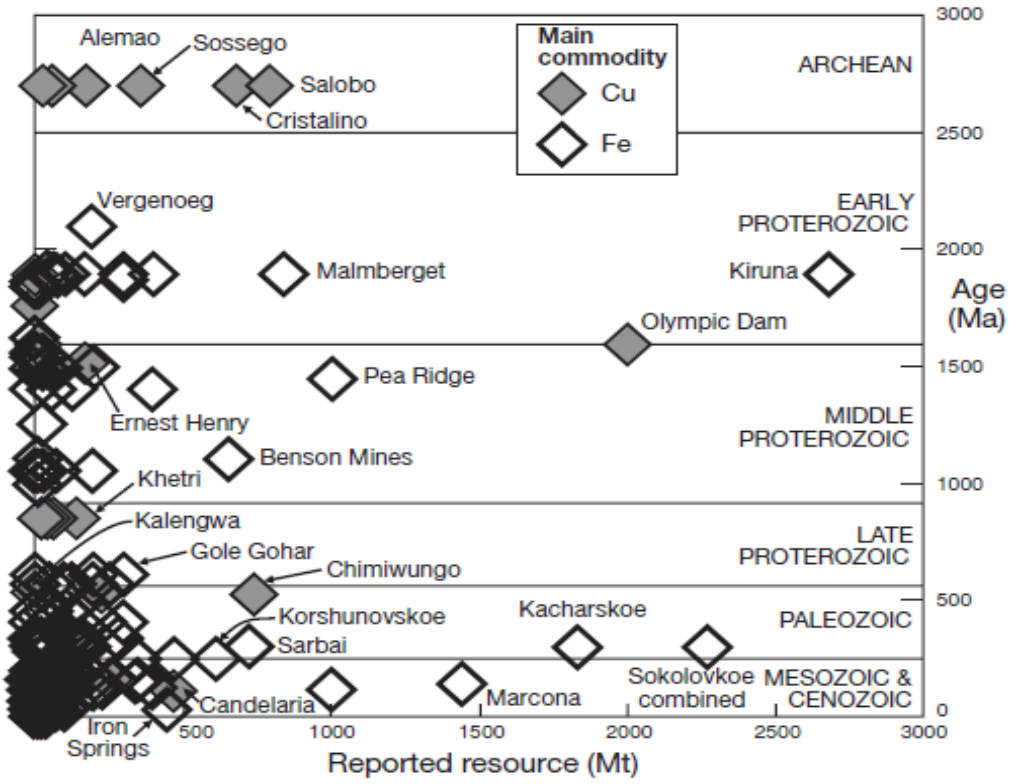

Figure 1.6: Age distribution of IOCG deposits (shaded diamonds) and iron oxide deposits (magnetite-apatite and skarn grouped together as unshaded diamonds) (Barton and Johnson, 1996), divided on the basis of the main commodity recovered (copper or gold). The deposit data are derived from publicly available data (Johnson and Barton, unpublished compilation).

1.5 Classification of IOCG deposits

Definition of IOCG deposits is still highly debated to date, with divergent views as to whether the magnetite-apatite deposits or some of the carbonatite-related Cu and REE deposits are bona fide members of the IOCG ore deposit family (Skirrow, 2015). Further, sources of fluids, ligands and ore metals, as well as the different relationship with other groups of ore deposits, have not been fully demonstrated (Williams, et al., 2005). With these various controversies the most realistic and simplest classification is to divide them into calc-alkaline and alkaline groups in accordance with their rock composition (Williams, et al., 2010). In terms of mineralogy and alteration, the deposit is further subdivided with each of the subtypes named after a particular deposit/district, as shown in Figure 1.7.

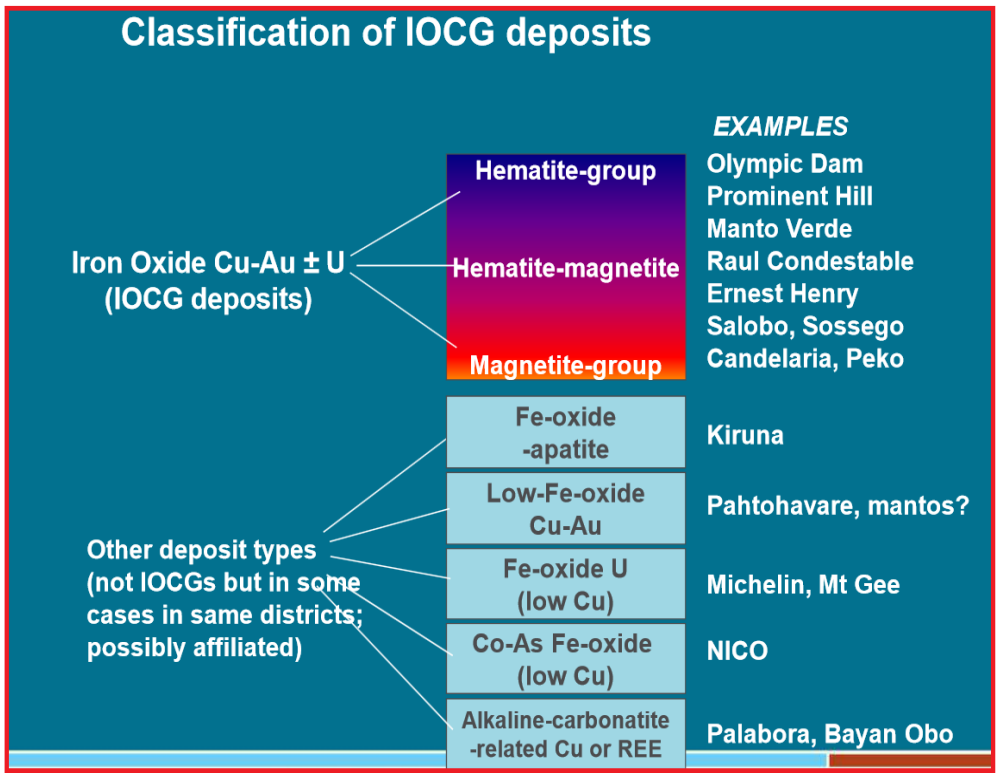

Figure 1.7: Classification of IOCG deposits (from Skirrow, 2014). The classification is based on alteration and mineralization. Upper group belongs to IOCG class with hematite, magnetite and hematitic/magnetite alteration assembly while the lower group are not necessary IOCG type but have some affiliations.

1.6 Alteration and Mineralisation

One distinguishing feature of most IOCG deposits is their alteration zones. The large volumes of alteration imply that the confined ore occurrences are products of very large hydrothermal systems (Barton and Johnson, 1996). There are three main types of alteration: Magnetite-bearing sodic-calcic alteration (3–6 km) dominated by replaceable albite within the felsic host rocks and albite-actinolite-diopside. Potassic alterations (1–3 km), which tend to post-date sodic and sodic-calcic alteration, are characterised by orthoclase-magnetite in the dominated felsic rocks and biotite-magnetite in dominated mafic rocks. They can be replaced by hematite at structurally high-level systems and sericite alteration and silification occurring at very shallow depths (< 1 km) (Hitzman, et al., 1992, 2005). There is a strong correlation between the alteration type and depths that are attributed primarily to the temperature increases that are associated with greater depths. Specifically, Na/(Na+K) ratios in

hydrothermal fluid systems tend to decrease with increasing temperature (Orville, 1963; Dilles and Einaudi, 1992; Hitzman, et al., 1992; DeJong and Williams, 1995; Barton and Johnson, 1996; Pollard, 2001).

Mineralisation in IOCG deposit systems occur in the form of vein and/or stock-work within a range of breccia types. These mineralisation features tend to be structurally controlled; they occur where there are fault intersections, shear zones and major lithological contacts (Williams, et al., 2005). Magnetite and hematite form the dominant iron oxide minerals deposited, with magnetite commonly forming earlier than hematite and associated with greater depths. For Cu-sulphides, chalcopyrite and bornite represent the major Cu ore minerals and together with pyrite and gold often overprint earlier oxide deposition. Iron sulphides constitute a minor component when compared with iron oxides (Porter, 2000, 2013). Uranium mineralisation generally occurs as uraninite or brannerite within Cu-enriched zones in association with Cu-Fe-sulphides (Hitzman and Valenta, 2005). Most often the copper-sulphide minerals associated with the IOCG appear as disseminated mineralisation. Thus, EM methods do not tend to play a significant role in exploration, but in theory Induced Polarisation (IP) could work.

1.7 IOCG Host Rocks

IOCG deposits are hosted by a various array of rocks, which includes coeval and/or pre-existing sedimentary rocks as in the case of Wernecke Mountains, Bayan Obo and igneous rocks as in the case of Olympic Dam, the Lightning Creek prospects and Candelaria (Gillen, 2010). Silicate, carbonate, ironstone and evaporite-hosting sequences form the major composition of sedimentary rocks while the igneous host rocks range from mafic to felsic composition (including volcanics). Most of host rocks are usually metamorphosed, with green schist to granulite faces represented (Hitzman, 2000; Harrison, 2009). However, in the Australia context, (e.g., Olympic Dam) the host rocks seem emplaced at shallow-crustal levels (Williams and Pollard, 2003). The divergence of these host rocks is an indication that the type or composition of host rock is not a serious factor in the evolution of these deposits

even though differences in the host rock are responsible for some of the differences in mineralogy between deposits.

Most IOCG deposits are affiliated with magmatism and large-scale intrusions. The Olympic Dam deposit for instance occurs within the Hiltaba Suite of granitoids with breccias intruded by different mafic, ultramafic and felsic dykes, usually connected to hydrothermal activity (Haynes, et al., 1995, Pollard, 2006). In Salobo, the Carajás district (Brazil), the deposits occurred in association with granitoid magmatism during the late Archean evolution of the Carajás province (Requia, et al., 2003). In the Ernest Henry and Eloise deposits in the Cloncurry district, Australia, mineralisation is related to specific relatively local intrusive events, where the cover sequence is intruded extensively by granitoids at 1760 to 1720 Ma, (Pollard and McNaughton, 1997; Page and Sun, 1998). This type of association with intrusive events has led researchers to suggest a genetic link between IOCGs and magmatism.

Though other deposits have a general inferred association with intrusions, it remains unclear how IOCG deposits are specifically linked with a magmatic body, For example, the Osborne deposit is spatially related to the Naraku batholiths, but at approximately 1595 Ma it predates the intrusion of the nearby batholiths (Gauthier, et al., 2001). Further, recently determined mineralisation ages at the Tennant Creek district, the Bayan Obo deposit and the Wernecke Mountains in Canada, are said to be incompatible with a temporal association with magmatism (Duncan, et al., 2009; Skirrow, 2000; Smith and Chengyu, 2000; Hunt, et al., 2007). One major conclusion from this weaker link with magmatism in these districts is a pointer to the fact that IOCG deposits can be formed with or without an identifiable related intrusion. However weak the link is, the identification of such intrusions may be a helpful clue when exploring for IOCG deposits.

1.8 Aims and Objectives of the Research

IOCG deposits contain enormous mineral wealth throughout the world and are of a key importance to mineral industry. However, IOCG deposits are difficult to explore because of very complex overburden and low velocity contrast between the target formation the background. Also, they typically have a subtle geophysical signature and, if at a depth greater than several hundreds of metres, they produce an unmeasurable gravity and magnetic response. The only method that could be effective for deeply situated IOCG systems is seismic. Consequently, this research is aimed at investigating the feasibility of using a seismic reflection survey to detect IOCG deposits from camp-to-regional scales, while the specific objectives are:

- ❖ Evaluate seismic signatures of iron oxide copper-gold deposits in the Gawler Craton at larger survey scales (camp to regional)
- ❖ Investigate high resolution seismic response over an IOCG deposit and evaluate its potential for resolving internal structure of such complex system
- ❖ Analyse whether it is cost-effective to use seismic reflection surveys at camp-regional scale for discovery, as well as the role the method might play within the existing exploration methodology.

1.9 Research Methodology

In order to achieve my research objectives, various geological models, representative of study areas (Hillside, Olympic Dam, Vulcan and Mount Gunson), were created with each model designed with a good correlation with respect to previous geological interpretations obtained from drilling. Synthetic seismic responses were computed over these models, compared, and evaluated against seismic surveys conducted in the past, except for Mount Gunson, which has no seismic data. All available information such as existing geological models, logs, core measurements and published elastic properties of similar mineral systems and rocks were used to populate the synthetic geological models. To achieve meaningful comparative analysis between field and simulated data, a high quality numerical schemes that can accurately propagate waves through such complex models were required.

2 Seismic Imaging Techniques

2.1 Overview of Seismic Exploration in hard-rock Environments

Application of seismic reflection methods to explore for mineral deposits in hard-rock terrains dates back to 1878 when Ferdinand Fouqué carried out an experiment with the aim of detecting seismic waves in granites (Fessenden, 1914; Tertyshnikov, 2014). Despite this early application of hard-rock seismic measurements, it was not well publicised. One of the earliest experiments in the application of using seismic methods for hard-rock terrain was done in USSR in 1927 to explore for mineral deposits (Gamburtsev, et al., 1952). From 1940–1950, different high-resolution seismic experiments were conducted across Russia and Europe to explore for ore bodies as well as to delineate the vertical-layered structures (Tertyshnikov, 2014).

From 1980s to present, there has been a tremendous increase in the application of seismic methods for mineral exploration in hard-rock environments with most of the scientific papers coming from Australia, South Africa, Canada and Northern Europe. In Australia, especially Western and South Australia, some pioneering work has been done by Greenhalgh et al. (2000) who carried out research on in-mine seismic delineation of mineralisation and rock structure at Kambalda nickel mines, where the results indicated that hard-rock layering (contacts that identify Ni prospectively) could be imaged. Urosevic et al. (2005), carried out re-processing of many seismic surveys in Western Australia to address the lack of imaging of complex structures and poor shallow imaging missing from the original 2D regional sections, then instigated many other surveys later designed to address these issues. It was reported that many deposits in the Yilgarn are typically found in complex geological structures associated with crustal scale shear zones (Urosevic, et al., 2005) where the prospective geology is commonly hidden by colluvial and alluvial deposits plus deep weathering.

In Sweden, Juhlin and Palm (2003) demonstrated reflections associated with granite interfaces as well as sub-horizontal fissure regions at depths below 2 kilometres. Salisbury et al. (1997) investigated sulphide imaging of hard rocks using a combination of 2D seismic and vertical seismic profiling (VSP) to image horizontal

reflectors. In the Canadian Shield region, a group of authors (Salisbury et al. 2000, Milkereit et al. 1997; 2000; and Boerner and Milkereit 1999) documented the potential of seismic methods for hard-rock mineral exploration to a depth range of about 2.5 km. Also, in 2000 a large blind massive sulphide was imaged at the Halfmile Lake Area of the Bathurst Mining camp in Canada (Salisbury, et al., 2003), fully reprocessed and reported by Malehmir et al. (2008). Pretorius (1997, 2000) further researched 3D images made of the Ventersdorp Contact 'Reef' gold ore body in South Africa, with results showing the approximate position were ore-deposits might be found, but was unable to pinpoint structural events within the data set for underground mining.

Pretorius et al., (2000) carried out 3D seismic surveys over goldfields in South Africa and the results indicated that seismic method can be effectively used to directly delineate deep seated mineral-bearing structures provided there are flat, sub-horizontal rock layers and a large impedance contrast sufficient to produce clear reflections. High-resolution data was also used to delineate 3D geological structures in order to evaluate the size, geometry and distribution of mineable structures in the Bushveld complex area of South Africa (Duweke, et al., 2002). Larroque (2002) further documented the possibility of using 3D seismic surveys to directly detect sub-layered ore deposits within the shallow depth of around 800 m. Various 2D regional seismic lines were also recorded over gold bearing structures on the Yilgarn craton to assess seismic methods in Western Australia, with results showing that imaging for deep structures important for gold mineralisation (>2 km) can be achieved (Drummond, et al., 2000). Stuart and Jolly (1999) and Stuart et al. (2000) carried out a 3D survey in 1997 in the Witwatersrand basin with reflections on the seismic image correlating well with the known faults in the mining operation within three meters to enhance faults imaged in the seismic data.

In the last few years, the usefulness of seismic exploration has been further demonstrated with encouraging results from different 2D and 3D surveys across the

globe (Malehmir, et al., 2012; Urosevic, et al., 2012; White, et al., 2012, Urosevic et al., 2017).

2.2 Challenges with Seismic Exploration in Hard Rock Environment

Despite the relative successes in the application of seismic reflection method in hard rock environment, it is yet to gain their relevance in the exploration for mineral deposits. The problems stem from the nature of the environment: usually characterised with high velocities and densities, steeply dipping structures as well as low signal-to-noise ratio. Propagation velocities of seismic waves in the regolith strata are generally significantly lower than the velocities in the base hard rocks. Such a high velocity contrast between formations produces strong wave conversions and reverberations that affect the quality of seismic reflection images often in the prime mining window 200 - 1000 m depth or 100 - 400 ms on time section (Urosevic et al., 2005; 2007). Another challenge is related to deep and complex regolith that causes travel time delays. If unaccounted properly, these delays can degrade or even completely destroy seismic image. There has also been a considerable lack of understanding of how to relate seismic "wiggles" to hard rock structures and particularly different rock types. The task of interpreting seismic images is much more cumbersome than is the analysis of potential field data. The primary reason is that seismic images are of much higher resolution and related to differences in elasticity rather than conductivity or magnetisation. It therefore appears that true integration of seismic images with other, main stream geophysical techniques will take a bit more time while the mineral exploration industry absorbs the lack of exploration success in many regions and the potential value that seismic acquisition brings to exploration.

2.3 Forward Modelling Techniques

Seismic forward modelling is the computation of seismic responses of a geologic model (Carcione, et al., 2002). Seismic forward modelling is numerical simulation of wave propagation through different types of rocks. The process involves creation of a numerical model representing particular geological setting and propagating either

acoustic or elastic waves through it. Acoustic wave propagation simulates "liquid rocks" and is often in use as it produces simplified seismic response that can be comprehended easier that is the case with elastic wave propagation.

The overall objective of seismic modelling is to produce seismic response of different geological structures or cases from which we can draw valuable understanding that will enable us to interpret real data seismic images. Thus, we often compare synthetic seismic response to field data. This process may need to be repeated number of times until reasonable match is achieved. If there is some level of correlation between the model and real data, the geological model used can be regarded as a reasonably accurate model of the subsurface (Carcione, et al., 2002). This process may be automated in the near future through application of novel methodologies such is the Full Waveform Inversion - FWS (Urosevic et al., 2017).

Seismic modelling can be utilised at any stage of the exploration process. Prior to acquisition, seismic modelling can be used to ensure that the geological objective of the survey will be seismically visible (Anderson and Cardimona, 2000). Seismic modelling can also help to verify whether a geologic target can be effectively imaged, given its geometry and the limitations of the field techniques that can be implemented. If a target is readily resolved on a synthetic seismic section, there is a reasonable probability it will also be resolved on properly acquired and processed seismic profiles (Anderson, and Cardimona, 2000; Robertson, et al., 2007). Lastly, we can compare our modelled data with real data and learn which rock types in contact or rock alterations are responsible for producing seismic response of a particular characteristic.

The two most common methods in seismic modelling are i) asymptotic and ii) direct methods, with the latter method used in this study. Direct methods of seismic forward modelling involve numerical solutions of the wave equation, sometimes called full wave methods, since it provides the entire wavefield. Direct methods include Finite Difference (FD) and Finite Element. (Alterman, and Karal, 1968;

Claerbout, 1971) and they require a density model as well as a P-wave and S-wave velocity model to work. The finite difference (FD) method used for this study calculates the seismic wavefield from different grid point by approximating derivatives of the wave equation with finite difference formulas and solving the resulting difference equation recursively (Carcione, et al., 2002).

For the various case studies in this research, all Synthetic seismograms were computed using stress-velocity formulation (Virieux, 1986) implemented in Tesseral-2D modelling software. The choice of modelling techniques (Acoustic or Elastic) depends on the nature of problem that is being investigated. For the purpose of this study, 2D acoustic modelling was chosen as a starting point due to several factors. First, we are mainly interested in predicting P-wave seismic responses over IOCG deposits by detecting the presence of an intrusive structure, possibly around fault zones. Using acoustic modelling, which takes into account only density and P-wave velocity, we can easily achieve our set objective: to see what a conventional P-wave survey and processing approach might provide over these deposits. Acoustic modelling is often justified by the fact that the reflection data processing favours only primary wavefield and attenuates all other modes. Hence, our primary objective is often achieved with acoustic modelling and simplified processing of acoustic wavefield rather than tedious processing of full elastic numerical data. Furthermore, elastic modelling is computationally expensive and since the starting model can hardly compensate for complexity of the surface, achievement gained compared to effort is limited.

Elastic synthetic response is hard to comprehend and hence the learning from it may be limited. Thus, I assume that the elastic effect will be negligible and that acoustic modelling results will be valid without loss of generality. Lastly, 2D modelling, whilst it does not seem particularly innovative as an approach, is capable of closely resembling field data, particularly regional 2D seismic data that were available for this study. For the above reasons I used 2D acoustic modelling approach to analyse seismic response over several IOCG mineralisation.

2.4 Parametrisation of the models

To produce a numerical model representative of the geological situation under study is not trivial. A "realistic" model has to contain structures that mimic closely existing geology and then it has to be parametrised or populated with elastic parameters that are indeed found in situ rocks. To produce final seismic response appropriate source wavelet of a frequency content found in the real field data has to be chosen while the waves have to be propagated in a non-dispersive manner by selecting optimum numerical grid parameters. The reflected wavefiled needs to be "recorded" using the same or similar geometry to the one used in the field survey.

3 Geology of the Gawler Craton and Petrophysical Attributes

3.1 Geology of Gawler Craton

The Gawler Craton (Figure 3.1) coving about 450,000 square kilometres of South Australia consists of Archean to Mesoproterozoic metasediments, volcanic and igneous intrusive. The region has also recorded a prolonged period of crustal growth and sedimentation (Daly and Fanning, 1993; Daly, et al., 1998; Ferris, et al., 2002). Tectonically, the Gawler Craton has been relatively stable except for minor epeirogenic movement since 1450 Ma when regional cooling and reactivation of some of the major shear zones took place (Thomas, 1976; Parker, 1990, 1993). The geology of the Craton is still not fully understood when compared to other cratonic regions within Australia, as a result of its sparse basement outcrop.

The Craton is divided into different geological provinces based on geological and geophysical data, with each region said to be bounded by major structures and stratigraphic breaks (Ferris, et al., 2002). Due to the scarcity of outcrops in the craton, the boundaries can be sharply defined by geophysical data, especially in terms of magnetic characteristics as well as magnetic anomalies, which are interpreted as bounding faults and shear zones (Ferris, et al., 2002). Some of the various domains within the Gawler Craton include the Nawa, Coober Pedy, Mount Woods, Christie, Fowler, Wilgena, Harris Greenston, Peake and Denison, Nuyts, Coulta, Cleve and Olympic Domains. For the purpose of this study, we shall briefly discuss the geology of Olympic Domain were all our case studies are located.

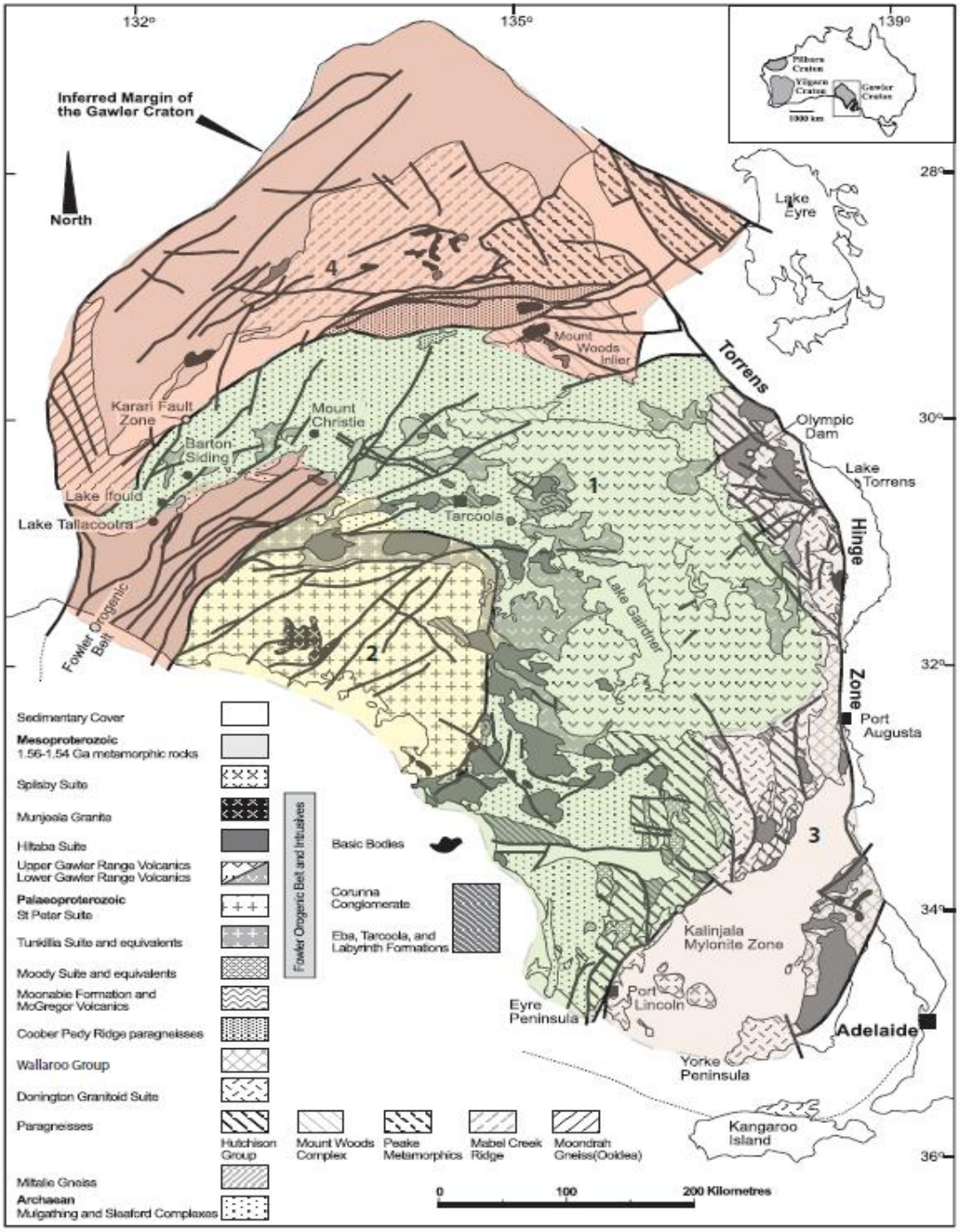

Figure 3.1: Modified sub-surface geology map interpreted from Gawler, South Australia, with simplified domain classified on the basis of geological affiliations.1 Central Domain, 2 South-west Domain, 3 Olympic Domain and 4 North-west Domain (After Daly et al., 1998)

3.2 Olympic IOCG Domain

The Olympic Domain (Figure 3.2), which hosts the world class Olympic Dam deposit, is situated on the eastern flank of the province, which partially coincides with and overprints, the enlarged Paleoproterozoic terrane of <2000 to 1740 Ma metasedimentary and metavolcanic rocks that is bounded to the west by the Mesoarchean to early Paleoproterozoic core of the Gawler province (Porter, 2012, Hayward, and Skirrow, 2010; Connor, et al., 2010).

The oldest known rocks in the domain are the granites of the Donington Suite, which have an age range of 1850 ± 4 Ma to 1860 ± 4 Ma and may be some 10 Ma older than granites reported in the adjacent Spencer Domain (Jagodzinski, 2005). The process or movement of these deposits has been interpreted to be partially associated with the ~1.59 Ga Hiltaba Suite granitoids. The Hiltaba Suite granites found in this domain consist mostly of Roxby Downs granites (RDG), which intrude into the Wallaroo Group (Porter, 2012; Creaser, 1989, 1996; Stewart and Foden, 2003; Hand, et al., 2007).

The Gawler Range Volcanics are overlain by the Pandurra Formation due to deposition. These deposits consist primarily of a medium-to coarse-grained quartz-rich and lithic-rich sandstone (Flint, et al., 1993). The Olympic Domain, apart from the giant Olympic Dam also hosts the three most significant copper discoveries, namely: Carrapateena, Prominent Hill and Hillside (Skirrow, 2004). The geology of each of these deposits is fully discussed in each case study (Chapters 4–7).

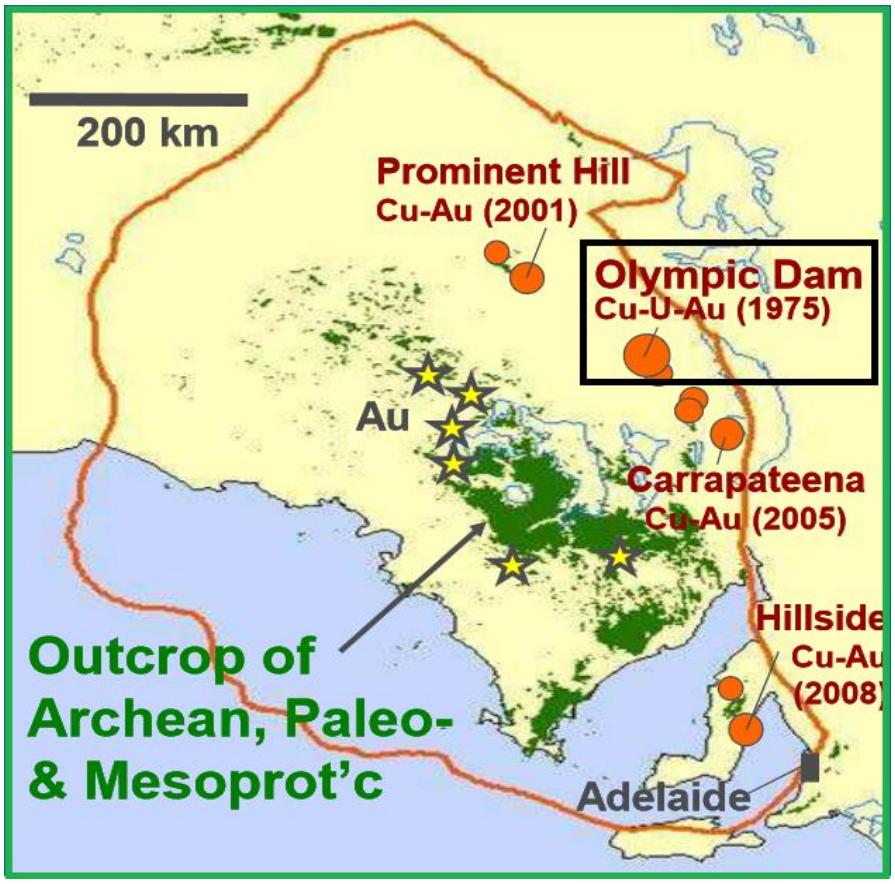

Figure 3.2: Simplified map of Olympic IOCG-Uranium Domain which hosts the world class Olympic Dam deposit (from Skirrow 2014). The oldest known rocks in the domain are the granites of the Donington Suite, which have an age range of 1850 ± 4 Ma to 1860 ± 4 Ma and may be some 10 Ma older than granites reported in the adjacent Spencer Domain. Examples of economic deposits within the Olympic Dam domain include Olympic Dam, Prominent Hill, Carrapateena and Hillside.

3.3 Petrophysical Attributes of Gawler IOCG Deposits

Petrophysical data has historically been used to deduce information on the organic content of source rocks, mechanical properties, and reservoir quality of formations of interest. Core data is commonly expensive and limited across the prospect and vertical interval of the formation. Open-hole logs, however, are continuous and are widely available in most drilled wells. This section presents results from petrophysical investigations aimed at characterising IOCG deposit lithologies in the study area. These measurements are an integral part of study that includes geological and geophysical data acquisition on the property. Generally, most mineral deposits are known and identified due to their spurious and anomalous properties, particularly densities and P- and S-wave velocities. Obtaining petrophysical data that is accessible via public domain about IOCG deposits has proven very difficult, especially seismic properties. However, we gathered an extensive amount of core information from the Hillside deposit and were able to compare these to data from Olympic Dam and Vulcan and know that there are no significant differences in the seismic properties of various lithology types (with the caveat of when the rock is not heavily fractured).

Petrophysical properties have extensive applications from early stages of exploration through to feasibility and mine design (Hearst, et al., 2000; Lipton, 1997). When properly analysed, processed and calibrated, they have the potential for effective characterisation of ore behaviour for a truly representative suite of samples. The measurements are usually very quick, non-destructive and relatively cheap and can be recorded either downhole or in a core facilities. Petrophysical measurement is also very fundamental for geological modelling, especially for determining how the changes in elastic properties relate to changes in mineralogy as well as predicting these elastic parameters in areas with no borehole logs. As in the case of study areas, (Gawler Craton), the petrophysical data collected is particularly useful for resource mapping and also provides invaluable background information for other geophysical data acquisition and interpretation programs being conducted, with a view at delineating the ore deposit.

Although petrophysical contrasts between ore and host rock may not be enough for direct geophysical detection of the economic mineral phases of copper and gold and other base metal exploration, an association may exist between the ore and an associated mineral (presence of pyrrhotite as a magnetic mineral in sulphide deposits) which renders the ore detectable by geophysical methods. Correlation between uranium content and gold grade in South African mines for instance, has led to prediction of gold grade using natural gamma logging (Campbell, 1994). Similarly, conductivity has also proved to be a good indicator of grade for some base metal sulphide ores at the Enonkoski nickel deposit in Finland (Hattula and Rekola, 2000). In the case of IOCG deposits the expectation is that the associated iron-rich minerals will make the rocks heavier with possibly higher seismic impedance.

For the purpose of building a realistic geological model of the study areas, measurements were carried out on different core samples. The suite of rock of samples that was analysed includes velocity, density and magnetic susceptibility. For the purpose of building, simulating and processing synthetic data, accurate representations of these P- and S-wave velocities and density are needed to produce realistically geological models (Smith, 2010).

3.4 Alterations as Seismic Target

From geological perspective, it is possible to establish the presence of hydrothermal alteration and succeeding mineralisation, thereby providing further justification for the application of seismic reflection techniques (Smith 2010). Rock alteration defines the changes in mineralogy of a rock due to some variations in depositional properties occasioned by variations with respect to chemical conditions, temperature and pressure or a combination of both. Significant mineralogical alteration occurs as a result of close contact with hot fluids from the surrounding igneous intrusions (Smith, 2010). Such contact causes the withdrawal of isolated minerals, thereby changing the physical characteristics of the rock. Thus, significant alteration will often be associated with physical changes associated with the changes in minerology and rock textures.

The seismic reflection technique as an exploration tool, acts fundamentally on variations in many of these physical changes in the rock, particularly the seismic impedance of a rock (product of velocity and density). Further, most IOCG deposits are well defined by distinctive minerals and dominated by hematite and magnetite, which tend to have higher impedance than most host rocks; thus, making both deposit types detectable using the seismic method.

3.5 Elastic Properties

Variation in elastic properties is one of the fundamental factors governing the seismic response of an orebody. Individual velocities and densities are controlled by factors like mineralogical content, fractures, pressure and fluid saturation especially in in-situ conditions. Laboratory measurements and borehole logging are used to constrain these parameters. Previous studies have shown most sulphides lie far to the right of the well-known Nafe-Drake curve in a large velocity-density field controlled by the properties of pyrite, which is fast and dense (8.0 km/s, 5.0 g/cm^3), pyrrhotite, which is very slow and dense (4.7 km/s, 4.6 g/cm^3), and sphalerite and chalcopyrite, which have intermediate and very similar velocities and densities (~5.5km/s, 4.1 g/cm^3) (Havey, 1997; Salisbury, et al., 1996, 2000, Malehmir, 2012). However, these measurements tend to relate to massive sulphide mineralisation and nearly all IOCG deposits have disseminated sulphide mineralisation in breccia or vein stock-work. Our investigations on samples (in the laboratory) from Hillside suggest that the sulphide-bearing rocks tend to have high velocities, but it would largely appear due to the related iron oxide minerals associated with the economic minerals. Whilst the breccia complex associated with the deposit may have been fractured and weak at one point in history, once the Fe-rich minerals and sulphides are emplaced the velocities and densities tend to increase as per the overall trend in Nafe-Drake curve.

The sulphide-containing rocks generally have high densities and therefore high impedances, that provide for contrast in imaging via seismic methods. Constraining

these elastic parameters provides necessary information for adequate assessment of the potential for using seismic and gravity methods for imaging IOCG deposits.

3.5.1 Magnetic Susceptibility (k)

Magnetic susceptibility measures the ability of a substance to become temporarily magnetised in a magnetic field. It is a reliable parameter to predict the presence of ferromagnetic minerals such as magnetite and pyrrhotite in rocks. As most IOCG deposits are sharply defined and dominated by magnetite minerals with high impedance contrast, it becomes an excellent target for seismic methods. For a given magnetite content, susceptibility decreases with decreasing grain size of magnetite (Schön, 1996). Considering the effect of compositional variations of rock on ore breakage and recovery, variation in susceptibility could play an important role in ore characterisation provided that magnetic mineralogy (e.g., magnetite or pyrrhotite) is present.

Susceptibility measurements have also been used for lithological interpretation, grade prediction, estimation of degree of homogeneity and alteration (Ellwood, 1980; Schonharting and Abrahamsen, 1984). In some cases, susceptibility measurements have proven to be correlated to rock quality (i.e., degree of fractures). In the study areas for example, magnetic susceptibility estimates ranging from 0.000087 to 0.721 were found (Figure 3.4). Low values of magnetic susceptibility (<0.0001 SI) corresponded to altered zones with many fractures while high magnetic susceptibility (>0.01 SI) correspond to unaltered and non-fractured zones. However, the type of nearby intrusive in IOCG formations plus the later magnetite deposition phase development, will dictate much of the magnetic characteristics.

3.5.2 Density Measurement

Different researchers have investigated the behaviour of the velocity of P-waves, S-waves and density for different rocks and minerals and they all found different values

(Tables 3.1–3.2). The summary of velocities and densities measured from cores in this study is shown in Table 3.3. Variation in these velocities and densities could be as a result of several factors such as variations in geology of the areas, mineralogical content, fracture intensity, pressure and fluid saturation especially in in-situ conditions (Bongajum, et al., 2009).

A total of 304 measurements were made on cores from selected drill holes at the Hillside mine site (Figure 3.3). The density values in Gabbro ranges from 2.600 g/m^3–3.887 g/m^3 with a mean value of 2.910 g/m^3, granite values obtained ranges from 2 6 g/m^3–3.840g/m^3 with an average value of 2.720 g/m^3, metasediment samples range from 2.600 g/m^3 – 3.200 g/m^3 with 2.780 g/m^3 as its mean value while the mineralised host rock, the value ranges from 2.630 g/m^3–4.810 g/m^3 with an average value of 3.020 g/m^3

Density measurements were performed manually since the use of a nuclear-sourced gamma-ray logging tool was not possible. The density of each core sample was computed from two measurements of mass, one with the sample suspended in air and the second with the sample suspended in water. Assuming the water has a density of 1.0 g/cm^3, this simple procedure provides an estimate of the dry density of the rock. Though these rock samples were no longer in in-situ conditions, we assumed densities would not have changed significantly over time as the samples were relatively intact (and largely incompressible) and the measurements were a close representation of the in-situ conditions of both the sulphide mineralisation and the host rocks.

The low densities (<2.9 g/cm^3) and the high densities (>3.2 g/cm^3) correlate very well with alteration and mineralisation zones respectively. Figure 3.4 shows the correlation between measured density and mineralisation. Further analysis of the petrophysical data suggests most of the mineralisation is either hosted within skarn/metasediment packages as in the case of Hillside Cu-AU deposit or granitic breccias/gabbro materials as in the case of Olympic Dam and Vulcan Cu-Au deposits.

Minerals	Density in g/cm^3	Vp Km/s	Vs Km/s	References
Pyrite	4.91	7.99	4.94	Havey, (1997)
Pyrite	5.01	8.44	5.61	Babaska and Cara (1991)
Pyrite	5.016	8.48	5.71	Bass, (1995)
Pyrite	4.65	7.78	5.32	Telford et al. (1990)
Pyrite	5.02	-	-	Klein and Hurlbut (1985)
Sphalerite	4.07	5.44	2.80	Havey, (1997)
Sphalerite	4.088	5.59	3.30	Bass, (1995)
Sphalerite	4.0	-	-	Klein and Hurlbut (1985)
Sphalerite	4.7	-	-	Thomas et al. (2000)
Chalcopyrite	4.28	5.12	2.49	Havey, (1997)
Chalcopyrite	4.06	5.36	-	Salisbury et al. (1996)
Chalcopyrite	4.02	-	-	Telford et, al 1990
Chalcopyrite	4.02	-	-	Klein and Hurlbut 1985
Pyrrhotite	4.71	4.62	2.73	
Pyrrhotite	4.62	-	-	Klein and Hurlbut (1985)
Pyrrhotite	4.65	4.89	2.86	Telford et al. (1990)
Pyrrhotite	4.63	4.68	-	Salisbury et al. (1996)
Pyrrhotite	4.71	4.60	2.73	Havey, (1997)
Pentlandite	4.68	4.56	2.95	,,
Pentlandite	4.80	4.42	2.81	Mateck, (2007)
Pentlandite	4.72	-	-	Bass, (1995)
Bornite	5.16	-	-	
Bornite	5.07	4.40	2.07	Havey, (1997)
Galena	7.51	3.69	2.11	Christensen (2000)
Galena	7.59	4.09	2.60	Hallenberg (1984)
Galena	7.50	-	-	Klein and Hurlbut (1985)

Table 3.1 P-Wave, S-Wave and density for sulphide minerals at 3000 PSI confining pressure as reported by different authors.

Rocks	Vp Km/s	Vs Km/s	Density g/cm^3	References
Sedimentary Rocks				
mudstone (sandy)	3.05-3.11	-	2.27-2.76	Barrett et al. (2012)
Limestone	4.0-6.4	2.3-3.7	2.6	Willia
Siltstone (red & grey)	4.20-4.52	-	2.55-2.72	Barrett et al. (2012)
Limestone	2.0-6.0	-	-	Kearey and Brooks (1991)
Shale	3.4-4.3	1.7-2.6	2.2-2.5	Williams et al. (2003)
sandstone	3.7-6.6	2.4-3.6	2.4-3.0	
Sandstone	2.0-6.0			Kearey and Brooks (1991)
Sandstone	5.23-5.51	-	2.62-2.64	Barrett and Froggat (2012)
Dolomite	7.65	4.92	2.79	Bass
Dolomite	3.2-7.1	2.8-4.0	2.5-2.9	Williams, et al. (2003)
Dolomite	2.5-6.5	-	-	Kearey and Brooks (1991)
Basalt	5.84	-	2.90	Palomeras et al. (2010)
Diorite	6.45	-	2.65	
Diorite	6.7	-	2.7	Birch (1961)
Igneous Rocks				
Granite	6.20	-	2.78	Birch, (1961)
Granite	4.69-4.72	-	2.60-2.64	Barrett et al. (2012)
Granite	5.5-6.0	-	-	Jearey and Brooks (1991)
Granite	5.7	3.4	2.7	Elena et al. (2004)
Gabbro	7.6	-	3.2	Birch (1961)
Gabbro	7.04	-	2.92	Palomeras et al. (2010)
Gabbro	7.2	4.1	3.5	Elena et al. (2004)
Gabbro	6.10-6.14	-	2.88-2.94	Barrett et al. (2012)
Gabbro	6.5-7.0	-	-	Jearey and Brooks (1991)
Diabase	6.64	-	2.78	Palomeras et al. (2010)
Diabase	7.5	-	3.1	Birch, (1961)
Andesite	6.6	3.6	2.7	Elena et al. (2004)
Metamorphic Rocks				
Schist	6.74	-	2.60	Elena et al. (2004)
Schist	4.71	-	2.69	Barrett et al. (2012)
Gneiss	5.44	-	2.71	,
Quartz	6.03	4.09	2.66	Babaska and Cara (1991)
Granulite	6.76	-	2.82	

Table 3.2 P-Wave, S-Wave and density of some sedimentary, igneous and metamorphic rocks at 3000 PSI confining pressure as reported by different authors.

Hole No	Tray No	Depth	Length	Vp	Vs	Vp/Vs	SG	MagSus
HDD 009	12	70	50.60	5206	3213	1.620	2.7	0.000133
,,	65	363.2	25.95	-	-	-	2.8	0.000482
,,	76	419.5	50.50	5208	3206	1.624	2.7	0.00137
HDD 060	64	242.2	30.79	6126	3605	1.700	2.8	0.000412
,,	92	350.7	29.73	6077	3337	1.821	2.7	0.000508
HDD 062	35	128.2	32.76	6231	3548	1.7658	2.7	0.000782
,,	33	125.2	33.65	6011	3389	1.774	2.7	0.00234
HDD 064	21	76.8	30.38	5624	3519	1.598	2.7	0.000385
,,	26	93.5	29.44	6141	3482	1.763	2.7	0.000769
,,	66	253.8	34.29	6210	3453	1.798	2.9	0.00161
,,	85	331.7	30.76	6106	3810	1.603	3.2	0.00087
,,	87	337.5	30.88	7328	4238	1.729	3.4	0.00104
,,	88	342.7	30.18	5448	3517	1.549	3.3	0.00207
167	4	95.2	29.02	6159	3455	1.783	2.6	0.0053
441	60	203.0	28.08	5039	2931	1.719	2.7	0.000261
,,	63	217.6	29.11	6231	3393	1.836	2.9	0.00328
,,	69	240.3	27.89	6021	3594	1.675	2.7	0.000483
,,	71	247.0	27.51	6179	3897	1.586	2.8	0.000615
,,	73	257.3	27.08	6339	3592	1.765	2.9	0.000878

Table 3.3 Summary of velocities, densities and magnetic susceptibility measured from the Hillside Cu-Mine site. The measurement on the core samples was done under normal room temperature and pressure. Petrophysical data used for Olympic Dam, Vulcan and Mount Gunson copper-gold deposits modelling are not available in the public domain, but they have similar geological environment to Hillside and thus these values are used in the seismic forward modelling for all test sites

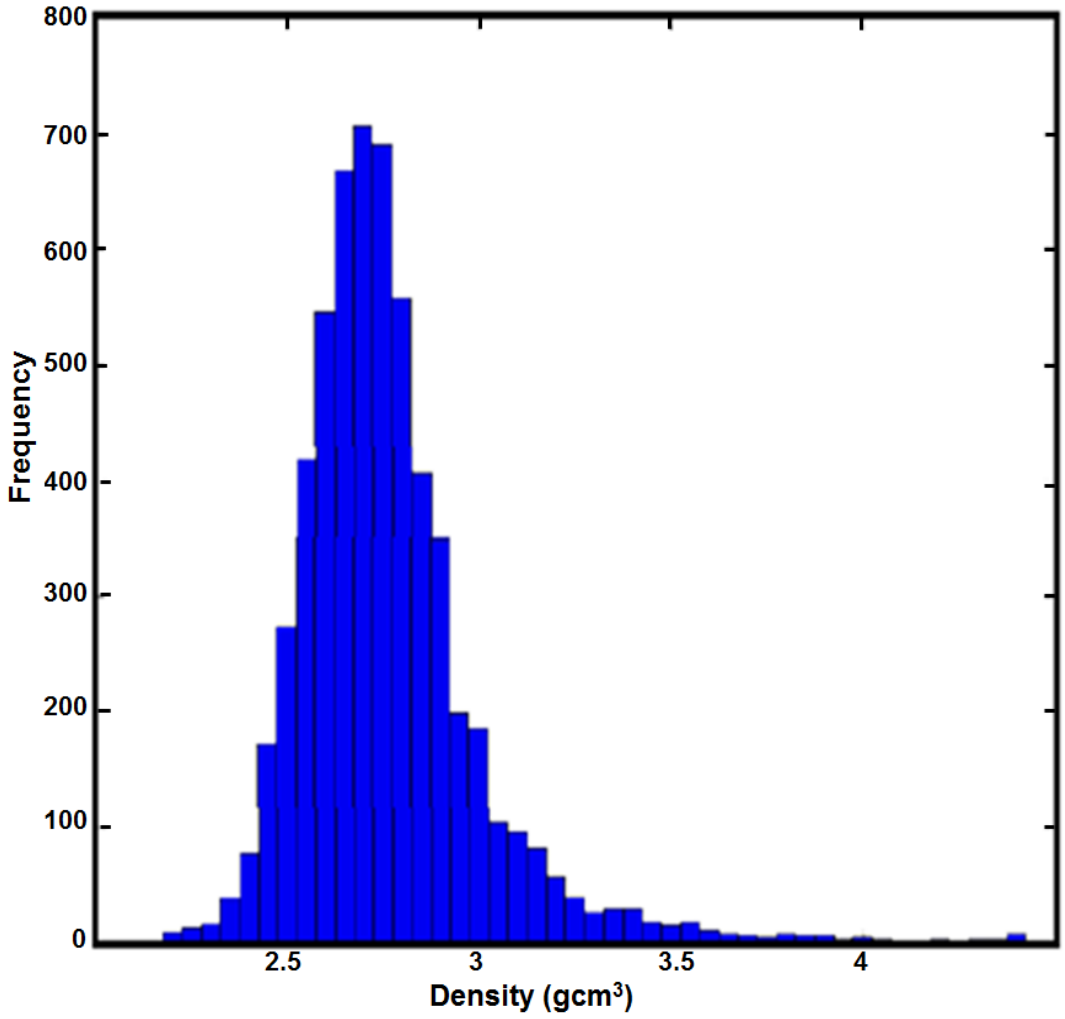

Figure 3.3: Density distribution. A total of 304 measurements were made on cores from selected drill holes at Hillside. Low densities (<2.9 g/cm^3) and the high densities (>3.2 g/cm^3) correlate very well with alteration zones and mineralisation zones respectively.

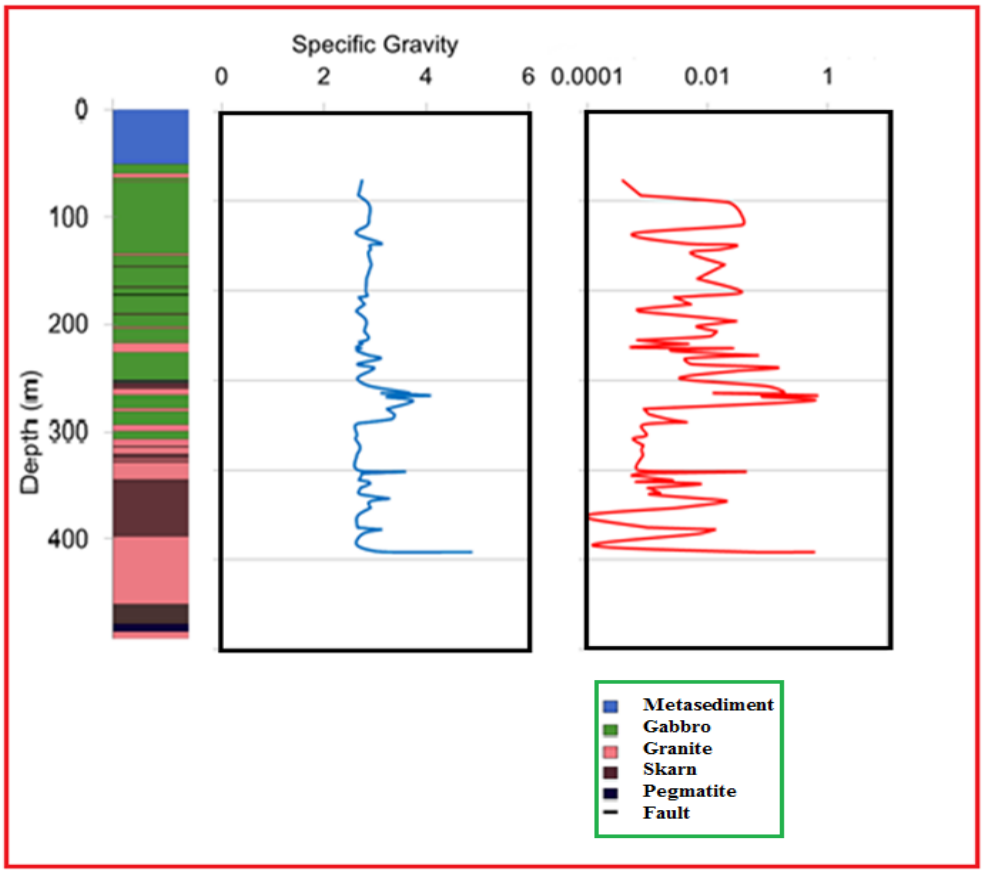

Figure 3.4 density log and mineralization from Hillside Petrophysical measurements. Magnetic susceptibility estimates ranging from 0.000087 to 0.721. Low values of magnetic susceptibility (<0.0001 SI) corresponded to altered zones with many fractures while high magnetic susceptibility (>0.01 SI) correspond to unaltered and non-fractured zones

3.5.3 Velocity Measurement

The velocities were determined from a suite of cores of ore and host rock with dimensions ranging from ~18.5–51.3 mm in length. These cores were representative of the characteristic lithologies found in the Gawler Craton. The compressional wave velocities were measured using the pulse transmission method, that is, a pair of piezoelectric sensors placed on opposite ends of the cylindrical rock sample such that

one sensor triggers an acoustic pulse that propagates through the sample and thereafter is recorded by the second sensor at the opposite end. Measurements were done under normal room temperature and pressure and measured with a portable oscilloscope.

Compressional and shear wave velocity measurements from representative core samples ranges from ~4.46 km/s (highly altered) to ~7.76 km/s. The low velocity values correspond to rocks with a high degree of alteration though some studies (Iturrino et al, 1991) have showed that in some instances, presence of Fe can increase densities, but lower Vp. Figures 3.5 and 3.6 are plots of P-wave vs S-wave velocities and P-wave velocity verses specific gravity.

To further characterise the acoustic velocities, the measured values were plotted against the well-known Nafe-Drake curve (Nafe and Drake, 1963), which highlights a general relationship between velocity and density that silicate host rocks and sulphide minerals tend to occupy at a confining pressure of 200 MPa (Figure 3.7). This relationship should still work at lower confining pressures if the crystalline rock mass is relatively free of open fractures. As velocity properties are severely affected by fractures or cracks, the measured values tend to increase to the crack free value with confining/overburden pressure as the cracks are progressively closed (Schmitt, et al., 2003; Salisbury, et al., 1996).

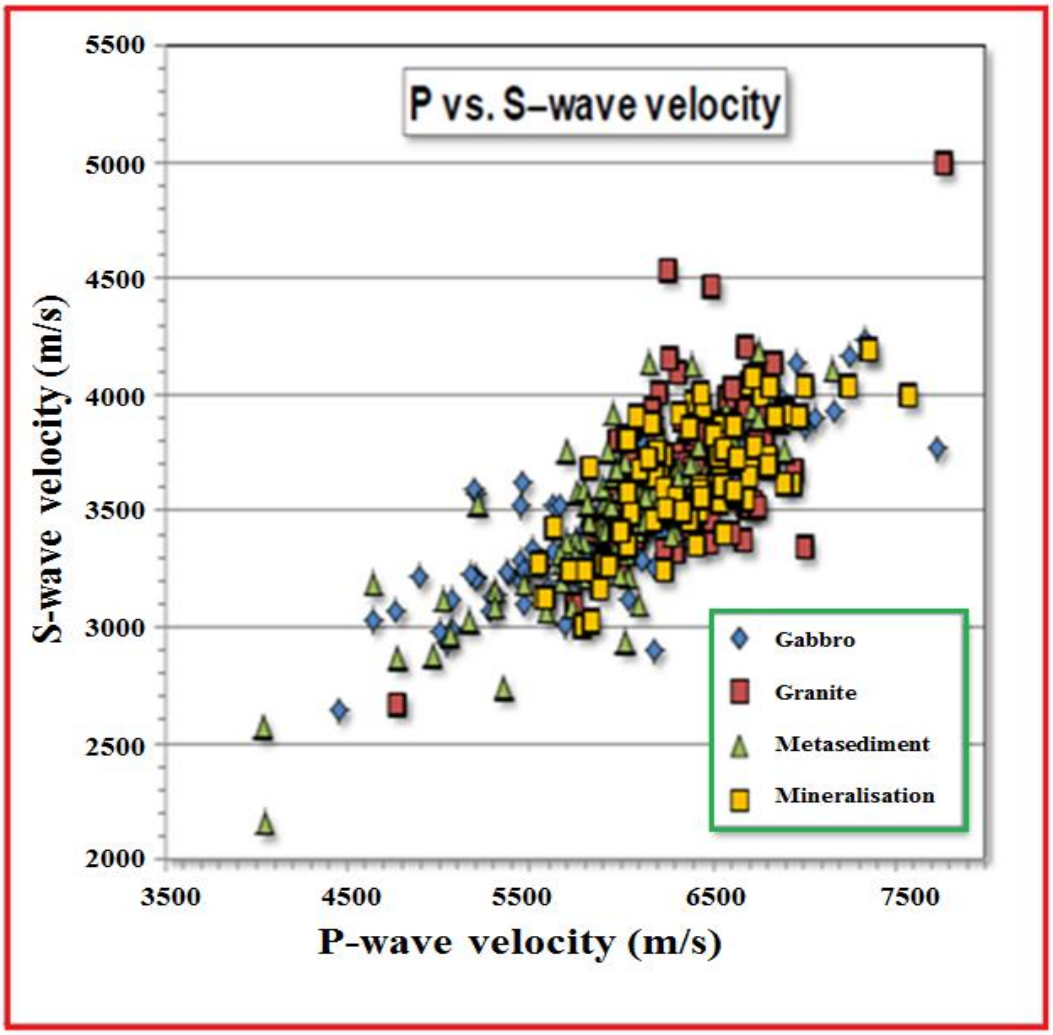

Figure 3.5: Crossplots of P-wave and S-wave velocity from Hillside core measurements. The metasediments have lower velocity, as well as the gabbros, and the mineralised rocks and granites have higher in velocity in Hilside. Note that typically sulphide minerlas and iron oxides are filling the cracks and voids of a breccia and often form the minor component of the minerilised rock. Thus, rocks tend to gain density and velocity with mineralisation, but will not deviate too much from the host rock. The result is that range of values of Hillside mineralsation (as with most disseminated deposits) will overlap signficantly with host-only properties.

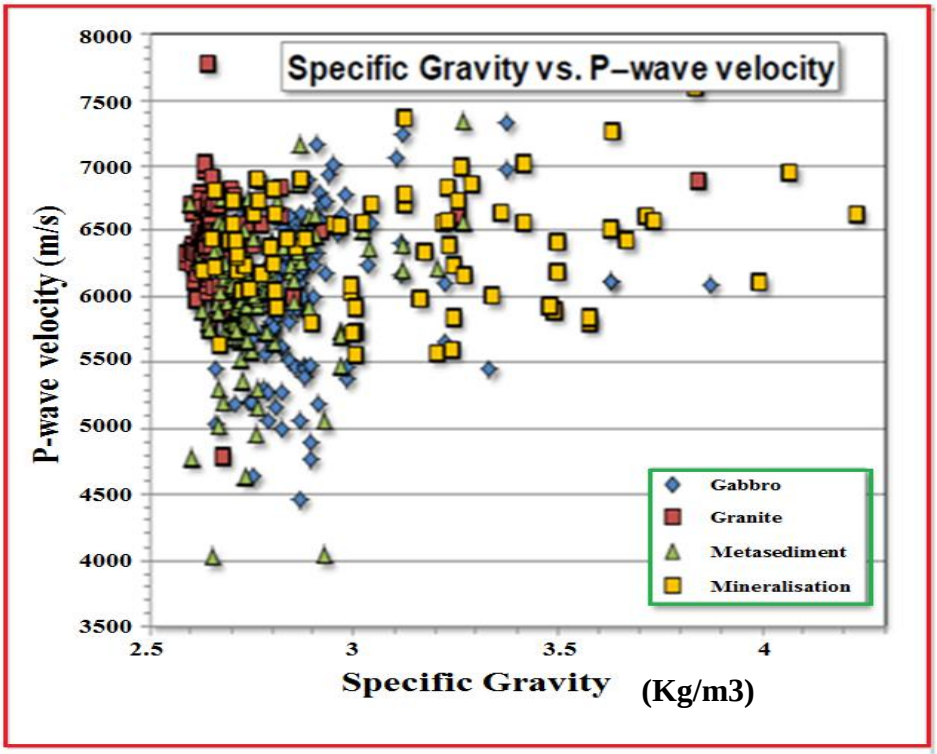

Figure 3.6: Crossplot of specific gravity and P-wave velocity from Hillside core samples. Though values appear to be fairly represntative of the properties of common lithologies in the Gawler Craton, it must also be emphasised that the high density of mineralised samples does not necessary mean high velocity as many sulphide minerals equally have lower velocites.

Further analysis of the petrophysical database indicates that velocities tend to increase as pressures changes (densities change varies slightly over same pressure range) (Salisbury, et al., 1996). Increases in compressional velocities with pressure also results in a slight increase in densities with pressure, thereby causing acoustic impedance differences to be inconsistent with confining pressure (Salisbury, et al., 1996). For the depths of interest in this study, less than 3 km, the differences are only really noticeable in the upper 100 m, where there is typically sediment cover in the majority of the Gawler Craton.

Figure 3.7 show the rocks rich in sulphide minerals are acoustically distinguishable from the host rocks since R=0.06 (reflection coefficient) is the threshold for producing a detectable reflection after allowing for noise. The data from Figure 3.6

broadly agrees with this prediction; however, Gawler IOCG mineralisation is rarely a "pure" sulphide phase and these minerals are usually a minority component in an iron-rich silicate mineral matrix.

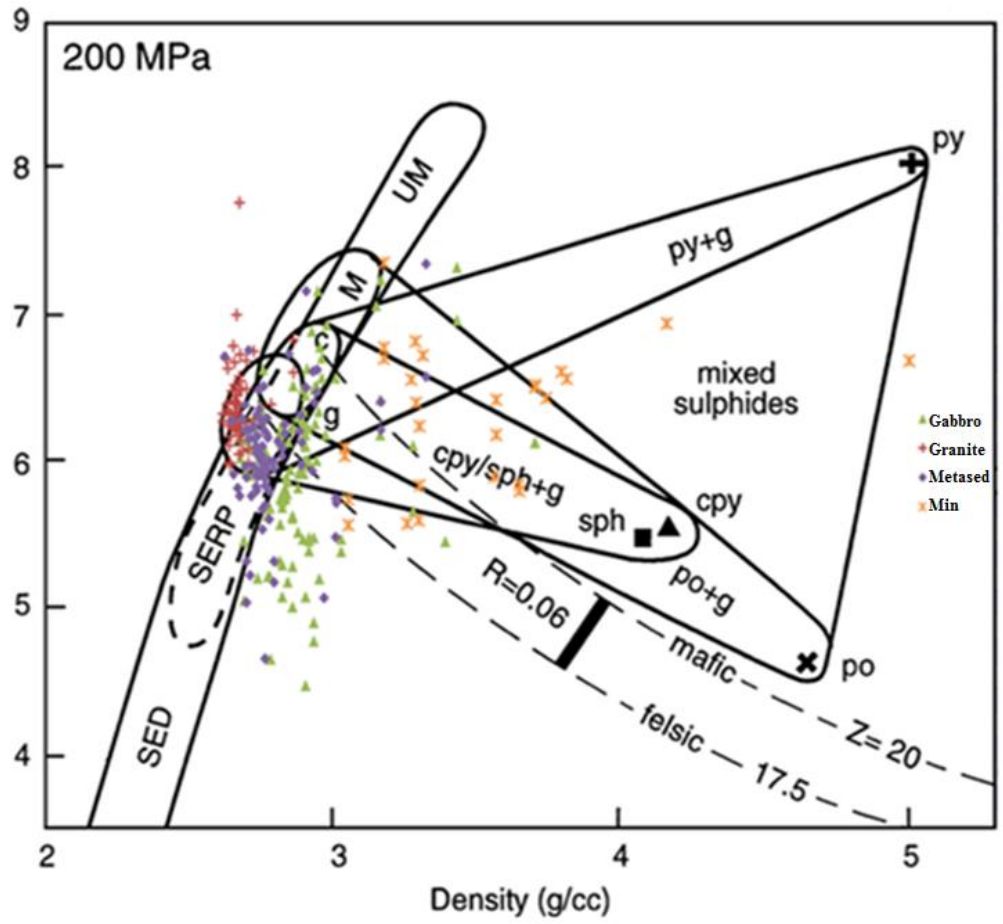

Figure 3.7: Projected Compressional wave velocity versus density for rock samples from Hillside Superimposed on the Nafe-Drake curve for common silicate rocks, and selected base metal ore minerals (after Salisbury, et al., 1996). In this plot only the heavily mineralised samples are plotted as "min", whereas in figure 3.6 the mineralised are the "economic zones", where the host rock properties tend to dominate due to the prevalent disseminated mineralisation.

3.6 Uncertainties in Petrophysical Measurements

All petrophysical data have uncertainty and limitations. Factors such as core thickness, traveltime measurement, delays due to sonic gel coupling on small samples, delay of the transducer and delay due to core boat for instance all add to uncertainties in P-velocity measurements; while core thickness, calibrator and gamma fluctuation and temperature influences density measurements (Dewan, 1983; Theys, 1997, 1999). In short the core measurements have errors that are more random than systematic. Lastly, the results of sonic measurements on the cores are likely to be significantly affected by their removal from the in-situ conditions.

For susceptibility, one of the factor that impacts the measurement is core thickness. Temperature range encountered during core measurements at the Hillside mine site is less significant to have an effect on magnetic susceptibility measurements. Thus, measured magnetic susceptibility values have less variation than the sonic measurements.

4 Hillside Modelling Experiment

4.1 Introduction

Hillside is a newly-discovered, undeveloped copper deposit resources related to Mesoproterozoic Hiltaba Suites of intrusive along the crustal-scale Pine Point fault on the eastern margin of the Gawler Craton, South Australia. Although small-scale historical mining is recorded in the area, the resources currently considered as the Hillside Cu-Au deposit was discovered in 2008 (Rex Minerals, 2012, Porter, 2013). This future mine site was selected as one of the case studies in this research for a number of reasons. Most of existing copper mines around the globe are in high-risk locations or at great depth with significant capital costs and the Hillside copper deposit is very different in that access is relatively easy and shallow.

The large scale, copper-gold-magnetite deposit is 'hidden' under thin layer of cover rocks extending almost to the surface. Magmatic fluids associated with mineralisation have been emplaced in the faulted network and have infilled many faults and joints (Porter, 2013). This deposit was a study area of the research group that I was working with (within DET CRC) and we were able to publish results with relative ease. Further, a variety of petrophysical data provided by Rex Minerals, operators of Hillside copper project, and 2D and 3D seismic experiments conducted by Curtin University Department of Exploration Geophysics, are available for comparative study (Tertyshnikov, 2014). The principal downside of Hillside is that it doesn't have the type of exploration issues that seismic reflection surveys address best. Thus, most of the geophysical research in DET CRC was spent upon evaluating seismic for in-mine definition.

4.2 Location and Geology of Hillside Copper Deposit

The Hillside copper deposit (Figure 4.1a and b) is situated within the striking Pine Point Fault Zone (PPFZ) which runs along the eastern coast of the York Peninsula, about 15 km south of Ardrossan and approximately 455 km south of Olympic Dam

(Porter 2013). Inferred resources as of 30th July 2012 are 330 Mt at 0.6% Cu and 0.16 g/t Au, at a 0.2% Cu cut-off (Rex Minerals, 2012)

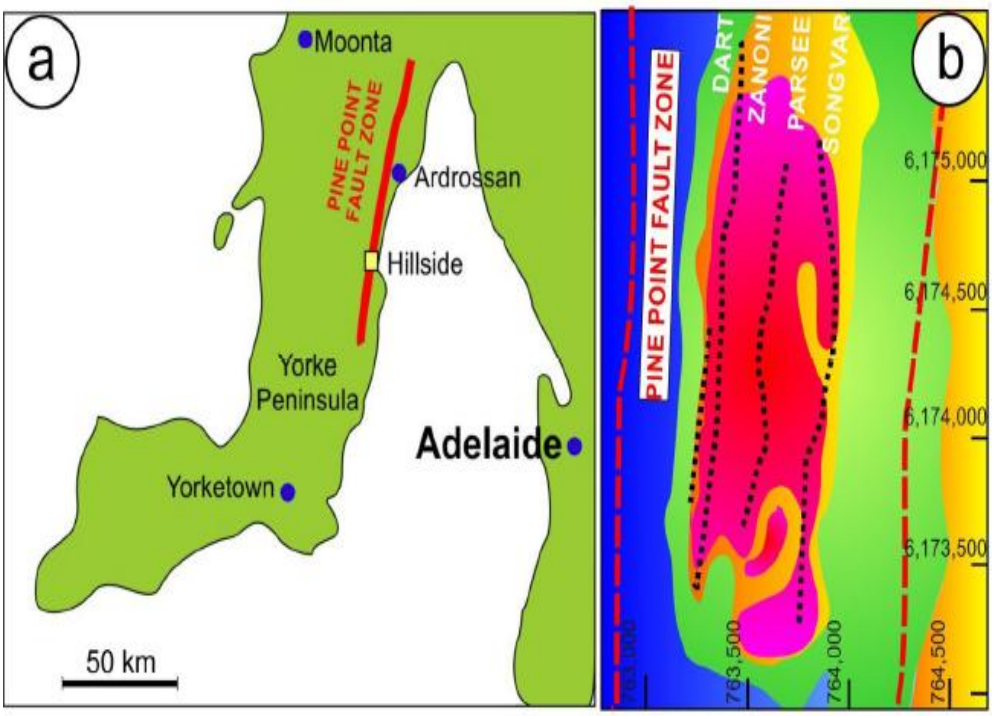

Figure 4.1: (a) Map showing the location Hillside deposit and the Pine Point Fault Zone along the eastern margin of the Yorke Peninsula, (b) Residual magnetic anomaly defining the Hillside with the four mineralised zones (faults) parallel to the Pine Point Fault Zone (modified after Conor et al, 2010).

The Hillside deposit is covered by sequences of recent sediments consisting unconsolidated sand spreads and inland dunes, silty sandstone, siltstone, and limestone of the Rogue Formation, which ranges in age from 1570 Ma to 1700 Ma (PIRSA, 2003; Okan, et al., 2015). Additionally, much of the cover is weathered basement rocks forming a regolith cover of typically 30 m. The tectonic setting of the Hillside copper-deposit is shown in Figure 4.2 A–D. The arrows in (a) show the fluid movement and shearing, (b) transfer of heat, (c) exsolution of magmatic fluid,

(d) descending of meteoric waters, while the dark vertical line shows the major structure associated with the early pine point fault. Such vertical structures associated with Pine Point fault (where mineralisation is known to accumulate) might be detected with seismic reflection surveys by either detecting the fault offsets or strong diffractions (stacked in) associated with the tops of these features. They are hosted by highly deformed and folded metasediments intruded by the Tickera Granite and Curramulka Gabbro equivalents, consisting different phases of granite and gabbroic intrusions (Skirrow, et al., 2004; Olsen, 2010; Rex Minerals, 2010).

The complex distribution of rocks types associated with the Hillside Deposit is shown in Figure 4.3. Majority of faults and fractures encountered occur in the gabbro-skarn-metasediments package, which host orebody, while the hanging wall and footwall units are less fractured. Further, it is believed that the magmatic fluids related with mineralisation is emplaced in the faulted network and have infilled the faults and joints. Thus, seismic reflection methods can be used to provide high resolution images of the subsurface, facilitating the interpretation and research on structural complexity related to IOCG mineralisation (Malehmir, et al., 2012).

The gabbro skarn metasediments assemblage, where the majority of the faults and fractures occur, could have high impendence contrast compared to the hanging wall and footwall due to delays in wave propagation through the faults and fractured zones. Unfortunately the significant structures are near-vertical and not well imaged using conventional 2D seismic image processing. Regardless of the various seismic impedance contrasts within the Hillside deposit complex, the magnetic data and other drilling data indicate that Hillside is identifiably abnormal from nearby host formations because of its relative complexity; thus, it is a candidate for a breccia trap (near a major fault) for IOCG mineralisation.

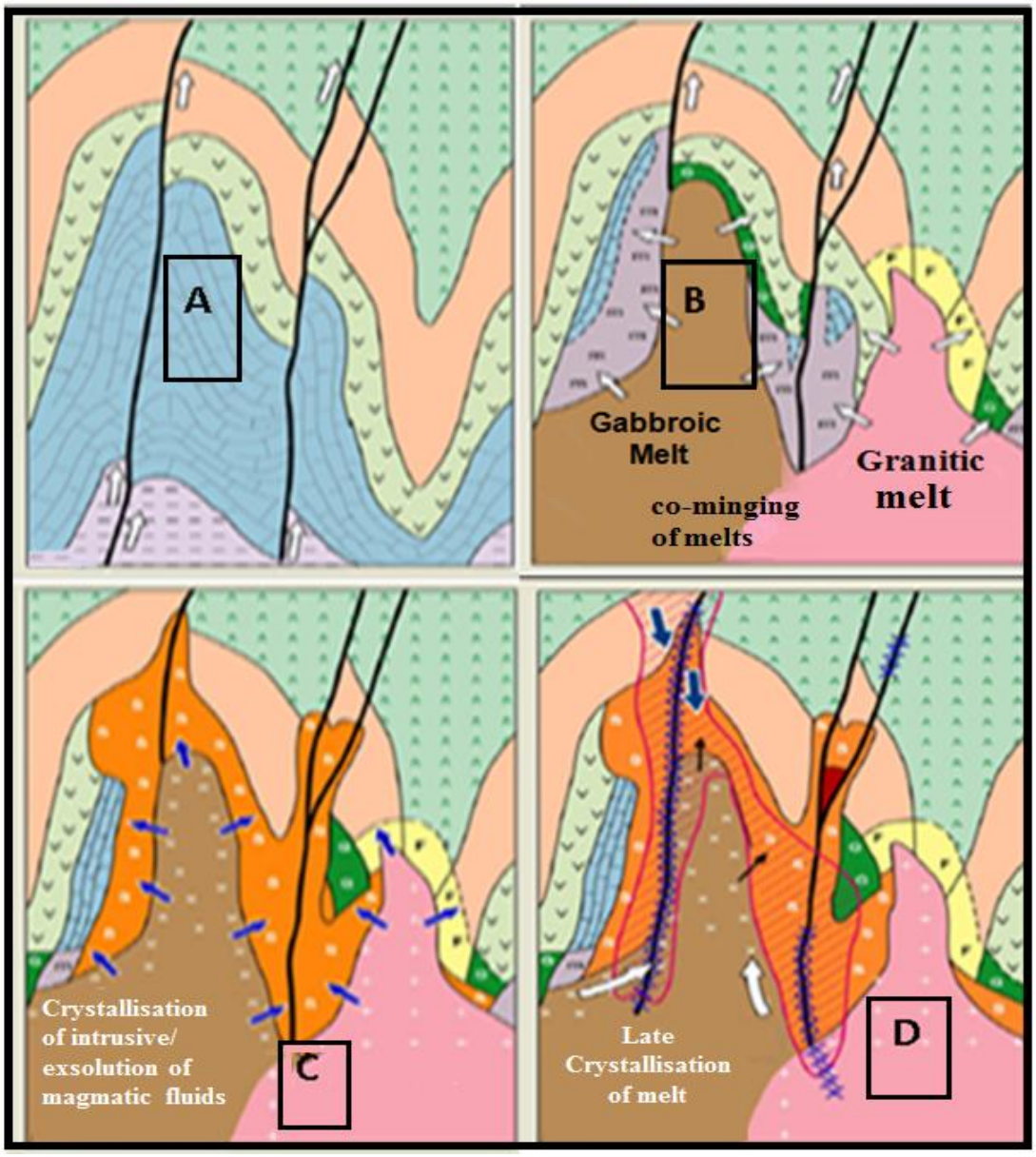

Figure 4.2: Different stages of evolution of Hillside IOCG Skarn deposits. The arrows in (a) show the fluid movement and shearing, (b) transfer of heat, (c) exsolution of magmatic fluid, (d) descending of meteoric waters, while the dark vertical line shows the major structure associated with the early pine point fault. (modified from Marc, T., & John, B., 2013). Such hidden vertical structures associated with Pine Point fault (where mineralisation is known to accumulate) might be detected with seismic reflection surveys by either detecting the fault offsets or strong diffractions (stacked in) associated with the tops of these features.

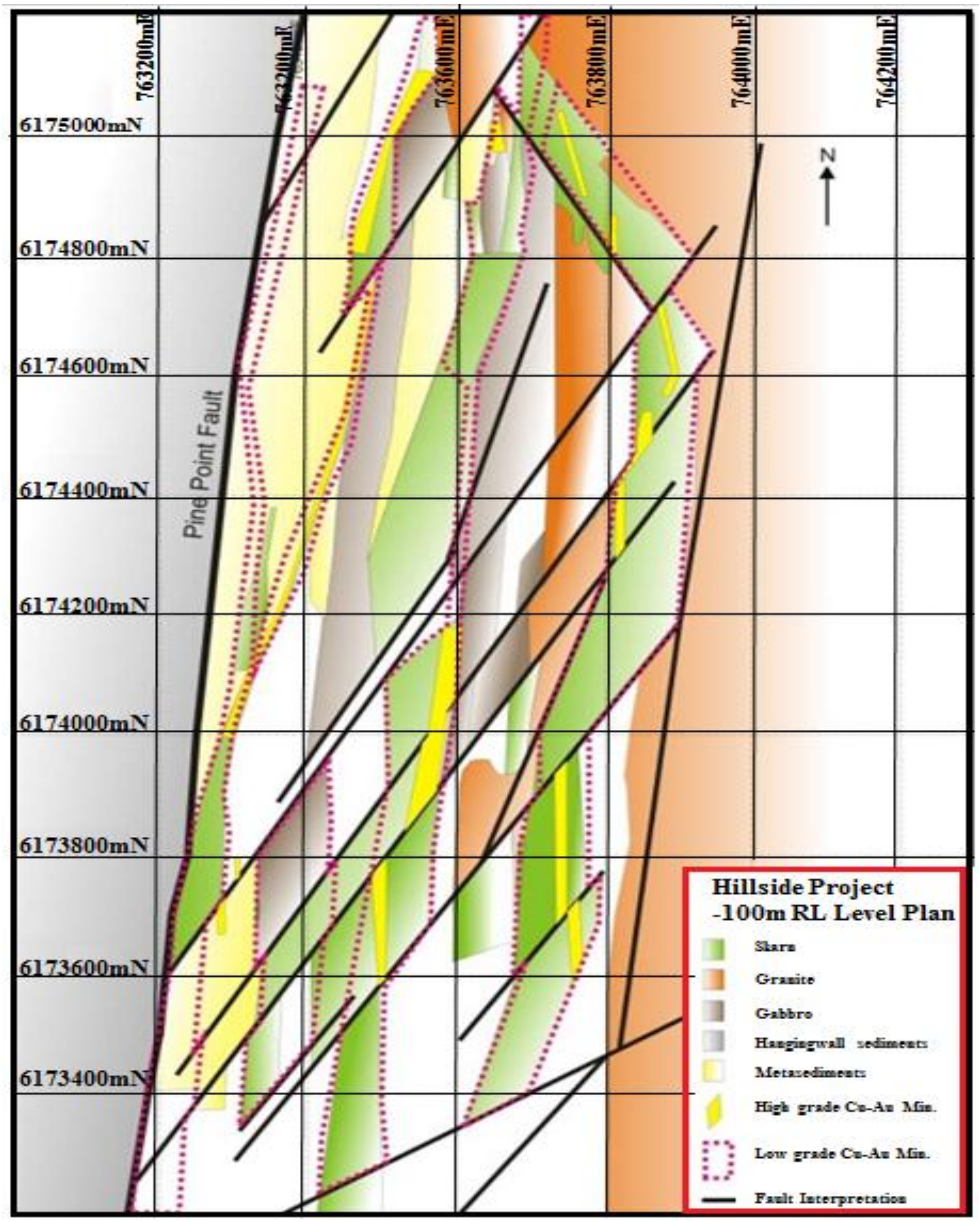

Figure 4.3 Distribution of different rocks and structuring affiliated with the Hillside Deposit (after Rex Minerals, 2010). The majority of faults and fractures occurs in the gabbro-skarn-metasediments assemblage or cluster, which host the deposit, whereas the hanging and footwall units are significantly less fractured. Such faults and fractures zones depending on rock and minerals composition should have high impedance contrast, which makes it excellent target for seismic reflection surveys.

Mineralisation in Hillside occurs within the metasediment, granite and the gabbro and skarn assemblage, which is spatially connected with regional Pine Point fault zone (Okan, et al., 2015). Primary copper mineralisation occurs within the vertical to

sub-vertical magnetite-hematite-rich block while secondary copper mineralisation occurs within a shallow sequence of weathered basement rocks (Conor, et al., 2010; Aldam, 2014; Rex, 2010). The dominant economic minerals are chalcopyrite with lesser amounts of bornite and chalcocite, while magnetite is replaced by hematite±chalcopyrite (Porter, 2013). Pyrite is said to be more in some domains, though is mostly replaced by chalcopyrite during skarn retrogression.

4.3 Magnetic Modelling with upward continuation filtering

One of the objectives of this study is to investigate the response and the resolving power of magnetic responses to IOCG deposit at greater depth. Hillside is unusually shallow compared to most other Gawler IOCG deposits, which are typically 400–1000 m deep. We expect that the magnetic method isn't really feasible for detecting intrusive structures (potential mineralisation zones greater than 250 m depth) unless the deposit is very large. To test this postulate, the initial magnetic response was plotted using Oasis Montaj (Geosoft) software before upward continuation filtering was applied to simulate the deposit at deeper levels.

Generally, the process of transforming a data set so that it can be measured at a different height is called continuation. When the potential is calculated at an altitude higher than the measured field or the anomaly is moved further away from the source, it is called upward continuation and when the data is moved toward the source, it is called downward continuation (Clarke, 1969; Henderson and Zietz, 1949; Jacobsen, 1987; Pawlowski, 1995). It is considered a clean filter because it producces almost no side effect that may require the application of other filters or process to correct. Because of this, it is often used to remove or minimise the effects of shallow anomalies. Jacobsen (1987) further made a strong case for using upward continuation filtering as a method of seperating causative sources for different target depths. He associated upward continuation to a low pass filter attenuating higher frequency components while enhancing low frequency components that would be analogues to deeper targets.

In the case of Hillside magnetic modelling, I applied upward continuation filter because it is reliable, in that the field is continued into free space where there are no casuatives bodies to perturb the field further as in the case with other filtering methods (Jacobsen, 1987). The method effectively attenuates near surface anomalies, thus providing a way for examining deeper structures.

Different testing elevations (100 m to 1000 m) were trialled. Figure 4.4 shows the results of magnetic responses when upward continuation filters were applied. It is very clear that magnetic method is good to approximately 250m depth. Farther from this depth, though some anomalies within the target zone appear can be seen and a broad anomaly exists, its efficacy diminishes. Thus, useful deposits might be missed as a result of decrease in magnetic response. This implies that magnetic approach is still useful at about 250 m, but no longer very trustworthy once the depth to source is greater than 250 m. A quick inspection of figures 4.4E and 4.4F shows that the responses become fuzzy and indistinct blob. No visible anomalies in the upward continued map. This is consistent with the upward continuation algorithm as it tends to suppress subtle features at the expense of longer wavelength anomalies (Jacobsen, 1987). It is now an anomalous limb and would not likely rank as a high priority target for investigation; thus, demonstrating the limitations of the most used exploration methods for deep IOCG exploration.

.

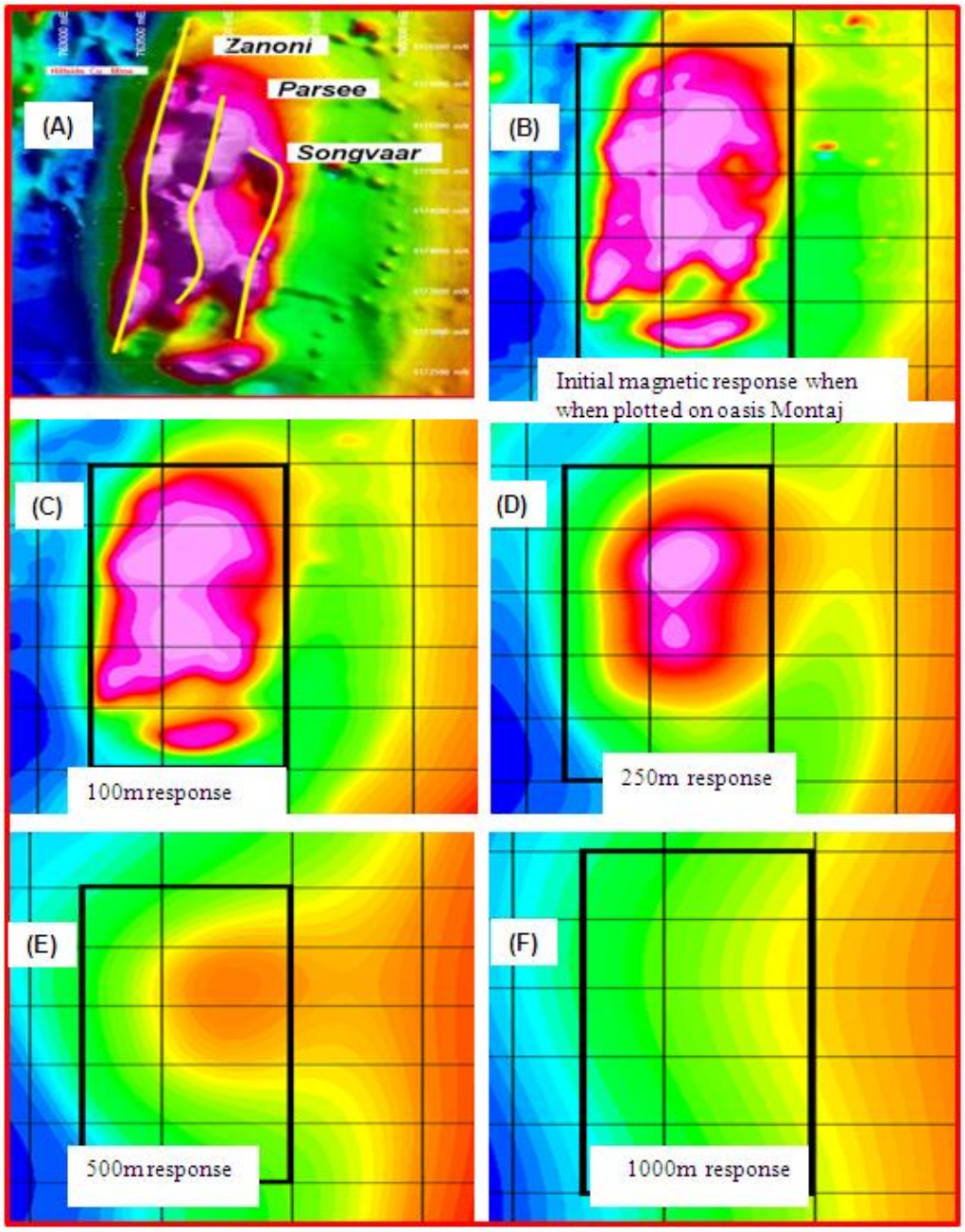

Figure 4.4 A) magnetic map of the Hillside deposit used for geological modelling, B) initial response when plotted on Oasis before applying upward continuation filters, C) response at 100 m, D) response at 250 m, E) response with a 500 m and F) response at 1000 m. In (C), we can see the anomaly at this depth range, which suggests that for shallow investigation, the magnetic approach could still be used to directly delineate the presence of deposits anomalies. In (D), though some anomalies within the target zone appear can be seen and a broad anomaly exists, its efficacy diminishes with increasing depths. Further filter (Figures E and F) do not show visible anomalies in the upward continued map. The responses becomes smear and fuzzy.

4.4 Seismic Modelling of the Hillside Intrusive Structure

Having demonstrated the ambiguity in magnetic responses with respect to an increasing depth of ore-bodies, we now focus our attention on seismic forward modelling of Hillside. The generation of a reliable geological model for synthetic data analysis is very significant; hence, deliberate attention is placed on the realism of input parameters. However, an overly complex model incorporating all available geological data may produce a good fit but is undesirable, as not much might be learnt for other IOCG deposits that are similar. A balance was sought in including enough geological data to make a realistic stacked image and general enough to make a conceptual model in order to extrapolate the learnings to similar deposits.

Rex Minerals provided a number of geological cross-sections derived from many previous drill-hole data. The geological cross-section that has been used for modelling is shown in Figure 4.5. As was the case with magnetic modelling, I vary the depths of intrusive package starting with 50m to 250 m, 500 m, 750 m and 1000 m respectively, to look at detection limits, which are predicted to vary little. For Hillside case study, two model scales representing mine and regional scales were used, respectively (Figure 4.6).The first model is 1000m long and only 500m deep (Figure 4.6 A), while the second model is 10 by 2 km in dimensions (Figure 4.6 B).

I used similar acquisition geometry to the available 2D seismic data. The petrophysical data used for Hillside modelling are based on many core measurements available from many selected drill holes across the mine site. For the 1000 by 500 m modelling experiment, as for the field survey both the source and receivers spacing was kept at 2m with a 48 channels spread while the offset was 24m from the first and last geophone of the spread. A dominant Ricker wavelet source frequency (35 Hz) was used to match field data. Free fall weight drop and highly attenuative and heterogeneous regolith zone effectively lower down the dominant frequency in the data. Record length was set to 2 seconds and sample rate 0.5 ms to avoid grid dispersion.

For the second modelling experiment (10km length by 2km depth), three cases were considered. In the first case, 480 source points at 20 m intervals were utilised for the modelling. Roll along split-spread acquisition geometry was used as often utilised in field studies. Again, zero-phase 1000 active receivers at 10 m intervals were used for the modelling resulting in maximum offset of 4800 m offset. This geometry is representative of a modern regional 2D survey that is last two years implemented by Geoscience Australia (Fomin, 2017 personal communication). The choice of line length is important for imaging and understanding the geology under cover. For the second and third cases, source shot intervals were simulated with 40 and 80 m intervals respectively (very wide spacing for a shallow target, but much lower in cost for deeper targets) across the entire model, maintaining the same source positioning (rolling split-spread) and same dominant frequency. Receivers were spaced at 20 and 40 m respectively. These sparse survey parameters mimic the large scale regional survey geometry used until recently to study deep crystalline structures.

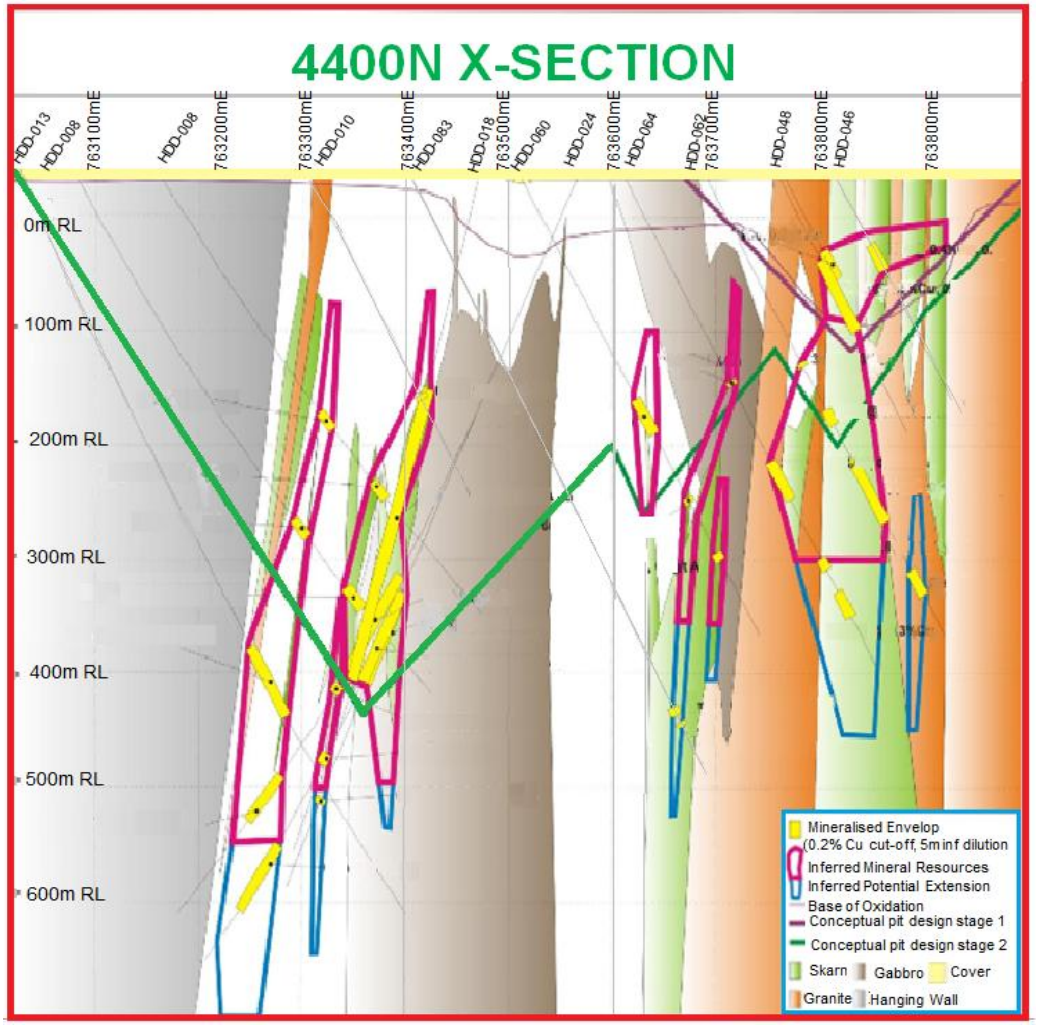

Figure 4.5: The geological cross-section interpreted from borehole measurements, which was used for modelling. (modified Rex Minerals, 2009). The complexity of the Hillside structural geology was further demonstrated from this cross-section; plus all the significant structures are near-vertical, which is not a particularly good situation for seismic imaging with limited offsets.

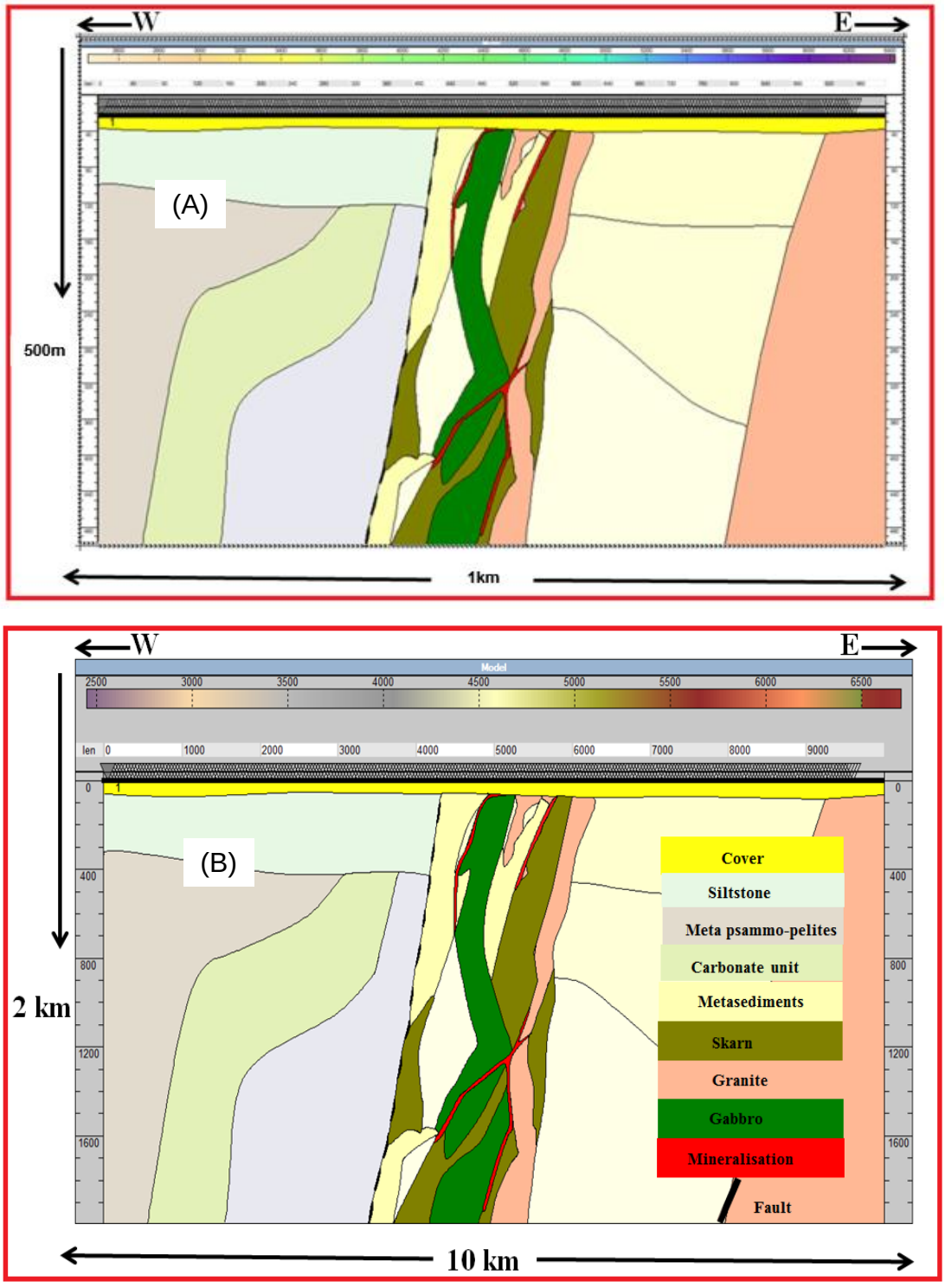

Figure 4.6: The synthetic geological model from the cross-section in Figure 4.5 with incorporated lithological units used for modelling: A) 1km x500m and B) 10km x 2km. Note that one detectable aspect of the mineralised zone is greater structural complexity compared to the host rock formations.

Table 4.1 and 4.2 summarise acquisition parameters and velocity-density used for Hillside modelling experiment.

Acquisition parameters used				
Model(s)	1km x 500m	10km x 2km		
		Case 1	Case 1	Case 3
Parameters	Value	Value	Value	Value
Source depth (m)	0	0	0	0
Receivers depth (m)	0	0	0	0
Shot interval (m)	2	20	40	80
Centre frequency (Hz)	35	35	45	35
Receivers spacing (m)	2	10	20	40
Record length (s)	2	2	2	2
Sampling rate (ms)	0.5	0.2	0.2	0.2

Table 4.1 Hillside Acquisition parameters used for the synthetic modelling.

#	ROCK Type	Vp (m/s)	Density (Kg/m^3)
a	Cover	2465	2070
b	Siltstone	2822	2615
c	Meta psammo-pelites	2350	2079
d	Carbonate unit	4462	2450
e	Metasediments	4630	2414
f	Skarn	5215	2542
g	Granite	6148	2655
h	Gabbro	6445	3410
f	Mineralisation	6635	4120

Table 4.2: Velocity-Density table for the Hillside synthetic geology model. Note that the "mineralisation" values are used for the occasional very rich sulphide zone. Most of the low-grade orebody is within the skarn and gabbro units.

4.5.1 Processing of Synthetic Data

Synthetic shot records were output from the geological model in SGY format for further processing using the RadexPro package with basic processing steps shown in Figure 4.7.

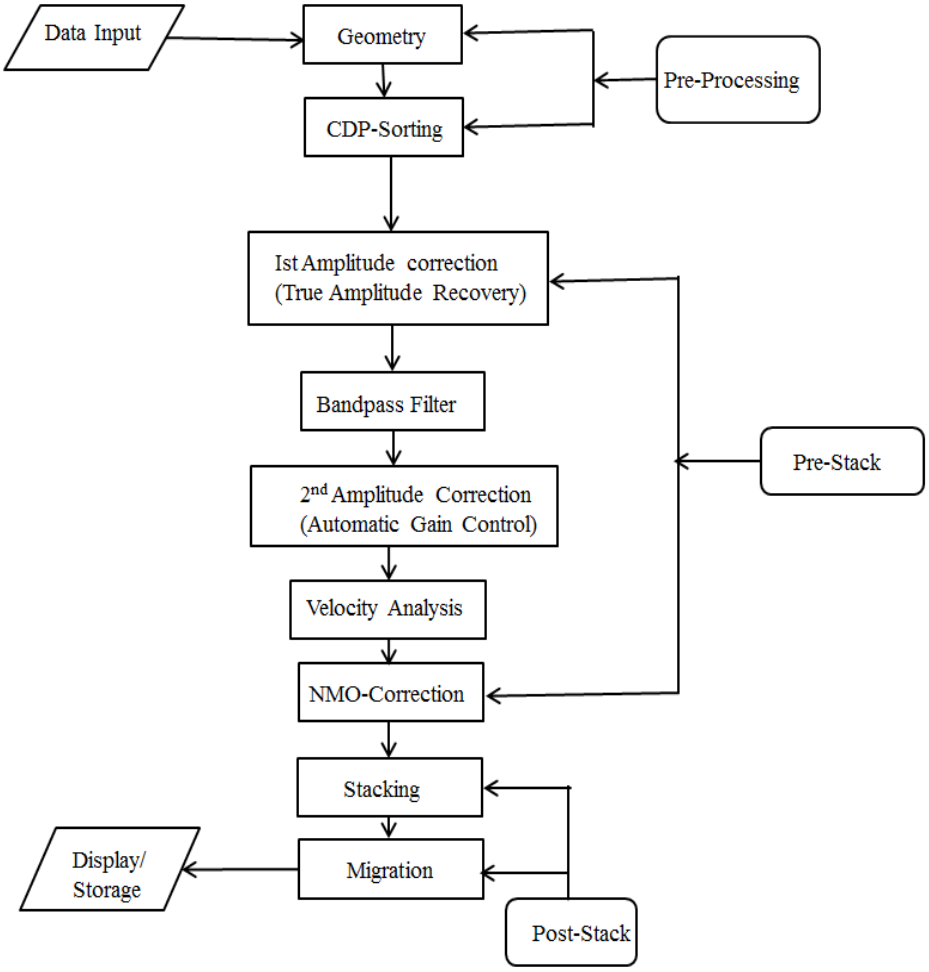

Figure 4.7: A basic processing flow used in all the case studies.

Note that the second correction used an amplitude non-preserving process - automatic gain control or AGC. The reason is that this step is often necessary in field data processing particularly when reflectivity is poor and hence signal to noise ratio low (Urosevic, 2017 personal communication). The processing was similar to the conventional processing used for reginal scale mineral seismic. The last step in the processing involved post-stack migration, followed by depth conversion. A smoothed velocity model derived from the stacking velocities were utilised in F-K migration algorithm. Further improvement in the processing of the data was achieved by applying F-X deconvolution before migration.

4.5.2 Results and Discussions

In this section, we present results from both seismic modelling experiment; 1km length by 500m depth (using similar acquisition parameters with available real 2D seismic data and regional scale experiment (10km length by 2km depth) with varying depth cover at 100 m, 250 m, 500 m, 750 m and 1000 m and different survey parameters. Figure 4.8 is an example of a noise-free synthetic shot record for source number 85 displayed from 0–5000 ms.

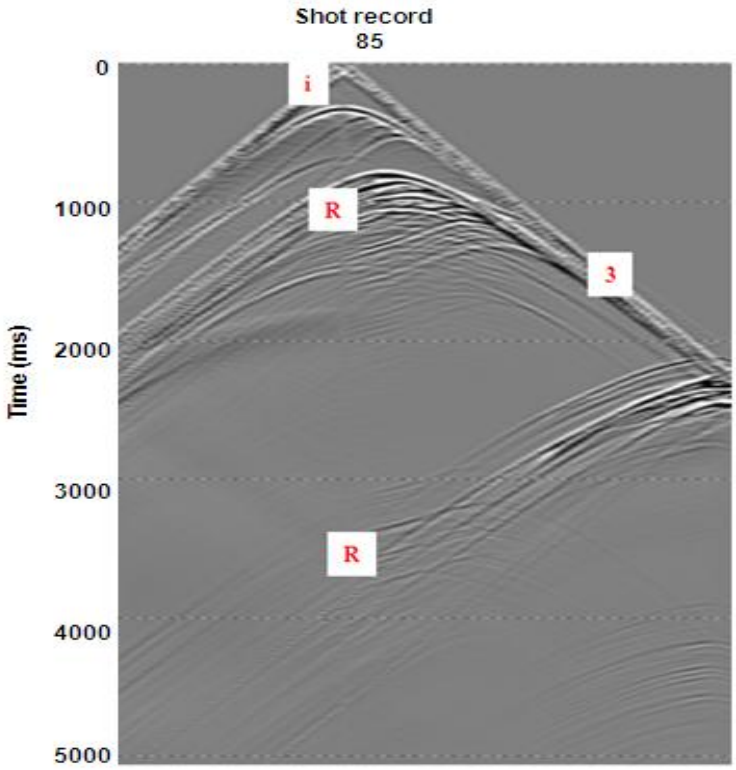

Figure 4.8: An example of noise-free synthetic shot records for source number 85 from the Hillside intrusive model: (1) Direct arrival signals, (R) reflections signals, (3) direct/refracted signals. The shot is displayed using true relative amplitude without correction for spherical divergence. The shot gathers were produced using a Ricker wavelet source cantered at 35 Hz recorded from 0–5000 ms but reflections event are more visible up to 3000 ms.

Generally, for seismic techniques to detect or map a reflective surface, (1) reflection coefficient must be greater than 0.06 to produce a clear reflection, (2) there must be a

minimum resolvable thickness quoted as 1/3 to ¼ of the wavelength and (3) the dip or plunge of less than 45–50 degrees dipping surfaces (Salisbury et al 2003). For the Hillside modelling experiment, the reflection coefficient was well above 0.06 to produce a strong reflection at different layers/lithological units, thus satisfying condition 1. Similarly, the minimum velocity used for modelling was 2465 m/s with base 35 Hz frequency; hence, the wavelength calculated was 70 m or less. Thus, the minimum resolvable vertical thickness is of the order of 17 m, which is greater than the limit of seismic detectability usually in the order of $\lambda/30$.

The Fresnel zone (horizontal resolution) width is expressed as $w^2 = 2d\lambda + \frac{\lambda^2}{4}$ were d is depth to the reflector (Salisbury et al 2003). Therefore, a wavelength of 70 m, at 2 km depth, will produce a reflector of 530 m length, which is greater than (350 m), the minimum Fresnel zone length. As a principle, when the reflector is equal or greater then Fresnel zone, the edges becomes farther from the source and thus lead to a better resolution. In most cases, reflectors in the subsurface are greater than the Fresnel zone yet some diffraction is still visible especially at the edge of the reflector. However, the third condition is usually an issue in exploring for mineral deposits as most structures hosting the ores are usually steeply dipping and/or almost vertical, as in the case of the Hillside Cu-deposit. This has potential to cancel reflections from the target.

4.5.3 Results from migrated depth section from 1000 length by 500m depth

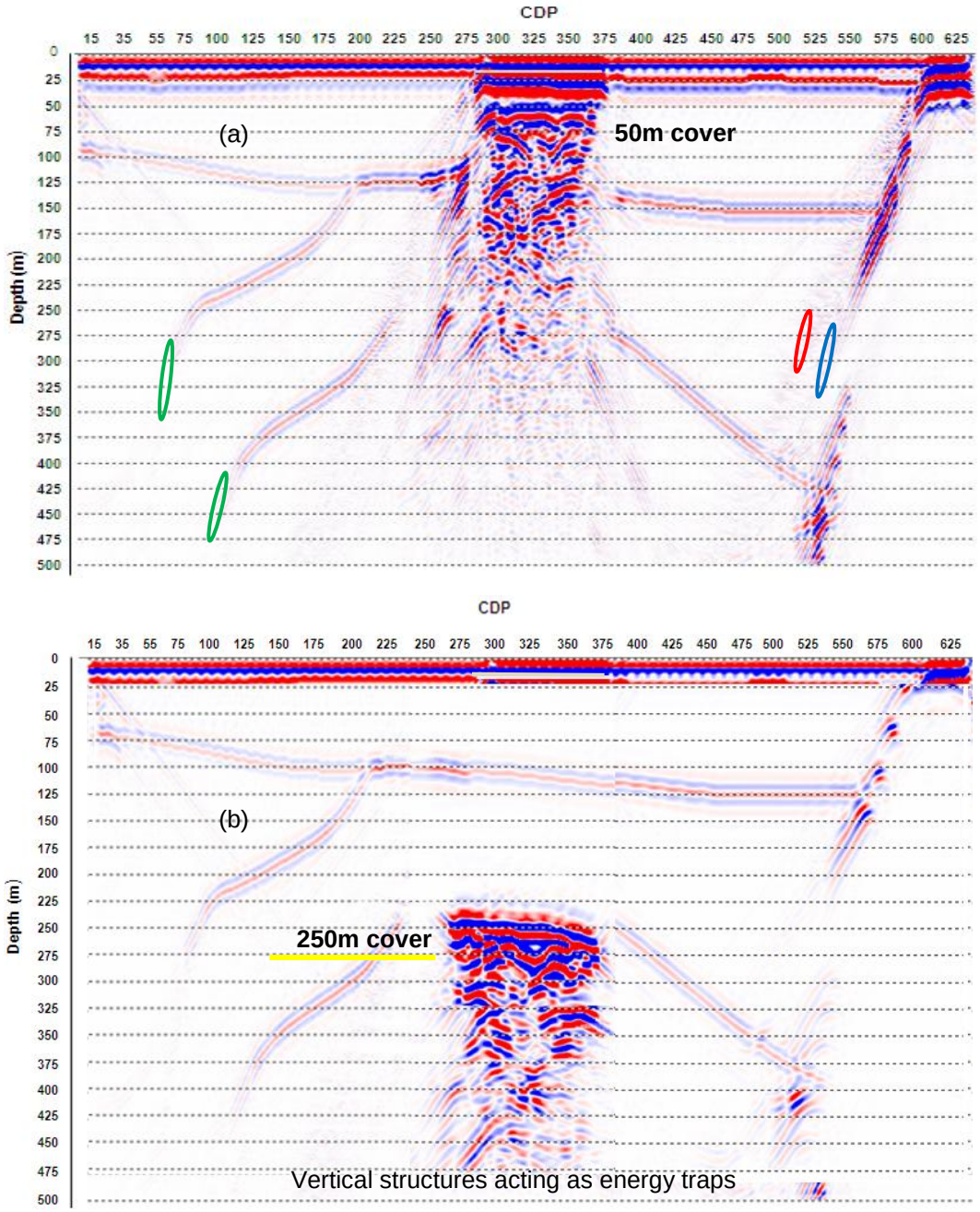

Figure 4.9: The final migrated stacked sections of the simulated seismic data (1000m x 500m) at a) 50m depth cover, b) 250m depth cover. Strong reflectivity associated with the intrusive block is due to the presence of gabbro and granite units. Both the hanging and foot wall are largely recovered when compared with results from regional scale experiment (Figures 4.10-4.14). Dense acquisition parameters used (2m source and 2m receiver) spacing may be responsible. We can also see that the migrated seismic section has successfully delineated the intrusive block (possible mineralised zone) from a depth of 50m to 500m without losing resolution.

4.5.4 Results from migrated depth section from 10km x 2km

Migrated synthetic sections converted to depth are shown in Figures 4.10–4.14

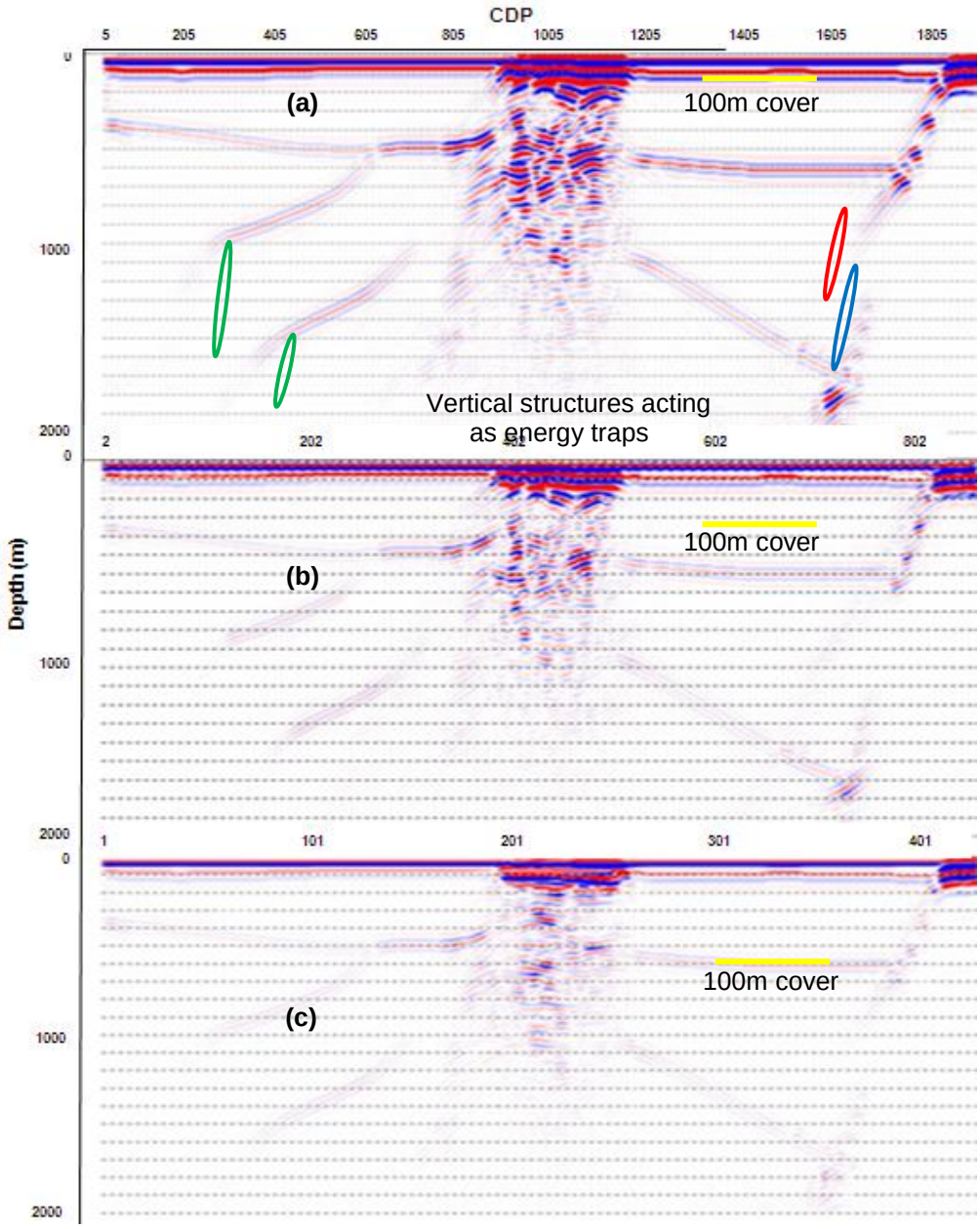

Figure: 4.10: Noise-free depth-migrated sections at 100 m cover a) 20 m source and 10 m receivers spacing b) 40 m source and 20 m receivers spacing c) 80 m source and 40 m receivers spacing. In all cases, the layers between the cover and siltstone are well image while the layers within the hanging wall sediment (green circle) and foot wall (eastern granite) (blue circle) are not fully recovered because of the aperture of the survey. The intrusive block is well imaged but the individual structures within the block are undefined. We observed some artefacts (red circle) which might be due to processing errors.

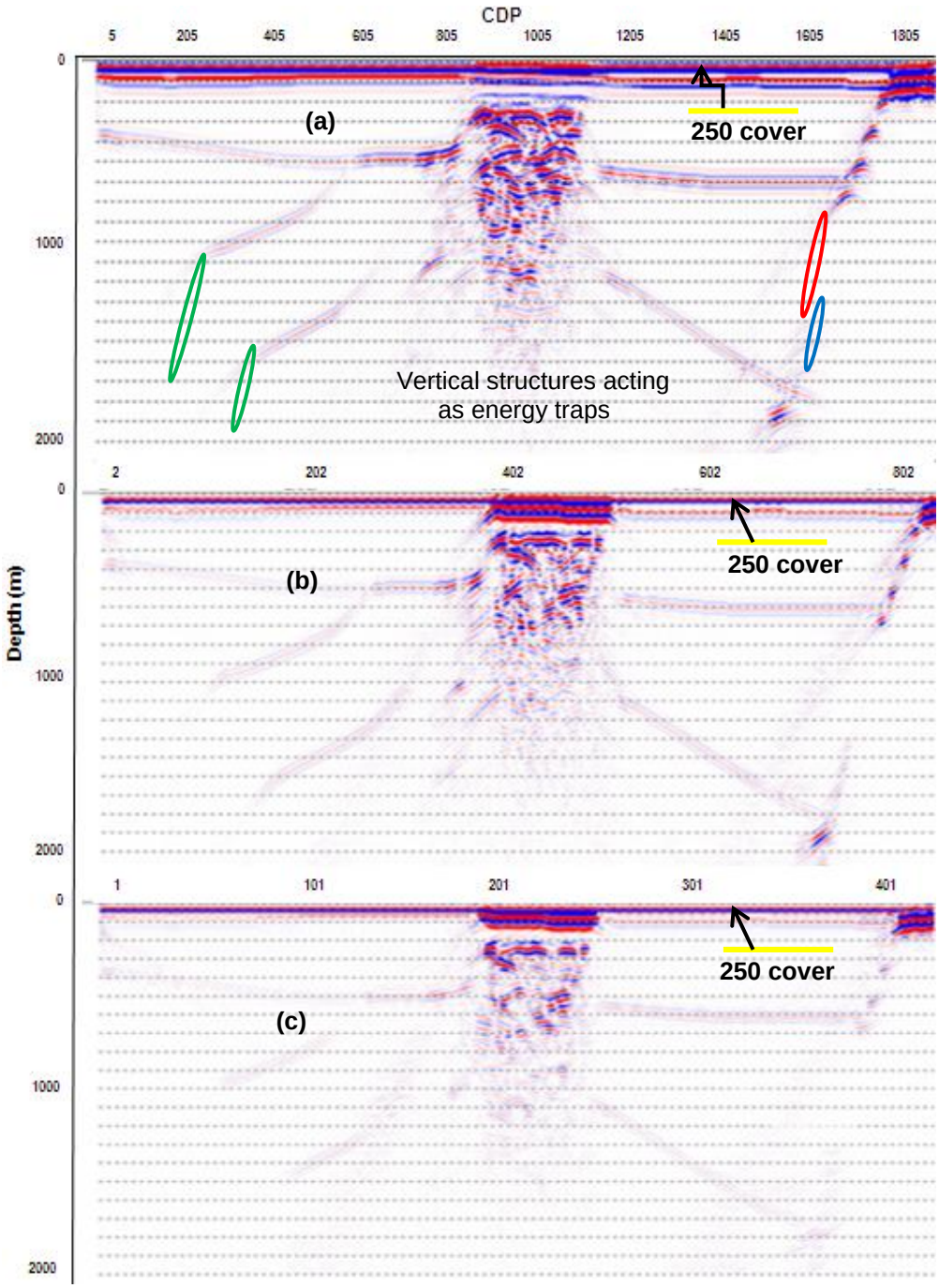

Figure 4.11 Noise-free depth-migrated sections at 250 m depth cover tested with different survey parameters; a) 20 m source and 10 m receivers spacing b) 40 m source and 20 m receiver spacing c) 80 m source and 40 m receiver spacing. Again, the layers between the cover and siltstone are well recovered but not so within the hanging wall sediment (green circle) and foot wall (blue circle) probably due to the aperture of the survey. The intrusive block becomes very obvious but the individual structures within the block are still unresolved. The red circle indicates some weak artefacts which are becoming stronger now, especially on the foot wall (red circle) and are likely due to processing errors.

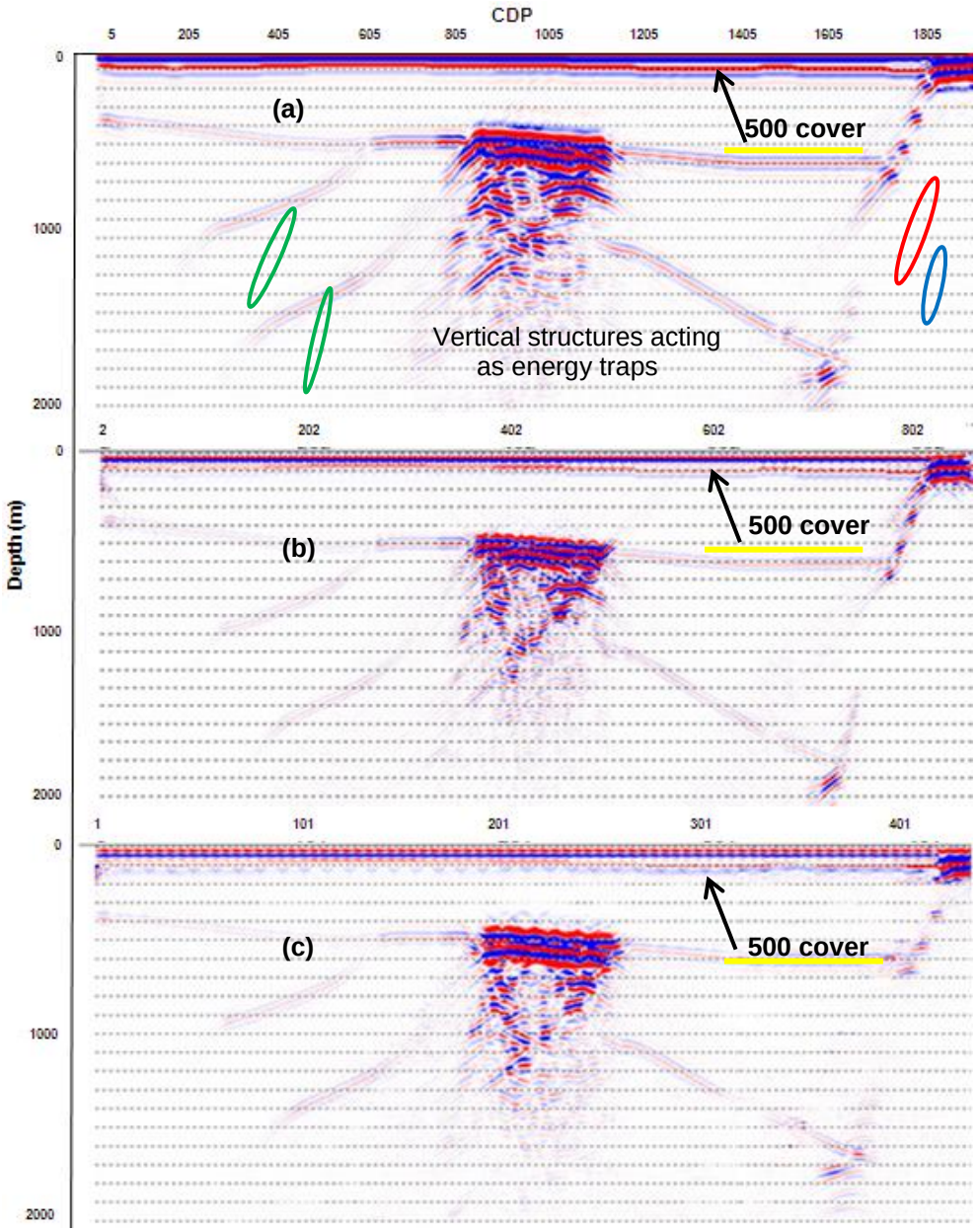

Figure 4.12 Noise-free depth-migrated sections at 500 m depth cover tested with different survey parameters; A) 20 m source and 10 m receivers spacing b) 40 m source and 20 m receivers spacing c) 80 m source and 40 m receivers spacing. For cases both the layers between the cover and siltstone within the hanging wall sediment (green circle) and foot wall (eastern granite) (blue circle) are becoming very weak image wise. The top of the intrusive block is well imaged but little within the block is imaged. Thus, at the typical depth limits for economic mining for IOCG deposits we are able to detect the presence of an anomalous package of intrusives, which could be a trap for sulphide minerals.

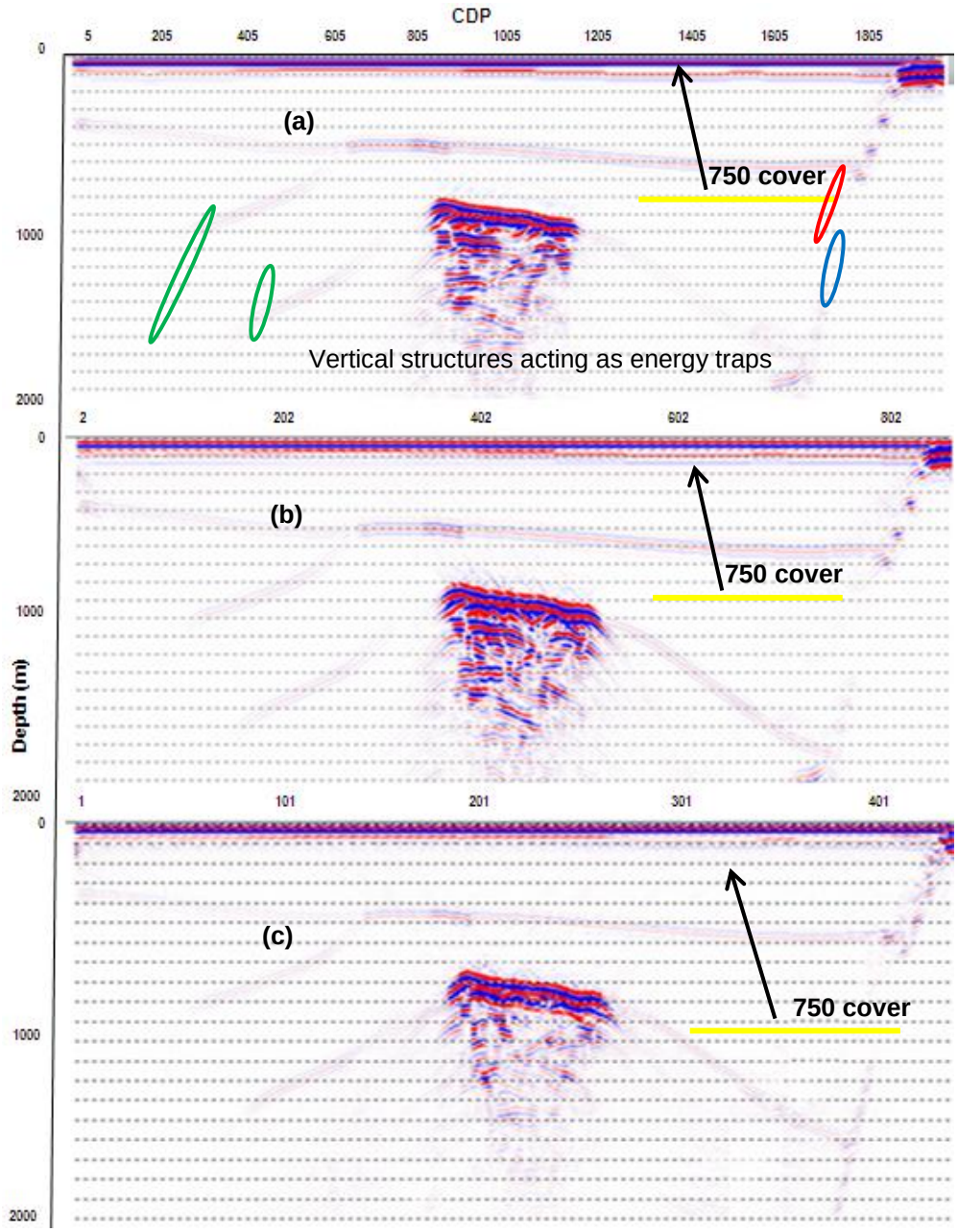

Figure 4.13 Noise-free depth-migrated sections at 750 m depth cover tested with different survey parameters; a) 20 m source and 10 m receivers spacing b) 40 m source and 20 m receivers spacing c) 80 m source and 40 m receivers spacing. The migrated image replicated the cover as well as the metasediment layers. For both cases, the layers within the footwall (blue) and the hanging wall (green) are partially recovered due to the vertical nature of the structures. Reflection within the intrusive block is also visible but the individual structures and the mineralisation zone cannot be imaged. The large circle in red indicates some artefacts due to processing errors.

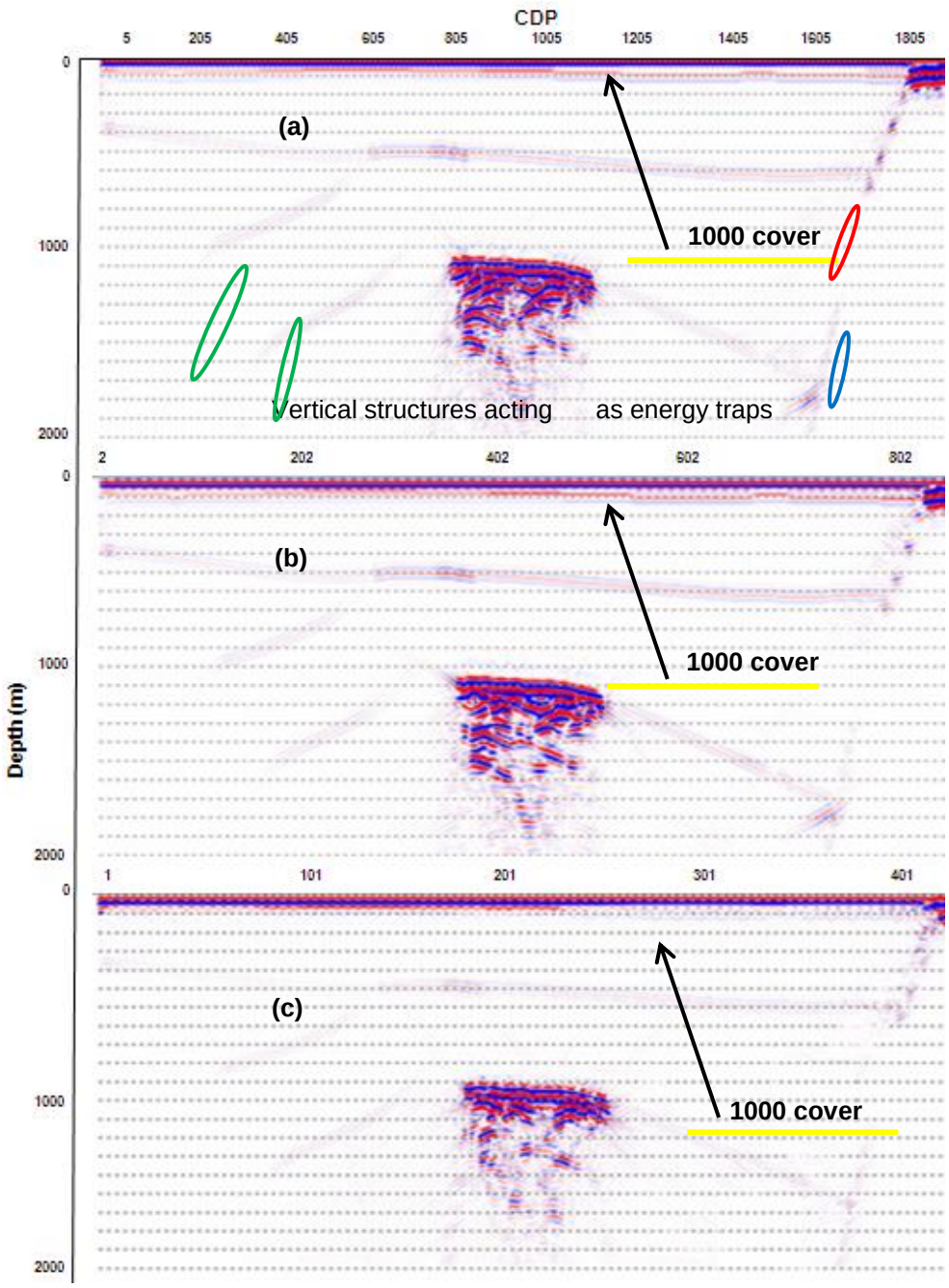

Figure 4.14: Noise-free depth-migrated sections at 1000 m depth cover tested with different survey parameters; a) 20 m source and 10 m receivers spacing b) 40 m source and 20 m receivers spacing c) 80 m source and 40 m receivers spacing. Due to the vertical nature of the structures, layers within the footwall (red arrow) and the hanging wall (blue arrow) in all cases are not well recovered. However, resolution is maintained with depth as we can still see reflections within the intrusive block when the cover is increased to 1000 m. Red circle indicates some artefacts as a result of processing errors We can also see reflections within the intrusive package but the individual structures and the mineralization zone cannot be imaged**.**

A superior result, as expected, has come from the 2m source and 2m receivers (Figure 4.9a and 4.9b). Interesting results also comes from 20 m source and 10 m receivers test parameters (Figures 4.10a, 4.11a, 4.12a, 4.13a and 4.14a). Strong reflections were observed at the contact between the intrusive structure and the sedimentary cover. This is expected as the rocks within the intrusive structure have a very high velocity and density. In all parameters tested, we can observe that the top of the intrusive structure can be detected. Reflections around the edges of intrusion are visible for all the cases; however, the individualised structures within the intrusive zone cannot be imaged. The effect of scattering of energy as a result of diffraction could obscure imaging of the individualised structures within the intrusive package. Also, even with large offsets the ability to image steep structures is not possible without more sophisticated processing methodology, which is not the focus of this study.

The layers within the hanging wall (sediments) were partially recovered. This is due to the complexity of the Hillside deposit where highly deformed and folded metasediments are intruded by different faces of nearly-vertical granitic and gabbroic dykes. These vertical intrusive structures cause the energy to be trapped and most of the reflections never return to the surface. In some cases, the vertical structures generate a very complex reflected wavefield, which has the potential of concealing reflections from the target. To be able to see these sub-vertical structures, we require wide-angle reflection recovery.

The footwall (eastern granite) was also recovered but there are some artefacts that may be due to an attempt to explain the elastic data with acoustic modelling, processing errors and the vertical angles of the boundary. However, by applying band pass filters, the artefacts are substantially reduced. Low reflectivity was observed outside the main intrusive block or structures. The lower values of the assigned reflection coefficients, coupled with the fact that there is no general decrease in reflection amplitude due to attenuation, may be responsible for this observation. Also, a lack of noise observed in the migrated images from the

geological model are due to the modelling technique used (acoustic), which takes into account only P-waves and density.

We also see from this experiment that seismic reflection events from complex intrusive structures have some corresponding relationship with ore bodies. They could produce superposed reflections from different azimuths with varying time functions. However, it is unclear which of the reflection events lie accurately in the imaging. The appearance as well as the position of reflections is related not only to a single structure, but also to combinations of structures within the intrusive package. Although resolution enhancement (post-stack deconvolution perhaps) might improve the corresponding relation of reflection events and ore bodies, it is difficult to enhance the resolution sufficiently to resolve the single ore body using real seismic data.

The modelling and processing techniques are two-dimensional; the data coming out of the plane on the 2D profiles as well as the structures will be seen on all profiles that are larger than the required window. This will have an effect on the Fresnel Zone due to contraction or reduction in 1D but could still expand its full width perpendicular to the line. Thus, to address this effect of out of plane effects, additional surveys beyond the target area of interest can be added to aid interpretation.

Overall, this modelling experiment demonstrates the suitability of seismic reflections survey in detecting deeper structures, as well as the complex fault (Pine Point) and fractures zones that could potentially host ore bodies. However, in practice, a traditional seismic data interpretation method, which predicts the layer structures on the basis of the reflection event distribution, will have some challenges. Therefore, the seismic data interpreter should bear in mind that the reflection events in this type of target and geology do not represent the “layers” and the “layers” may not have corresponding events. Further, due the heterogeneous nature of the upper crust and hard-rock environments hosting most ore bodies, using an accurate and reliable 3D

geological model, VSP, tomography and well-logging information will be important to map out the fine detail. Regardless of these methods, the iron-rich intrusive package from the 2D modelling experiment is identifiable compared to the host rocks.

To look at the reliability of the seismic method assuming noise is present, 25% Gaussian noise was added, resulting in noisy data. Such noise levels were evident in our real seismic data from Hillside (Tertyshnikov, 2014, Urosevic, 2017), but it is not as evenly spread as in the synthetic tests. Figure 4.15 is an example of the resulting seismogram with 25% Gaussian noise. There is a considerable difference when compared to the noise free seismogram in Figure 4.8. Some migrated images with 25% Gaussian noise are displayed in Figure 4.16. The images from the noisy data are slightly blurred; however, the contact between the eastern granite and that of the metasediment package as well as the instructive structure are largely recovered.

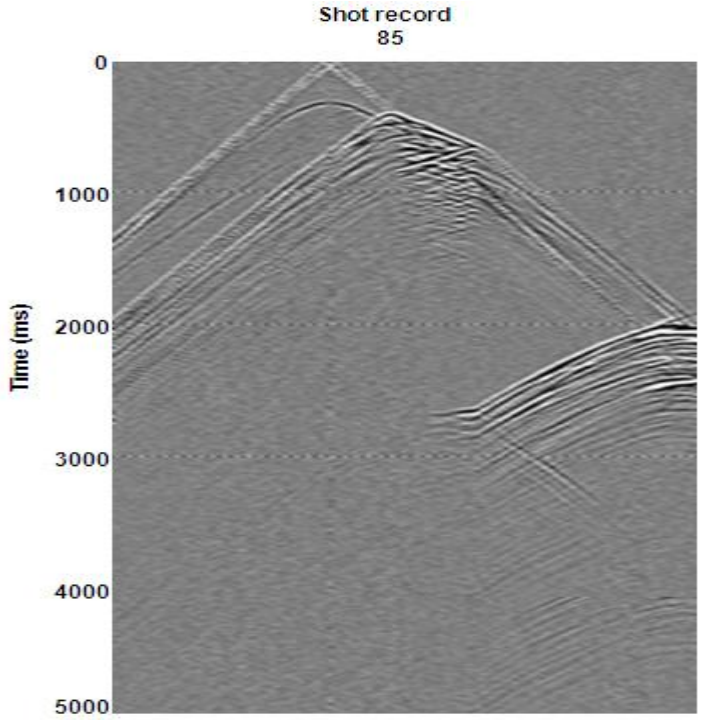

Figure 4.15: Synthetic shot records with 25% Gaussian noise. Recorded from 0–5000 ms but reflections events are visible up to 3000 ms.

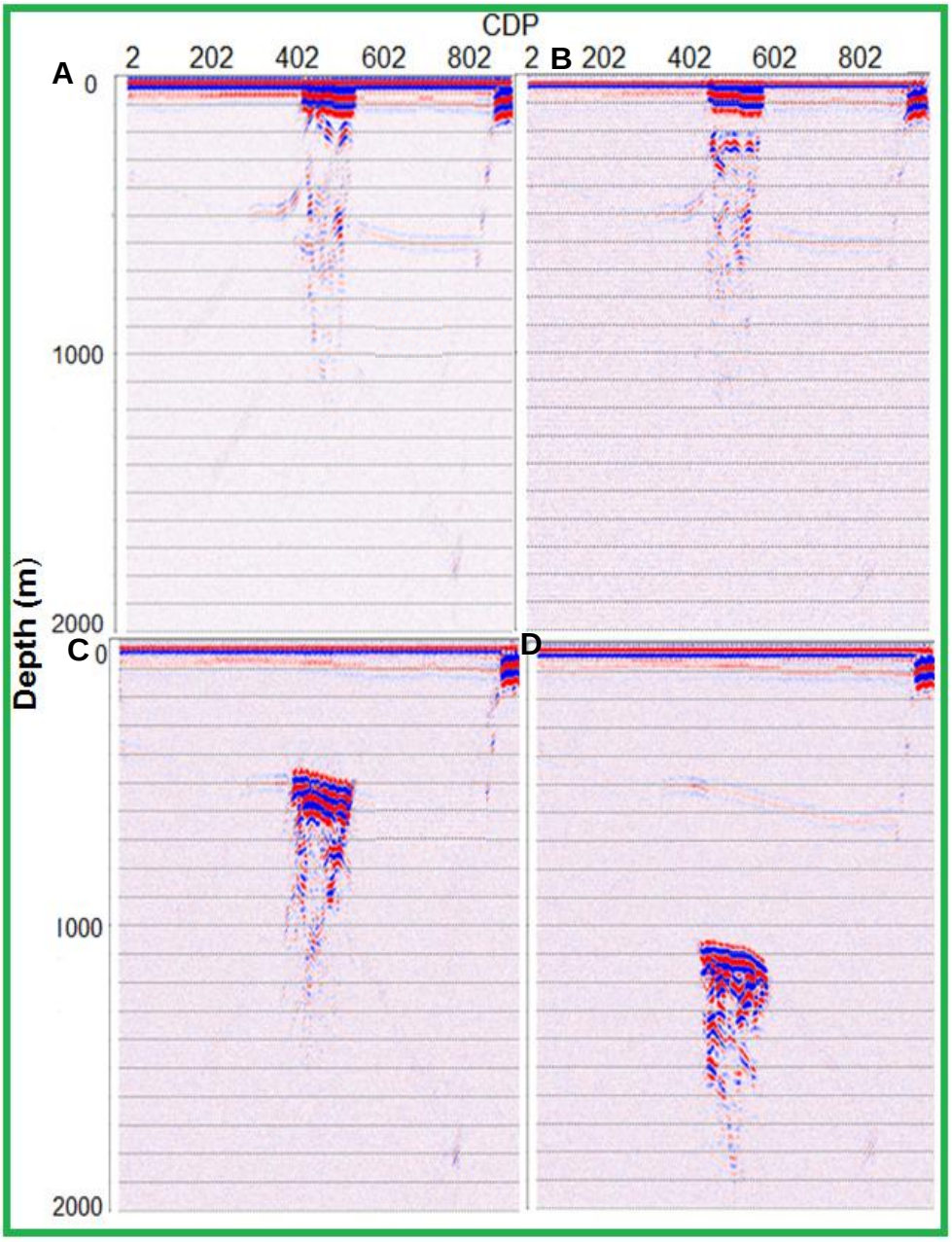

Figure 4.16 Depth migrated sections with 25% random noise at different depth covers tested with different survey parameters: A) 100 m cover, B) 250 m, C) cover 500 m cover D) 1000 m cover. As expected, layers within the sediments are slightly blurred and, in some cases, completely absent while reflection within the intrusive structure is very visible.

Comparing magnetic responses in Figures 4.4 with noise free seismic responses in Figures 4.9–4.14 as well as the responses from the 25% noisy images in Figure 4.16,

it is clear that magnetic methods can only be useful for shallow investigation up to a depth of 250 m (at best) depending on the target. As the depth of the orebody increases, magnetic response becomes smeared or practically uninterpretable.

The images from the noise-free model look cleaner and the various lithological contacts within the sediments (hanging wall) are largely recovered. Reflections around the edges of intrusion are visible from all the cases considered though the individual structures within the intrusive block cannot be imaged due to the effect of scattering of energy and background heterogeneity, which produces a high degree of noise thereby concealing or overshadowing the reflections. With the addition of 25% random noise to the data, the migrated images become blurred. Particularly, reflections within the metasediments are not very visible. However, the reflections around the edges of intrusion are still very noticeable.

Overall, the results from the Hillside modelling experiment using different test parameters are encouraging. Even with the addition of 25% Gaussian noise, we can still see the presence of some of the major IOCG features, and where the intrusives overprint the reflections from the basement geological structures and the cover sediments. Worthy of mention here is that the presence of steep deep structures within the intrusive block could be inferred from the seismic data directly or indirectly by observing a "zone" of a changed reflection character. The fact that seismic resolution and detectability are largely maintained with depth gives hope that the same ore zone recognition principles can be applied for any depth range; unlike potential field methods.

The outcomes of these results support the initial proposition that seismic reflection surveys are likely to be useful in detecting the presence of IOCG mineralisation within an overall intrusive structure.

4.6 Seismic Reflection Surveys

4.6.1 Motivation

Due to high metal prices and increased difficulties in searching for shallower deposits, the exploration for and exploitation of mineral resources is expected to move to greater depths. Accordingly, seismic methods will become a more important tool to help unravel the structures hosting mineral deposits at great depth for mine planning and exploration. Seismic methods can be used to directly target mineral deposits at depth and could support exploration drilling programs by providing high-resolution images, although they are currently not widely used in the mining industry compared to potential and electromagnetic techniques.

Hillside mineralization is hosted by a highly deformed sequence of metasedimentary rocks belonging to the Moonta-Wallaroo Group, Mesoproterozoic and Hiltaba Suite granites, and gabbros. The mineralized skarn occurs along four distinct faults, part of a major structure in the area - the Pine Point Fault. Also, there are some other difficulties such as complex geology, steep dips, complex fault zones and fractures and alteration zones in the hard-rock environment of base-metal deposits. Seismic should be one of the most powerful geophysical methods to overcome most of these challenges or say to "respond" to such geological features.

4.6.2 Hillside 2D Seismic Survey

The Curtin University Deep Exploration Technologies CRC conducted a 2D seismic experiment at the REX Minerals, Hillside deposit in 2011 (Tertyshnikov, 2014, Urosevic, 2012). A 2D line, comprised of two segments approximately 1000 m long orientated west-east was acquired. The line location is shown on Figure 4.17

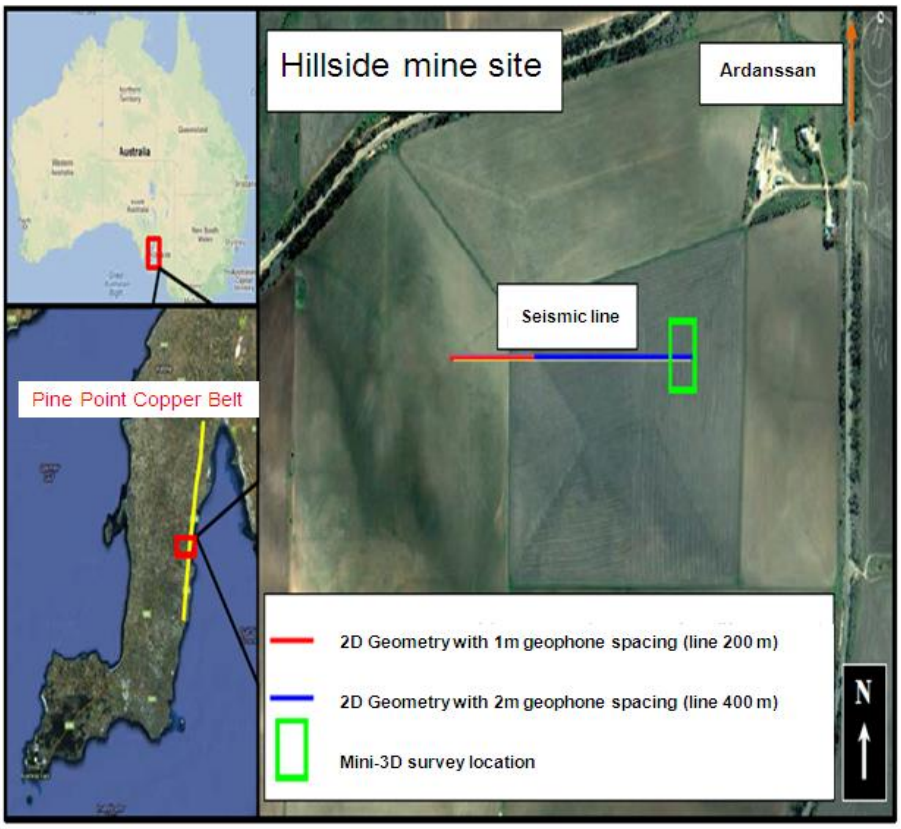

Figure 4.17 Schematic map showing the location of Hillside seismic survey lines (Adopted from Tertyshnikov, 2014). A 2D line, comprised of two segments approximately 1000 m long orientated west-east was acquired. The blue and red lines indicate the position of a 2D seismic line.

4.6.2.1 Field Equipment

The main objective of the Hillside seismic experimental survey was to test the performance of high resolution seismic methods when using a small number of active seismic channels and a portable weight-drop in a hard rock environment to image a regolith structure. Proving such a concept would enable rapid and inexpensive surveys which could allow for its widespread application for exploration of certain type of mineral deposits by using dynamic seismic acquisition systems such as land streamers or 'dragable' geophone arrays. Different seismic data analysis techniques were analysed such as reflection, refraction and surface wave analysis.

The 48-channel seismic system EX-6 with 10 Hz geophones was used to collect data. This distributed system consists of several acquisition units, each of them collecting 6 channels of data. A 45 kg accelerated weight drop was assembled on a trolley and used as a source of seismic waves. This source was easily moved by two people and was suitable for a highly repeatable shooting (Figure 4.18). The Wireless Triggering Box (WTB) and piezoelectric sensor attached to a force spreading plate were used to synchronise shooting and recording. Table 4.1 shows the acquisition parameters used for the 2D seismic surveys acquired at Hillside mine site.

.

Figure 4.18 Field Equipment used for the 2D seismic survey at the Hillside mine. Distributed seismic array (above panel, 300 ch) and weight drop (below panel).

Two short 2D seismic lines were acquired along the same traverse with an overlap of approximately 50 m. The first 200 meters (Line 1) geophone spacing was 1 m. Distance between shots was 2 m. Each spread had 48 channels; the offset was 24 m from the first and the last geophone of the spread. Shots were fired through the spread and the spread was then moved by 24 channels. For the next 400 meters (Line 2) geophone spacing was 2 m; shot increment was 4 m (Figure 4.19). Same shooting pattern was implemented. The record length was 2 seconds; sample rate 0.5 ms. Three shots were stacked at each source position. Table 4.3 summarises the acquisition parameters used for the 2D seismic surveys acquired at Hillside mine site. The quality of acquired data was reasonably good for processing and interpretation (Figure 4.20). Still the most prominent events on the seismograms correspond to surface and refraction waves.

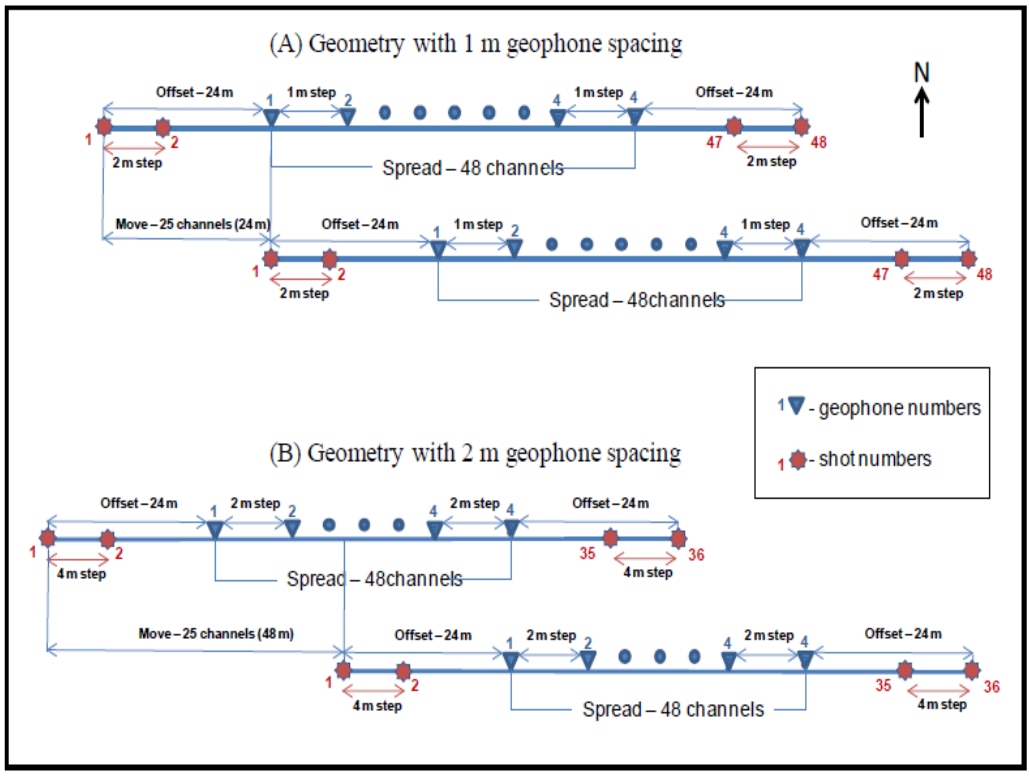

Figure 4.19: 2D Survey geometries. (A) Geometry of Line 1 (1 m geophone spacing); (B) Geometry of Line 2 (2 m geophone spacing)

Source	45 kg accelerated weight drop
No of Line geometry	2
Line 1 geophone spacing	1m
Shot spacing	2m
Offset	24m
Spread	48 channels
Line 2 geophone spacing	2m
Shot spacing	4
Offset	24
Spread	48 channels
Record length	2s
Sample rate	0.5ms

Table 4.3 Acquisition parameters used for the 2D seismic surveys at Hillside.

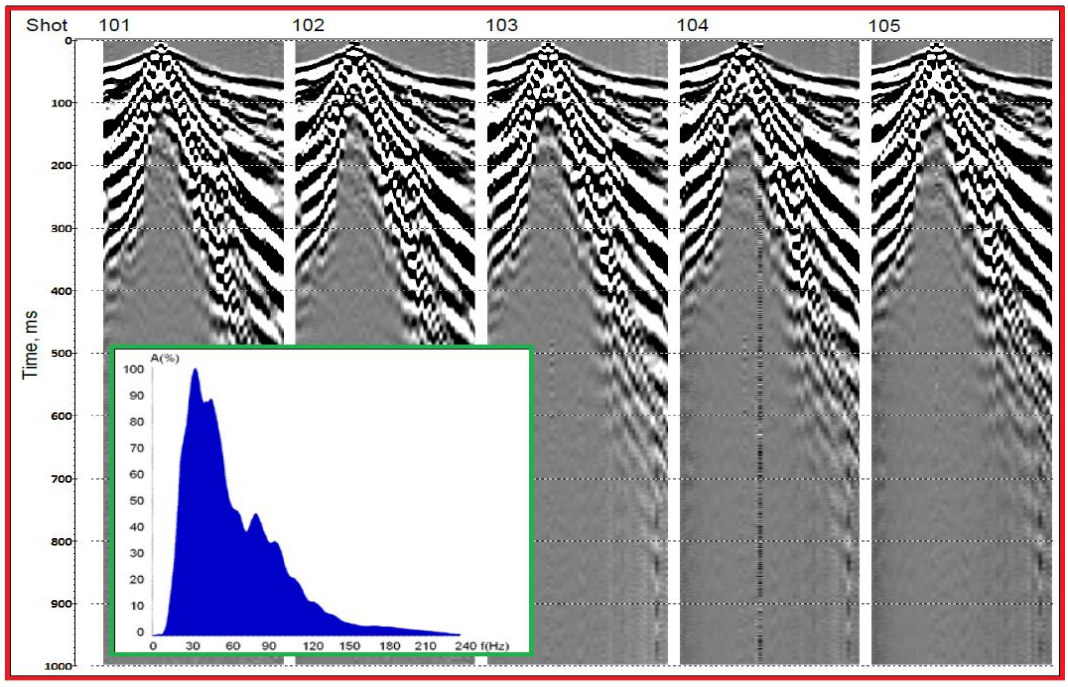

Figure 4.20 Selected 2D shot gathers of Line 1. The power spectra shown were computed for the first shot gather.

4.6.2.2 Processing and Results

In 2D seismic reflection, conventional data processing as well as pre-processing, refraction static corrections and Dip Move-Out (DMO) processing was applied in order to prepare the CMP gathers. After stacking the CMP gathers, the sections were migrated both with stacking and tomography velocities. Promax software was used

to process the reflection data. Surface wave noise attenuation, predictive deconvolution, bandpass filtering and automatic gain control are some of the applications used in pre-processing the reflection data. After pre-processing, refraction static corrections and DMO were applied in order to prepare CMP gathers. 2D seismic sections were migrated from stack sections by using a combination of stacking and tomographic velocities (Figure 4.21).

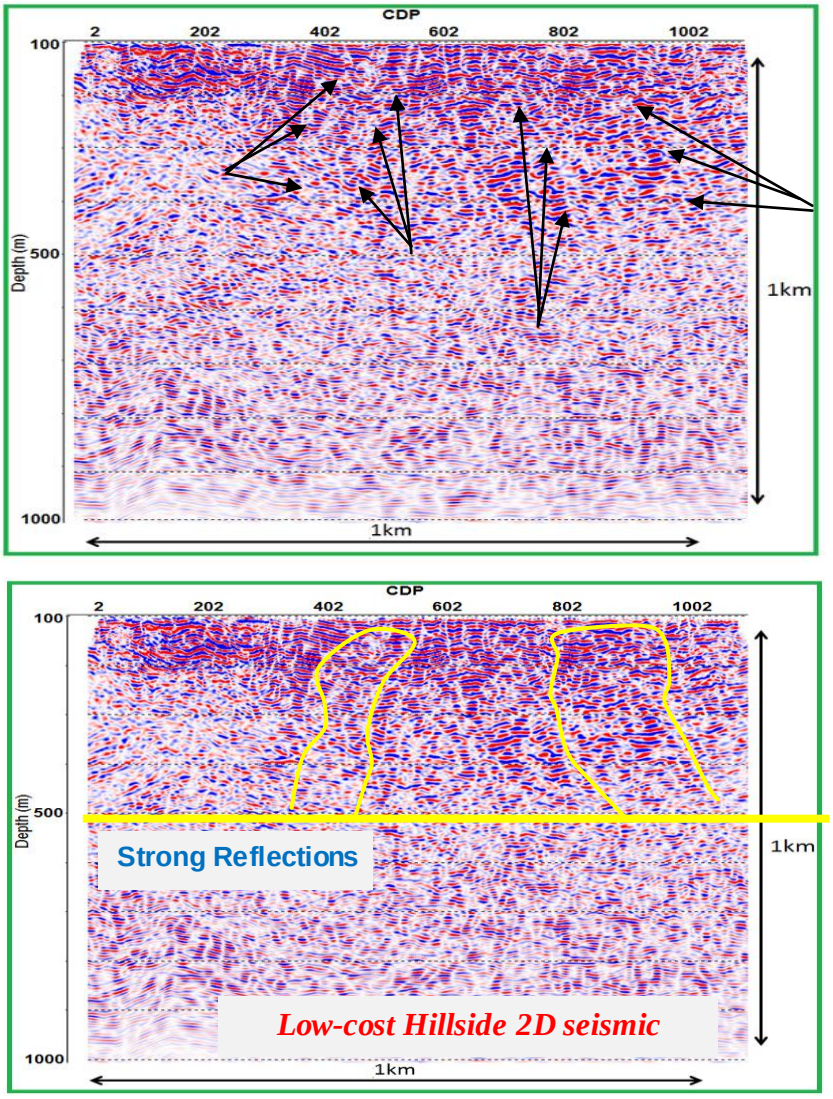

Figure 4.21 Migrated 2D seismic section converted to depth (Tertyshnikov, 2014). The presence of a steeply dipping intrusive structure (indicated by yellow lines in the bottom panel and based on the reflection termination points indicated by black arrows in the top panel) is indicated as one possible interpretation. While "disruptions" to the reflection continuity are visible, individual structures within the intrusive package cannot be resolved. The overall complexity of the seismic image is high and additional, similar alignments of event terminations can be interpreted.

4.6.3 Hillside 3D Seismic Survey

To further demonstrate the proof of concept of using integrated high-resolution surface seismic for delineating complicated structures predominant in hard-rock terrains, Curtin University conducted a 3D seismic survey at REX Minerals, Hillside mine site, between the 22nd of November and 13th of December 2012. The survey, which covered approximately a 0.85 km^2 area, was an intergral part of the DET CRC research project 3.1 "3D Seismic Exploration for Hard-Rock Environments". Hillside copper-gold mineralization areas are associated with subvertical fault zones The survey location and the fold map resulting from a simple orthogonal 3D design are shown in Figure 4.22.

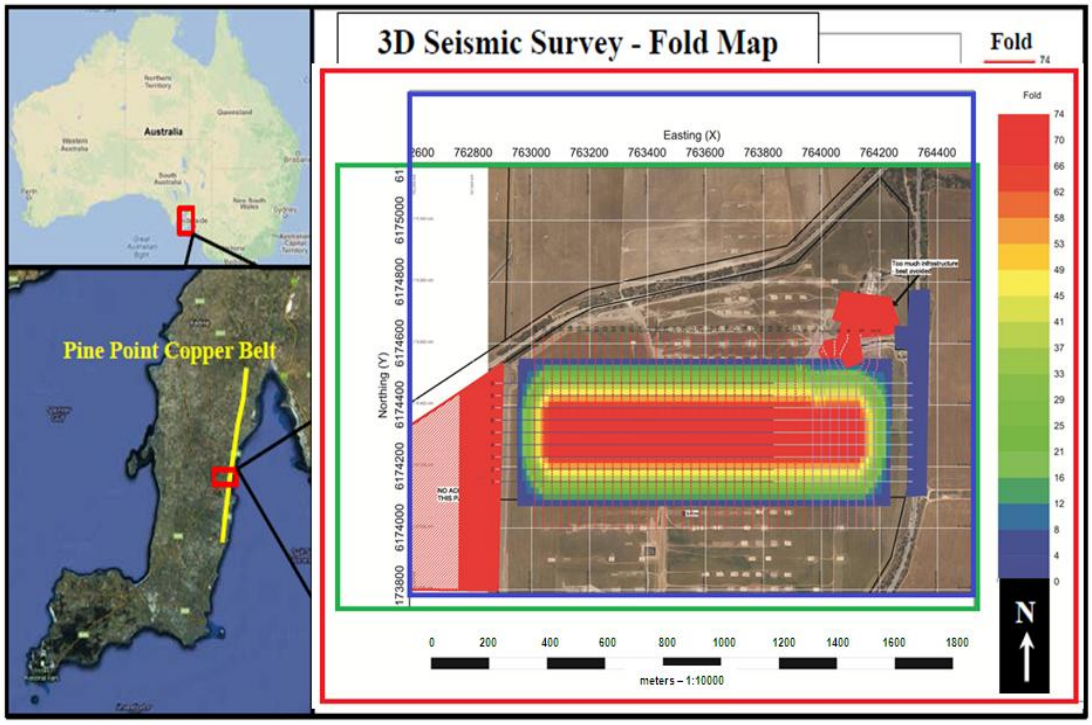

Figure 4.22 Location of the 3D seismic survey at the Hillside mine site (South Australia) and a CDP fold map of the survey. The survey covered approximately 0.85 km^2 area while the data were acquired from east to north. (Images provided by Google Earth2011).

The 3D seismic data were acquired using a modern EX-6 distributed seismic system with 864 channels and SM24 10 Hz geophones. A weight drop of about 45 kg was used as energy source while a wireless triggering box with a piezoelectric sensor was used to synchronise shooting and recording. Figure 4.23 shows the equipment used at the Hillside site.

Figure 4.23 Field equipment: A) a bobcat with an accelerated weight drop, B) solar panels. The 45 kg weight drop was used as energy source while a wireless triggering box with a piezoelectric sensor was used to synchronize shooting and recording. The solar panels was used to supply energy to the acquisition units during the survey period

The survey covered 0.85 km2 and the data were acquired from east to west. The data was collected over 10 m shots and 5 m receiver spacing for all the five patches. In each patch, there were nine receiver lines with 96 stations and eight shot lines with 64 stations. While the receiver line spacing was 30 m, shot line spacing was 40 m and the offset was 155 m. The recording length was 2 s while the sampling rate was 1 ms. the acquisition parameters of the seismic survey are listed in Table 4.4.

Source	720 kg weight drop
No of patches	5
Source points per patch	512
Source spacing	10m
Source line spacing	40m
Receiver lines per patch	9
Receiver line spacing	30m
Receiver point spacing	5m
Record length	2 s
Sample rate	2 ms
Patches overlapping	50%

Table 4.4 Acquisition parameters used for the 3D seismic surveys.

Two Navcom SF–3040 pole–mounted StarFire/RTK GNSS Survey Receiver units were used to collect GPS data with decimetre–level (~10 cm) accuracy. The units were initialised and stabilised at the base stations provided by REX Minerals Ltd on a regular basis before data acquisition. Receiver locations were pegged with a maximum tolerance of 3 cm and shot locations were stacked with a tolerance of 10 cm. The communication between the handheld GPS and the GPS rover was maintained.

Bluetooth Navcom Fieldgenius Survey software was used on the handheld to log GPS data and the data was downloaded on a laptop computer using Microsoft Active Sync 4.5. A 720 kg F9 Hurricane accelerated weight drop was assembled on a bobcat and used as a source of seismic waves while 20 solar panels were used to supply

necessary energy to the survey equipment. A Wireless Optical Triggering Box (WTB) and piezoelectric sensor attached to a force spreading plate were used to synchronise shooting and recording. The length of the record was 2 seconds; sample rate was 2 ms

The processing of the acquired 3D seismic dataset was focused on overcoming the regolith heterogeneities and increasing signal to noise ratio. To compensate travel times through the low velocity weathered regolith overburden the refraction static corrections and residual reflection static were applied to the seismic volume. The following processing procedures were used to address noise issues: amplitude compensations, single-channel and 2D filtering. DMO corrections and F-X deconvolution preceded post-stack migration.

4.6.3.2 Results

The geology at the Hillside camp is highly complex, and to reveal geological structures and delineate mineralization zones, interpretable inline and crossline reflection sections were produced with conventional data processing of the seismic data (Hossain, 2016). The migrated cube was converted to depth using a 95% reduction of the stacking velocities. Figure 4.24 shows the intersection of inline 6174300 and a crossline 763600. Several moderately strong but patchy reflections can be observed within the two zones indicated by yellow solid lines in Figure 4.24. These zones were interpreted jointly with my colleague Dr Mohamad Hussein by following the “lines” or terminations of the reflected events. This is still one of the several possible interpretations. The ambiguity is to some extent caused by the amplitude non-preserving processing which is performed to enhance structural elements. Additional uncertainties are related to the subjectivity inherited in the process of geological interpretation of un-calibrated seismic images (Urosevic, 2018, personal communication).

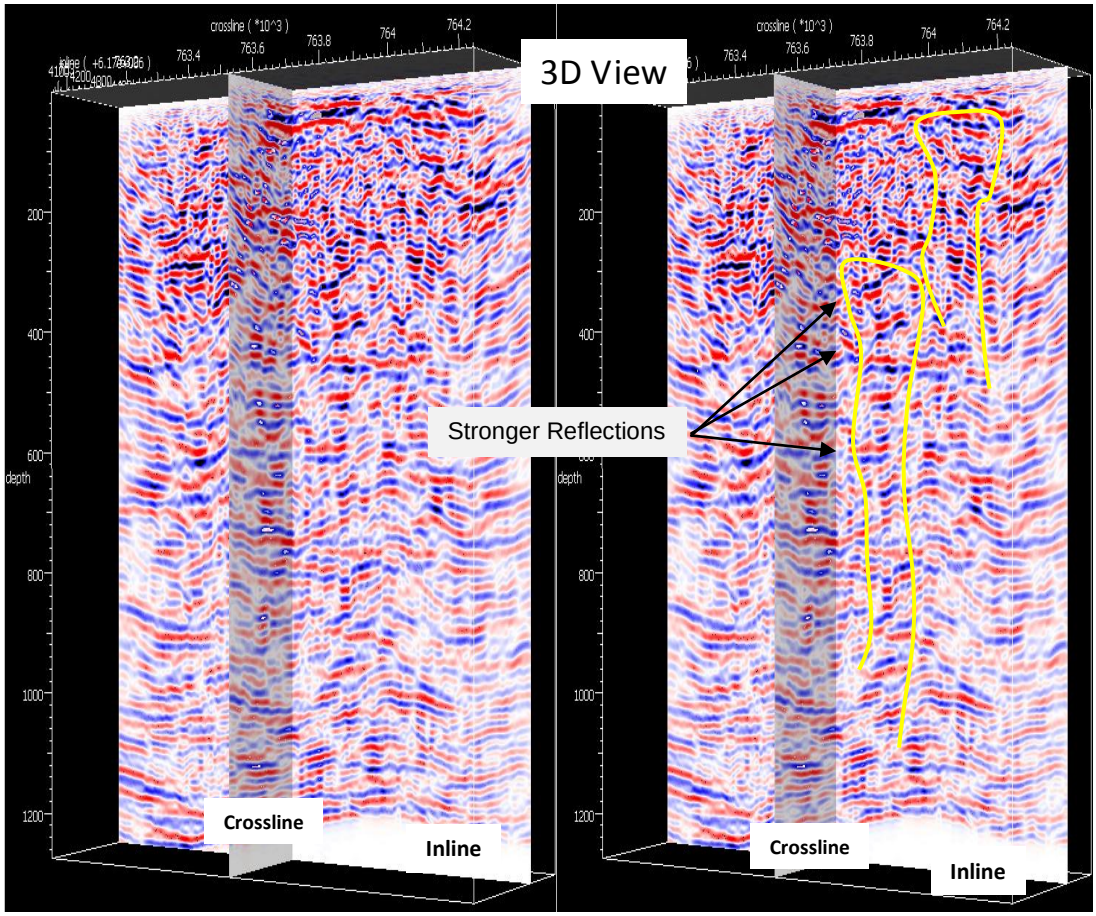

Figure 4.24 3D view from GoCAD of an inline section 6174400 and a crossline section 763600. The interpreted borders of steeply dipping intrusive structures (indicated by the yellow lines in the right panel, provided with the help of Dr Mohammad Hossain) are interpreted by tracing successive terminations of different seismic events. Several moderately strong reflection events can be seen within the regions denoted by the yellow lines.

4.7. Real data versus simulated data

The simulated 2D data acquired over 1 km length by 500m depth is shown in Figure 4.25 and will be used to compare both the 2D and 3D real data in Figures 4.21 and 4.24. Comparison of the modelled and real data is further investigated in Figures 4.26 and 4.27.

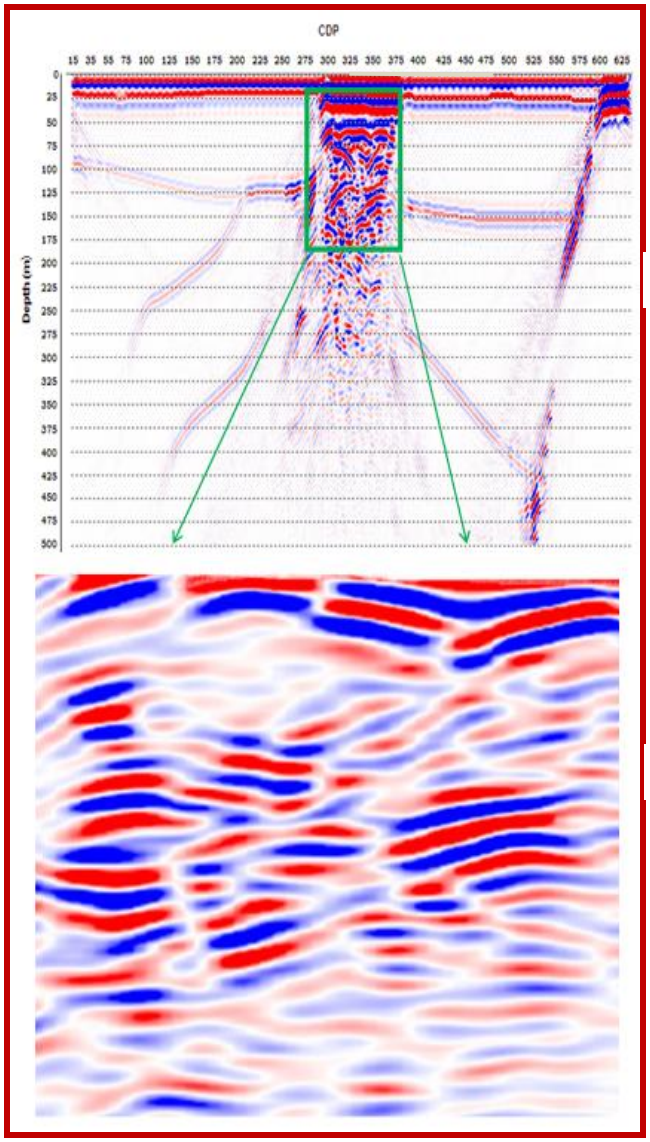

Figure 4.25 a) Noise-free depth-migrated sections for 100 m cover with 2 m source and 2 m receiver spacing's and b) an expanded section of the intrusive structure within the green rectangle.

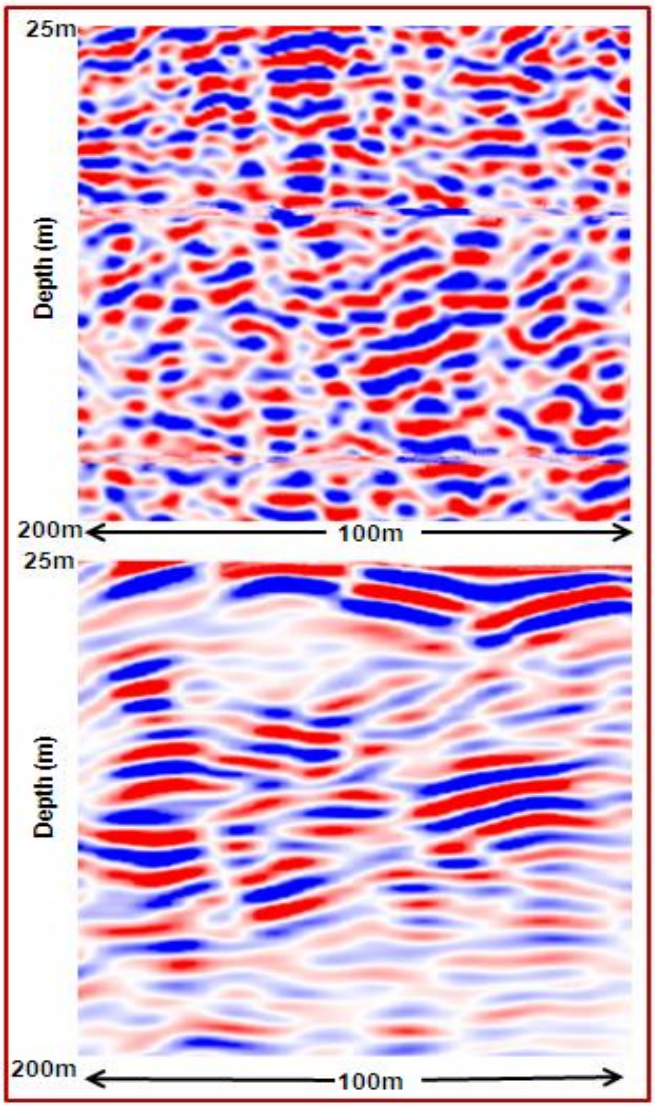

Figure 4.26 Field and synthetic seismic data: a) an expanded section extracted from the 2D field data acquired at the Hillside mine site and b) an expanded section from the noise-free synthetic data. The difference in the amplitudes are expected but may have been amplified by a multiple application of short window AGC used in the real data processing.

.

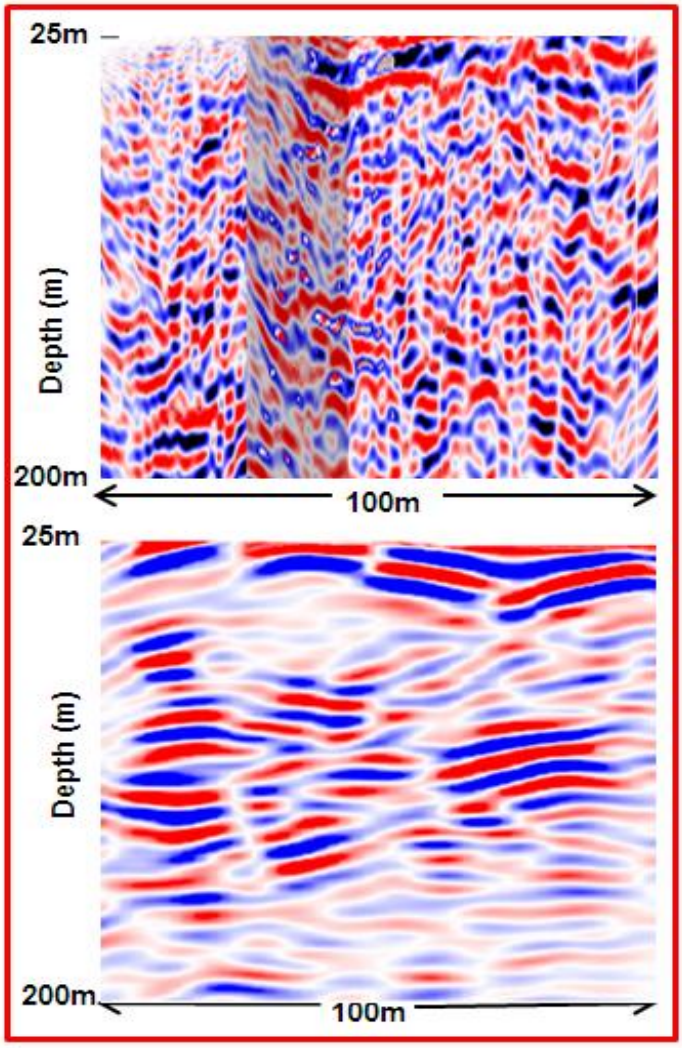

(a)

(b)

Figure 4.27 3D field and 2D synthetic data: a) 3D cube from inline section 6174300 and cross-section 763600 and b) corresponding segment of a section from the noise-free synthetic model. Both 3D data and 2D data have similar resolution. With respect to 2D seismic, the imaging of the deeper targets was improved in 3D data. It can be observed that there is a small difference in the amplitudes inside and outside the outline anomaly in 3D migrated image when compared to the synthetic image.

4.8. Seismic superposed on Geological model magnetic section

Figure 4.28 shows the superposition of a geological interpretation of the Hillside mine based on borehole data and the migrated section of the simulated data. Small discrepancies between the geology especially (hanging and footwall) and seismic may be due to steeply dipping nature. Weak reflections are observed between siltstone/meta psammo-pelites and carbonate/metasediment contacts as predicted from the petrophysical measurement. Strong reflections comes from the intrusive block and are associated with series of highly deformed gabbro and granite, hence becomes very easy to image with seismic reflection methods because of their geometry, cutting through existing rocks in sheet-like surfaces. The nature of the contacts within intrusive package is however more complex and therefore cannot be image individually. This perhaps maybe related to the way successive lavas were erupted.

Overall, superposition of simulated seismic data on geology and magnetic in Hillside mine site has given new insights into the nature of seismic reflectivity. Clearly, lithological contacts are the main source of the observed seismic reflectivity. Due to their high acoustic impedance against host rocks, granitic and gabbroic intrusions flows remain potential candidates to generated strong reflections. This implies that direct detection of mineriased zones is possible.

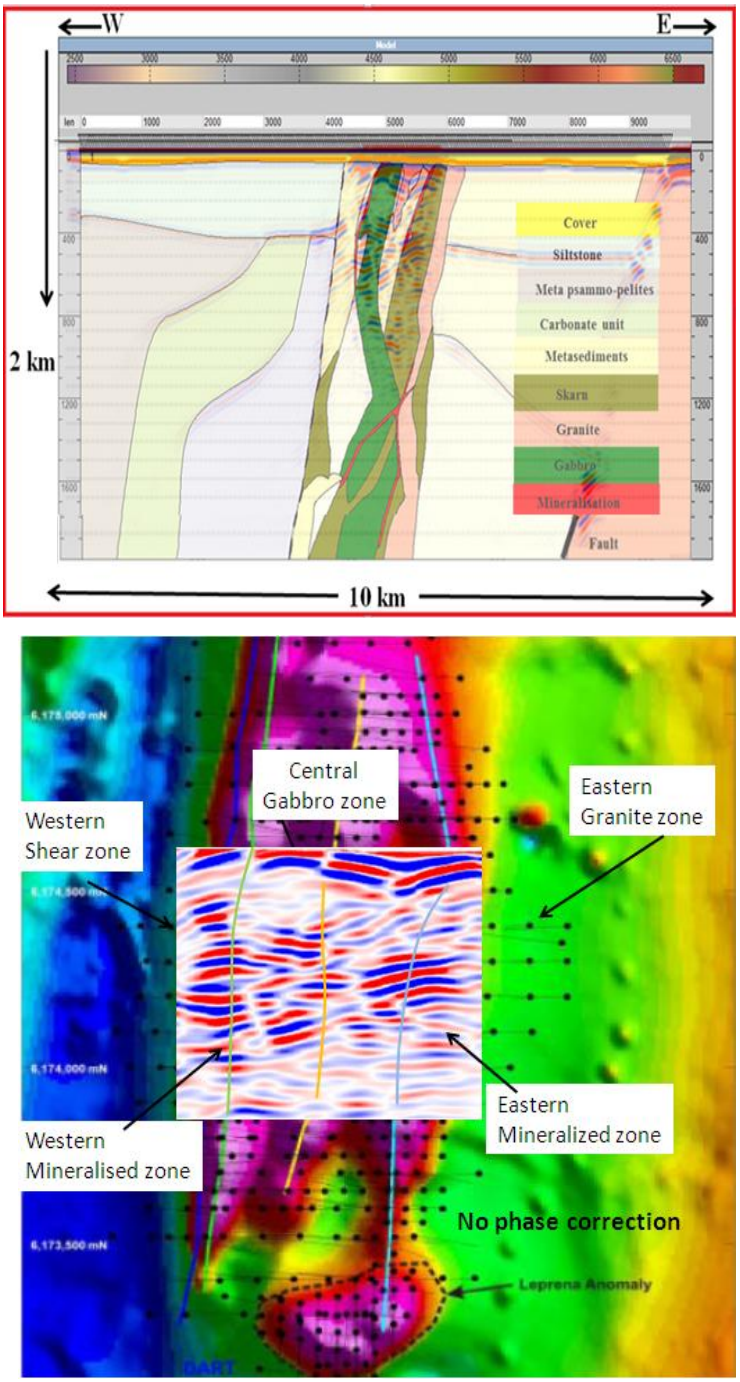

Figure 4.28 A) migrated seismic images converted to depth and superposed on the geological model derived from the geological cross-section interpreted from borehole measurements and B) magnetic section with a segment from the synthetic line overlaid. Both the migrated section and the geological model correlate fairly well. Good agreement between reflection seismic and geology suggest high potential of the application of seismic methods for exploration at this site.

4.9 Conclusion

From the forward modelling experiment at Hillside, it appears that the seismic reflection method could be used for detecting the possible presence of copper-gold deposits related to intrusives at the mine-to-regional scale. This is not the case for the magnetic method as the resolution decreases or practically absent as the depth to the orebody increases. The real data does not entirely test the initial hypothesis because neither the 2D nor 3D survey clearly indicates the presence of the Hillside intrusive package.

In the real seismic data there is little difference in the scattered and reflected amplitudes within and outside the orebody zone in 2D and 3D migrated images when compared to the synthetic image. However, the real seismic surveys never ventured properly off the intrusive structures that host the Hillside deposit; hence, there was no difference in the reflection character. The synthetic model lacks of many internal structures outside the intrusive package as this is a defining characteristic of the proposed means to detect an IOCG deposit, that is, the detection of changes/overprinting due to the mineralisation process. Also, the 3D data should have better resolution when compared to the simulated image due to the efficiency of 3D imaging in complex environments as well as some differences in dominant frequency and the acquisition parameters used. Though similar acquisition geometry was used for mine scale and real data, however, even with the sparser acquisition parameter (regional scale), it was feasible to map the different layers and intrusive contact between the complex structures and the cover sediments thus demonstrating its cost effectiveness, as 2D surveys tend to be easier to mobilise and run than 3D surveys.

While 2D surveys could be used to locate the structures hosting deposits, it may not be enough to warrant drilling based upon seismic alone, by potential investors. Drilling campaigns based on 2D seismic surveys pose a risk as it is very common to image out-of-the-plane structures, especially in a region with very complex geology,

such as Hillside, where the structures hosting the deposit are almost vertical (Malehmir, et al., 2010). 3D seismic remains the best approach for detailed and concise delineation of known ore deposits as well as targeting nearby prospects. The methods, apart from the huge potential of improving seismic resolution, also have the capability in constraining seismic interpretations, as well as allowing for the prediction of rock composition (Bohlen, et al., 2003; Snyder, et al., 2008). Even sparse 2D reflection surveys may generate targets and help increase the confidence in drill placement. This could also be used as an alternative exploration approach with shallower IOCG deposits like Hillside.

5 Olympic Dam Modelling Experiment

5.1 Introduction

Following the discovery of the Olympic Dam copper deposit in 1975, the entire Gawler Province has undergone intense scrutiny in search of similar deposits. The discovery is indeed legendary in the history of Australian mineral exploration as it was found using a conceptual exploration model initially designed for sediment-hosted strata-bound Cu deposits and was interpreted to be variety of sediment-hosted mineralisation (Roberts and Hudson, 1983). The deposit is unique and significant to this study because it serves as a reference point in the search for similar deposits across the globe. Further, two regional seismic lines were conducted across the Gawler Craton in 2003 by Geoscience Australia with one of the lines, EW (03GA-OD1) just south of Olympic Dam. This seismic data set is available for comparison to modelled responses.

5.2 Location and Geology

The Olympic Dam ore deposit (Figure 5.1) is situated approximately 520 km NNW of Adelaide and 275 km NNW of Port Augusta, South Australia (30° 26' 24"S, 136° 53' 22"E) within the mature Stuart Shelf geological province of the currently preserved Gawler Craton (Parker, 1993). The deposit is covered with younger flat lying sedimentary rocks (about 350 m) comprising limestone, quartz, shale and conglomerate. At the basement of these cover rocks is the undeformed and unmetamorphosed Roxby Down Granite (RDG). A large oval-shaped breccia complex developed within the RDG where the orebody is hosted. The breccia complex is an elongated zone approximately 1.5 km wide and about 5 km long and is loosely zoned from the granite breccia on the periphery of the deposit (Figure 5.2).

.

The outward area of the breccia complex compares to the limits of the Olympic Dam breccia complex (ODBC), where a deeper magnetite-carbonate-chlorite-pyrite±chalcopyrite zone marks the transition to the magnetite-K feldspar±actinolite±carbonate package (Ehrig, 2013). The breccia complex is associated with Roxby Downs granite (Creaser and Cooper, 1993). This Roxby

Downs granite in collaboration with the Gawler Range Volcanics (GRV), constitutes the Gawler large igneous province (Flint, 1993; Direen and Lyons, 2007). The upper part and RDG is said to be significantly altered during meso–to–neoproterozoic, after which the sedimentary rocks were deposited. The ODBC is believed to have been intruded by various ultramafic, mafic and felsic dykes with irregular shapes (Reynold, 2000). They are less than one meter at the top of the deposit but become thicker at depth.

Alteration assemblages within the deposit are dominated by a sericite-hematite ±chlorite ± quartz ± siderite with subordinate magnetite paragentically earlier than hematitie-phyllosilicate alteration and concentrated in deeper parts of the system (Reynolds, 2000). Hydrothermal alteration like the brecciation event, appear polycyclic in nature, but zonation patterns could be developed within the deposit and around individual breccia zones. Within the fractured granite occur weak sericite- and Fe-metasomatism, but become highly intense towards breccia zone, where sericite, hematite, chlorite and epidote become dominant. Towards the centre of the breccia bodies hematite is more visible; thus, the iron rich minerals overprint all other styles of alteration (Reynolds, 2000). The chlorite-siderite alteration becomes more visible at depth and on the peripheries of the deposit and seems to be associated with magnetite-dominated alteration and chalcopyrite mineralisation (Reynolds, 2000).

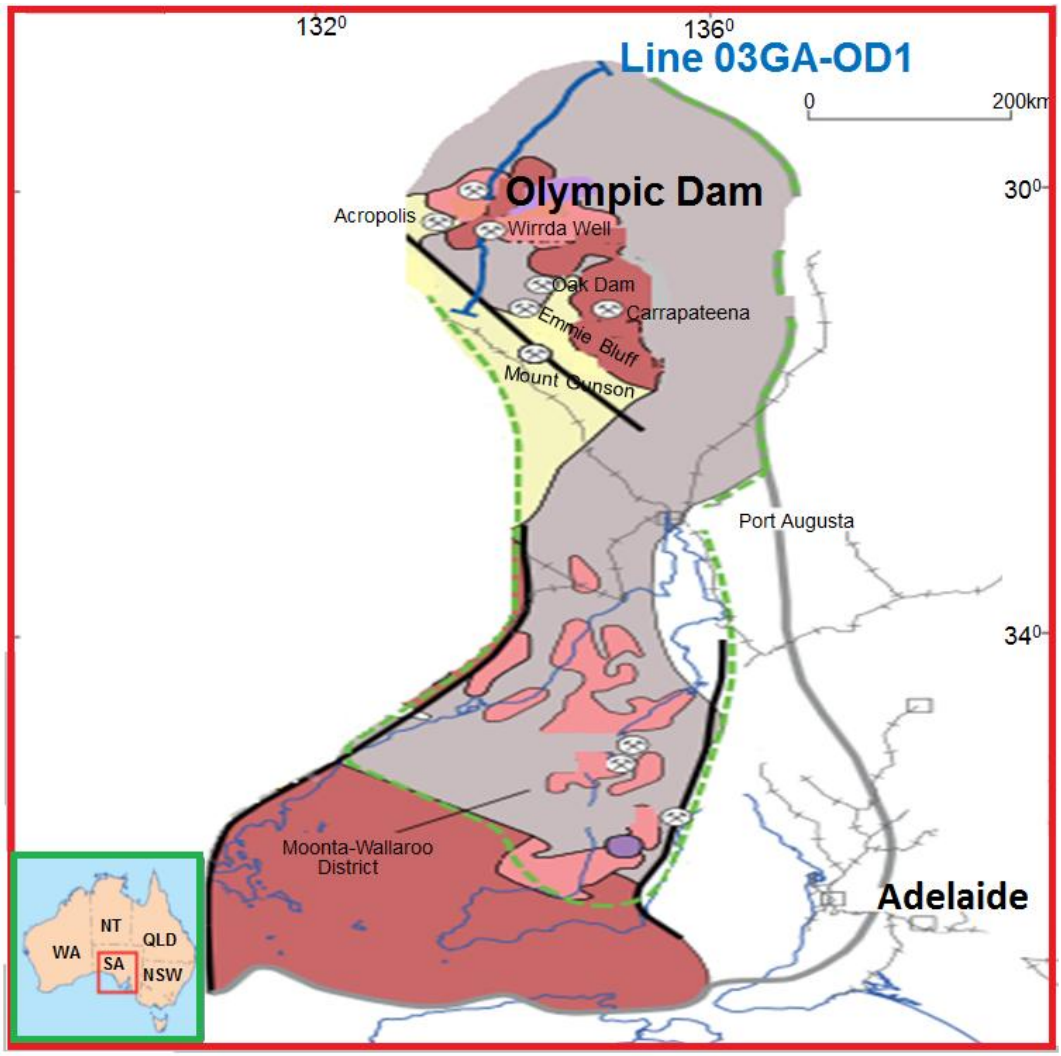

Figure 5.1 Location of the Olympic Dam copper deposit with seismic line 03GA-OD1 shown (modified from Hayward and Skirrow, 2010). The deposit is cover with younger flat lying sedimentary rocks (about 350 m in thickness) comprised of limestone, quartz, shale and conglomerate.

Mineralisation is characterised by a hydrothermal hematite-quartz rich breccia that looks dyke-like in appearance and up to 100 m wide (Oreskes and Einaudi, 1990; and Reeve, et al., 1990). Strongest mineralisation at the outer barren core compares well with the best-developed hematite-granite breccias and lower margins of the ODBC zone mappable (Reeve, et al., 1990; Reynolds, 2000; Ehrig, 2013). Over the upper margin, sulphides become scarce while little copper mineralisation is seen within the vicinity of hematitic breccias. In the lower margin, a very fast transition to chalcopyrite, with lesser copper grade, and which corresponds to an increase in the

pyrite: chalcopyrite ratio is observed (Reeve, et al., 1990; Reynolds, 2000; Ehrig, 2013). A broad anomaly was detected in the gravity data over the Olympic Dam. The actual extent of the mineralised zone extent and internal structures remained unresolved. This is where seismic could provide some addition value. Previously, seismic surveys have not been conducted because seismic cannot be used to map sub-vertical structures such as often found in an IOCG system. However, seismic method can be used to map steep structures.

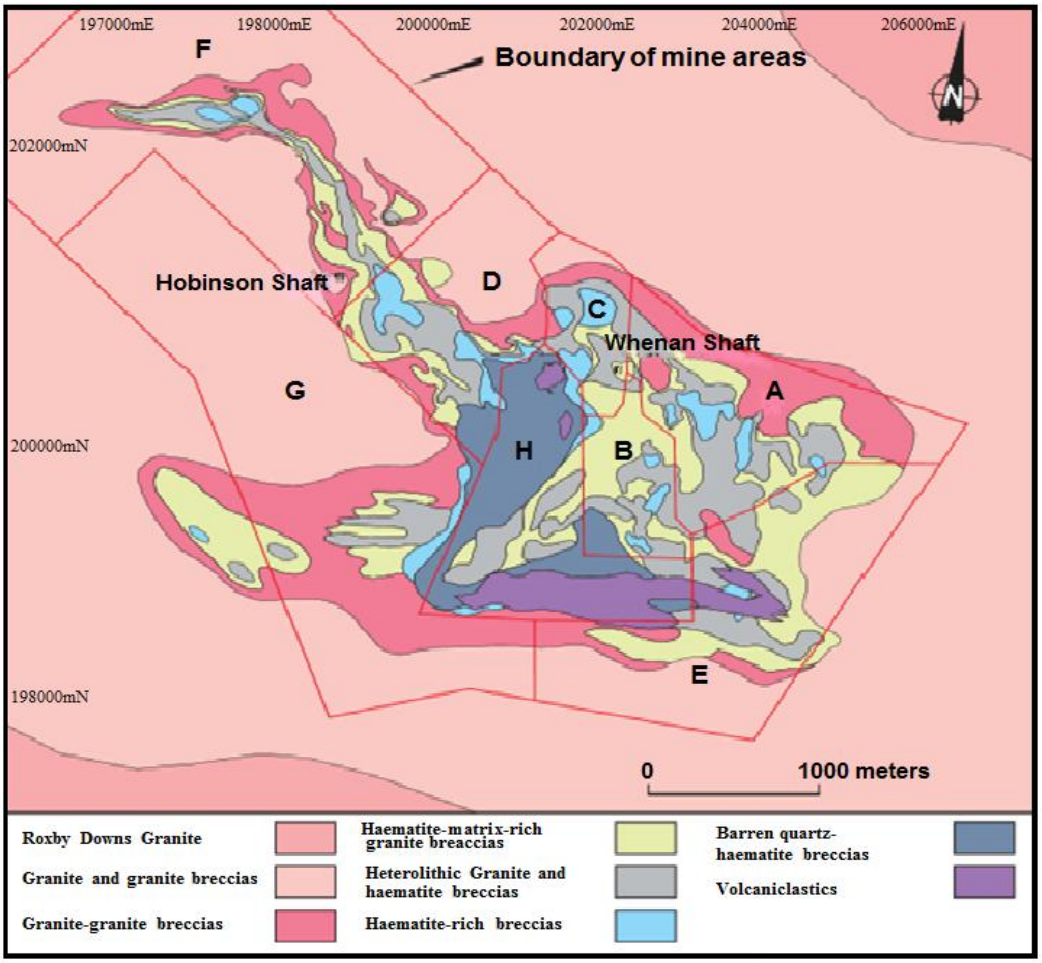

Figure 5.2 Simplified geology of the Olympic Dam Breccia Complex showing distribution of different breccias. The large zonation from the host granite at the margins of the breccia complex to progressively more hematite-rich lithologies in the centre should be noted (from Reynolds, 2000).

5.3 Modelling Experiment

Seismic modelling of the Olympic Dam IOCG deposit was carried out to investigate whether this type of IOCG deposit produces a seismic signature at the regional scale. For this purpose, models have been designed in line with the geological predictions from past seismic surveys carried out by Geoscience Australia. Three cross-sections B–D, indicating the overall distribution of main breccia units, are shown in Figure 5.3 with cross-section D used in seismic modelling, while Figure 5.4 shows the geological model created from cross-section D. The principal areas of interest (ODBC) were situated within the central 2 km.

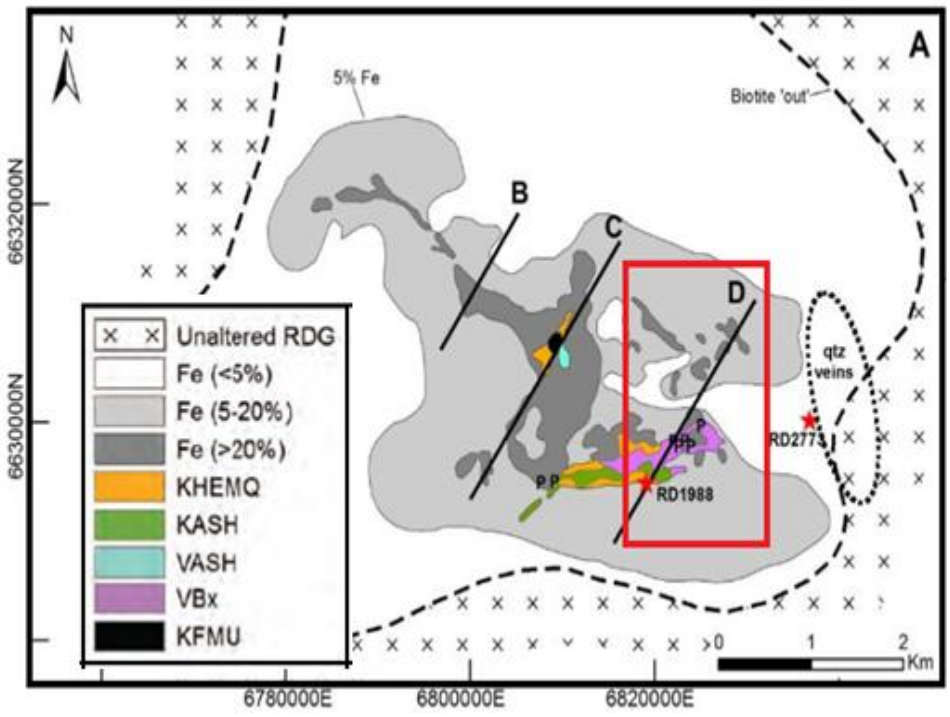

Figure 5.3 Simplified geologic map with cross sections (B-D) of the Olympic Dam Breccia Complex, showing the distribution of unaltered Roxby Downs Granite, outer limits of significant brecciation and iron metasomatism (5 wt % Fe contour), granite-rich breccias (5–20% Fe), hematite-rich breccias (>20% Fe), chlorite-bearing, laminated sandstone and mudstone (KASH), well-bedded, hematite-rich sandstone, mudstone, and conglomerate-breccia (KHEMQ), thinly laminated, very hematite-rich mudstones (VASH), polymictic volcanic conglomerate (KFMU), hematite-rich breccias consisting of porphyritic felsic volcanic clasts (VBx). The locations of drill holes with picrite lavas are labeled with "P". The stippled area shows the locations of thick quartz veins. Section (D) in rectangle is used for modelling (reproduced from Ehrig, 2013).

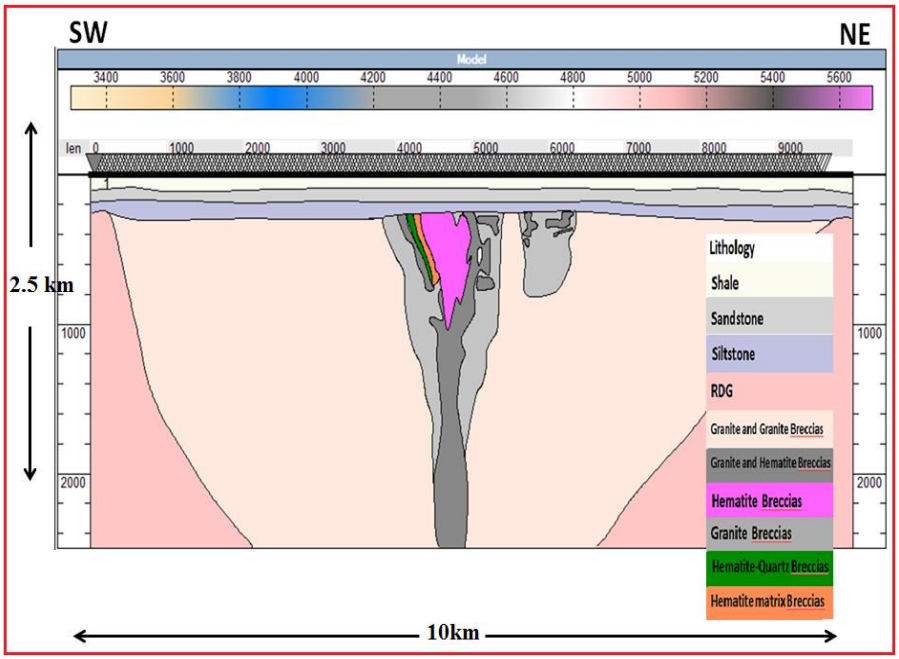

Figure 5.4 2D synthetic geology model of the Olympic Dam based on cross-section D in Figure 5.3. The depth cover was increased to 750 m and 1000 m (adapted and simplified from Ehrig, et al., 2013).

5.4 Survey design, Modelling and Processing of Synthetic Data

The synthetic survey for the Olympic Dam case study was designed with similar parameters to the 2003 Gawler Craton seismic survey conducted by Geoscience Australia. Synthetic seismograms were subjected to the full processing flow including filtering, NMO corrections, stacking and migration as shown in Figure 4.7.

Split-spread survey geometry was used with the source at the middle of the spread while four different survey parameters were used for this experimental numerical modelling test. A total of 1000 geophones at 10 m intervals and 500 geophones at 20 m intervals were placed along the model in the first and second case. For the sources, 480 and 240 synthetic shots with 20 and 40 m interval were placed at the surface over 10 km of the model. An impulse Ricker source wavelet with a centre frequency of 35 Hz was used to generate synthetic shot records (correlated records from a Vibrator source). In the third and fourth cases, synthetic data were collected over

120 and 100 source shots, modelled at 80 and 100 m intervals respectively across the entire model maintaining the same source positioning (rolling split-spread) and dominant source frequency (35 Hz) Ricker wavelet. Receivers were spaced at 40 and 50 m respectively. The objective was to find out the minimum level of sparsity of seismic data that could give rise to a positive seismic response over the Olympic Dam system. Acquisition parameters and velocity-density used for Olympic Dam are shown in table 5.1 and 5.2 respectively.

Acquisition parameters				
Parameter	Case1	Case2	Case 3	Case 4
Source depth (m)	0	0	0	0
Receivers depth (m)	0	0	0	0
Shot interval (m)	20	40	80	100
Receivers spacing (m)	10	20	40	50
Centre frequency (Hz)	35	35	35	35
Number of shots (no)	480	240	120	100
Record length (s)	2	2	2	2
Sampling rate (ms)	0.1	0.1	0.1	0.1

Table 5.1 Acquisition parameters used for Olympic Dam synthetic modelling

#	ROCK Type	Vp (m/s)	Density (Kg/m^3)
a	Shale	3310	2243
b	Sandstone	3425	2618
c.	Siltstone	3620	2572
d.	Roxby Dawn Granite (RDG)	5074	2905
e.	Granite and Granite Breccia (GGB)	4850	2810
f.	Granite and Hematite Breccias (GHB)	5365	2756
g.	Hematite Breccias (HB)	5626	3510
h.	Granite Breccias (GB)	4665	2930
i.	Hematite-Quantize Breccias (HQB)	5475	3912
j.	Hematite mineralisation	4992	4310

Table 5.2 Velocity-Density table for the Olympic Dam synthetic geology model; These assigned values are based on personal verbal communication with my supervisor. Also, there are many gravity models of this deposit with density published.

Petrophysical data used for Olympic Dam, Vulcan and Mount Gunson copper-gold modelling are based on personal verbal communication with my supervisor, (who was privy to Olympic Dam rock property data as a geophysicist with Western Mining Corporation Resources Limited (WMC)), and with HiSeis Pty Ltd, who have collected some core measurements on Olympic Dam and Vulcan prospect core. These data are not in the public domain due to commercial confidentiality issues and I was not provided with any actual measurements, instead guided to use "reasonable" values. However, these values appear to be relatively accurate as the results from the models matched well with real seismic data plus they correspond well to other published physical properties of similar rocks. The synthetic seismic records generated were then used to determine if an expected geologic target would produce interpretable signatures.

5.5 Results and Discussion

For the Olympic Dam modelling experiment, the reflection coefficient is equal or greater than 0.06 so as to produce a strong reflection at different layers/lithological units. The minimum velocity is 3310 m/s with a frequency of 35 Hz; hence, the wavelength is 96 m long. Thus, the minimum theoretical resolvable vertical thickness is of the order of 24 m. In practice that would be 32 m or more. The Fresnel zone is large, close to 694 m, which is not favourable for the detection of sub-vertical bodies. This was a motivation for the detailed modelling studies.

Simulated results from an Olympic Dam model with overlying cover of varying depths at 350 m, 750 m, and 1000 m and using different survey parameters are presented in this discussion. The variations are to look at whether the seismic approach would work as well at depths greater than the current Olympic Dam situation, and if we were to use wide-spaced sources and receivers would we miss an Olympic Dam style deposit at shallower depths. It thus appear that the brecciated intrusive structure hosting Olympic Dam deposit can be detected at any depth by using even sparse survey geometry.

Figure 5.5 is an example of noise-free synthetic shot records for source number 99 displayed from 0–5000 ms. Some diffraction is noticeable in the shot records; this is always the case when seismic wave comes in contact with a feature whose dimensions are comparable to or smaller than the wavelength. The shot records also contain some artefacts due to an attempt to explain the elastic data with acoustic modelling. After applying F-K filters, the diffractions and artefacts were substantially reduced.

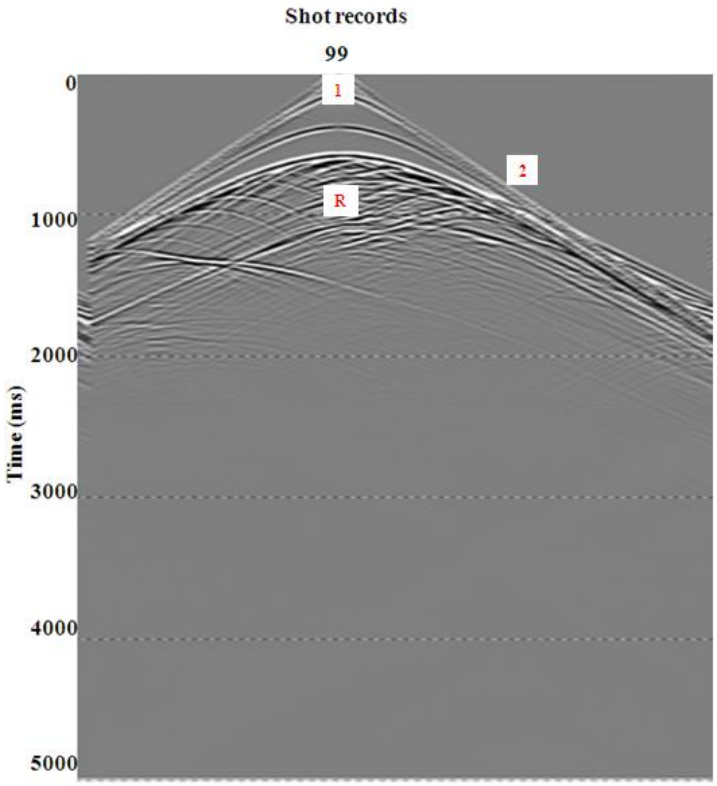

Figure 5.5 Noise-free synthetic shot records for source number 99 from the Olympic Dam breccia complex model shown in Figure 5.4 (1) direct wave, (2) refracted signals (R) reflection signals. The shots are displayed using true relative amplitude without correction for spherical divergence. Shot depth for all gathers is 0 m and they were produced using Ricker wavelet of 35 Hz.

Migrated sections tested with different survey parameters are shown in Figures 5.6–5.8. Superior results come from test parameters with 20 m source and 10 m receiver spacing as well as 40 m source and 20 m receiver spacing (Figures 5.6a and b, 5.7a

and b and 5.8a and b. The stacked amplitudes from the other test parameters decrease due to the sparse source-receivers spacing. Layers within the sediment cover have low signal-to-noise as expected due to low impedance contrast (low velocity and density was assigned to these layers).

The steeply-dipping structures of the ODBC model shown in Figure 5.4 were effectively imaged down to a depth of 1.4 km, 2000 km and 2300 km for 350 m, 750 m and 1000 m cover respectively (Figures 5.6- 5.8). Imaging of the steep dipping boundaries is not due to any special migration techniques; it is simply due to the discontinuity of reflections and diffractions arising from the breccia complex of ODBC when we move away from the deposit. Most of the geological models do not have as much complexity in the host rocks; thus, the seismic models follow these characteristics. A strong reflection between the cover sediments and the basement rock in all the parameters tested was observed as a result of high density-velocity values.

Anomalous reflectivity due to acoustic impedance change (density*velocity) across contacts between fragmentals and lavas within the large intrusive area (indicated with black arrow) is visible. This suggests that imaging various dense breccias from any geological model with appropriate petrophysical data is relatively feasible even with very sparse seismic reflection surveys (80 m source and 40 m receivers spacing).

We can also see the offset of layers, abrupt change in reflection character or layer thickness as well as low reflectivity (indicated with orange) at the base of the large intrusive area (Figure 5.6). A possible explanation for this scenario is because the base of the large intrusive area has only one structure (granite and hematite breccia) and the surrounding granite and granite breccia as shown in Figure 5.4. The Roxby Dawn Granite (RDG), granite and granite breccia host the Olympic Dam Cu-U-Au deposit, and are imaged as a region of no-reflectivity. Note that this is also the case with the real data (03GA-OD1). There is substantial difference in amplitudes

between reflections recorded from the RDG/GGB and the reflection recorded on the outer part of the mineralised zone.

Though influence of attenuation have course the energy to diminishes, seismic reflection method was still able image to a depth of 2.3 km. However, the steep near-surface reflectors could not accurately image, due to the vertical and horizontal resolution. The vertical fault and structures that is well identified in the results above is largely because the fault is imaged by its effect (displacement of reflection layers) and not necessary by reflections from it.

Effect of the 3D over the 2D approach is one of the major limitations of this modelling experiment as all features expected cannot be captured in 2D. This is because the acoustic modelling used only takes into account P-waves while in reality the earth is elastic in nature (a combination of P-waves, S-waves and surface waves). Another issue is that the wavefront propagates in 2D on a circle while in actual fact wavefront propagates spherically so that the attenuation seen on 2D is quite different from 3D. Lastly, since the modelling and processing techniques are two-dimensional, the data coming out of the plane on the 2D profiles as well as the structures will be seen on all profiles that are larger than the required window. This will have an effect on the Fresnel Zone due to contraction or reduction in one dimension but will still extend its full width perpendicular to the line.

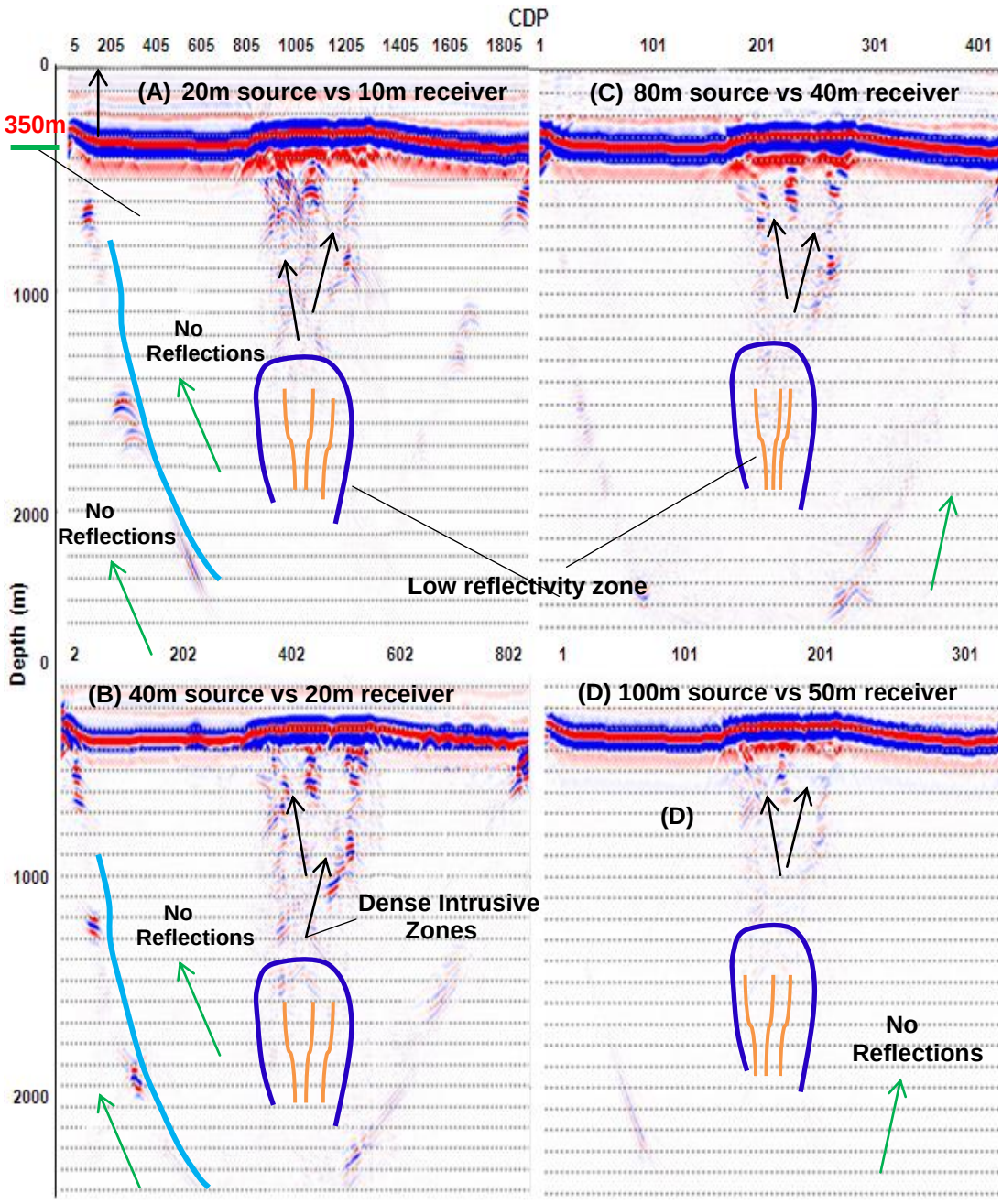

Figure 5.6 Noise-free depth-migrated sections for 350 m depth of cover tested with different survey parameters; A) 20 m source and 10 m receivers spacing, B) 40 m source and 20 m receivers spacing, C) 80 m source and 40 m receivers spacing and D) 100 m source and 50 m receivers spacing. Reflections across contacts between fragmentals and lavas within the hematite rich breccia plus clast are visible. The layers within the cover sediment have low impedance are fully recovered while the boundary between the Roxby down granite and Hematite rich breccias is partially recovered. Lack of internal structure within the unit may be a possible explanation for this partial recovery.

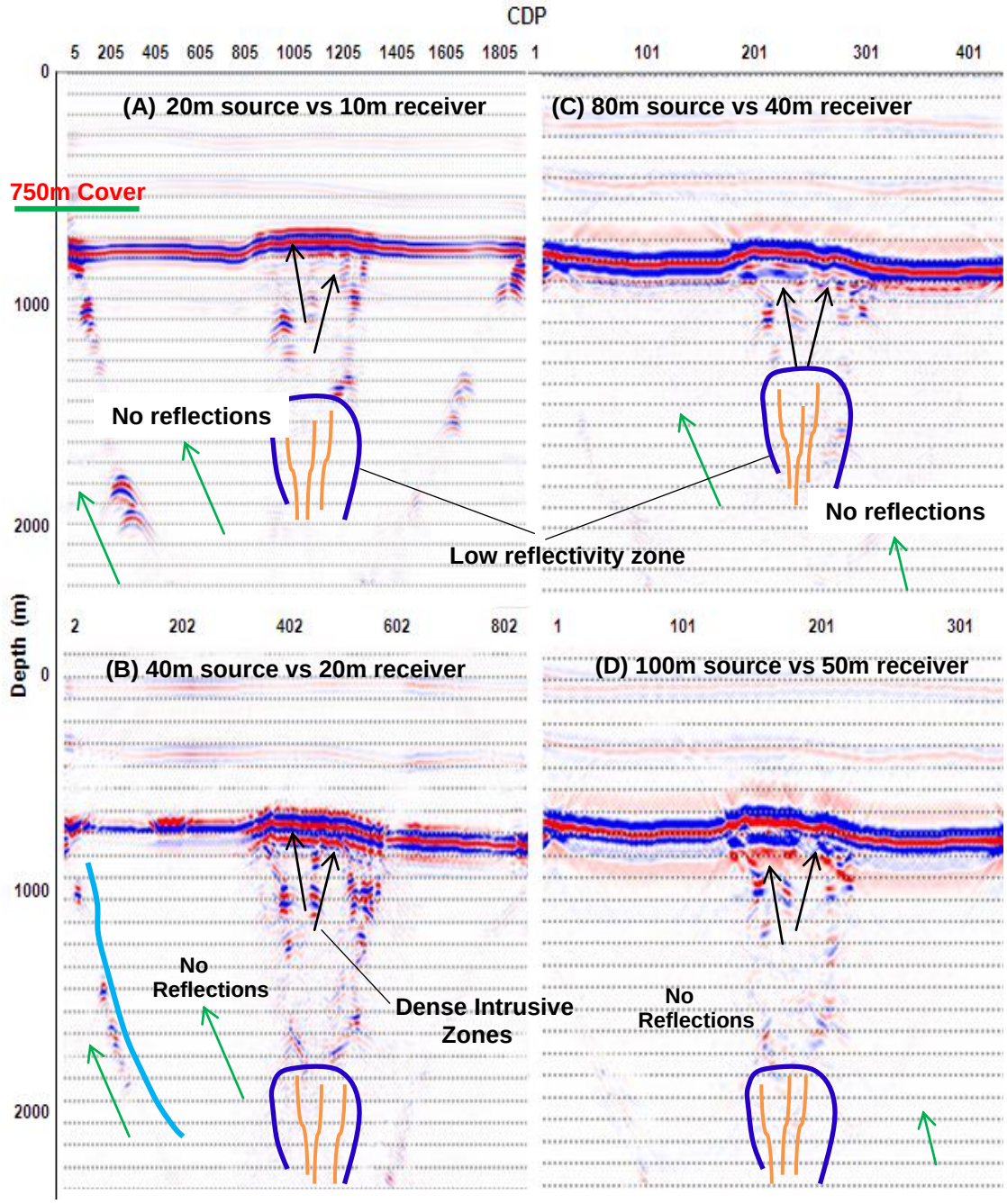

Figure 5.7 Noise-free depth-migrated sections for cover depth of 750 m tested with different survey parameters: A) 20 m source and 10 m receivers spacing, B) 40m source and 20 m receivers spacing, C) 80 m source and 40 m receivers spacing and D) 100 m source and 50 m receivers spacing. For all the test parameters, resolution is maintained with depth as we can still see the various layers and intrusive structure when the depth increases to 750 m. Layers within the sediments have low impedance contrast due to low velocity.

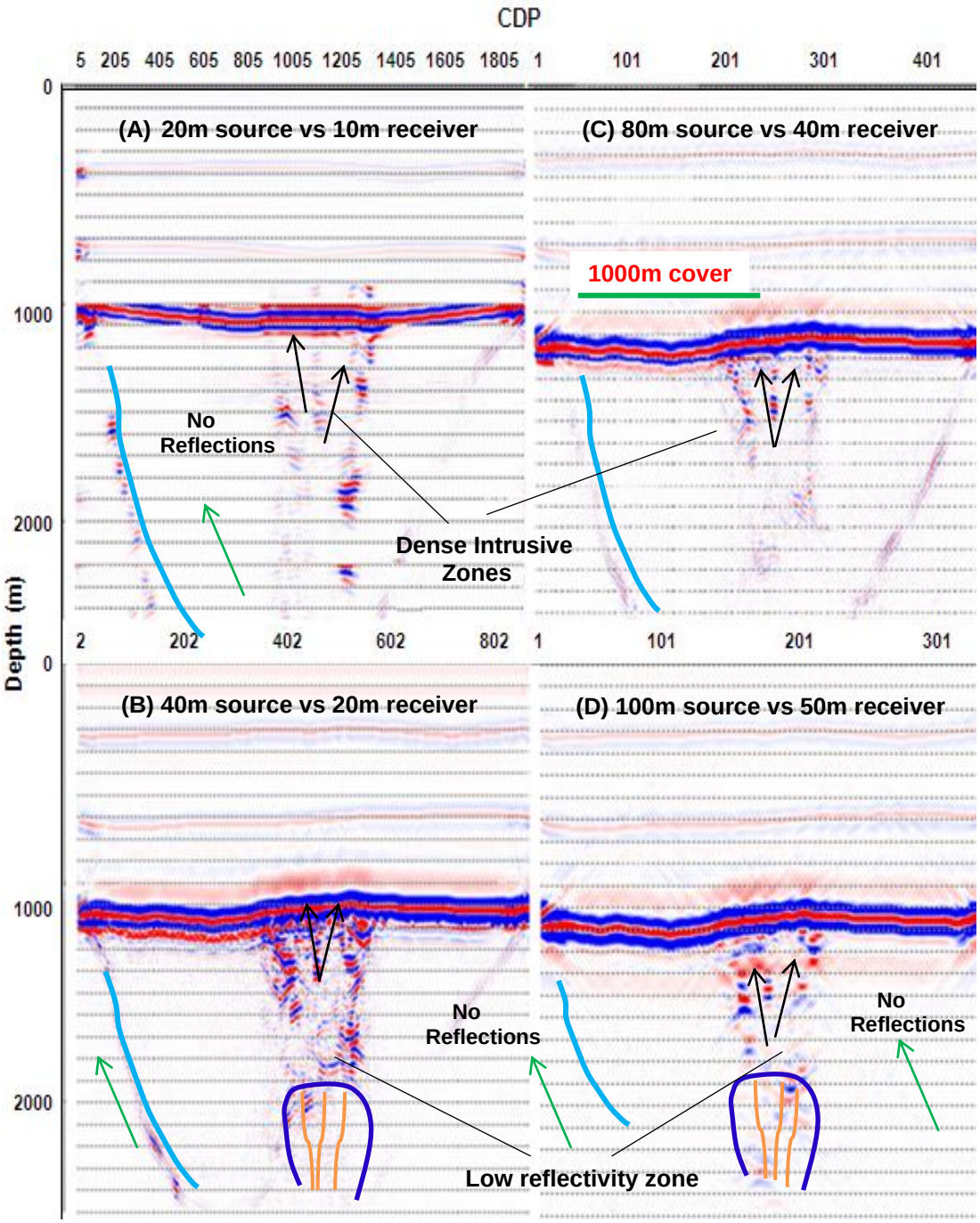

Figure 5.8 Noise-free depth-migrated sections for 1000 m thick cover tested with different survey parameters: A) 20 m source and 10 m receivers spacing, B) 40 m source and 20 m receivers spacing, C) 80 m source and 40 m receivers spacing and D) 100 m source and 50 m receivers spacing. The most striking feature of this result is that even at 1000 m cover, resolution is maintained as the both the intrusive structure and the cover sediments are fully recovered except the boundary between the Roxby dawn granite and the Hematite Rich Breccias that is partially recovered.

Gaussian noise of 25% (relative to signal on each trace – unrealistic, but no simulated noise appears to be realistic) was added to further demonstrate the suitability of the model when noise is present. The frequency band was kept same as that of the noise-free data. The resulting synthetic shot gathers with 25% Gaussian noise Figure 5.9b is compared with noise free synthetic gathers Figure 5.9a of the same shot 99.

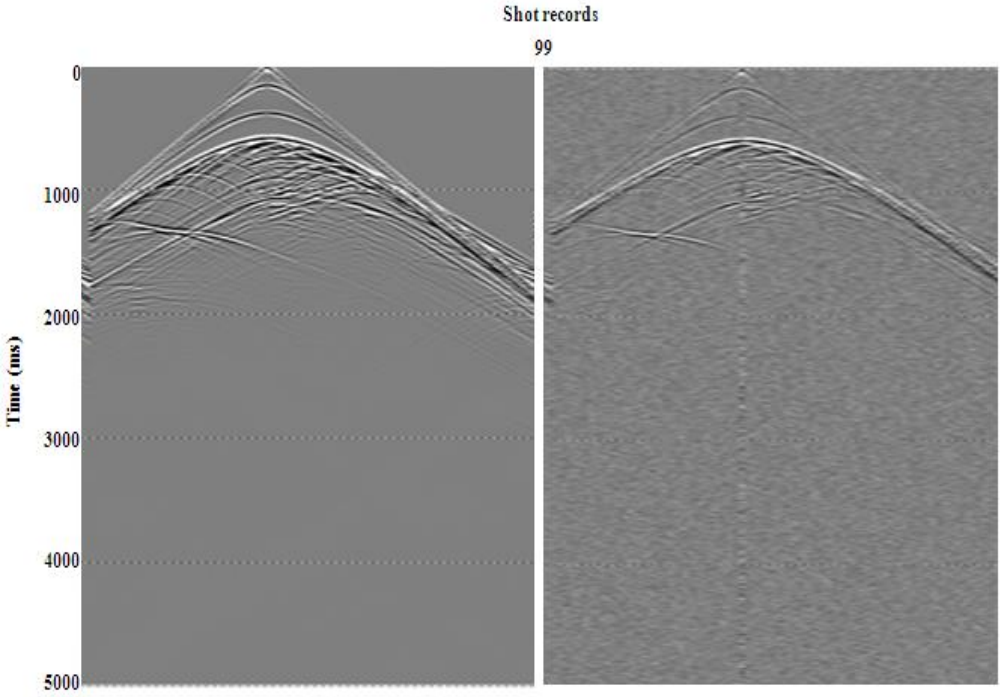

Figure 5.9 A) noise free synthetic shot B) with 25% Gaussian noise both for shot no 99. Record from 0–5000 ms

The migrated section with 25% Gaussian noise level is shown on the right panel in Figure 5.10. It shows similar change in reflection character over the ore zone, which is of course quite prominent with the noise-free migrated sections on the left panel. The presence of the ore zone is however likely to be detected by observing subtle change in the reflectivity across the ore zone. The Olympic Dam Breccia Complex (ODBC) structure was reconstructed fairly when compared to the noise free migrated section.

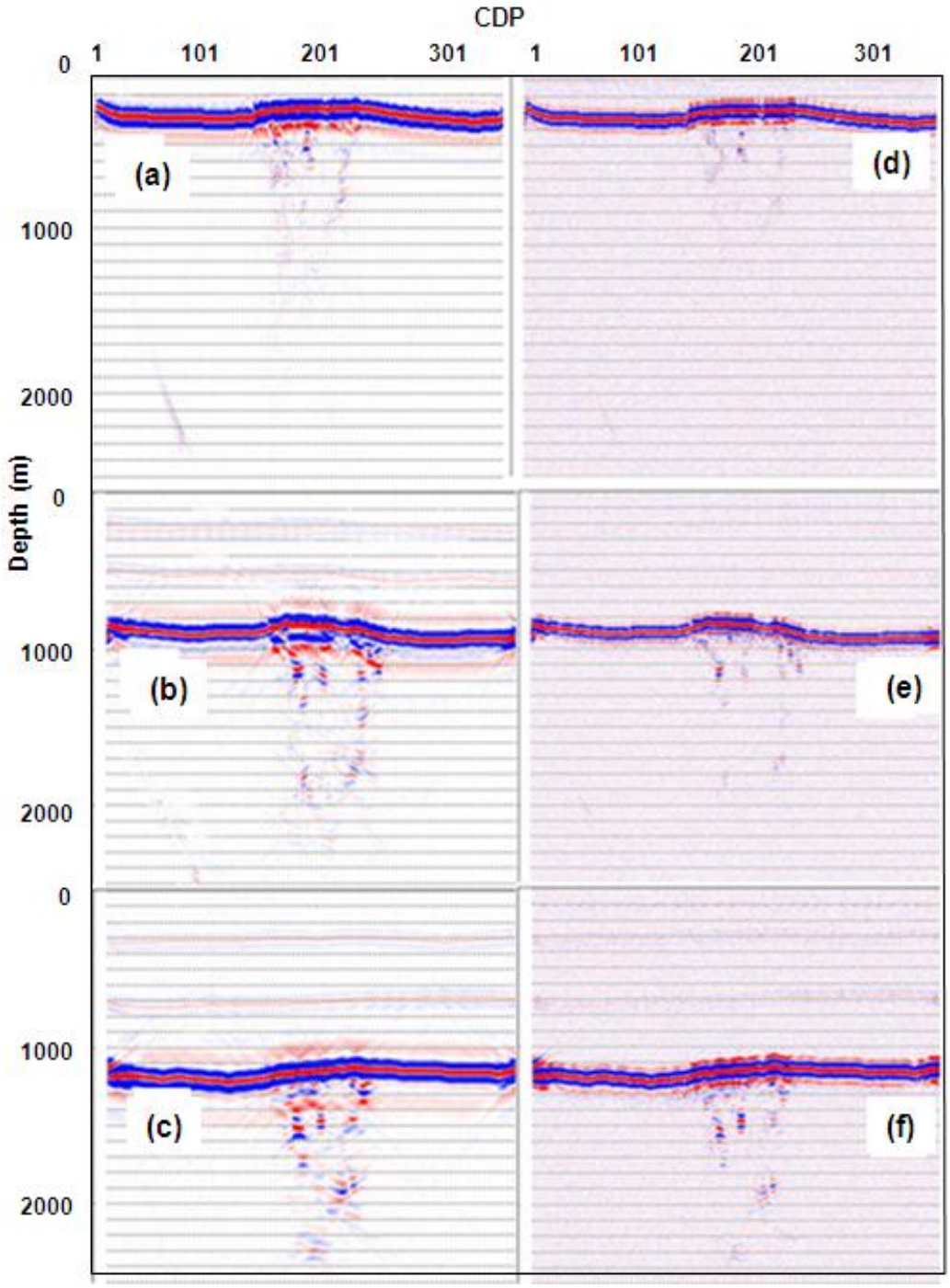

Figure 5.10 Depth migrated synthetic sections: a,b,c) are noise-free images for 350 m, 750 m and 1000 m of depth cover, respectively and d.e.f) corresponding images with 25% of Gaussian noise added. The images with 25% Gaussian noise added are slightly blurred. Still the contact between the basement rock and that of the cover sediments as well as the intrusive structure are recovered to a satisfactory extent.

5.6 Gawler Craton Seismic Surveys

The 2003 Gawler Craton Seismic Survey (L163), situated in the Roxby Downs area in South Australia consists of 2 lines. The EW line (03GA-OD1) is just south of Olympic Dam and NS line (03GAOD2) is an expanded section of Olympic Dam (Figure 5.12). The survey was conducted by Geoscience Australia with the overall goal of mapping and delineating the tectonic setting of Olympic Dam, define the IOCG deposit and provide further information on the nature of the Torrens Hinge Zone (THZ) among others (Lyons and Goleby, 2005). The seismic profile is shown in Figure 5.11.

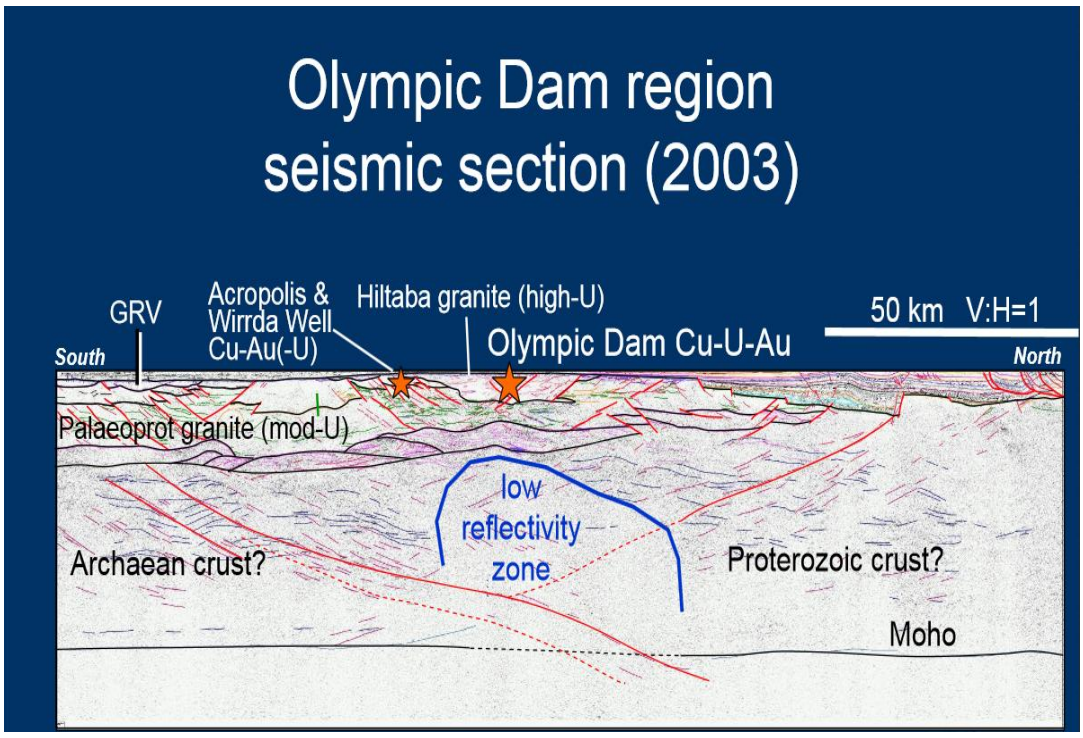

Figure 5.11 Olympic Dam seismic profile acquired and interpreted by the Geoscience Australia (From Lyons and Goleby, 2005)

The seismic reflection data were acquired along roads. Station coordinates were surveyed using differential GPS by Dynamic Satellite Surveys (2003). A split-spread geometry was used with the source nominally at the centre of the spread. Receiver groups were centred between station pegs, while the source array was centred on the peg. Three IVI Hemi-60 (60,000 lb) vibrators were used in-line; with move up between each of three various sweeps. Sweep parameters were chosen from experiments conducted at the beginning of the survey. An ARAM 24-bit 240 channel recording system was used to record and correlate the seismic data. Table 5.3 below shows the acquisition geometry used

Direction	N to S
Length	193.36km
Stations	1000-5834
CDP Range	2000-11546
Source interval	40m
Receivers interval	80m
Geophone Group pattern	12 inline @ 3.33m
Source type	3 x IVI Hemi-60
Sweep type	3 x 12 s: 7-56, 12-80 & 8-72Hz
Channels	240
Fold (Nominal)	60
Sample interval	2ms

Table 5.3: Summary of acquisition parameters for Olympic Dam regional seismic survey.

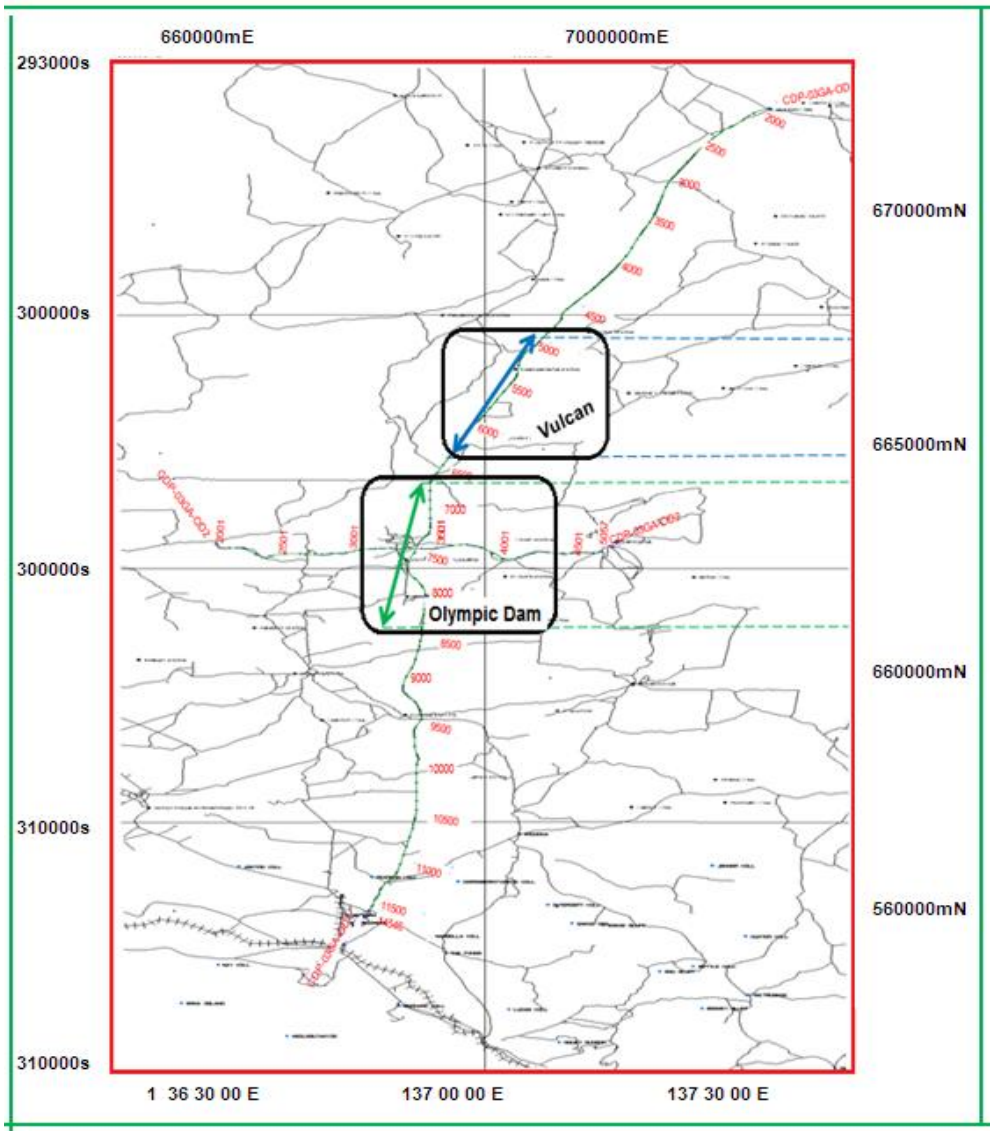

Figure 5.12 Location of the 2003 Gawler Craton deep seismic reflection traverses. The Olympic Dam geological cross-section (D) Figure 5.3 used for modelling is located within the rectangle indicated with green arrow and corresponds to CDP 6630–8350, while the Vulcan geological cross-sections (A–B) Figure 6.4 used for modelling is located within the rectangle indicated with blue arrow and corresponds to CDP 6250–5250. Both segments were extracted from a larger reprocessed seismic section for a comparative analysis with synthetic data.

5.7 Comparison of Gawler Seismic Results with Model Data and Discussion

A segment from the Gawler craton seismic field data (low-resolution regional deep crustal survey) of Olympic Dam (EW 03GA-OD1) is shown in Figure 5.13. Data are reprocessed at Curtin University (Urosevic, 2018). Figure 5.14A is the 2.5 km by 10 km section extracted from 5.13 while Figure 5.14B is the expanded section directly below projection of Olympic Dam onto the seismic line. Results from our modelling experiments using the geological model in Figure 5.4 are shown in Figure 5.15A with an expanded section shown in Figure 5.15B. The Olympic Dam geological cross-section (D) used for modelling in Figure 5.3 is located within the triangle indicated with green arrow and corresponds to CDP 6630–8350.

The Roxby down granite and granite breccia that host the Olympic Dam copper-gold deposit is imaged as a general zone of non-reflectivity**.** A close relationship between the idealised noise-free numerical data and very sparse deep crustal data may be observed. This is better seen when comparing Figures 5.14A–B with 5.15A–B. A subtle change in the reflection character in field data is seen at the edge of mineralised complex. The difference in the amplitude between the field data and simulated data is because of real data having much more complex wavelength while the geological model is a simplification, real attenuation, scattering and the fact that elastic behaviour of seismic waves is not considered in the model. The dominant frequency used for the field data is higher than the one used for the synthetic data hence, the real data has slightly higher resolution.

Ideally, for field data acquisition in hard-rock terrain, to properly capture the response from an orebody, high frequencies (up to 120 Hz) are needed because ore deposits are rather small and high frequency improves resolution. This is because the hard-rock environment itself is “hard” and is characterised with noise (random and coherent) with high potential to affect the quality of the data. However, since this is synthetic model (noise-free), we anticipate that starting with 35 Hz dominant frequency we can equally achieved our goal without loss of generality.

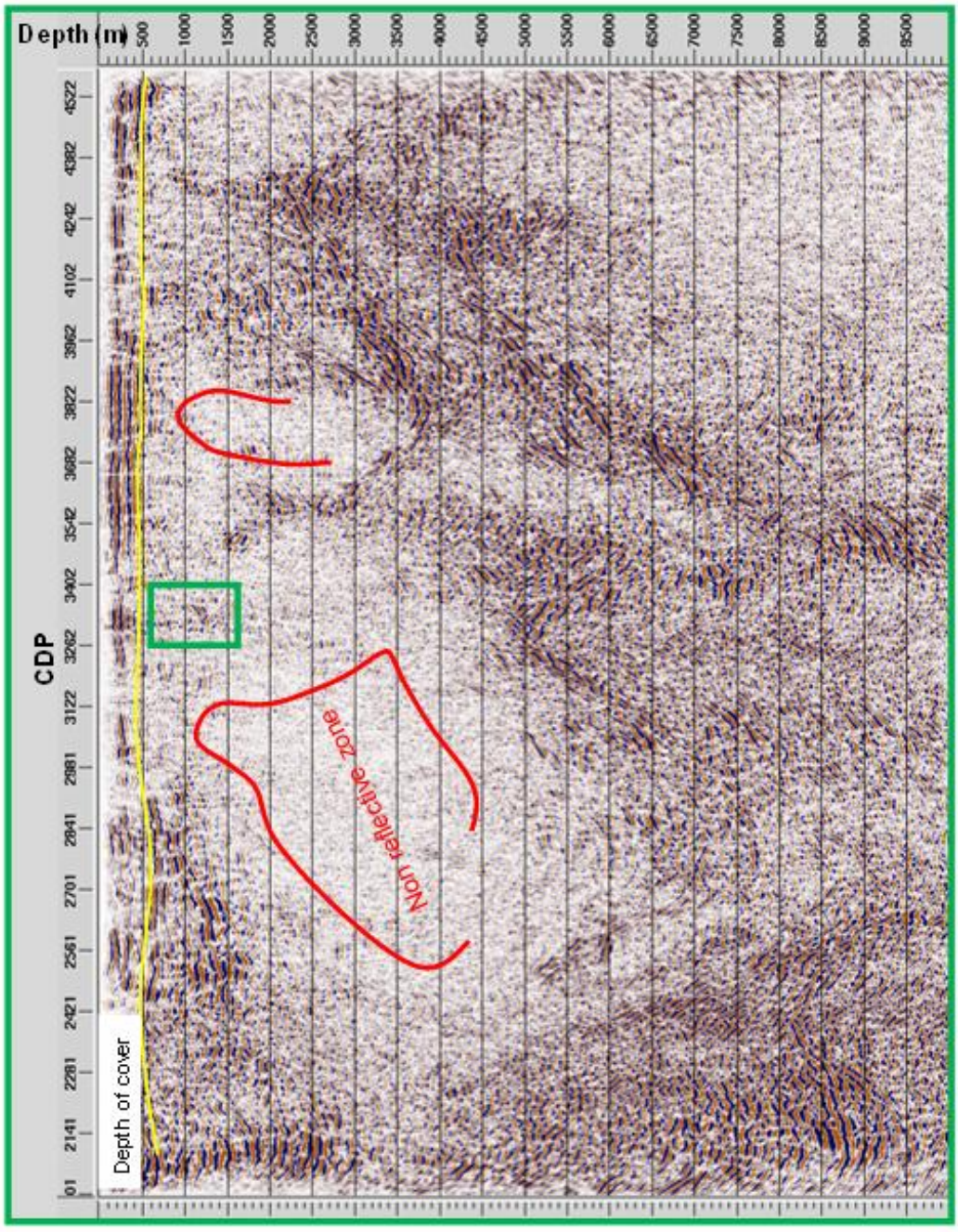

Figure 5.13 *Geoscience Australia E-W seismic line just south of Olympic Dam (preserved amplitude processing).*

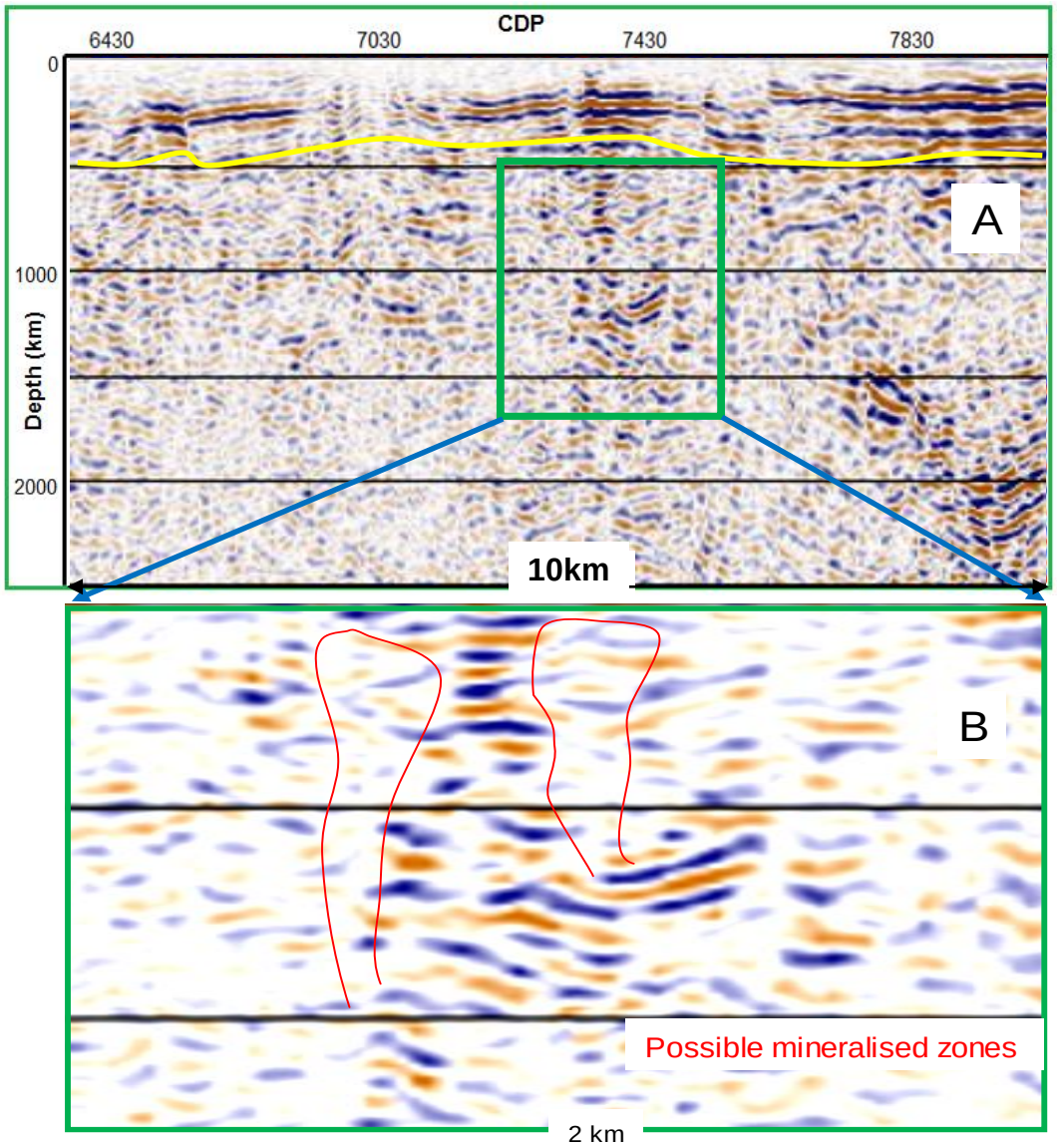

Figure 5.14 A) 2.5 km by 10 km section of EW seismic line just south of Olympic A segment of the line extracted from CDP no 6630–8350 as indicated in Figure 5.13 by the green rectangle and B) Expanded section directly below projection of Olympic Dam onto seismic line. Image is brightened to enhance non-reflective and reflective regions. The Roxby Down granite, granite and granite breccia, which hosts the Olympic Dam deposit is indicated with red as a no-reflectivity region.

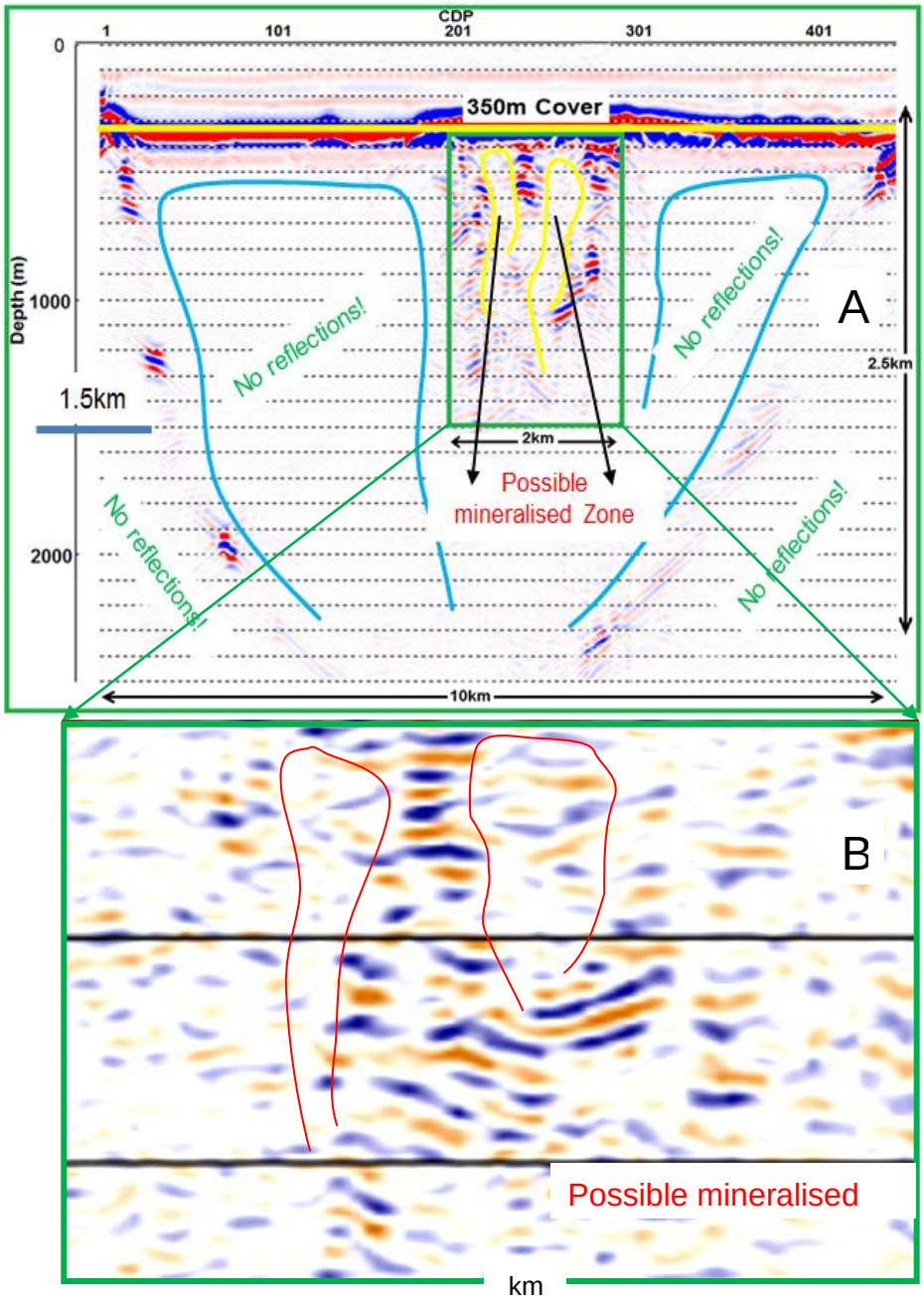

Figure 5.15 A) Noise-free depth-migrated section from the geological model in Figure 5.4 using the cross-section D in Figure 5.3 with 80 m source and 40 m receivers spacing and B) Expanded section. The Roxby Down granite, granite and granite breccia (indicated with red line in Figure 5.14B) host to the Olympic Dam Cu-U-Au deposit is imaged as a non-reflective region and this was also the case with the real data (03GA-OD1). No-reflectivity in this region is probably due to the geometry (steeply dipping), low impedance contrast or perhaps low velocity gradient related to alteration. The extent of possible mineralised zone is now modified in light of modelling results.

To further corroborate the relationship between the migrated seismic sections, I superpose it on the geological model (Figure 5.16). The migrated seismic section matches very well with the geological model except for the steeply dipping structures (almost vertical) which cannot image entirely.

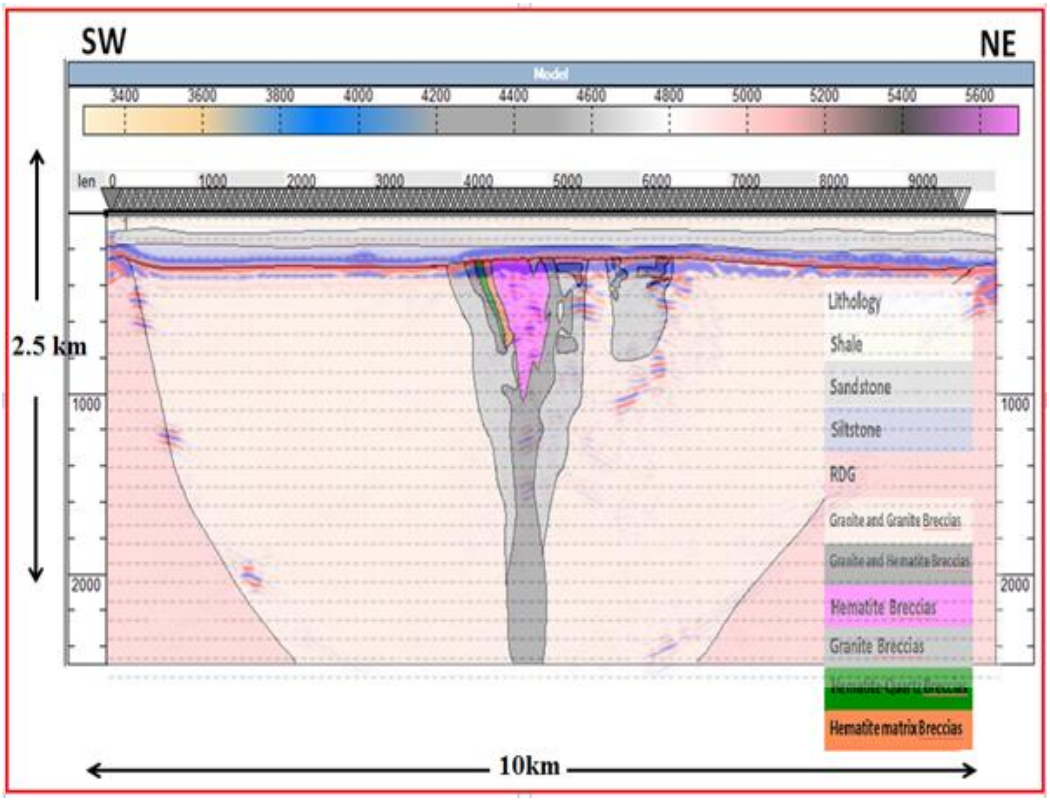

Figure 5.16 Migrated seismic data from Olympic Dam processed to accentuate the Olympic Dam Breccia Complex features superposed onto geological cross section from boreholes for comparison.

5.8 Conclusion

This modelling experiment and comparison with field data (with 2D surveys) has indicated that seismic reflection surveys can be very useful geophysical methods for mapping deep seated ore-bodies hosted by complex structures typical in Gawler Craton (our study area). Even with very sparse 100 m source and 50 m receivers spacing we can still see the complex structures, abrupt changes in reflection character as well as low reflectivity at the base of the large intrusive area. In fact, at the camp-scale the host rock is not particularly complex, but the breccia zone is evidently complex.

Anomalous seismic responses were seen within the intrusive package and are probably due to mineralogy composition, which has different impedance contrast in combination with discontinuities. For instance, velocities and densities within the sulphide zone are usually controlled as a result of mixture in properties of sulphide end-member with its host rocks. Thus, mixture of pyrite-felsic rocks causes an increase in velocity with density, while ores with chalcopyrite, sphalerite or pyrrhotite end members decrease in velocity with increasing density (Salisbury, et al., 2003).

The Roxby Down Granite (RDG) and granite and granite breccia, host to the Olympic Dam copper-gold deposit, are identified or mapped as non-reflectivity region, while low reflectivity at the base of the large intrusive area is observed. Lack of internal structures, the nature of the geometry and low impedance contrast (small reflection coefficients values) assigned in addition to the complex deformation, which partially destroyed reflection continuity, may be responsible for this observations. It should be noted that large granitic units imaged in seismic surveys in Western Australia also tend to lack "internal" structure (Urosevic, et al., 2007).

A close similarity between the idealised noise-free numerical data and very sparse deep crustal data over Olympic Dam especially in terms of reflection patterns can be

observed. In the three cases considered using different test parameters, burial at greater depth do not downgrade the resolution significantly. The difference in the amplitudes and frequency characteristics between the field data and simulated data is due to many differences between the model and real data conditions.

The major reason for the anomalous reflectivity seen in all the sections is interpreted to represent both lithological variations in faults and shears zones. However, the similarity of the Olympic Dam response is quite remarkable given that there was only one iteration of model building before the simulated data was compared to real data. Clearly, the geological models of Olympic Dam are fairly mature and incorporating these geological models with sensible petrophysics (personal communication with my supervisor, P. Williams and D. Pridmore of HiSeis Pty Ltd., all ex-WMC geophysicists) results in a good match with real data.

An issue still to be resolved is whether sparse survey geometries would in fact allow for the detection of an Olympic Dam style orebody near the surface, due to the vertical and horizontal resolution obtainable. For steeply-dipping structures, which characterize the Olympic Dam style of deposit, horizontal resolution less than 300 m on an unmigrated section will not be feasible, even at the highest frequencies. Thus, further research, using a more realistic 3D seismic modelling approach as well as the use of VSP/crosshole and tomography is required to resolve these issues.

6 Vulcan IOCG-Uranium Modelling Experiment

6.1 Introduction

Vulcan was a previously identified IOCGU target, further developed in 2009 by Tasman Resources. This Project was selected as one of the case studies in this research work because it has geophysical similarities (a very large gravity anomaly) comparable to Olympic Dam with a proven potential for exploration. Also, HiSeis (a Curtin University spin-off) performed some 2D seismic surveys in 2010 and looked at the feasibility of seismic reflection. Whilst the HiSeis information is commercial-in-confidence, their general learnings and knowledge in operating in this area was useful to this research. The case study tests the high-resolution power of seismic reflection surveys as the deposit is covered by approximately 850 m of "flat" lying sediments. Lastly, there is an existing seismic line acquired in 2003 by Geoscience Australia (G.A), available for comparative study; thus, we can test our ideas (feasibility of seismic reflections surveys to detect typical IOCG deposits at varying scale in Gawler Craton).

6.2 Location and Geology of Vulcan IOCGU

The Vulcan IOCG-Uranium deposit (Figure 6.1-6.2) is located in the Lake Torrens area within the eastern Gawler craton, South Australia. Vulcan mineralisation was discovered some 30 years beforehand by WMC Exploration, (personal communication, P. Williams, ex-Chief Geophysicist, WMC), but considered too deep for commercial exploitation at the time. The first drill hole in the area was drilled in 1981 by WMC, but this hole was drilled off Tasman's current Vulcan target and no significant mineralisation was intersected (Tasman, 2013). It was later identified as a primary IOCGU target by Tasman Resources in 2009 due to the presence of a large and previously untested gravity anomaly with key tectonic lineaments very important to the discovery of Olympic Dam (Tasman, 2012, 2014). The prospect is defined by geophysical anomalies intersected by diamond drilling.

The deposit occurs within basement rocks beneath approximately 850 m of younger, flat-lying sedimentary cover rocks, which have been dated at 1,586 +/-8 million years old, the same as Olympic Dam (Proterozoic age). Only a very limited number of drill holes have been completed within a large target area. The deposit is hosted by metasediments, granite and volcanics with similar characteristics to Olympic Dam. It is dominated by a large hematite IOCGU system (~12km^2) 30 km north of Olympic Dam and 150 km away from Prominent Hill mine with very thick and strong alteration including 100's metres of hematite breccias, low-grade IOCGU mineralisation (Cu, U, Au, Ag, Mo and REE).

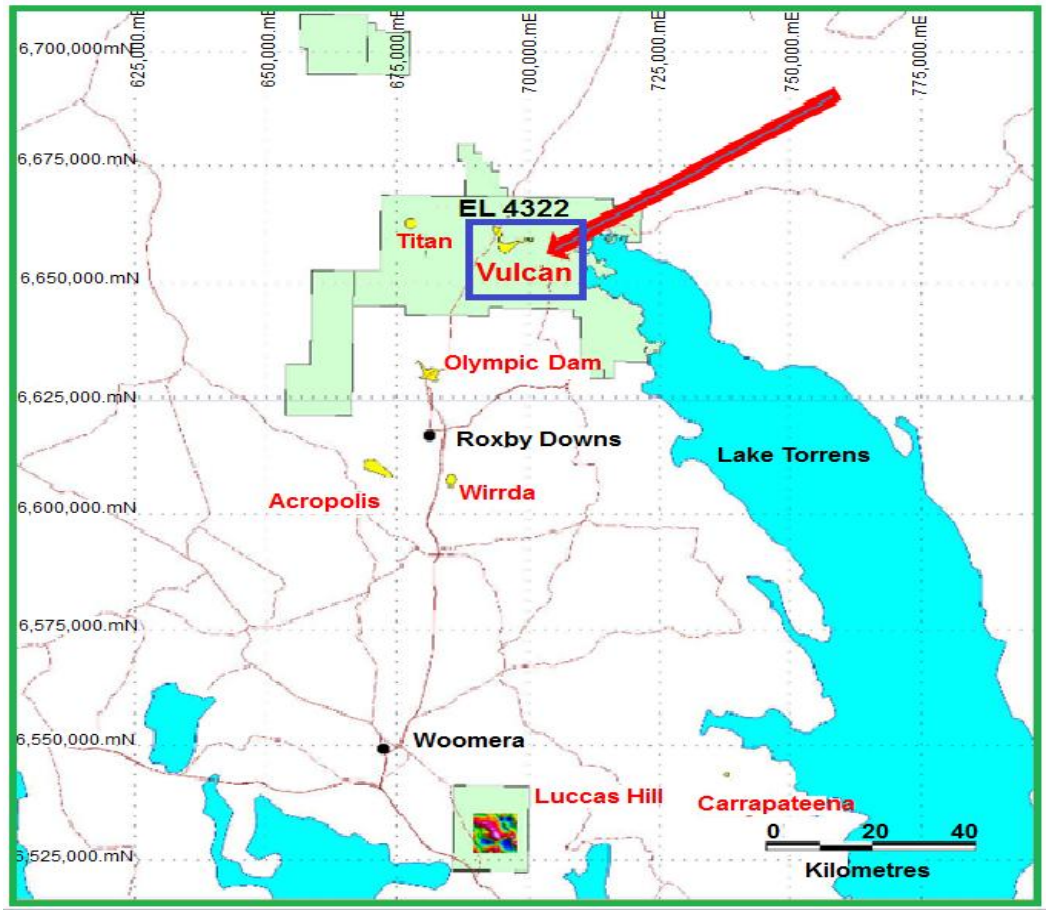

Figure 6.1 Location of Vulcan IOCGU deposit within the Lake Torrens Area (after Tasman, 2009).

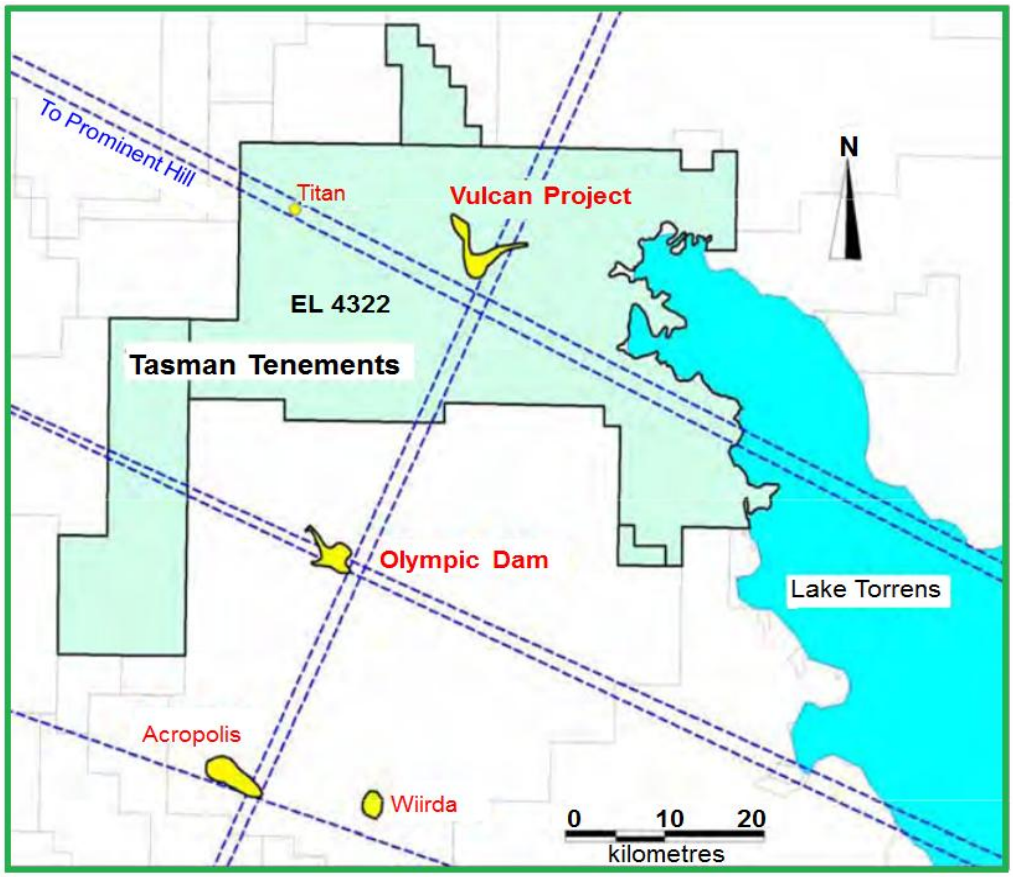

Figure 6.2 Location Plan of the Vulcan IOCGU Project with various key tectonic lineaments indicated by dashed blue lines (After Tasman, 2009)

The mineralisation style of Vulcan is very similar to that of the nearby Olympic Dam deposit (Tasman, 2011) and comprises of disseminated pyrite and chalcopyrite, which is hosted within the breccia rich zonation consisting fine black grained to steely-grey hematite. Near the bottom of the main discovery hole the pyrite-chalcopyrite mineralisation weakens and host rock clasts become quite abundant. Lesser grade uranium is visible throughout the interval but diminishes close to the bottom of the hole (Tasman 2011). Mineralisation is said to occur as a series of different and weak-to-moderate intersections in the drill holes, while others occur within the hematite dominated breccias. It is thought that the highest-grade copper mineralisation is probably remobilised and occurs within the upper portion of a mafic

dyke (Tasman web site, 2011). Thus, structural controls for fluid migration are important.

There are many reasons why seismic might be considered for a Vulcan type of deposit. First, the deposit is sited under approximately 850 m sedimentary cover, which is far beyond the ability of potential field methods to resolve structures below 500 m depth. Secondly, some of the ore zones may be associated with structures that remain hidden by the overburden and can only been detected using seismic methods. Also, Vulcan mineralisation comprises Fe oxides plus disseminated pyrite and chalcopyrite that have higher velocity and density than the surrounding rocks thus making a basis for a seismic reflection survey.

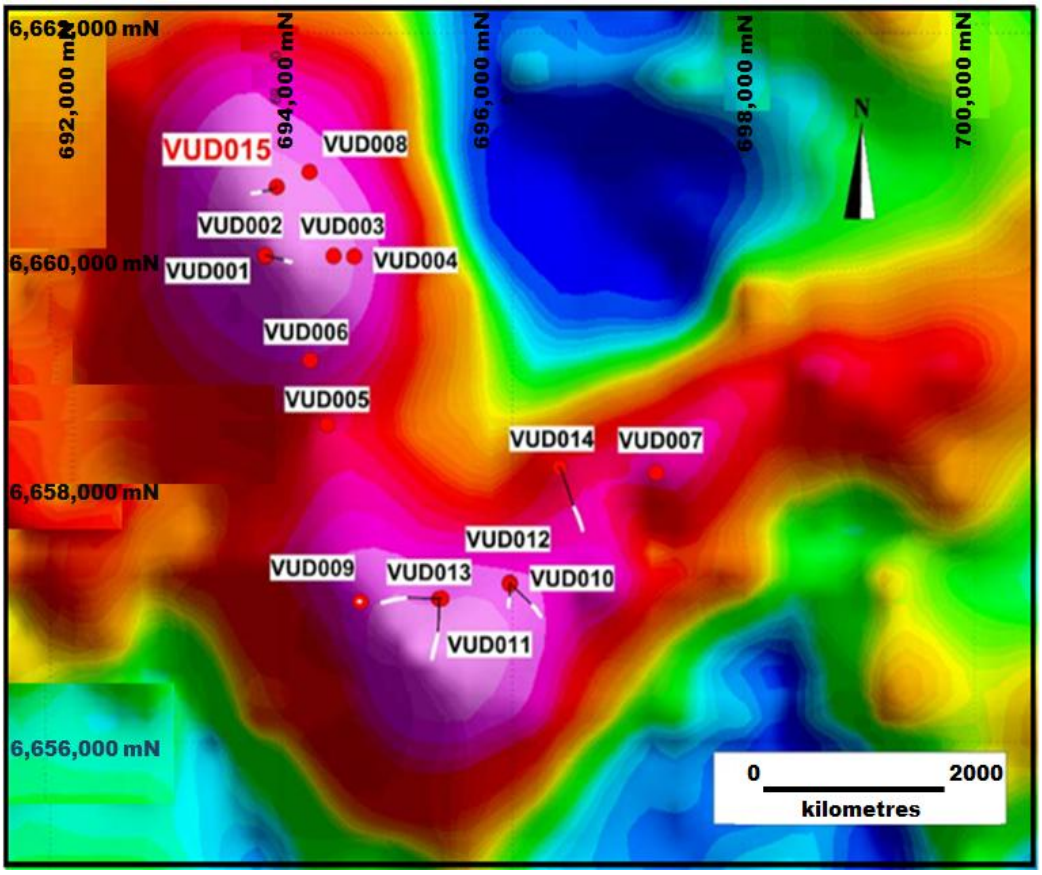

Figure 6.3 Vulcan residual Bouguer gravity with exploration boreholes shown as red solid circles (after Tasman, 2013).

6.3 Vulcan Seismic Modelling Experiment

To further demonstrate the feasibility of using a seismic reflection survey to detect IOCG deposits at regional scale, the Vulcan deposit was modelled and simulated using petrophysical information described in Chapter 3 and corroborated from personal communications with staff performing sonic core testing done at Curtin on behalf of HiSeis Pty Ltd. Figure 6.4 and 6.5 shows the schematic geological plan of the Vulcan IOCGU indicating the location of the cross-section A–B and the synthetic geological model respectively. Gravity modelling was used to assist interpolation between holes.

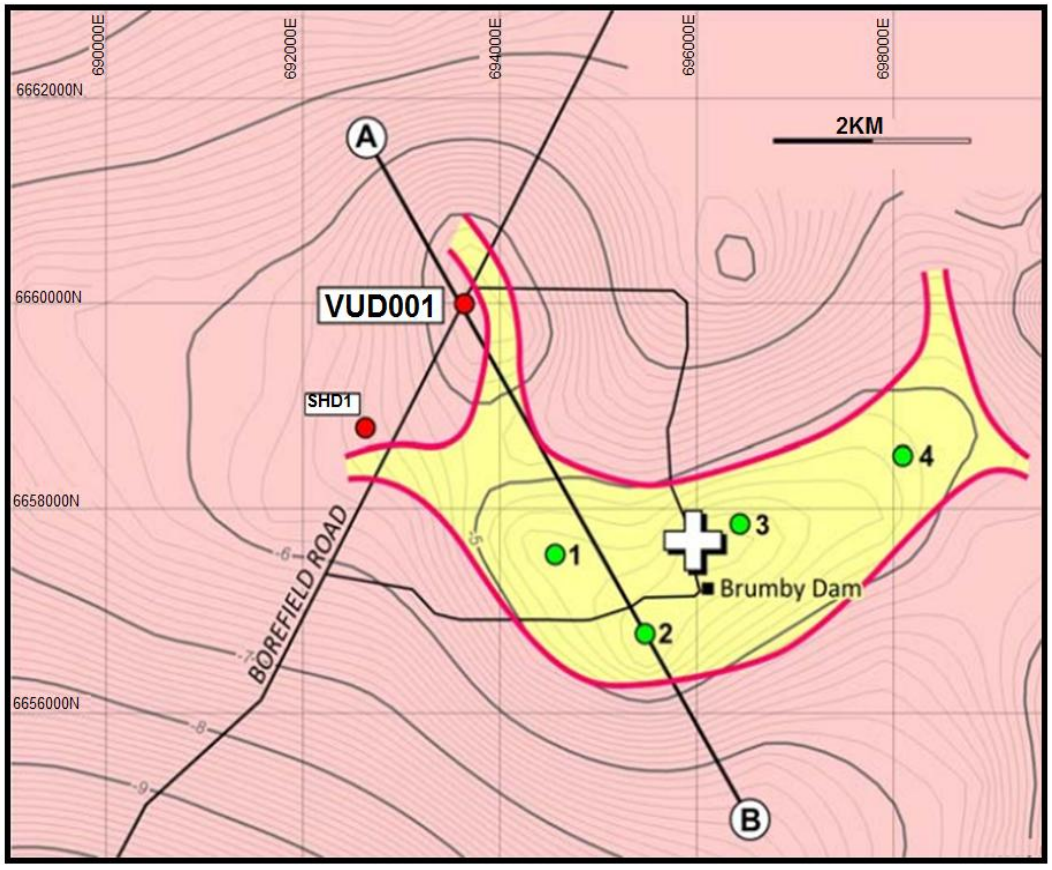

Figures 6.4 Geological extent of the Vulcan project overlaid onto Bouguer gravity contours as based on the results of Hole VUD 001 and available geophysical data (after Tasman, 2010).

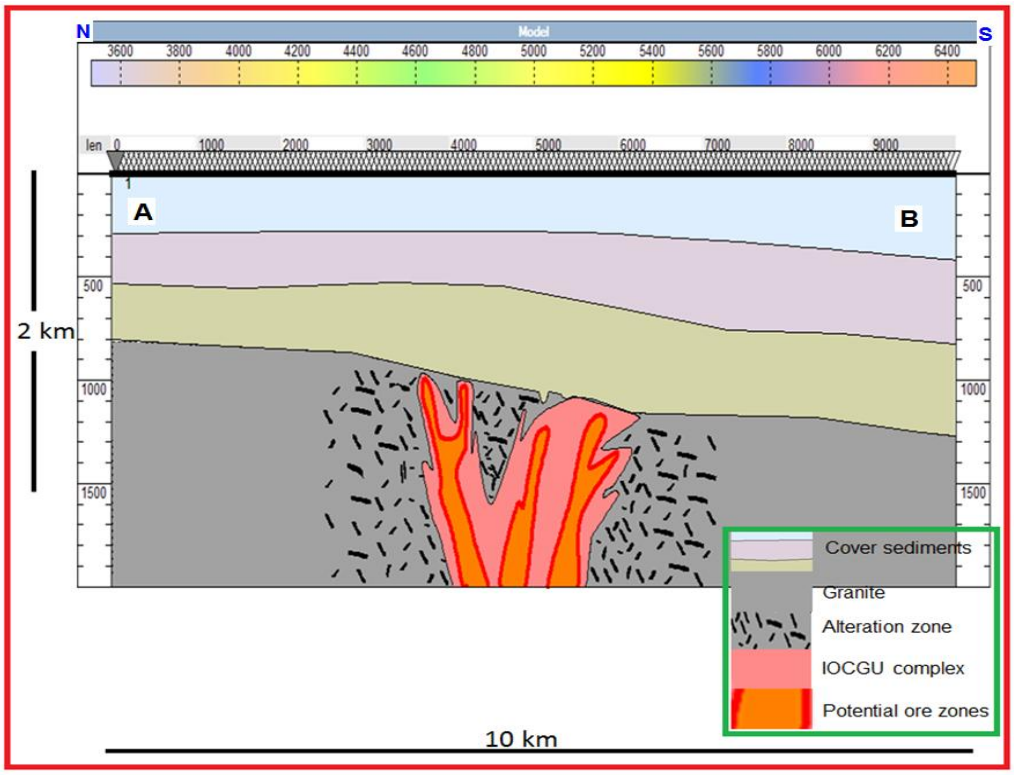

Figures 6.5 A simplified synthetic geological model along cross-section A–B shown in Figure 6.4.

6.4 Survey Design, Modelling and Synthetic Data Processing

Again, the synthetic survey for the Vulcan IOCGU modelling case study was designed to correlate with the seismic reflection profile used by Geoscience Australia on the expanded section of Olympic Dam (OD1). This involved 10 km x 2 km geological model where the primary zones of interest were situated within the central 2 kilometres of the modelled data. A split-spread geometry was used with the source positioning located at middle of the spread with four different survey parameters used to collect the data. In the first and second case, data was taken across the 480 and 240 source shots, simulated at 20 m and 40 m shot intervals, with a dominant source frequency of 35 Hz and a Ricker wavelet. Receivers were spaced at 10 and 20 m intervals respectively.

In the third and fourth cases, data was taken across 120 and 100 source shots, simulated at 80 and 100 m intervals respectively across the entire model maintaining same source positioning (a sparse rolling split-spread) and a dominant source frequency of 35 Hz (Ricker wavelet). Receivers were spaced at 40 and 50 m respectively. Table 6.1 and 6.2 shows the acquisition parameters and velocities and densities respectively used for the synthetic modelling. Acoustic modelling was again followed by the full processing as shown in Figure 4.7.

Acquisition parameters				
Parameter	Case 1	Case 2	Case 3	Case 4
Source depth (m)	0	0	0	0
Receivers depth (m)	0	0	0	0
Shot interval (m)	20	40	80	100
Receivers spacing (m)	10	20	40	50
Centre frequency (Hz)	35	35	35	35
Number of shots (no)	480	240	120	100
Record length (s)	2	2	2	2
Sampling rate (ms)	0.1	0.1	0.1	0.1

Table 6.1 Acquisition parameters used for the Vulcan deposit synthetic modelling experiment.

#	ROCK Type	Vp (m/s)	Density (Kg/m^3)
a	Cover sediments	3450	2352
b	Granite	5920	2854
c.	Alteration zone	4328	2640
d.	IOCGU complex	6245	3630
e.	Potential ore zones	6430	4080

Table 6.2 Velocity-Density parameters used to populate the Vulcan synthetic geological model; these values are based on the limited core tests performed by HiSeis Pty Ltd). Gravity modelling by Kitzig, 2016 used similar values as provided in the table.

6.5 Results and Discussion

Some reflection coefficients used for the Vulcan modelling experiment are of the order of 0.64, which will produce strong reflections at various units or boundaries.

This is mostly in the transition to younger overlying sediments over altered and mineralised basement rocks. The minimum velocity was 3450 m/s with 35 Hz frequency hence wavelength was calculated to be 99 m. Thus, the calculated minimum resolvable vertical thickness of 25 m is still higher than the limit of seismic detectability usually in range of $\lambda/30$. For a 2 km depth with wavelength of 99 m, the Fresnel zone was calculated as 631 m.

Results from the Vulcan seismic modelling experiments using different survey parameters are presented below. Figure 6.6 is an example of noise-free synthetic shot records for source number 105. Primary reflection energy is evident in the time window ranging from 0–5000 ms. However, the various reflectivity events are visible up to 2000 ms. The complexity of the Vulcan IOCGU geological structure is visible by the pattern of reflections displayed on the shot records.

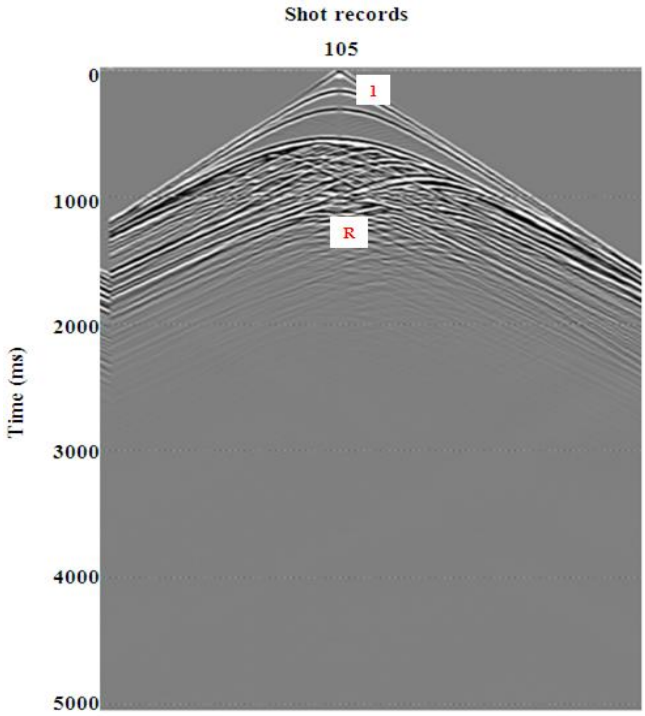

Figure 6.6 An example of noise-free synthetic shot records for source number 105 from the Vulcan complex model: (1) is the direct wave and (R) denotes numerous reflections and diffractions. Records are from 0–5000 ms while actual reflectivity events are visible up to 2000 ms. the shots are shown using true relative amplitude.

Migrated synthetic sections converted to depth are shown in Figures 6.7–6.10. The layers within the sedimentary cover have weak reflections due to the low-impedance contrast (low velocity-density values assigned). As expected, a strong reflection was noticeable between the granitic basement rock and sedimentary cover contact in all the parameters tested, which due to the high-impedance contrast. Anomalous reflectivity within the IOCGU complex area (indicated with yellow) due to mineralogy composition and/or different impedance contrast was also visible and this could be a possible target for drilling. As with Olympic Dam, modelling the Vulcan IOCGU deposit is visible as series of complex reflections and diffractions in an otherwise bland (with respect to reflectivity) crystalline basement. Older metasediments that are not "bland" and lie on the edge of the granitic intrusive host rocks, are not modelled. As seen in later 2D seismic data (Figure 6.14) the deposit sits sandwiched between this granitic intrusion and the metasediments, with some of the deposit perhaps overprinting the metasediments. It is quite possible the very large granitic intrusion that preceded the mineralising event produced a breccia, including the margins of even older metasediments and forming a trap for mineralised and Fe-rich fluids to migrate into.

We can see reflections within the mineralised intrusive regions even with the addition of some 25% Gaussian noises with all of the four cases of survey parameters. Thus, the cheaper sparse survey geometry is in theory able to detect Vulcan. This is in agreement with our started objective, which is to demonstrate that seismic reflection surveys could be a very useful tool for detecting presence of brecciated intrusive structures that may host iron oxide related mineralisation.

Overall, the results from the Vulcan numerical modelling experiment using different test parameters are very encouraging. The migrated images from modelling generally compare favourably with the available 2D data, indicating that the geometry of the seismic model is a reasonably representative of the internal structure of Vulcan deposit. Thus, the seismic reflection survey method is appropriate for detecting

mineralisation structures that are likely to be connected with IOCGU in the Gawler craton.

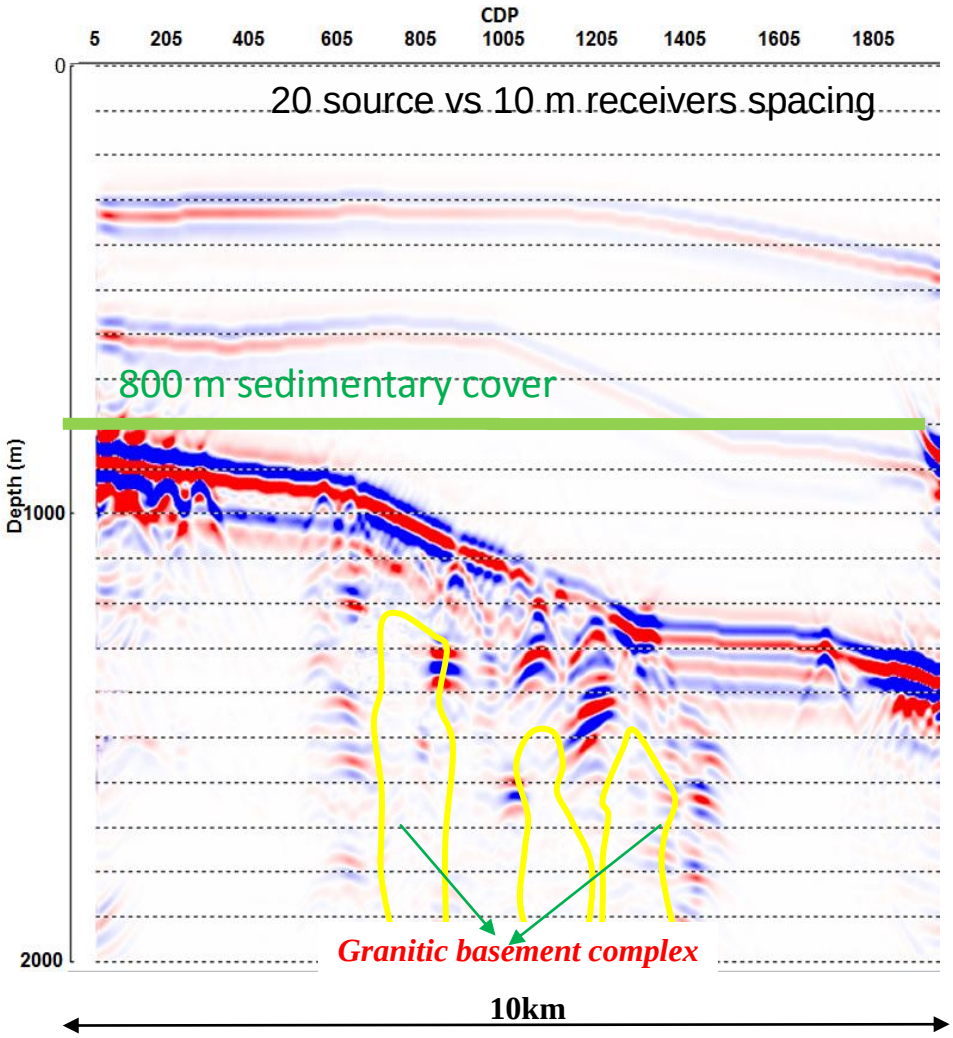

Figure 6.7 Depth-migrated sections (noise free) using 20 m source and 10 m receivers spacing. The layers within the sediments as well as the intrusive structure within the basement rocks are fully recovered. A strong reflection was also observed between the basement rock and the sedimentary layers due to high impedance contrast between the two layers.

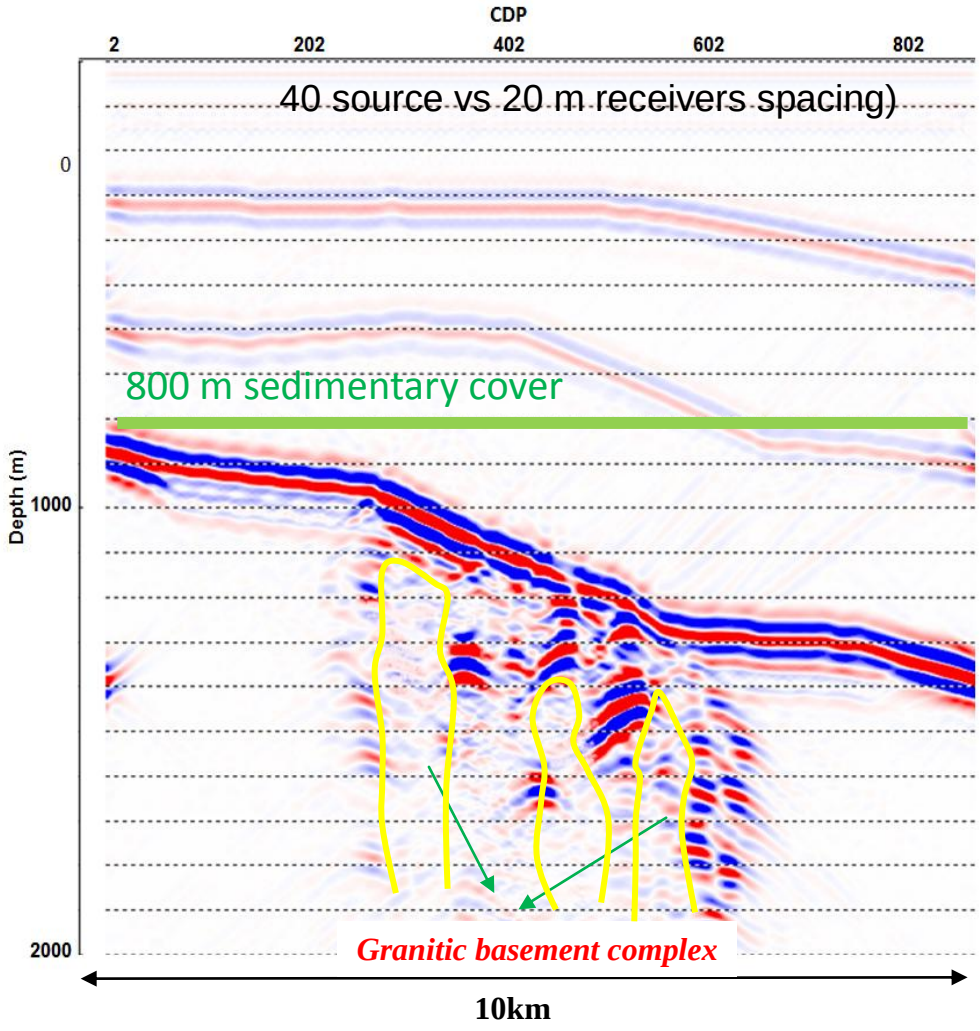

Figure 6.8 Depth-migrated sections (noise free) using 40 m source and 20 m receivers spacing. There is almost no difference in this result in comparison to the previous survey parameters. Both the sediments layers and the basement structures are also recovered. A strong reflection was also observed between the basement rock and the sedimentary layers due to high impedance contrast between the two layers.

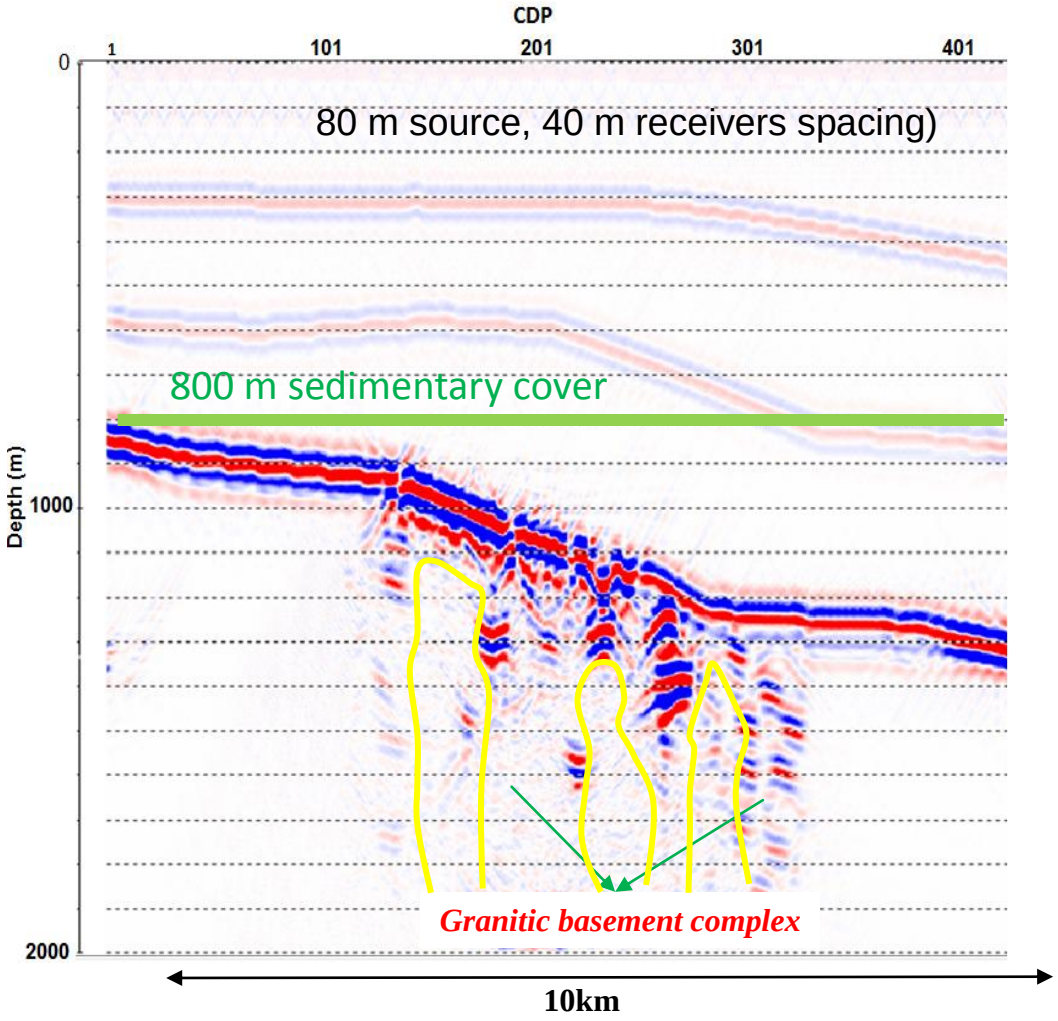

Figure 6.9 Depth-migrated sections (noise free) using 80 m source and 40 m receivers spacing. With 80 m source and 40 receivers, we can still see the layers within the sediments as well as the intrusive structure within the basement rocks though results from 20 m and 40 m source spacing and 10 m and 20 m spacing looks better. A strong reflection was also observed between the basement rock and the sedimentary layers due to high impedance contrast between the two layers.

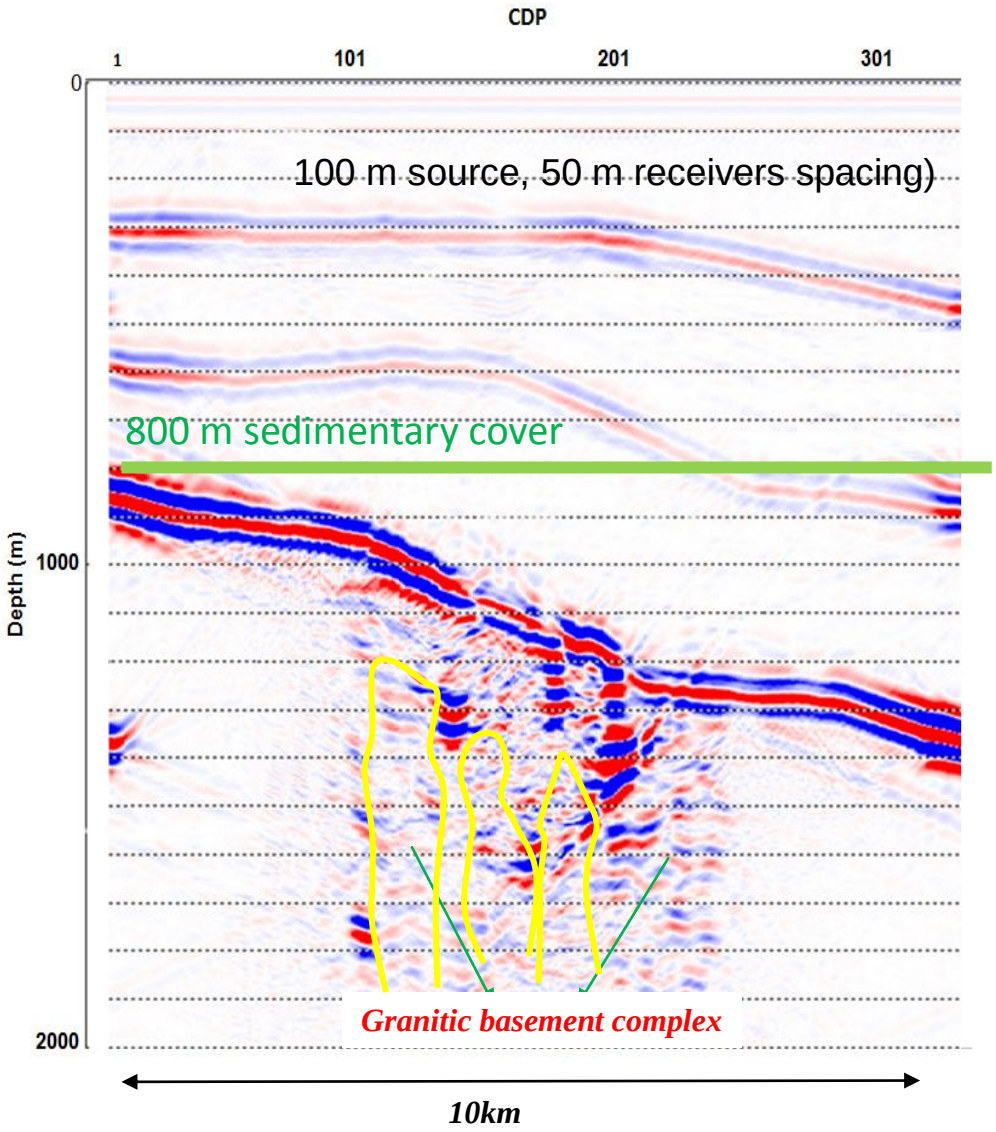

Figure 6.10 Depth-migrated sections (noise free) using 100 m source and 50 m receivers spacing. The migrated sections look poor when compared with previous parameters tested, which suggest that using this acquisition parameter might not be ideal for real seismic survey in hard rock environment.

To further investigate the reliability of our model assuming noise is present, we decided to add 25% Gaussian-noise to the data, resulting in noisier data, but same frequency was maintained. A typical seismogram containing 25% noise level is display in Figure 6.11 left panel. There is a considerable difference when compared to the same seismogram from the same modelling on right panel. The depth-converted sections from noise-free and 25% Gaussian noise are shown in Figure

6.12. The images from the data with 25% Gaussian noise are slightly blurred, but still compare favourably with the noise-free migrated sections except that geological boundaries within the sediments are only partially recovered. The contact between the cover sediments and granitic basement rock as well IOCGU complex structure are largely recovered when compared to the noise-free migrated section.

Comparison of noise-free and 25% Gaussian noise migrated images from very sparse parameters (80 m source versus 40 m receivers and 100 m source versus 50 m receivers) are shown in Figure 6.12. The images from the noise-free data look better than the noisy image for obvious reasons. However, the contact between the eastern granite and that of the metasediment package as well as the intrusive structure are fairly recovered. Given the large impedance changes this is expected.

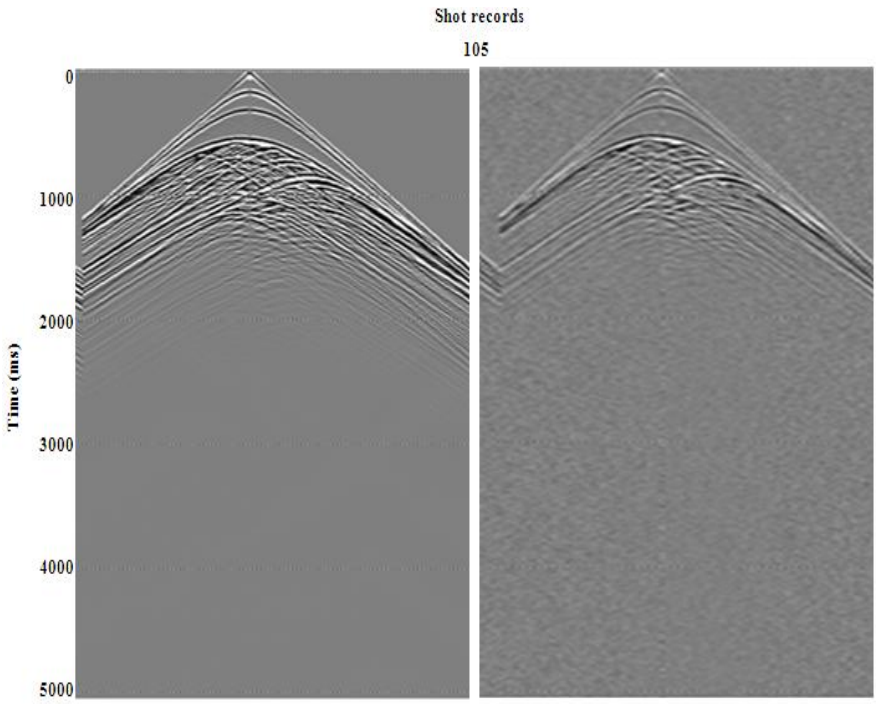

Figure 6.11 left panel noise free synthetic shot records, right panel) with 25% Gaussian noise for source number 105. Records are from 0–5000 ms but reflectivity event are visible up to 2000 ms.

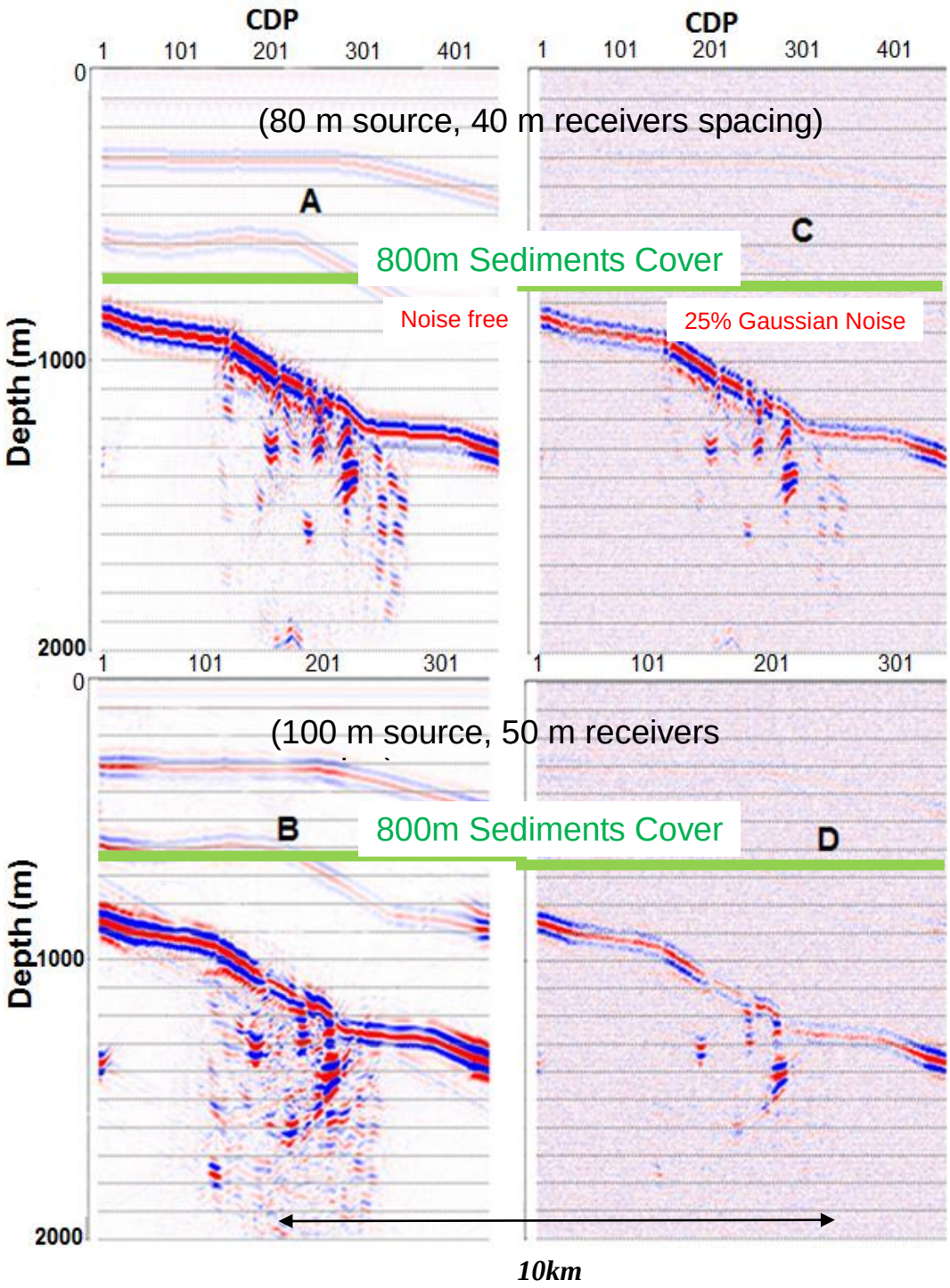

Figure 6.12 Noise-free and 25% noisy migrated images comparison. A–B) Noise-free depth-migrated sections, C–D) 25% Gaussian noise depth migrated sections. The images from the noisy data are slightly blurred compared to the noise-free image. The layers within the sediments indicated with yellow circle are basically unresolved, but the contact between the basements-cover sediments as well as the intrusive structures is detectable.

6.6. The Vulcan Real Seismic Survey

The Vulcan IOCGU deposit is part of the 2003 Gawler Craton Seismic Survey (L163), conducted by Geoscience Australia. A portion of the initial processed seismic section is shown in Figure 6.13 and can be obtained from public sources (Geoscience Australia website). New versions are becoming available (Figure 6.14) that have been reprocessed by Curtin University as part of deep exploration technology corporate research centre DET CRC research. The acquisition parameters used is as described in section 5.6 (Table 5.3). Vulcan deposit is an expanded section of Olympic Dam deposit.

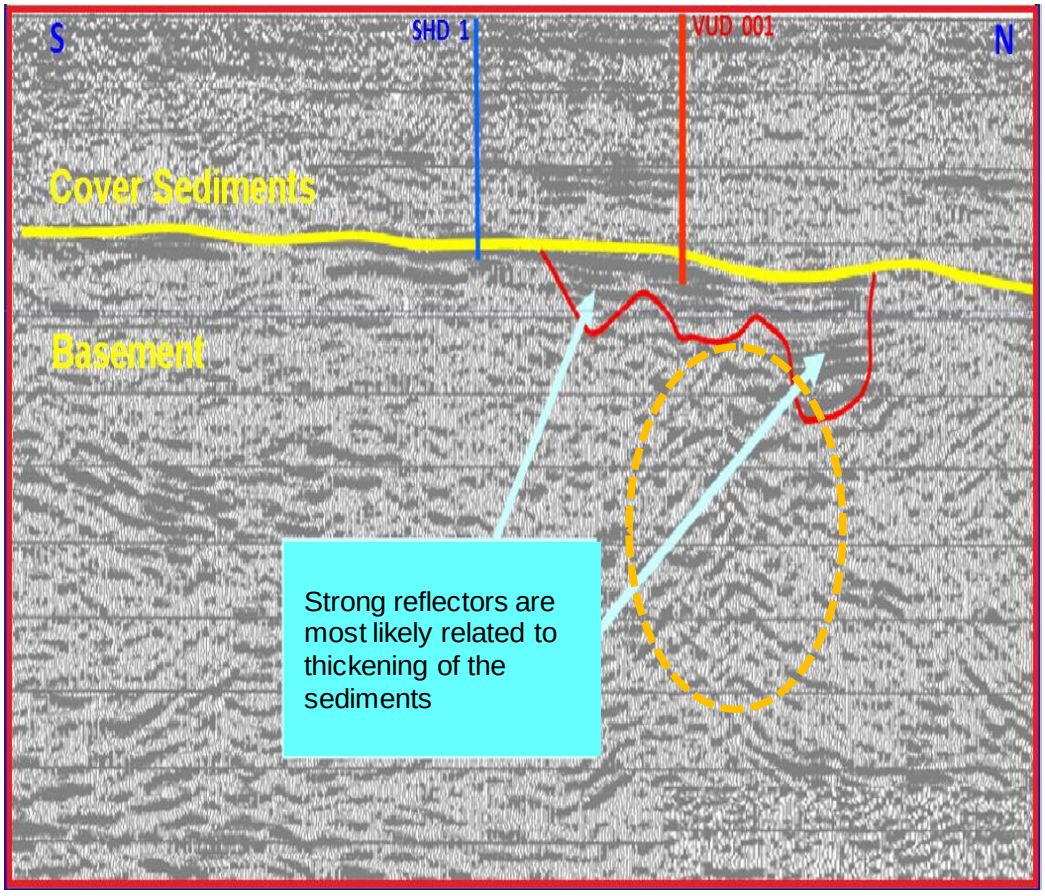

Figure 6.13 Vulcan SN seismic reflection profile from (Lyons and Goleby, 2005). An example of the early GA processing methodology. Thickening of the cover is marked with blue arrows. The orange ellipse is denoting the area where "chaotic" reflection character could be related to the ore zone.

6.7 Comparison of Gawler Seismic Results with Model Data and Discussion

Figure 6.14 shows the results from recently reprocessed GA Gawler Craton seismic field data (a relatively low-resolution regional deep crustal survey) of the Vulcan IOCGU deposit is displayed in an expanded section of the Olympic Dam (NS 03GA-OD2) processed seismic section. This processed section is an "enhanced version" reprocessed at Curtin University by Prof M. Urosevic to recover more near-surface detail and higher frequency content. We have used the reprocessed section for comparison with the modelled data. Figure 6.15A is the 2 km by 20 km section extracted from Figure 6.14 for the purpose of comparison with our synthetic model while Figure 6.15B is the expanded section directly below the projection of the Vulcan deposits. Note that the expanded section (green rectangle in Figure 6.14) largely encompasses the potential mineralised zones and it lies on the edge of a major intrusion into older metasediments. This is where we would predict an IOCG to be located as it lies on the edge of a significant intrusion near a major lineament; thus, in a zone of tectonic weakness for mineralisation to come from below.

The stacked and depth-converted results from our modelling experiments using the geological model in Figure 6.5 are shown in Figure 6.16A in comparison with the actual seismic section shown in 6.16B. The Vulcan geological cross-section (A–B) used for modelling in Figure 6.5 is located within the triangle indicated with blue arrow in Figure 5.15 of the long GA survey line and corresponds to CDP 6250–5250. There is a close relationship between the noise-free numerical data and sparse deep crustal seismic data. This is seen better when comparing Figure 6.15A–B with 6.16A–B. A subtle change in the reflection character in the field data is visible around the granitic basement and may indicate a potential ore zone.

The real data has slightly higher resolution when compared with the synthetic data, due to differences in source signature and processing flow. The real data contains a wealth of detail that were not included in the simplified model such as extensive metasediments. The layers within the modelled sediments also have weak reflection

due to the low-impedance contrast. Strong reflections, as expected, were noticeable between the basement rock and sedimentary cover contact.
Even with the addition of 25% Gaussian noise (Figure 6.12C–D) we can still see reflection characteristics within the granitic basement as well as the contact between sediment and basement rock. However, reflections within the sediments are blurred due to the presence of noise.

A short-coming of this experiment is 3D effects that cannot be seen with a 2D approach. Acoustic modelling was used for this study, while in reality the earth is elastic in nature (a combination of P-waves, S-waves and ground rolls) hence not all features and artefacts expected can be seen. Further, the attenuation seen on 2D data and amplitude recovery is quite different from that of 3D data. Also, the energy of wavefront propagating in 3D vanishes faster than that of 2D energy hence it is impossible to see all the features expected in 2D data. Finally, since the modelling and processing techniques are two-dimensional, the data coming out of the plane on the 2D profiles as well as the structures will be seen on all profiles that are larger than the required window. This will have effect on the Fresnel Zone due to contraction in 1D. Thus, to address this out of plane effect, adequate care should be taken during planning to ensure that the survey extends well beyond the area over which one intends to interpret amplitude. Regardless of all the small contentions listed above, the match between the images from a simple geological model and the real data is quite striking, even if both replicate the failings of using 2D methods. Lastly, the granitic host intrusive is many 10's of km in diameter; thus, the geology is effectively 2½ D and somewhat suitable for a 2D approach as long as the explorer crosses the deposit.

Overall, the application of seismic methods to Vulcan style IOCG deposits is promising as it not only locates the structures hosting the deposits, but can also maintain resolution with considerable depth, at 800–1000 m were the signature is clear.

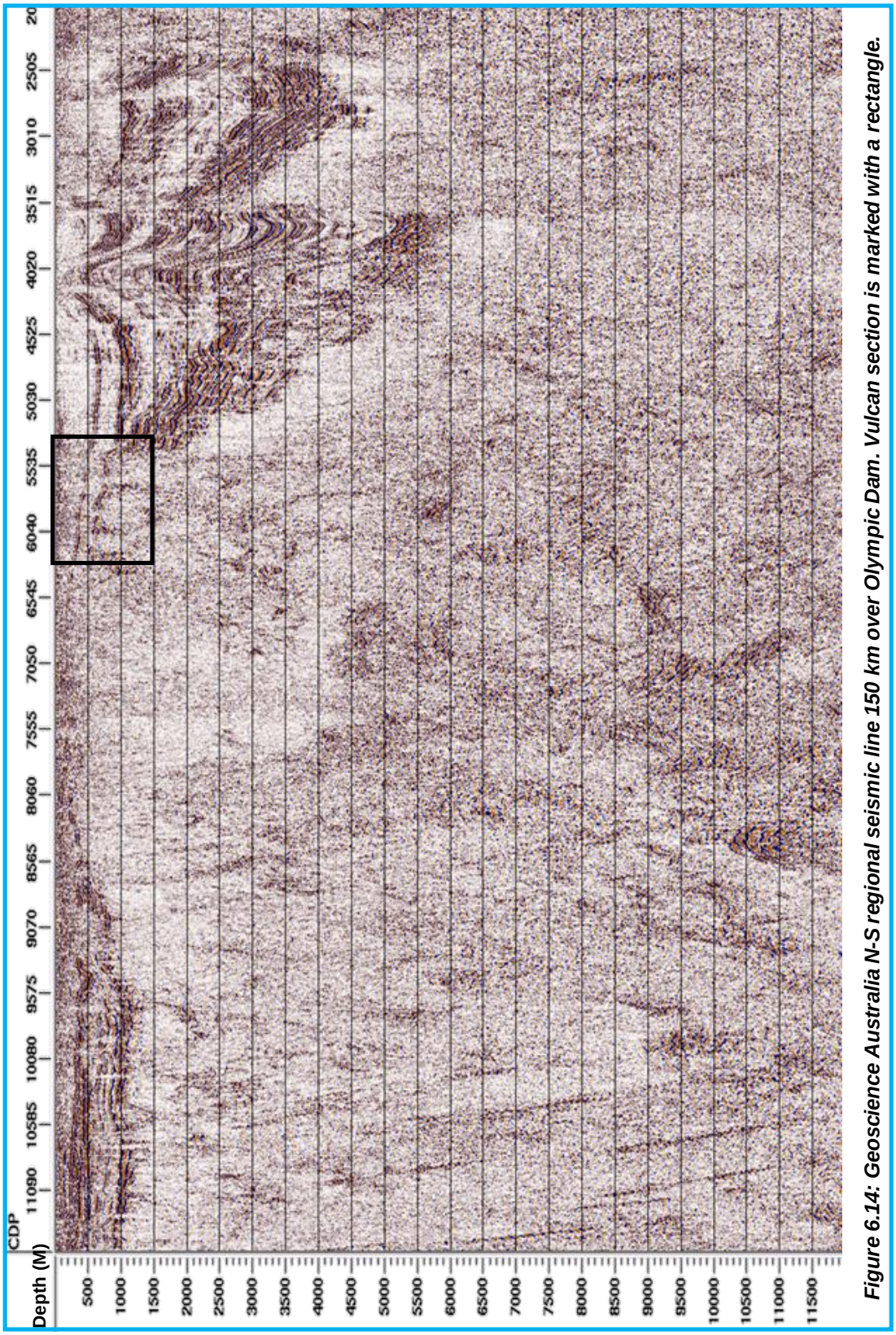

Figure 6.14: Geoscience Australia N-S regional seismic line 150 km over Olympic Dam. Vulcan section is marked with a rectangle.

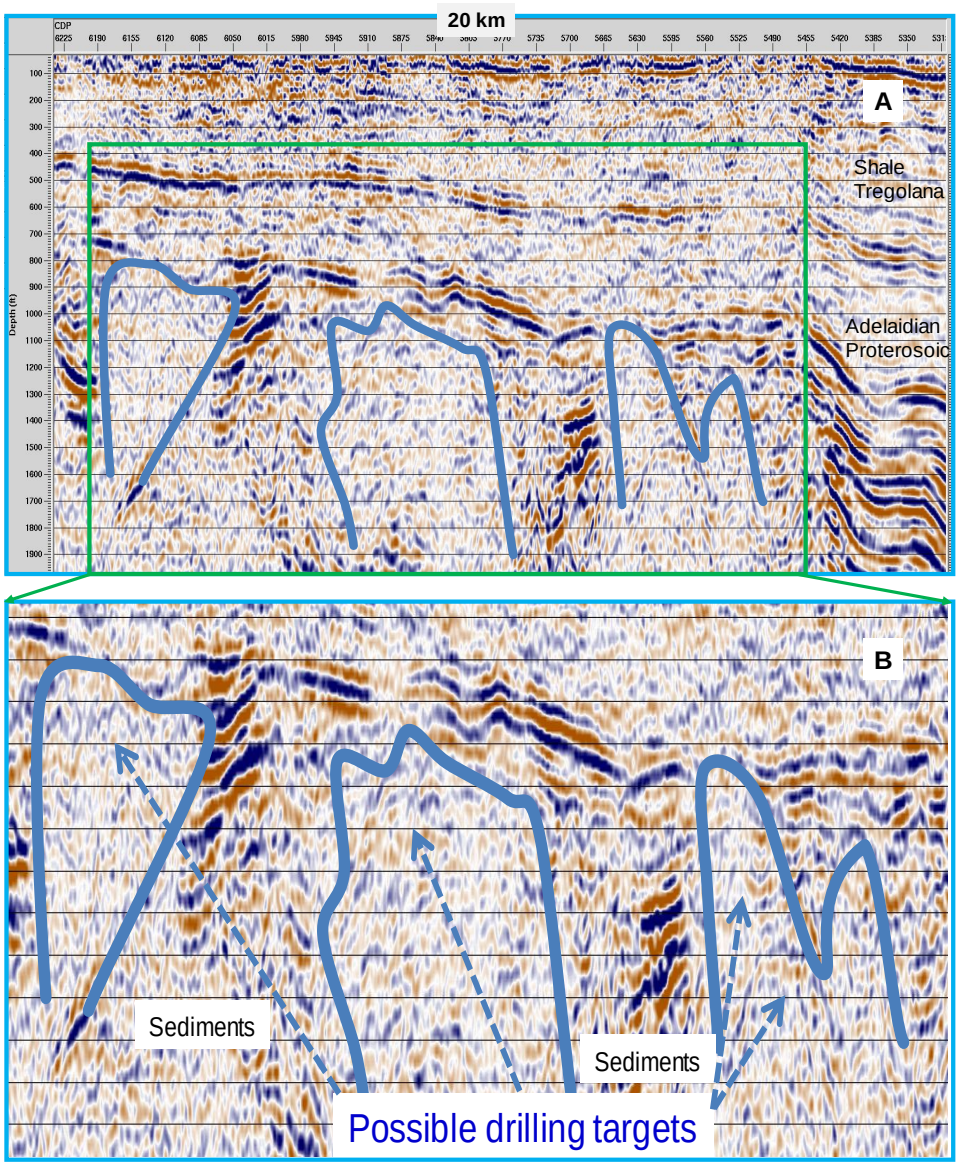

Figure 6.15 A) A 20 km long extract (CDP no 6250–5250) from the regional seismic line shown in Figure 6.14. A total depth of 2 km is displayed only. And B) Further expanded image below projection of Vulcan deposits (indicated with green rectangle). The blue lines indicate possible targets: intrusive or alteration zones.

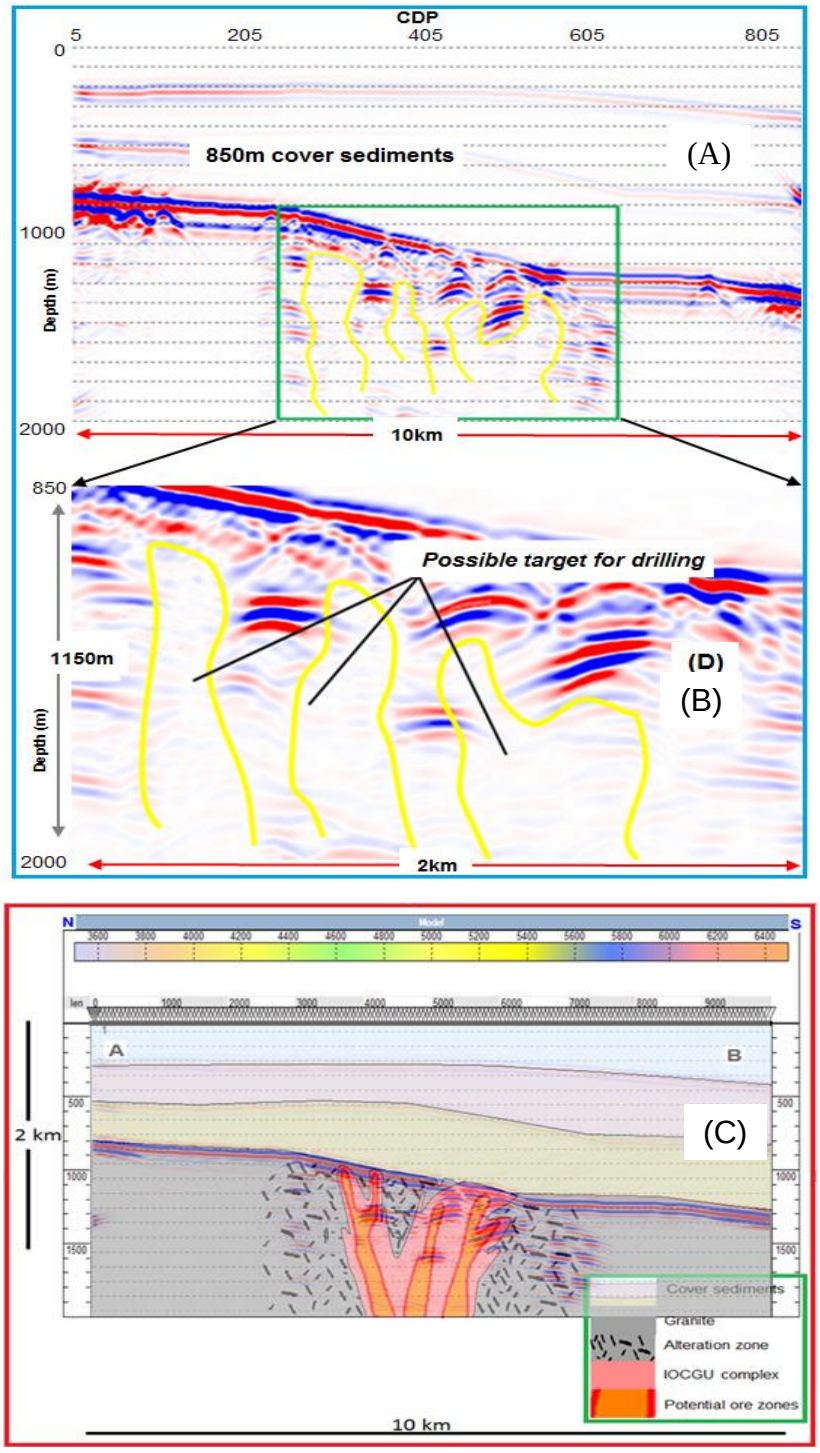

Figure 6.16 A) Noise-free depth-migrated section from the 2 km by 10 km geological model in Figure 6.5 using the cross-section A–B in Figure 6.4 with 80 m source and 40 m receivers spacing and B) expanded section of the Vulcan intrusive package as indicated with the green rectangle in 6.16A and C) migrated seismic data from Vulcan superposed with model derived from geological cross section constrain with boreholes

6.8 Conclusion

This modelling experiment has further suggested the ability of seismic reflection surveys to detect the presence of IOCG deposits, especially under significantly thick cover. Generally, the Gawler Craton geology is very complicated as the rocks are often highly deformed, so reflector continuity, although variable, is usually far shorter than that encountered within sedimentary environments. However, the results of the numerical modelling and field tests agree to a reasonable extent in terms of reflection patterns. Not all strong reflections in the modelled sections are from intrusive zones as identification of intrusive/fault zones depend on whether they link with surface outcrop.

The real data has slightly higher apparent resolution when compared with the synthetic data due to differences in the processing methodology as well as the acquisition parameters used. Overall, the migrated images compare well with the available real data as we can see the various horizontal layers as well as imaging intrusive block or package, suggesting that the geometry of the synthetic model may well be a fair representation of subsurface structure hosting Vulcan deposit. Even the relatively inexpensive seismic surveys with sparse survey parameters are able to detect the seismic signature of the breccia complex on the edge of the intrusive. While not every breccia complex will be mineralised, being able to detect such signatures in the Gawler Craton is very important.

Many, if not nearly all, IOCG deposits are located around fluid pathways in major lineaments and tectonically significant fault zones. Vulcan is an excellent example of such a situation. Given this association the Vulcan case study demonstrates it is feasible to use seismic surveying techniques to image both the intrusive structures to aid exploration drilling.

7 Mount Gunson Feasibility Study

7.1 Introduction

The Mount Gunson project offers a new deposit style that has not been looked at using the seismic reflection exploration approach. Specifically, the mineral transport system to the surface is different from other IOCG deposits and this could be a potential target for explorers. In the case of Mt Gunson, the mineralisation has been mobilised into what is normally the cover formations in other IOCG deposits in the Gawler region. Thus, such deposits will likely be closer to the surface and more economical to develop. Remobilised mineralisation can further concentrate the mineralisation as the Fe-rich minerals from the primary source may be left behind and the sulphides further concentrated in the new fluid traps closer to surface. Remobilised mineralisation is not new as both Olympic Dam and Vulcan are interpreted to have had multiple phases of mineralisation where earlier phases are pushed to the margins. Remobilised mineralisation into overlying sequences is noted by the current explorers at Mt Gunson. They believe they have found the "source" of Mt Gunson as weak IOCG mineralisation in the Gawler Range volcanics basement rocks (Torrens Pty Ltd. website, www.torrensmining.com.au).

The Mount Gunson copper deposit also lacks geochemical signatures because of small outcrops, confined drainage, sand cover and high salinity, especially in and around the playas (Creelman, 2005. Thus, conventional exploration techniques are unlikely to work well with this type of deposit. The deposit, Figure 7.1–7.2 is centrally located in the Olympic Dam copper-gold province (approximately 110 km south of Olympic Dam mine site), which is about 650 km long corridor along the eastern boundary of the craton. It is bounded to the east by the Torrens Hinge Zone, a major geological discontinuity (Creelman, 2005; O'Driscoll, 1986; Preiss, 1993).

Figure 7.1 Location of Mount Gunson copper deposit (after Lintern, et al., 1999)

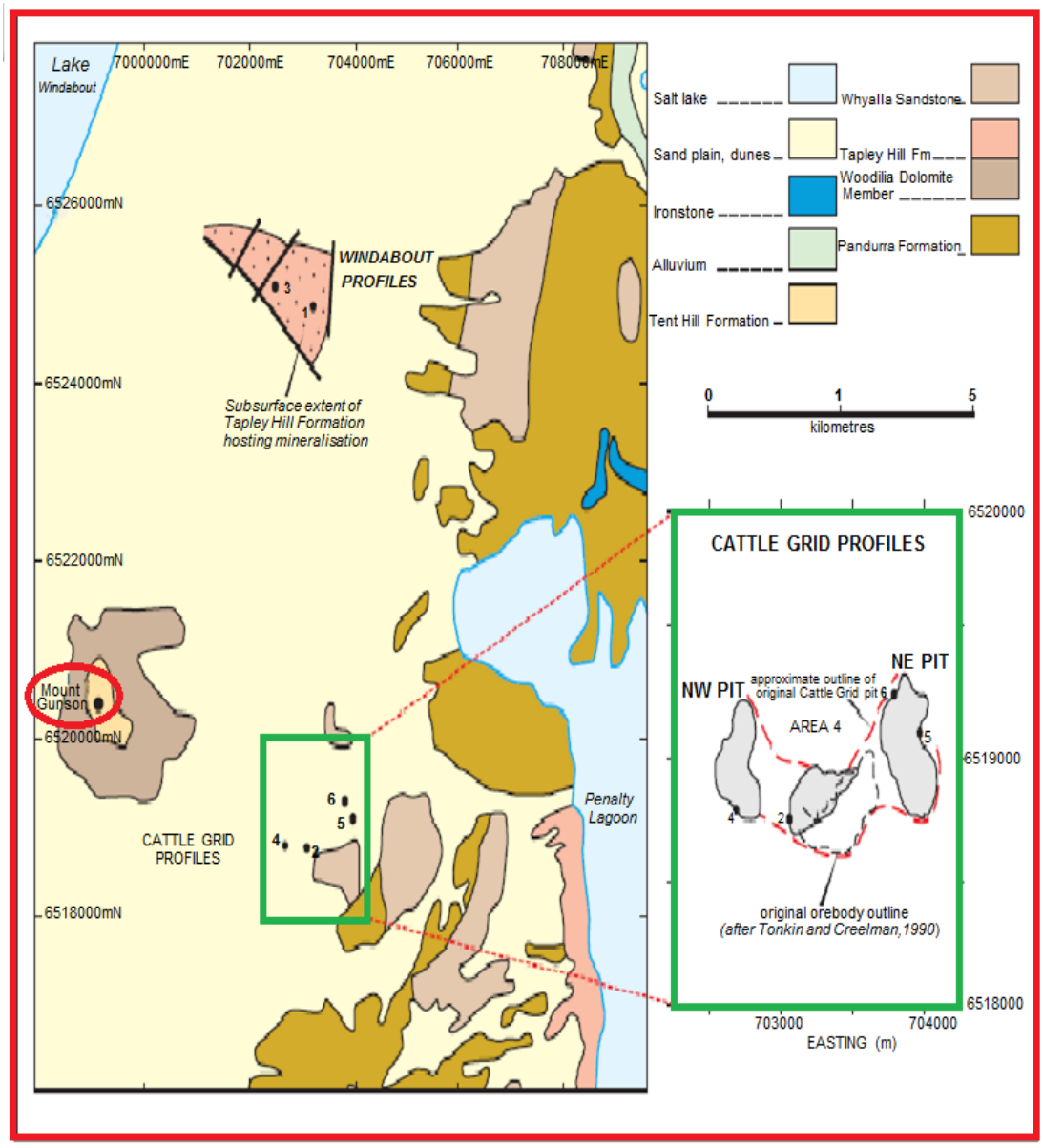

Figure 7.2 Geology of Mount Gunson indicating Cattle Grid and Windabout profile locations (after Johns, et al., 1981).

The Mount Gunson copper project is hosted by flat-lying undeformed terrestrial sediment rocks of the Late Proterozoic Age deposited on the Stuart Shelf. These platform sediments, often referred to as the 'Cover Sequence', host the gently dipping lenticular orebodies with thicknesses varying from about 3–10 m and depths varying from 10's of metres to up to 400 m deep (Porter, 2015). The cover sequence overlies igneous and metamorphic rocks of the eastern margin of the Archaean Gawler Craton. The deposit is intruded by minor dykes through the Pandurra Formation with one of such dyke containing some quantity of pyrite and copper sulphides, often closely connected with carbonate veins (Gersteling and Heape, 1975).

Mineralisation generally occurs along permeable stratigraphic horizons, especially within the disconformities; however, two major styles (Cattle grid and Windabout) are recognised. The Cattle Grid mineralisation, which is sandstone hosted, is mostly associated with the Pandurra Formation, a 1 km thick fluviatile sandstone unit which contains breccias in its base and top with an average of 4.5 m thickness (Williams and Tonkin, 1985; Preiss, 1987 Lintern, et al., 1998, 2007). Chalcocite is the dominant mineral with some bornite and chalcopyrite also present.

The Windabout shale-hosted mineralisation occurs in the Adelaidean Tapley Hill Formation units (Rattigan, et al., 1977). The mineralogical composition, mostly sulphide, is related to cattle grid style (Rattigan, et al., 1977; Tonkin and Creelman, 1990). The dominant sulphide minerals are pyrite, chalcopyrite and bornite (Porter, 2015). Figure 7.3 is the stylised sections of the Mount Gunson area showing stratigraphy and mineralisation hosts.

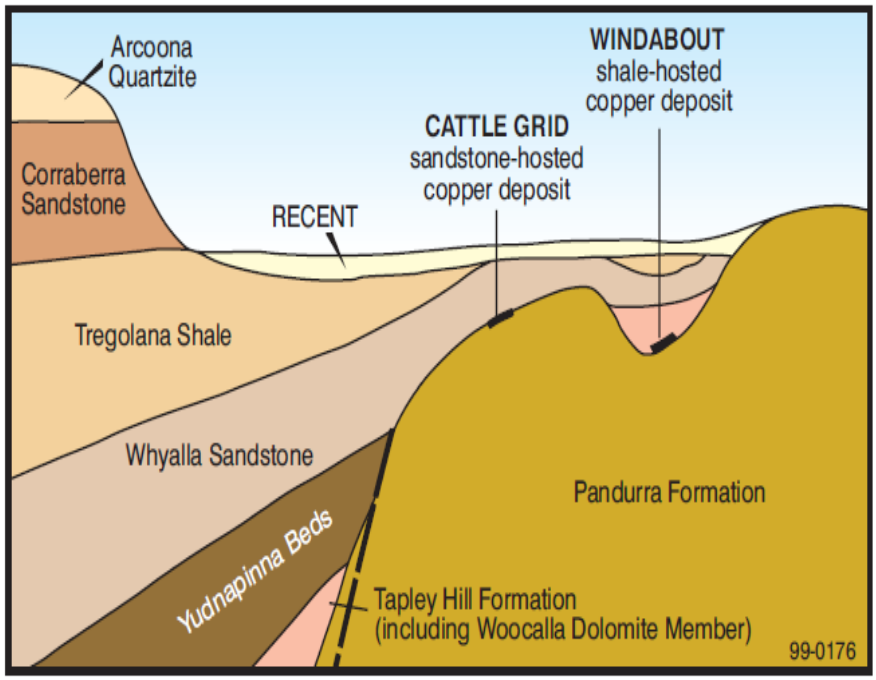

Figure 7.3 Stylised sections of the Mount Gunson area which shows stratigraphic and mineralisation zones (Tonkin and Creelman, 1990).

7.2 Mount Gunson Modelling Experiment

The Mount Gunson deposit has been reported to be detectable by potential field methods (Bampton, 2003). This modelling experiment will therefore focus on the feasibility of using the seismic reflection approach in detecting these thin mineralised lenses at slightly greater depth, where potential field methods cannot be used, but where such deposits would still be economic to develop. The geological cross-section that was modified for the modelling experiment is shown in Figure 7.4. The synthetic geologic model used for the modelling experiment is shown in Figure 7.5.

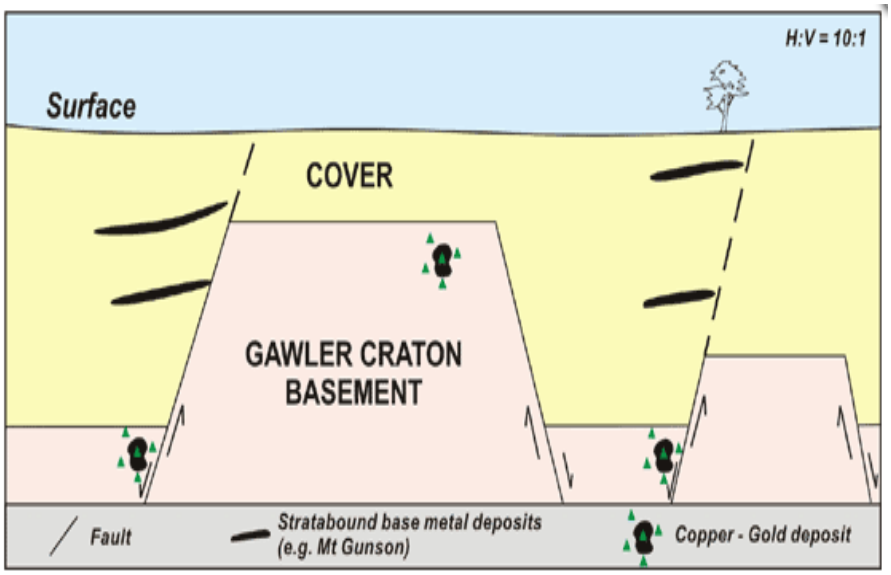

Figure 7.4 Diagrammatic cross-section of the Mount Gunson Copper deposit modified for modelling experiment (after Strandline Resources, 2015). It is actually unlikely that a second deposit would be above the lower one, using the same fluid pathway (fault). When the copper-bearing fluids hit the first redox boundary, most metal would precipitate and leave little else for a higher redox boundary. A higher-level deposit would probably get there via another pathway that does not see the lower redox boundary.

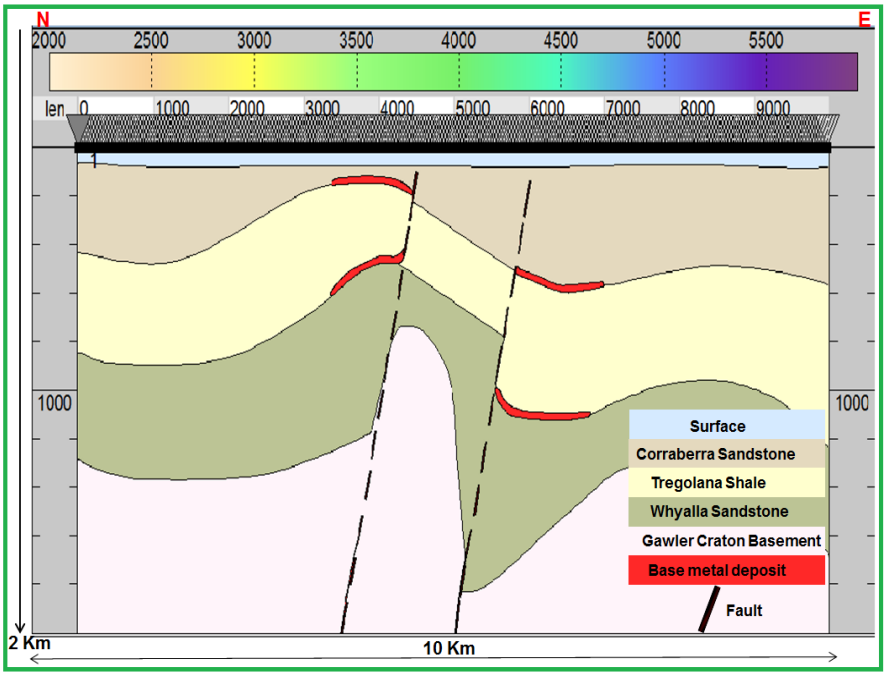

Figure 7.5: Synthetic geological model with inclusions of thin "lenses" of enriched host representing mineralisation.

7.3 Survey Design

The synthetic survey was designed and modelled with survey parameters akin to typical seismic acquisition parameters. This involved 10 km x 2 km synthetic geologic model of which the primary area of focus is situated within the central 2 kilometres of the geological model. The split-spread method was used with the source positioning located at middle of the spread. Data was then taken across the 250 m source shots, simulated at 40 m intervals and a dominant source frequency of a 35 Hz Ricker wavelet. Receivers were spaced at 20 m intervals which produce an offset of 5000 m. Synthetic seismogram was obtained from the modelling using sampling rate of 0.5 ms. Table 7.1 below shows the velocity and density used for the synthetic modelling.

#	Rock Type	Vp (m/s)	Density (Kg/m^3)
a.	Corraberra sandstone	2450	2182
b.	Tregolana Shale	2270	2154
c.	Whyalla sandstone	2640	2245
d.	Gawler craton basement	5560	3630
e.	Base metal deposits	5635	4080
f.	Fault	5074	3520

Table 7.1 Velocity and Density table used to parametrise geological model; these assigned values are based on estimates from the earlier modelling where it is assumed that the breccia-sandstone host are similarly enriched with heavy minerals and that the filling of pores and cracks substantially increased the velocity.

7.4 Null Model

A null geological model was first simulated to observe seismic response assuming there is no mineralisation. Modelling was limited to two layers within the cover sediments and the Gawler Craton basement as the responses at these interfaces have been proven in earlier modelling and as such, values can be confidently assigned. Representative units of the null model seismic responses are shown in Figure 7.6 while seismic response in the absence of mineralisation lenses is shown in Figure 7.7.

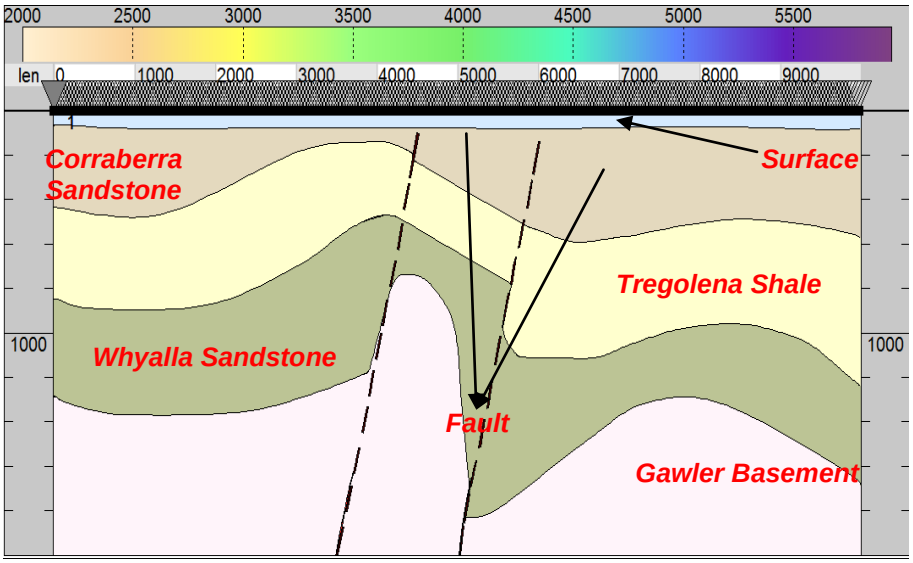

Figure 7.6 A null geological model. Sane layers as used in Figure 7.5 but without mineralization zones.

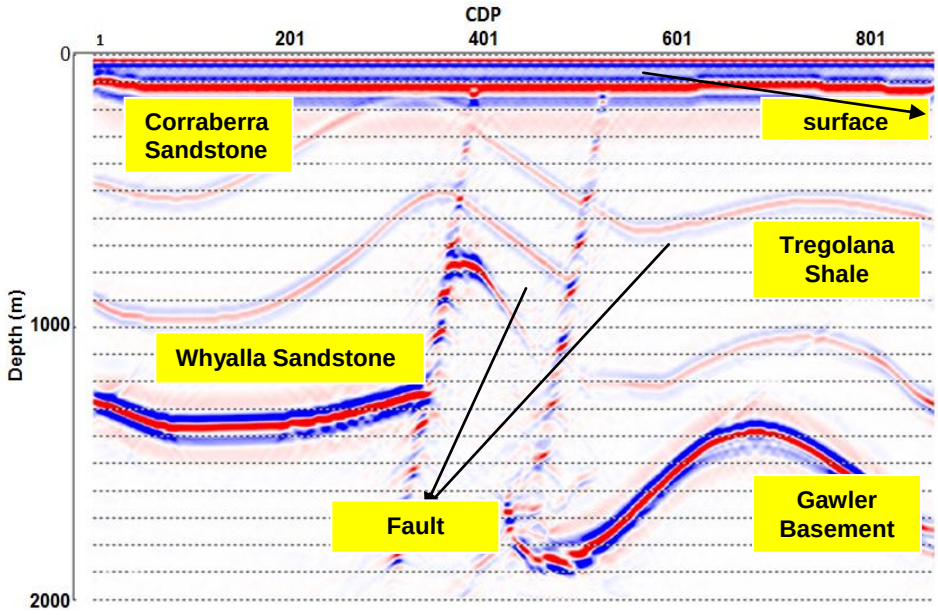

Figure 7.7 Synthetic seismic responses from the null model in the absence of mineralisation lenses. The impedance contrast within the sediment layers (Corraberra sandstone and Tregolana shale) is low compared to the impedance contrast between the Gawler basement and the Whyalla sandstone. The vertical faults above were identified as a result of the fault been imaged by an aligned "noise train" rather than reflection from it.

7.5 Modelling with Mineralised bodies

Different lenses were placed at various positions within the model with first and second lenses located at the boundary between Corraberra sandstone and Tregolana Shale in a flat-lying orientation around 150 m and 450 m depth respectively. The third and fourth zone of alteration lenses was located between Tregolana shale and Whyalla sandstone in similar orientation at around 600 and 1100 m respectively. The last mineralisation lenses were situated within the Gawler Basement. The overall ideal was to demonstrate seismic responses to sulphides filling up the pore spaces in these interfaces at different depth ranges with various mineralisation thicknesses.

Modelling situations representative of different lens thicknesses provides a clue of possible seismic responses with respect to some heavily mineralised ore zones. The input criterion was deduced in line with existing geological knowledge of the area as well as the relationship with Olympic Dam basement geology. As the Mt Gunson deposit was mined out long before any serious studies of the deposits provided petrophysical information, we need to make an educated guess as to the influence of sulphide minerals in the cover formations. For this reason, the various mineralisation lenses have been given a best estimate P-wave of 6052 m/s and density of about 4 kg/m^3. It should be noted that in the absence of noise that almost any contrast in the flatter layers will be faithfully reproduced in imaging and look much the same with a display AGC. Thus, the densities and velocities are not that critical to demonstrate that reflectivity will be detectable.

7.6 Synthetic Data Processing

All synthetic seismograms were generated as shot records, sorted to CMP and fully processed with the methodology discussed in section 2.3.2 using the processing flow in Figure 2.1.

7.7 Results and Discussion

Figure 7.8 is a typical noise-free synthetic shot record for source number 112 displayed from 0–5000 ms while Figure 7.9A shows the expected response from a post-stack depth-migrated section at 20 m thickness within the representative geological model. Responses due to decreasing lens thickness 15 m, 10 m and 5 m respectively, are shown in Figure 7.9B, 7.10A and 7.10B. As the thicknesses are less than ¼ wavelength of the seismic wave, we see that an increase in the thickness of mineralisation lens leads to remarkable surge in amplitude (as the top vs bottom reflections partially cancel). Figure 7.11A–D shows the comparison of responses between 5 m, 10 m 15 m and 20 m lens thicknesses.

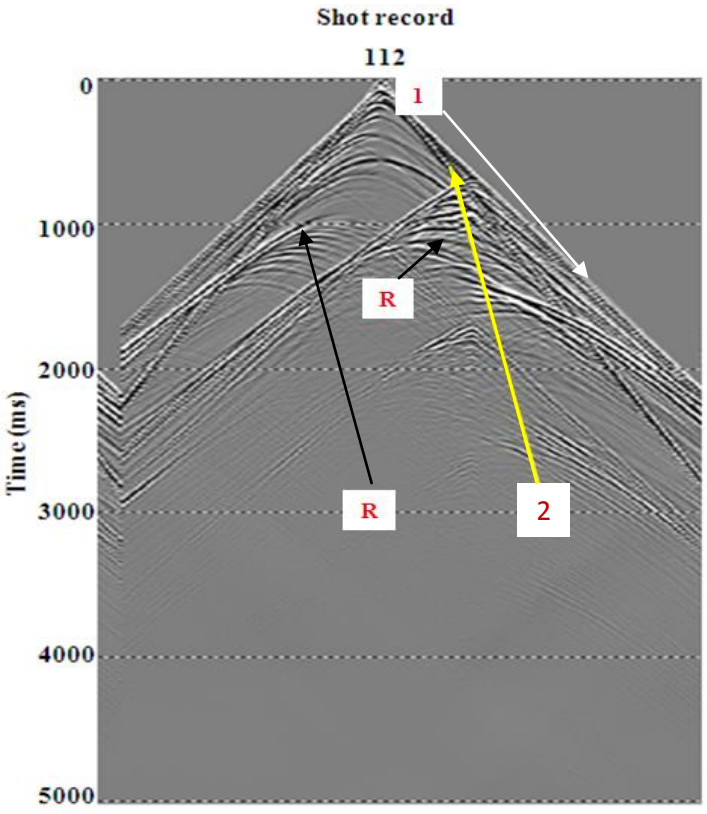

Figure 7.8 Example of a noise-free synthetic shot records for source number 112. The events labeled are: (1) refracted arrival, (2) direct wave and (R) reflected signals. The shots are displayed using true relative amplitude without spherical divergence. Shot gathers were created using a Ricker wavelet source cantered at 35 Hz. Record from 0–5000 ms but reflections event are visible up to 3000 ms.

The two major faults were easily recognised due to the way they disrupt layering, which includes offsets of layers across faults, sudden changes in reflection character, changes in dip and the existence of diffractions via terminated zones.

An important lesson from this modelling experiment using seismic reflection techniques is the potential to image the various lenses at greater depth, which is currently impossible with modern electromagnetic and potential field geophysics Smith, (2010). The modelling results suggests very well, the presence of high reflectivity events that correspond directly to the location of mineralised ore-bodies as well as contact between the Gawler basement and the cover sediments. The presence of these reflectivity events is evident with various modelled lens thicknesses, except for increase in amplitude, which is the only dominant variation.

Existence of flat-lying alteration zones within Carraberra sandstone/Tregolana shale zones responds with reflectivity amplitudes that are clearly delineated as a result of a remarkable increase in amplitudes. Also, despite a relatively thin 5 m thickness; we can still see an anomalous reflection response; however, the amplitude of reflection, even in idealised synthetics, maybe immaterial especially for real-life recognition. Further, addition of some Gaussian noise coupled with the general poor signal-to-noise ratio, which dominates most hard-rock environments, obtaining good imaging from a thin layer might be difficult if not impossible.

At shallower depths <500 m, adequate energy may be returned to the surface so that the likelihood of detecting 5–20 m thick lenses in reality is very promising. Furthermore, since the modelled lens thicknesses are lower than ¼ of the dominant wavelength of the geological model, it is likely unfeasible to map top and bottoms of each zone. Results from the migrated images fully demonstrate this as responses from 5 m, 10 m, 15 m and 20 m alteration zones have similar responses in terms of reflection patterns. The only visible major difference when decreasing alteration thickness is the reflection amplitude.

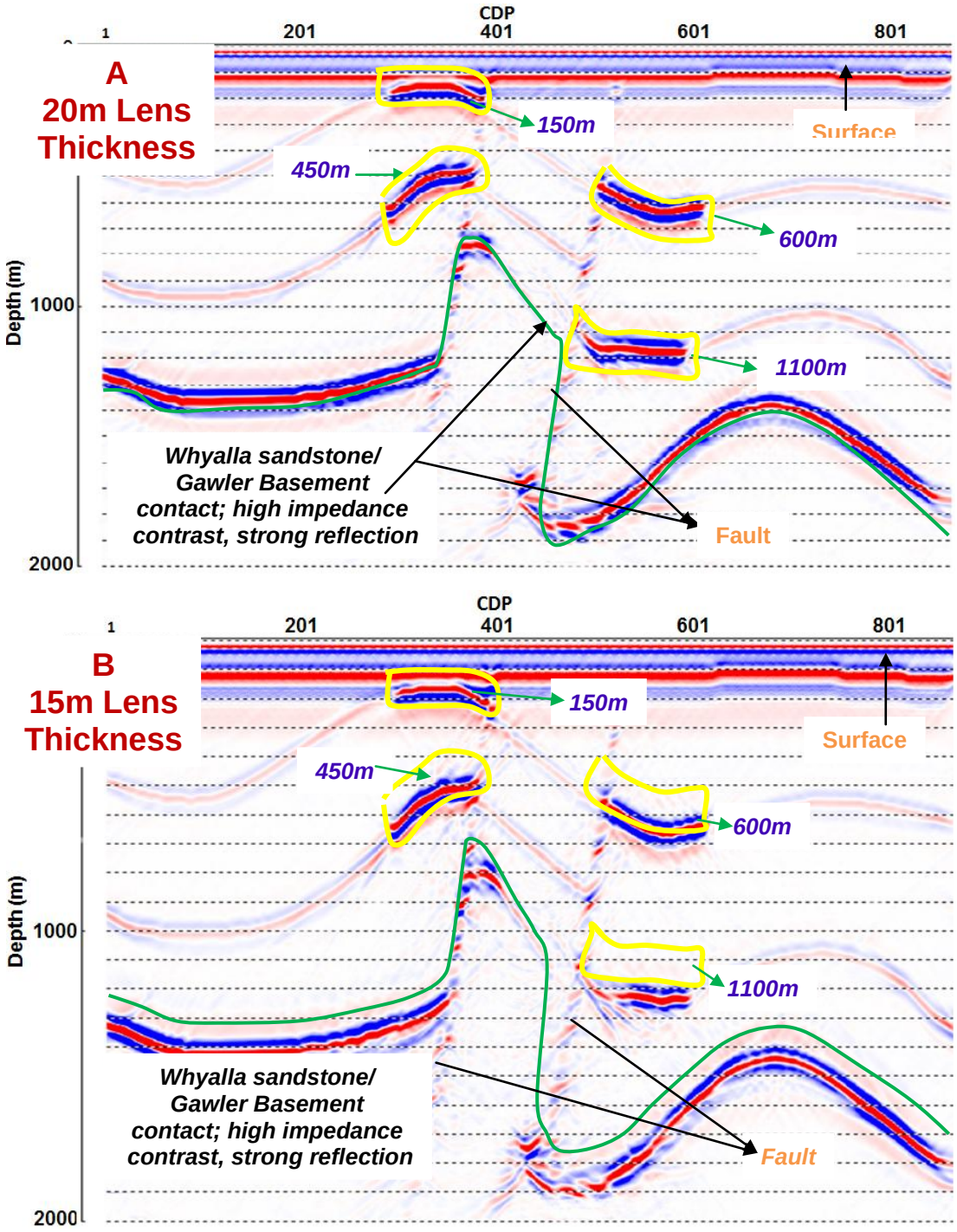

Figure 7.9 Poststack depth-migrated section of the expected response from; A) 20 m thickness; B) 15 m thickness. Seismic responses over the 20 m and 15 m thin lenses are visible. One notable feature with this result is the ability of seismic reflection to maintained resolution even at 1100 m depth. Strong reflection was equally observed between the Gawler basement rock and Whyalla sandstone.

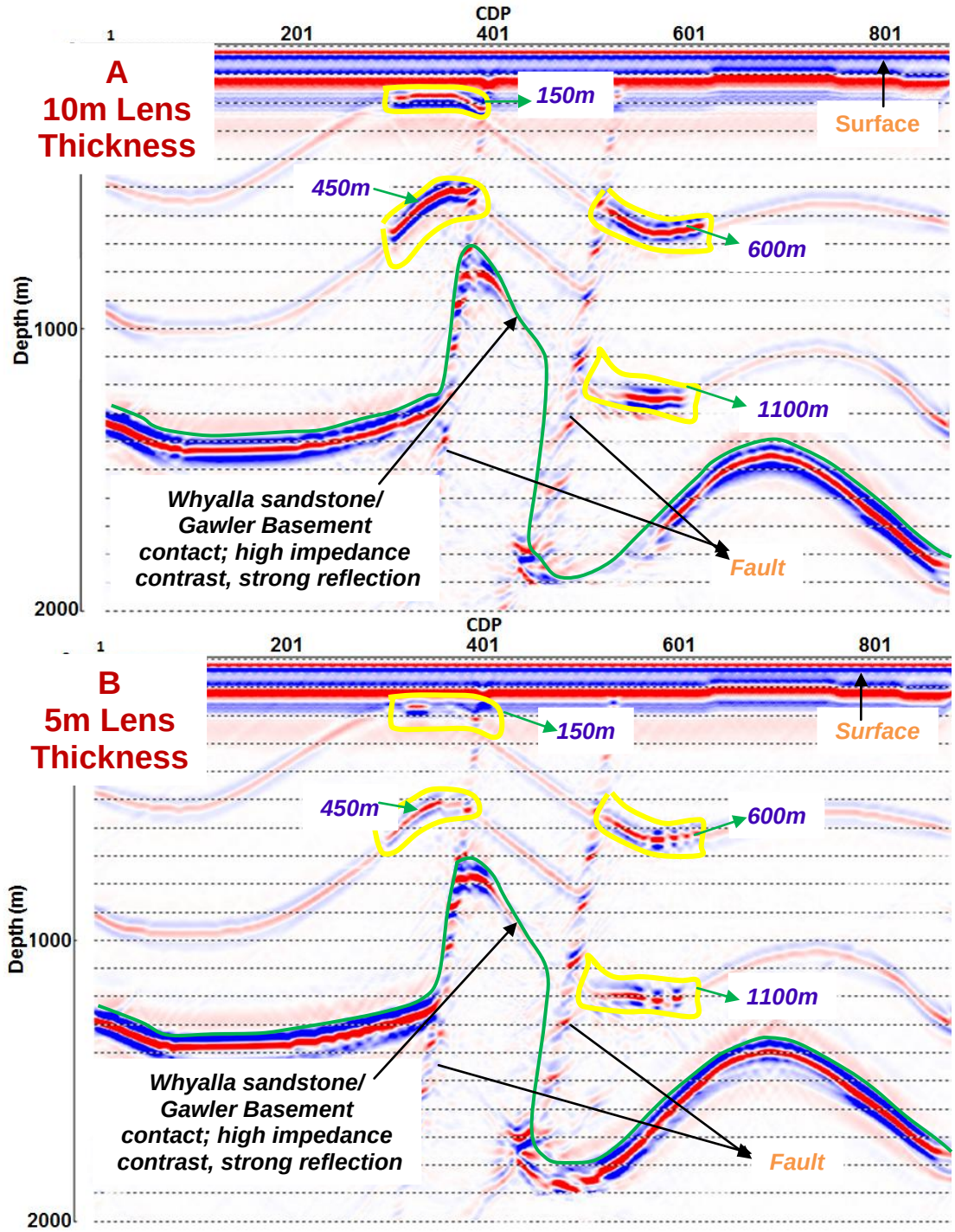

Figure 7.10 Poststack depth-migrated section of the expected response from; A) 10 m thickness; B) 5 m thickness. Though we can see reflection responses over 10 m and 5 m lenses, the amplitude of reflection decreases when compared with the 20 m and 15 m lenses. Overall, the resolution power of seismic reflection is fully demonstrated.

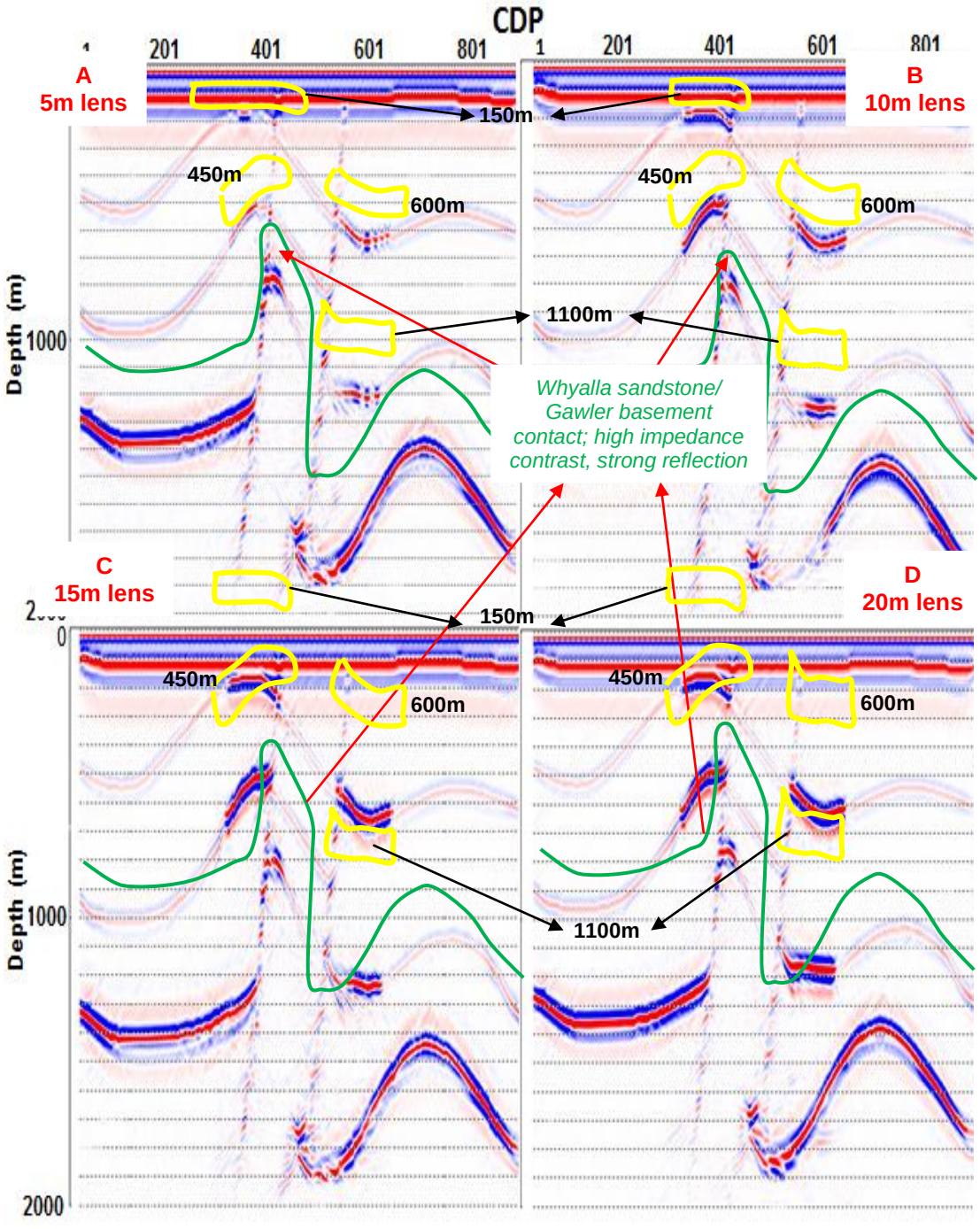

Figure 7.11 Synthetic seismic responses of various lens thicknesses placed at 150 m, 450 m, 600 m and 1100 m respectively; A) response from 5 m lens thickness; B) response from 10 m lens thickness; C) response from 15 m lens thickness and D) response from 20 m lens thickness. An inspection of the various responses above reveals amplitude increases as the only difference.

In order to establish the feasibility of seismic reflection technique assuming noise is present we added 25% Gaussian-noise to the data, which results in noisy data but maintains the same frequency range. Resulting synthetic shot gathers with 25% Gaussian noise is displayed in Figure 7.12. There is a considerable difference when compared to the same seismogram from the same modelling shown in Figure 7.8. The migrated images with a 25% noise level are shown in Figure 7.13–7.14. Images from the noisy data are slightly blurred, especially the various layers within the sediments. However, the contact between the Gawler basement rocks and the sediments cover as well as mineralisation lenses are largely recovered (as in the previous modelling studies).

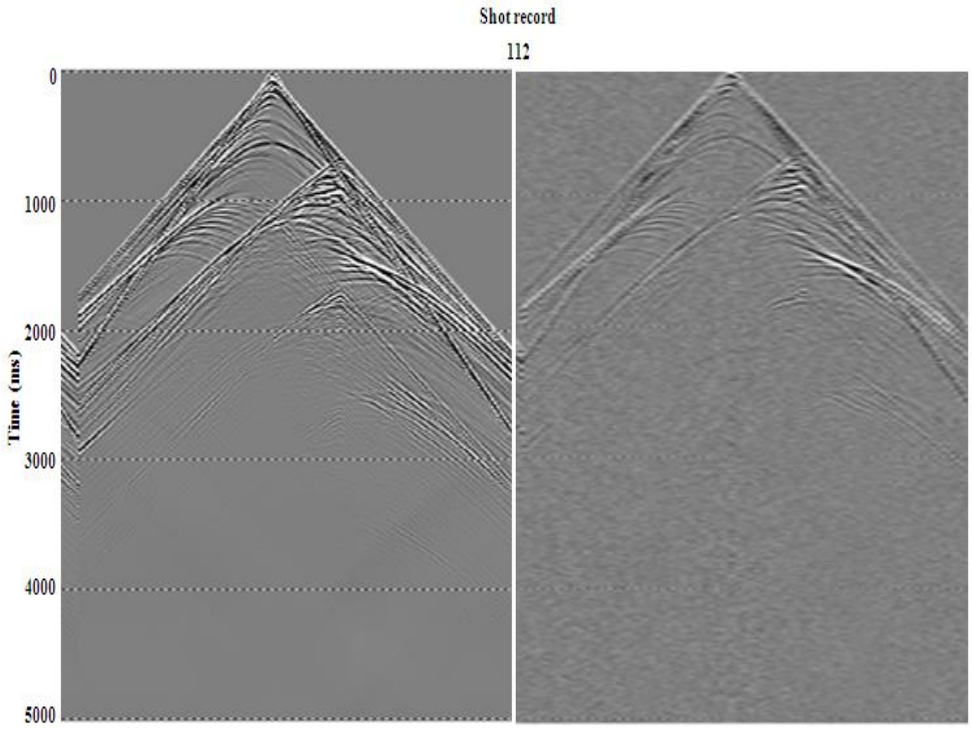

Figure 7.12 Shot record 112: left panel noise free synthetic gather and right panel synthetic gather with 25% Gaussian noise added both for. Weaker reflections are much less visible in the right panel.

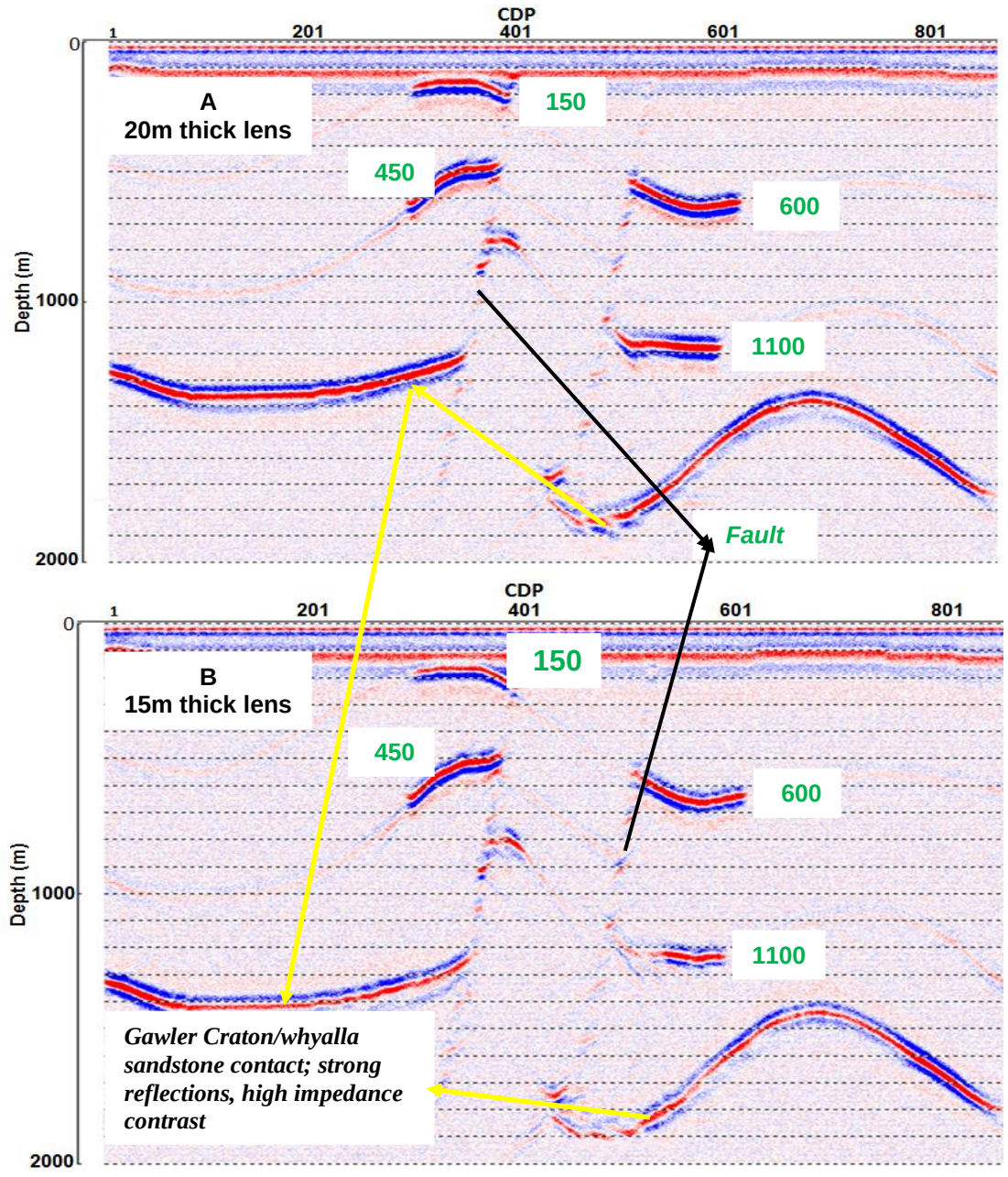

Figure 7.13 Poststack depth-migrated section of the expected response from A) 20 m thickness with 25% Gaussian noise; B) 15 m thickness with 30% Gaussian noise. The mineralisation lenses placed at various depths are visible and well imaged. Also, there is a strong reflection from the Gawler basement/Whyalla sandstone contact as indicated by the yellow arrow.

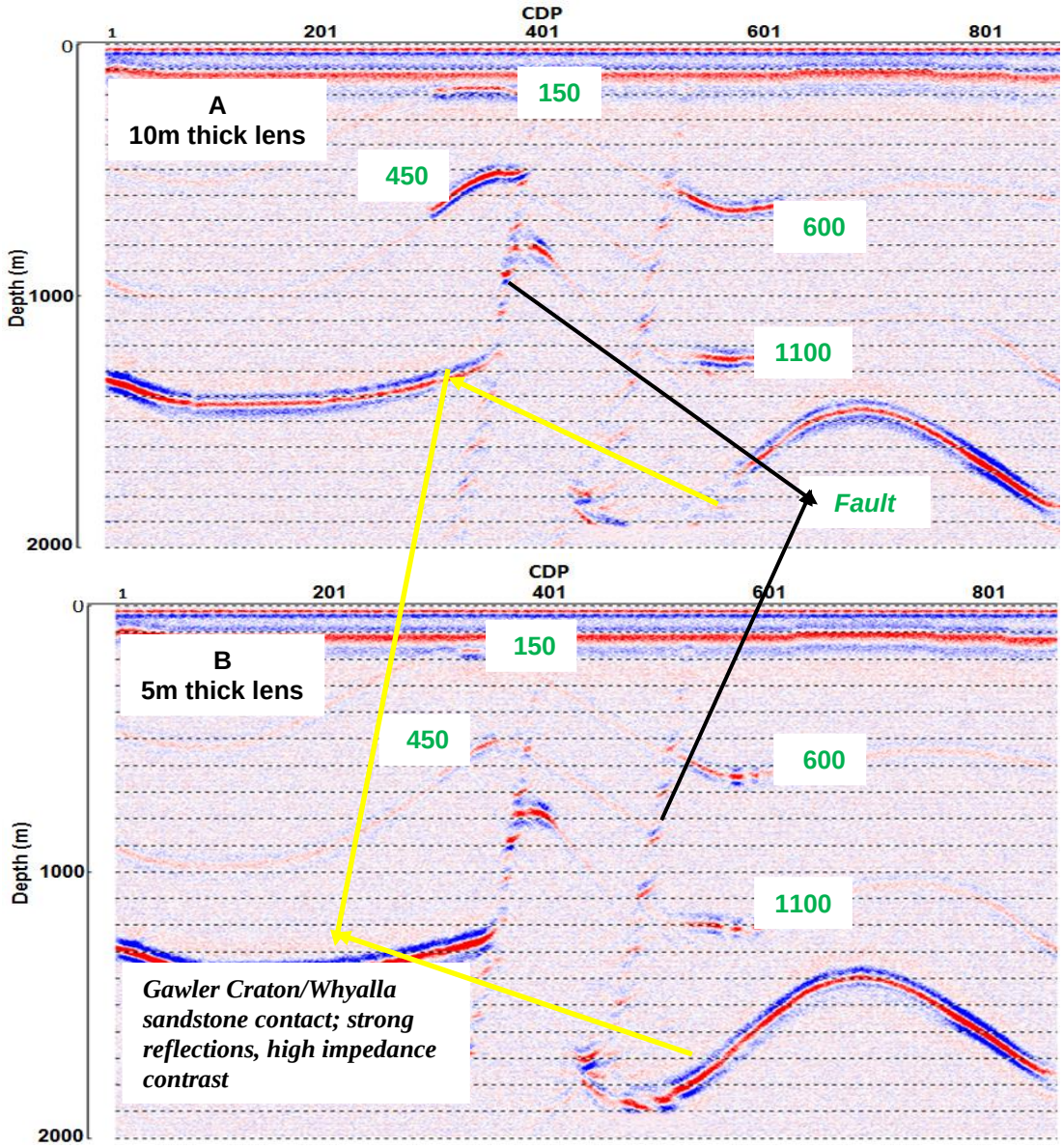

Figure 7.14 Poststack depth-migrated section of the expected response from A) 10 m thickness with 25% Gaussian noise; B) 5 m thickness with 30% random noise. Both the noise free and noisy migrated images obtained at different lens thickness and depths can be seen by comparing Figures 7.13–7.14 with Figures 7.9–7.10. The different lenses from the noise-free model look better and more visible compared to the noisy ones. The addition of 30% Gaussian noise also shows the sediment layers becoming blurred with weak reflections. However, reflections between the Gawler basement rock and the Whyalla sandstone are very strong in both the noise-free and noisy images.

7.8 Conclusion

Results from the Mount Gunson modelling experiment investigate different geological scenarios (the results still confirm that seismic reflection, as an exploration tool, has great potential for the detection of thin, remobilised IOCG mineralisation into the cover sequence. The Mount Gunson example is significantly different from other IOCG deposits in that the mineralisation is likely to be closer to the surface, flat lying, and more regular, as the mineralisation is in the cover sequence. Thus, the signature is expected to be very different compared to typical IOCG deposits. One similar aspect is the need to have a significant fault, lineament, or horst and graben features in the basement rocks to provide a conduit for the mineralisation that will be emplaced into the permeable formations above.

Forward modelling over areas representative of mineralised lenses with varying thickness responded as reflectivity zones, in which the amplitudes rises proportionally with respect to ore-body thickness. Reflectivity events from the zones of interest (lenses placed at different depths) have higher amplitude, as expected, than the local reflections resulting from sediment layers.

The use of seismic reflection surveys to detect a possible copper bearing location in Mount Gunson seems encouraging as lenses with varying thicknesses were largely reproduced. However, lenses of thickness 5 and 10 m responded somewhat weakly as reflectivity events, especially with the addition of Gaussian noise. On balance such thin mineralised zones are not likely to be detectable. Reflectivity over these responses is still subtle and taking into account problems involved especially poor signal-to-noise ratios makes the application of seismic for direct detection of ore deposits difficult. Conversely, with good survey design and seismic processing, we may be able to explore for this style of deposit, which has been largely overlooked in the exploration for large sediment copper near lineaments and intrusives.

8 Seismic Reflection Surveys – Cost Effective tool for Exploration?

8.1 Introduction

Appreciating seismic reflection techniques in a hard-rock environment and to consider the role it might play in the exploration chain, both technical and economic feasibility studies are required. We have so far technically demonstrated that IOCG deposits have distinctive seismic signatures and that seismic reflection surveys could be used for greenfield exploration campaigns, where deposits may be located within 10–50 k. Results from our seismic modelling experiments using different acquisition parameters suggest that seismic reflection surveys using relatively sparse source-receiver spacing can detect the intrusive structure hosting mineralisation, as was in the case of the Hillside copper deposit as well as the low reflectivity zone in the Olympic Dam case studies.

The success of seismic reflection surveys in hard-rock terrains cannot be fully appreciated by investors and explorers without analysing its cost effectiveness. Cost of a 3D surveys largely depends on many factors such as the shot density and size of the source area, required resolution to correctly delineate the area of interest (target), nature of the seismic source needed to map the target, condition of the surface and level of access permissible within the site (Joey, 1999). Furthermore, the quantity of available information with respect to the site and the ability to access such information can equally have a direct effect on the survey cost. For instance, a survey aimed at delineating shallower features, will require a very dense array and hence will be more capital intensive to process when compared to survey aimed at mapping deeper features. Also, as the resolution needed for surveys increases, the cost of processing equally increases.

In this section, we look at the economic feasibility of using seismic surveys by doing some basic cost analysis of carrying out seismic surveys in realistic situations.

The area around Olympic Dam is an excellent example of a prospective area, with many deposits within a 50 km radius (Figure 8.1). A regional 3D survey would likely discover other IOCG deposits that have poor or indistinct potential field signatures and map mineral bearing structures to surface. Thus, we look at a 1000 square km (20 km EW and 50 km NS) seismic survey with "sparse" survey geometry for reconnaissance exploration and targeting. The Omni 3D survey planning tool from Schlumberger (formerly Gedco) was used to create a survey plan and evaluate the anticipated illumination. The survey assumed up to 2000 receiver stations would be active; thus, about 3000 receivers would need to be deployed to have spares for pick-up and placement in preparation for rolling of the active spread.

Figure 8.1 A satellite photo of a Camp-scale area around Olympic Dam, approximately 3000 sq km of area to explore. There are at least four known IOGC deposits within the central corridor: Olympic Dam, Vulcan, Acropolis, and Wirda Well.

The Omni survey design "wizard" tool was used to optimise the design using 2000 active recording channel and an orthogonal survey layout. The active patch pattern used 50 m geophone intervals with 200 m line spacing and 50 m shot intervals with 2590 m line intervals.

Such a design produces perfectly even fold (effectively illumination) at 1500 m of depth (Figure 8.2). However, this is quite deep to economically develop such a deposit. The fold picture at an 800 m depth, which is still deep for low-grade deposits, is not as good. The fold has dropped to half of the deeper values (less than 50) and starts to show source-receiver footprint patterns. Thus the illumination of targets starts to become uneven (Figure 8.3).

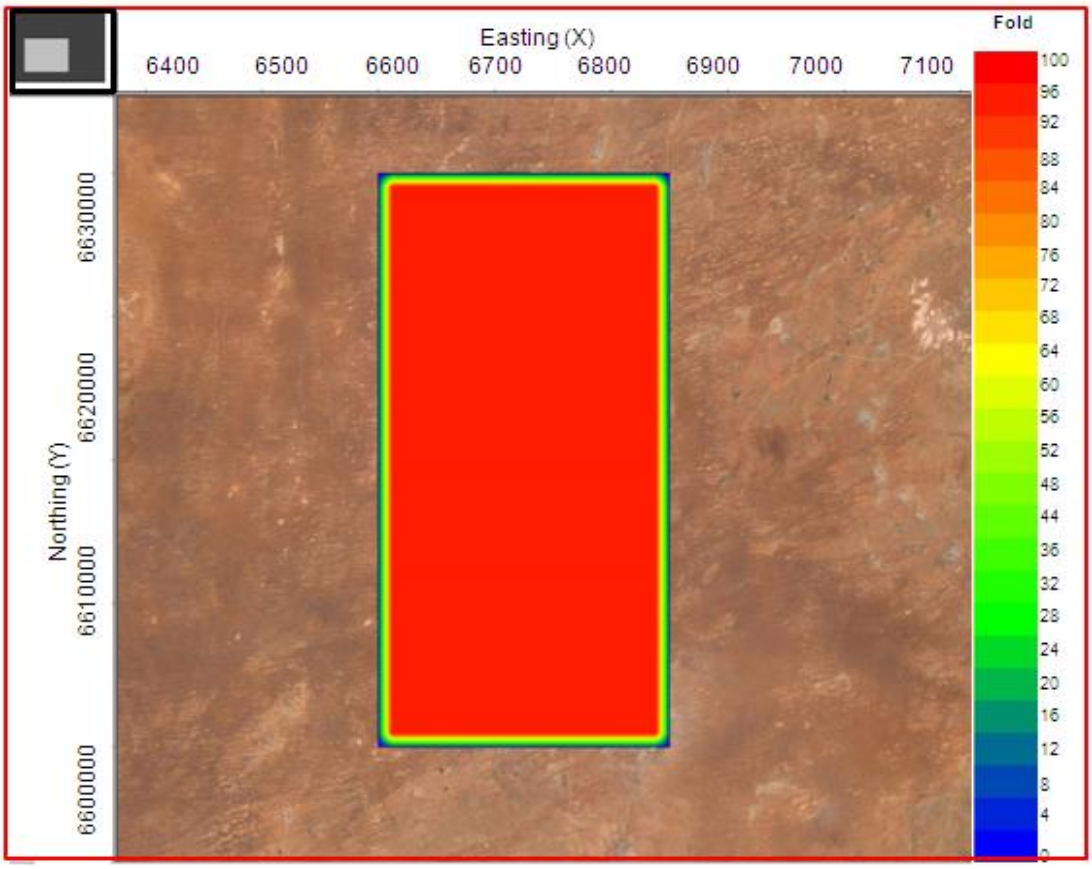

Figure 8.2 The field map at 1500 m depth overlain on a satellite photo of the area around Olympic Dam. Approximately 1000 sq. km of area is covered by the survey that uses an orthogonal design with survey geometries typical of many petroleum exploration surveys.

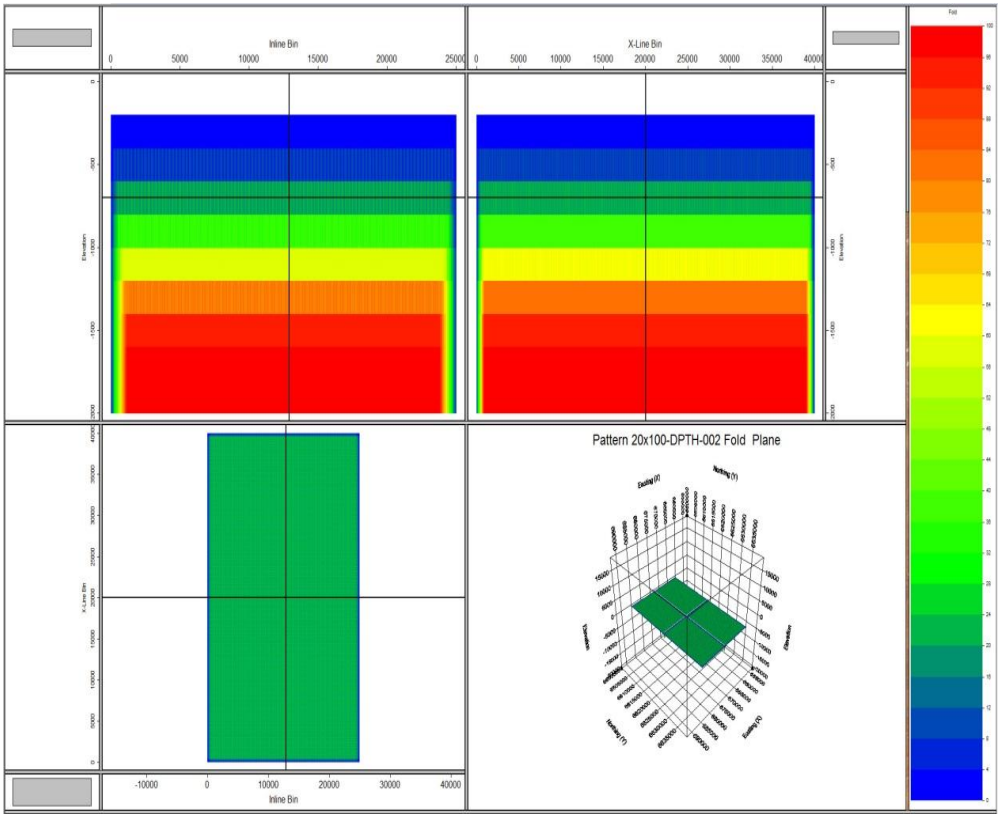

Figure 8.3 A picture from the Omni 3D survey design tool showing fold with depth and position. The fold at 1500 m depth is approximately 100, which is reasonably high. However, near the surface at 500 m the blue-green colours indicate that fold is less than 20, which is poor for low signal-to-noise environments such as complex structures in crystalline rock.

In the case of imaging targets shallower than 500 m, the wide angle reflections are significantly cut off by NMO stretch (set to 40%). So the final seismic image quality will likely fall off quickly close to the surface. If there is 500 m of overlying sediments, then this may not pose a significant problem. However, this simple illustration demonstrates that blanket coverage with higher receiver and source density precludes seismic surveys for regional exploration. The targets need to be big and deep to make the exercise worthwhile. It is estimated that this survey design would cost approximately A$8M to conduct over several months. To ensure that IOCG targets are not missed at 200–500 m would likely quadruple the cost to A$25M.

If large 3D surveys are too expensive to cover the upper 500 m reliably, then an option is to perform many smaller 2D or 3D surveys over the regionally significant structures identified by magnetics, gravity and possibly bedrock geochemistry. Below are estimates of smaller survey costs in Australia compared to grid drilling on a 10 x 10 square km area (100 square km):

8.2: Drilling Cost Analysis

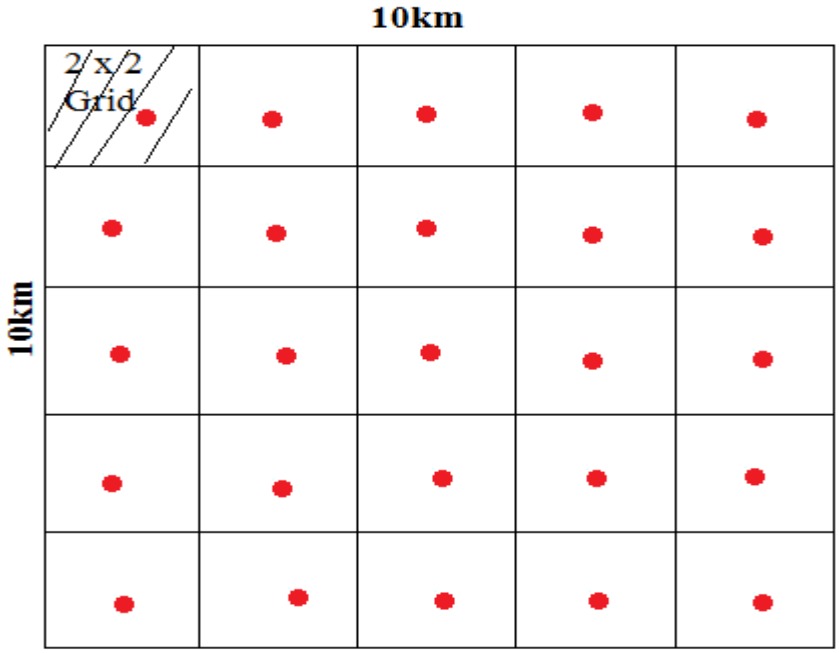

Table 8.1 A very sparse 10x10 km Grid Design.

No of holes in each grid of 2x2	=	1
Total no of holes in the entire area	=	25
Depth of drilling	=	500 m
Cost of drilling per meter	=	$200

Total cost of drilling to 500 m depth
25*500*200
$2,500,000.00

Representative costs of 2D and 3D surveys that are able to reliably detect IOCG deposits are used based upon the modelling results in Chapters 4 to 7.

Item	2D Seismic Survey	3D Seismic Survey	Drilling to 500m
	10 km at 15 m spacing 10 lines x 1 km apart	100 Shots/sq km 2000 receivers	100 sq km area 25 x 500m drill-holes
	$442,000	$870,000	$2,500,000

Table 8.2 2D/3D Survey cost vs Drilling cost

A basic cost analysis of a typical 10x10 square km area with 2D seismic surveys program will cost as low as $5k/km^2 (with large line separation though) while a sparse 3D survey with 100 shots per sq km, which is reasonable for IOCG exploration, would cost as low as $9k/km^2. Whereas, a drilling program with the same coverage using 25 drill holes on a 100 sq km area could cost up to $25k/km^2 or more for a depth range of only 500 m, barely penetrating the cover in many cases. Apart from seismic surveys being able to screen multiple km^3 and provide a framework for subsequent exploration, it is less time consuming compared to drilling. Rationally, seismic seems to win easily with any economic argument, 2D or 3D.

Presently, mining activities globally are shifting to underground following the structures of earlier diggings, as this is more cost effective than finding new deposits. However, the obstacle is for explorers and decision makers is to trust that the seismic reflection surveys will work. All of the above analysis indicates that seismic surveys will definitely complement other traditional methods to uncover deep-seated deposits and improve targeting, plus reduce the risk of missing targets associated with drilling.

Concluding Remarks

Discovering IOCG deposits will remain a challenge to explorationists due to their extraordinary variety of styles and extensive but typically unrecognised footprint as well as the structural complexity of the regolith typical in a hard-rock environment in Australia. In the Gawler Craton, the 'easy' and nearby deposits are already discovered and exploited, and current discoveries are under moderate to thick cover with weak geophysical or geochemical signatures. As potential field methods have limitations in terms of resolution (only very useful for mapping shallow targets, from a 0–500 m depth), there is not much hope to discover new IOCG deposits using the same methods as used in the last 40 years. Thus, the traditional approaches to finding IOCG deposits in the Gawler Craton are becoming less effective and more expensive, requiring alternative methods to be utilised in exploration.

The seismic reflection method represents this "new technology" as it offers many distinct advantages over other geophysical techniques due to the depth of penetration and superior spatial resolution. In many different geological terrains, seismic methods provide "3D mapability and/or detectability" of units within the stratigraphic column. The iron-rich rocks plus mineralising sulphides in IOCG deposits provide both a density and elastic change over the host rocks. Generally the IOCG deposits are made of materials that have higher acoustic impedance than the host rocks. Thus, IOCG deposits should be identifiable by their seismic impedance changes causing reflection and scattering of seismic waves. Overall, IOCG deposits are likely to show a distinctly different reflection character from the surrounding barren rocks. In addition, as most IOCG deposits tend to be concentrated around major structural lineaments, seismic reflection methods provide a structural model signature for interpreters to check in stacked images. Distinctive intrusive imprints over earlier units are a sign that there might be mineralisation. Both Olympic Dam and Vulcan have such overprints of existing geology in both real and modelled data. In the case of Olympic Dam it is a dense, complex package into barren featureless

granite. With Vulcan the Fe- and sulphide-rich mineral emplacement "mutes" the reflection signatures of older metasediments near a major lineament.

Regional Seismic Reflection Surveys for Exploration of IOCG Deposits

The comprehensive modelling experiments at the Hillside mine site, Olympic Dam and Vulcan reveals that seismic reflection surveys can be used to detect the presence of IOCG at many scales and in different geological settings. In the Hillside modelling experiment (Chapter 4) for instance, we could see the various contacts from the depth-converted migrated sections. Reflections from various lithological contacts and the lack of reflections from the edges of intrusions are identifiable when compared with the geological model. Expectedly, a close relationship of the depth-converted, migrated images with the geological models is seen and this is also the case when examining real 2D and 3D seismic surveys over these IOCG deposits. Even with relatively sparse acquisition parameters (80 m source spacing and 40 m receivers spacing), one can still see the various lithological boundaries. These are remarkable feats in that the top of the mineralisation deposits range from close to the surface at 30 m to 1000 m.

Results from Olympic Dam modelling experiments (Chapter 5), tested with different survey parameters at varying depths of 350 m; 750 m and 1000 m burial were very encouraging as it has further demonstrated that the seismic reflection method provides continuous detailed images of structures while maintaining resolution at depth. Reflections due to acoustic impedance (density x velocity) changes across contacts between fragmentals and lavas within the hematite rich breccia and clasts are also visible. Also, similarity between the idealised noise-free numerical data and sparse deep crustal real data can be observed in terms of reflection patterns within and outside the intrusive blocks. In the Vulcan modelling experiment (Chapter 6), changes in the reflection character in the migrated section are visible around the granitic basement and indicate that a mineralised zone is possible. There is no discernible difference in the results from different acquisition parameters, which

suggest that even with 100 m source spacing and 50 m receivers spacing, it would be feasible to image the intrusive related structures at the depths of Vulcan (1000 m).

One of the major short comings of these modelling experiments is the 3D effects that cannot be seen in 2D data. Because modelling and processing techniques are two-dimensional; the data coming out of the plane on the 2D profiles as well as the structures will be seen on all profiles that are larger than the required window. This will have effect on the Fresnel Zone due to contraction or reduction in one dimension but will still extend its full width perpendicular to the line.

Detection of IOCG Signatures: Geophysical methods, Geological mapping, or a combination?

Traditionally, discoveries of IOCG deposits are largely based upon potential field data (magnetics and gravity) and early success is then proven by drilling a grid of straight parallel holes. Though this method seems very effective, it however does not have the needed lateral and depth resolution to effectively understand deeper mineral deposits; particularly where thick cover is present. Also, over-reliance on these methods to identify drilling targets limits success as we don't know what deposits may have been missed by the absence of detectable magnetic and gravity responses.

In the case of the Hillside deposit (Chapter 4) mineralised lenses extend almost to the surface (<70 m); hence, it was feasible to detect it in the past using magnetic method. However, we anticipate that when the mineralised package is 250 m and deeper, the magnetic response might become ambiguous, or practically absent whereas seismic reflection techniques are largely able to detect the deposit. To test our prediction we apply upward continuation filters to the residual magnetics maps at Hillside. As expected, good magnetic responses was recorded for shallow mineralisation while smeared or indistinct responses was produced by deeper mineralisation with thicker cover, which suggests that magnetic method can only be effective for shallow investigations (0–500 m depths).

The ability of the seismic method to resolve targets at greater depths means not only the possibility to detect the alteration associated with mineralisation, but the possibility to detect the faults and former fluid conduits that enable the mineralisation. Both the Hillside and Mt Gunson modelling experiments show that the prospective faults for mineralisation are interpretable. Additionally, the GA data collected over the Vulcan deposit clearly shows both the prospective intrusive packages with iron-rich minerals and the main contact between older metasediments and the large granitic intrusion that helped the mineralisation reached surface. By detecting and correctly interpreting these geological features the risk of drilling false anomalies will be significantly reduced.

Seismic reflection surveys were also used to detect mineralisation with minimum thickness as low as 5 m (Chapter 7) in the Mt Gunson exercise. Forward modelling over areas representative of mineralised lenses with varying thickness responded as reflectivity zones, in which the amplitudes rises proportionally with respect to ore-body thickness. Reflectivity events from the zones of interest (lenses/zones placed at different depths) have higher amplitude than the local reflections resulting from sediment layers. A fairly high contrast was used in the Mt Gunson example, but it does illustrate that a good economic deposit is easily mapped with seismic reflection.

The major short comings of the seismic method in all the case studies are that it cannot be used (or appears to be very challenging) directly to image the individual structures within the intrusive blocks due to scattering. Further, the impedance contrast and reflection coefficients between most common igneous and metamorphic rocks and SNR ratio are low, thus making it difficult to delineate small scale complex structures in the host rock. Also, due to the small size of most deposits usually (often much less than 1 km), they tend to appear as diffraction patterns stacked instead of continuous reflection on seismic profiling, which is difficult to relate to structure but easy to notice when anomalous. However, the above statements are much more restrictive for all other widely used geophysical methods. Thus, while seismic is bad in many ways, it is better than all the other alternatives.

The results of the modelling studies and comparative analysis with available field data suggest that regional seismic surveys could be useful in detecting IOCG deposits.

Is the Combination of Potential, Drilling and Seismic Methods the best approach?

Geophysical surveys can be of great assistance in the early exploration stage. Their purpose is essentially to cut down the cost of exploration by limiting drilling to favourable targets. No geophysical survey (potential and seismic) can give results of the type commonly claimed for drilling and coring. A favourable indication obtained by means of a geophysical has no economic value until it has been tested by drilling. Geological surveys may identify a favourable structure or geological horizons, but this may be so large as to require an extensive drilling program to prospect it completely. Petrophysical analysis provides suitable information for modelling geophysical responses and assisting in depth conversion of the seismic data. Other than these, petrophysics plays a minor role in exploration. Any analysis of drill-hole data is restricted as each hole tests a small area and provides a limited context for further exploration. Thus, a combination of potential field methods constrained by seismic data, geological and petrophysical analysis may be the solution for exploration of mineral deposits in hard-rock terrain. Particularly, it will help in mapping contacts and structures while maintaining resolution at depth.

Cost effective seismic reflection and its role in exploration

One of the most limiting aspects for adoption of seismic reflection surveys for mineral exploration is the cost effectiveness and this is partially answered in Chapter 8, where the costs of different seismic survey programs were estimated and compared with the cost of grid-drilling for better decision making by investors and explorers at the very beginning of exploration. A typical seismic survey program can cost as low as \$150k/km^2 as opposed to drilling, which can cost at least \$300k/km^2, but often much more depending on the target and depth. Drilling in exploration is popular as it produces familiar data and only costs a little at a time. However, it is

like a bank loan taken over many years: the total paid over time becomes very large. To cover an effective volume requires much more drilling than wide-spaced grids where a whole deposit can sit between the holes. Each seismic survey screens multiple km^3 of volume, with no missing bits in between, and can also provide a framework for subsequent exploration. It is also less time consuming as 10–30 km^2 areas of data can be acquired and processed in 3 months. Explorers with large lease holdings should seriously consider blanket seismic reflection surveys to properly survey their holdings to save in the longer term with more efficient exploration.

From the results of numerous modelling experiments conducted in conjunction with the analysis of the existing seismic data, I am convinced that seismic reflection techniques can play significant role in the entire exploration package. In particular, a seismic reflection survey can provide additional information for modelling by defining the location of geological structures such as faults; especially as we have no idea as to what deposits have been missed due to the absence of detectable magnetic and gravity responses. Seismic surveys will further provide information with respect to the bedding in sedimentary formations plus the exact location of target deposits. Such a role, when complimented with a drilling program, will significantly lower the technical risk associated with drilling anomalies.

Future Work and Recommendations

Obtaining seismic signatures that are truly representative of subsurface geological structures is fundamental for successful mineral exploration. However, since seismic reflection techniques are still an emerging technology in hard-rock environments and the general complicity of the regolith, the suggestions for future research are stated below:

- Feasibility of using regional seismic reflection surveys to detect IOCG deposits was investigated using 2D synthetic models largely because the existing models and data were 2D. However, 2D seismic is not suited to image properly the highly three dimensional geology. This issue may be

addressed in different ways but the question of economic remains. For example further extension of studies of IOCG deposits might consider the use of multi-component seismology. How to best utilise the potential of such methods remains to be investigated.

- 3D geological models and better petrophysical data would allow for creation of more realistic synthetic seismograms that could be used to optimise survey design and refine the processing flow for 3D data.

- The geology of the study area (Gawler Craton) is highly complicated and 2D and perhaps not even 3D surface seismic may not image the individual structures within the intrusive block or package. VSP and crosshole surveys may be considered for that purpose. Borehole tomography may be used as to study internal structures or provide high quality velocity model for subsequent imaging. Such approach could help resource definition and mine planning.

- Exploration should plan to begin with the seismic reflection method especially as exploration for mineral deposits shift towards being located under deep cover. To use seismic reflection surveys only at a late stage of mineral exploration process when all other investigation techniques (potential, geology and petrophysical) have failed should be discouraged as we do not know what deposits may have been missed by the absence of detectable magnetic and gravity responses.

References

Adam, E., G. Perron, B. Milkereit, J. Wu, A. Calvert, M. Salisbury, P. Verpaelst, and D.-J. Dion, 2000, A review of high-resolution seismic profiling across the Sudbury, Selbaie, Noranda, and Matagami mining camps: Canadian Journal of Earth Sciences, **37**, (2–3): 503–516.

Adshead-Bell, N. D., P. Voulgaris, and V. N. Muscio, 1998, Osborne copper-gold deposit: in Berkman, D.A., and D. H. Mackenzie, ed., Geology of Australian and Papua New Guinea.

Aki, K.T., and P. G. Richards, 1980, Quantitative Seismology: Theory and Methods: **1**, W.H. Freeman and Co.

Aldam Geoscience, 2014, Hydrogeological Summary Report of Hillside Project: 19–23.

Allen, S. R., J. McPhie, G. Ferris, and C. Simpson, 2008, Evolution and architecture of a large felsic igneous province in western Laurentia: The 1.6 Ga Gawler Range Volcanics, South Australia: Journal of Volcanology and Geothermal Research, **172**, 132–147, doi:10.1016/j.jvolgeores.2005.09.027.

Alterman, Z. S., and F. C. Karal, 1968, Propagation of elastic waves in layered media by finite-difference methods: Bulletin of the Seismological Society of America, **58**, 367–398.

Anderson, N., and S. Cardimona, 2000, Forward seismic modelling: the key to understanding reflection seismic and Ground Penetrating Radar (GPR) techniques: Geophysics, **11-15**.

Australia's Identified Mineral Resources (AIMR) 2013: http://www.australianminesatlas.gov.au/aimr/index.html

Baker, T., and W. P. Laing, 1998, Eloise Cu-Au deposit, east Mt Isa Block: structural environment and structural controls on ore: Australian Journal of Earth Sciences, **45**, 429–444.

Barton, M. D., and D. A. Johnson, 1996, Evaporitic-source model for igneous-related Fe oxide-(REE-Cu-Au-U) mineralization: Geology (Boulder), **24**, 259–262.

Barton, M. D., and D. A. Johnson, 2004, Footprints of Fe-oxide (-Cu-Au) systems: SEG 2004 Predictive Mineral Discovery Under Cover – Extended Abstracts: Centre for Global Metallogeny, The University of Western Australia, **33**, 112–116.

Betts, P. G., and D. Giles, 2006, The 1800–1100 Ma tectonic evolution of Australia: Precambrian Research, **144**, 92–125.

Birch, F., 1961, The velocity of compressional waves in rocks to 10 kilobars, part 2: Journal of Geophysical Research, **66**, 2199–2224.

Boerner, D. E., and B. Milkereit, 1999, Structural evolution of the Sudbury impact structure in the light of seismic reflection data. Impact cratering and Planetary Evolution II, Boulder Colorado: Dressler, B., ed., and V. L. Sharpton, Geological Society of America, Special Paper, **339**, 419–430.

Bortfeld, R., 1961, Approximations to the Reflection and Transmission Coefficients of Plane Longitudinal and Transverse waves: Geophysical Prospecting, **9**, 485–502.

Campbell, G, 1994, Geophysical contributions to mine development planning—a risk reduction approach: XVth CMMI Congress, South African Institute of Mining & Metallurgy, **3**, 283–325.

Carcione, J. M., G. C. Herman, and A. P. E. Kroode, 2002, Seismic modelling: Geophysics, **67**, no. 4, 1304–1325.

Claerbout, J. F., 1971, Toward a unified theory of reflector mapping: Geophysics, **36**, 467–481.

C. E. Wadea, A. J. Reida, M. T. D. Wingateb, E. A. Jagodzinskia, and K. Barovichc, 2012, Geochemistry and geochronology of the c. 1585 Ma Benagerie Volcanic Suite, southern Australia: Relationship to the Gawler Range Volcanics and implications for the petrogenesis of a Mesoproterozoic silicic large igneous province Precambia Research: Precambrian Research 206–207, 17–35.

Conor, C., O. Raymond, T. Baker, G. Teale, P. Say, and G. Lowe, G, 2010, Alteration and mineralisation in the Moonta-Wallaroo Cu–Au mining field region, Olympic domain, South Australia: Hydrothermal Iron Oxide Copper–Gold and Related Deposits: A Global Perspective, **3**, 1–24.

Corriveau, L., 2005, Iron Oxide Copper -Gold (±AG ±NB ±P ±REE ±U) Deposits: A Canadian Perspective: Natural Resources Canada, Geological Survey of Canada.

Creaser, R. A. 1989, The geology and petrology of middle Proterozoic felsic magmatism of the Stuart Shelf, South Australia: La Trobe University, unpublished PhD thesis, 434.

Creaser, R. A., and J. A. Cooper, 1993, U-Pb geo-chronology of middle Proterozoic felsic magmatism surrounding the Olympic Dam Cu-Au-U-Ag and Moonta Cu-Au-Ag deposits, South Australia: Economic Geology and the Bulletin of the Society of Economic Geologists, **88**, 186–197, doi:10.2113/gsecongeo.88.1.186.

Creaser, R. A., 1996, Petrogenesis of a Mesoproterozoic quartz latite-granitoid suite from the Roxby Downs area:, South Australia: Precambrian Research, **79**, 371–394.

Creelman, R. A., 2005, Pernatty Lagoon-Mount Gunson Cu Deposits, South Australia.

Daly, S. J., and C. M. Fanning, 1993, Archaean, In: Drexel, J. F., Preiss, W. V. and Parker, A.J. (Eds), the Geology of South Australia, The Precambrian, **1**.

Daly, S. J., Fanning, and M. C. Fairclough, 1998, Tectonic evolution and exploration potential of the Gawler Craton, South Australia: AGSO Journal of Australian Geology & Geophysics, **17**, 145–168.

De Jong, G., and P. J. Williams, 1995, Giant Metasomatic System Formed During Exhumation of Midcrustal Proterozoic Rocks in the Vicinity of the Cloncurry Fault, Northwest Queensland: Australian Journal of Earth Sciences, **42**, 281–290.

De Wet, J. A. J., and D. A. Hall, 1994, Interpretation of the Oryx 3D Seismic Sur vey: in Anhaeusser, C.R., ed., Proc. XVth CMMI Congress: SAIMM Symposium Series S14, 3, 259–270.

Dilles, J. H., and M. T. Einaudi, 1992, Wall-rock alteration and hydrothermal flow paths about the Ann-Mason porphyry Cu deposit, Nevada –a 6 km vertical reconstruction: Economic Geology, **87**, 1963–2001.

Direen, N. G., and P. Lyons, 2007, Regional Crustal Setting of Iron Oxide Cu-Au Mineral Systems of the Olympic Dam Region, South Australia: Insights from Potential-Field Modelling: Econ. Geol., **102**, 1397–1414.

Dobrin, M. B., and C. H. Savit, 1988, Introduction to geophysical prospecting, New York: McGraw Hill Book Company.

Drummond, B. J., B. R. Goleby, A. J. Own, A. N. Yeates, C. Swager, Y. Zhang, and J. K. Jackson, 2000, Seismic reflection imaging of mineral systems: Three case histories: Geophysics, **65**, 1852–1861.

Duweke, W., J. C. Trickett, K. Tootal, and M. Slabbert, 2002, Three dimensional reflections seismic as a tool to optimize mine design, planning and development in the Bushveld igneous complex: 64th EAGE Conference and Exhibition, Florence, Italy, May 27–30, Extended Abstracts, D-20.

Eaton, D. W., B. Milkereit, and M. H. Salisbury (Eds.), 2003, Hardrock seismic exploration, **10**, SEG Books.

Ehrig, K., J. McPhie, and V. Kamenetsky, 2013, Geology and mineralogical zonation of the Olympic Dam iron oxide Cu-U-Au-Ag deposit, South Australia: Society of Economic Geologists Special Publication, **16**, 237–268.

Ellwood, B. B., 1980, Application of the anisotropy of magnetic susceptibility method as an indicator of bottom-water flow direction: Marine Geology, **34**, (3), M83–M90.

Ferris, G. M., M. P. Schwarz, and P. Heithersay, 2002, The geological framework, distribution, and controls of Fe-oxide Cu–Au mineralisation in the Gawler Craton, South Australia: Part 1 - Geological and tectonic framework. In: Porter, M. T., ed., Hydrothermal iron oxide copper-gold and related deposits: A global perspective: PGC Publishing, Adelaide, **2**, 9–31.

Flint, R. B., 1993, Mesoproterozoic, in Drexel, J. F., et al., ed.: The geology of South Australia, **1**: The Precambrian: Geological Survey of South Australia Bulletin, **54**, 107–169.

Fomin, T., 2017, Geoscience Australia, Personal communications.

Garry K.C. Clarke (1969). Optimum second-Derivative and Downward-Continuation Filters. Geophysics Vol. 34, Issue 3: Pages 424-437

Gamburtsev, G. A., Y. V. Riznichenko, I. S. Berson, A. M. Epinatieva, Y. V. Karus, and I. P. Kosminskaya, 1952, Correlation method of refraction waves: The USSR Academy of Science, Moscow (in Russian).

Gauthier, et al., 2001, The Osborne Deposit, Cloncurry Deposit; A 1595 Ma Cu-Au Skarn Deposit; 2001: A Hydrothermal Odyssey Extended Conference Abstracts, Townsville, 2001, 58–59.

Geoscience Australia & ABARE, 2010, Australian Energy Resource Assessment: Report 2010, Geoscience Australia, Canberra.

Gerstelling, R. W. and J. M. Heape, 1975, The Cattle Grid orebody, Mt. Gunson, South Australia: in Proceedings, The Aus. I.M.M. Conference. South Australia, June, 1975, The AusIMM, Melbourne, 103–112.

Gillen, D., 2010, A study of IOCG-related hydrothermal fluids in the Wernicke Mountains, Yukon Territory, Canada: Doctoral dissertation, James Cook University.

Greenhalgh, S. A., I. M. Mason, and C. Sinadinovski, 2000, In-mine seismic delineation of mineralization and rock structure: Geophysics, **65**, 1908–1919.

Hale, D., 1984, Dip-moveout by Fourier transform: Geophysics, **49**, 741–757.

Hand, M., A. Reid, and L. Jagodzinski**,** 2007, Tectonic Framework and Evolution of the Gawler Craton, Southern Australia: in Econ. Geol. **102**, 1377–1395.

Harrison, C., 2009, Feasibility of Rock Characterization for Mineral Exploration Using Seismic Data: PhD, Curtin Unversity.

Hattula, A., and T. Rekola, 2000, Exploration geophysics at the Pyhasalmi mine and grade control work of the Outokumpu Group, Geophysics, **65**, no. 6, 1961–1969.

Haynes, D. W., K. C. Cross, R. T. Bills, and M. H. Reed, 1995, Olympic Dam ore genesis: A fluid mixing model: Economic Geology, **90**, 281–307.

Hayward, N., and R. Skirrow, 2010, Geodynamic Setting and Controls on Iron Oxide Cu-Au (±U) Ore in the Gawler Craton, South Australia: in Porter T. M., ed., 2010 Hydrothermal Iron Oxide Copper-Gold and Related Deposits: A Global Perspective PGC Publishing, Adelaide, **3**, 119–146.

Hearst, J. R., P. H. Nelson, and F. L. Paillet, 2000, Well logging for physical properties: A handbook for Geophysicists, Geologists, and Engineers, 483, John Wiley & Sons.

Henderson, R.G and Zietz, I. (1949). The upward continuation of anomalies in total magnetic intensity fields. Geophysics, Vol. 14, Issues 4: Pages 517-534

Herglotz, G., 1907, Über das Benndorf'sche Problem der Fortpflanzungsgeschwindigkeit der Erdbebenstrahlen (in German), Physikal, Zeitschr, **8**, 145–147.

Herrington, R., 2011, Geological features and genetic models of mineral deposits. Sea, **1**, 1.3, 1–4.

Hitzman, M. W., N. Oreskes, and M. T. Einaudi, 1992, Geological characteristics and tectonic setting of Proterozoic iron oxide (Cu-U-Au-REE) deposits: in Gaal, G., and K. Schulz, ed., Precambrian Research, **58**, Amsterdam, Elsevier Science Publishers, 241–287.

Hitzman, M. W., 2000, Iron oxide-Cu-Au deposits: What, where, when, and why: in Porter, T. M., ed., Hydrothermal Iron Oxide Copper-Gold & Related Deposits A Global Perspective, **1**, Adelaide, Australia, Australian Mineral Foundation, 9–26.

Hitzman, M. W., and R. K. Valenta, 2005, Uranium in iron oxide-copper-gold (IOCG) systems: Economic Geology, **100**, 1657–1661.

Holm, J., B. (1977). A case for upward continuation as a standard separation filter for potential maps. Geophysics, 52. 10.1190/1.1442378.

Hunt, J. A., T. Baker, and D. J. Thorkelson, 2007, A Review of iron oxide-copper-gold deposits, with focus on the Wernecke Breccias, Yukon, Canada, as an example of a non-magmatic end member and implications for IOCG genesis and classification: Exploration and Mining Geology, **6**, 209–232.

Jackson, A., 2012, Ore Deposits 101 – Part 3 –Porphyries, Skarns and IOCG.

Jacobsen, B.H. (1987). A case for upward continuation as a Standard Separation filter for potential-field maps. Geophysics, 52. 390-398.

Jagodzinski, E., 2005, Compilation of SHRIMP U-Pb geochronological data Olympic Domain, Gawler Craton, South Australia, 2001–2003: Geoscience Australia Record, 2005/20, 211.

Johns, R. K., M. N. Hiern, L. G. B. Nixon, B. G. Forbes, and J. G. Olliver, 1981, TORRENS map sheet. South Australia. Geological Survey: Geological Atlas 1:250 000 Series, sheet SH53-16 (revised 2nd edition).

Juhlin, C., and H. Palm, 2003, Experiences from Shallow Reflection Seismic over Granitic Rocks in Sweden: Hardrock Seismic Exploration, **10**, 93.

Kallweit, and Wood, 1982, The limits of vertical resolution of zero-phase wavelets: Geophysics, **47**, no. 7, 1035–1046.

Karaev, N. A., and G. Rabinovich, 2000, Ore seismic prospecting: Geoinformmark, Moscow (in Russian).

Kitzig, 2016, Personal communication.

Knight, J., J. Lowe, S. Joy, J. Cameron, J. Merrillees, S. Nag, N. Shah, G. Dua, and K. Jhala, 2002, The Khetri copper belt, Rajasthan: Iron oxide copper-gold terrane in the Proterozoic of NW India: in Porter, T. M., ed., Hydrothermal iron oxide copper-gold and related deposits a global perspective, 2: Adelaide, Australian Mineral Foundation, **2**, 321–341.

Larroque, M., J. J. Postel, M. Slabbert, and W. Duweke, 2002, How 3D seismic can help enhance mining: EAGE 64th Conference & Exhibition, expanded abstract.

Lintern, M. J., M. J. Sheard, and D. J. Gray, 1998, Geochemical studies of the regolith at the Mt Gunson Copper Deposits, Stuart Shelf, South Australia: CRC LEME Report, 76R.

Lintern, M. J., M. J. Sheard, and D. J. Gray, 2007, Geochemical studies of the regolith at the Mt Gunson Copper Deposits, Stuart Shelf, SA: CRC LEME Open File Report 216, 71.

Lipton, I. T., 1997, A review of density determination methods for iron ore deposit evaluation in Iron making Resources and Reserves Estimation, Perth, WA: 51–56.

Lyons, P., and B. R. Goleby, 2005, The 2003 Gawler Craton seismic survey: Notes from the Seismic Workshop: Geoscience Australia, Record 2005/19, 81.

Malehmir, A., C. Juhlin, C. Wijns, M. Urosevic, P. Valasti, and E. Koivisto, 2012, 3D reflection seismic imaging for open-pit mine planning and deep exploration in the Kevitsa Ni-Cu-PGE deposit, northern Finland: Geophysics, **77,** no. 5: WC95-WC108.

Malehmir, A., G. Bellefleur, S. Taylor, and C. Müller, 2008, 3D seismic reflection imaging of VHMS deposits: Insights from re-processing of the Halfmile Lake data, New Brunswick, Canada: in 2008 SEG Annual Meeting, Society of Exploration Geophysicists.

Malehmir, A., and G. Bellefleur, 2009, 3D seismic reflection imaging of VHMS deposits, Insights from reprocessing of the Halfmile Lake data, New Brunswick, Canada: Geophysics,**74**, no. 6, B209–B219, doi:10.

Marc, T., and John B. 2013. “Hillside”, South Australia Delivering Australia Largest Underdevelop Copper Project. The AusIMM

Mark, G., and D. R. W. Foster, 2000, Magmatic-Hydrothermal albite-actinolite-apatite-rich rocks from the Cloncurry district, NSW Queensland, Australia: Lithos, **51**, 223–245, 2001.

Martin, F., 2012, 9th SA Exploration and Mining Conference, Adelaide.

McKay, A. D., Y. Meizitis, K. Porritt, D. C. Champion, A. Britt, A. Whitaker, D. Summerfield, M. Sexton, S. Jaireth, D. Huston, D. Hoatson, A. Schofield, L. Carson, R. Towner, and M. Huelatt, 2013, Australia's Identified Mineral Resources 2012. Geoscience Australia.

Minerals Council of Australia (MCA), 2012, 2013-2014 Pre-budget Submissions.

Milkereit, B., E. K. Berrer, A. Watts, and B. Roberts, 1997, Development of 3D seismic exploration technology for Ni-Cu deposits, Sudbury Basin: in Gubins, A. G., ed., Geophysics and Geochemistry at the Millennium: Proceedings of Exploration 97: Fourth Decennial International Conference on Mineral Exploration, GEO/FX, 439- 448.

Milkereit, B., E. Adam, A. Barnes, C. Beaudry, R. Pineault, and A. Cinq-Mars, 1992a, An application of reflection seismology to mineral exploration in the Matagami area, Abitibi Belt, Quebec: Current Research, Part C,13–18.

Milkereit, B., and D. E. Boerner, 1999, Structural evolution of the Sudbury `impact structure in the light of seismic data. Large meteorite impacts and planetary evolution 11 Special paper: Geological Society of America, **339**, 419–429.

Milkereit, B., E. Berrer, A. King, A. H. Watts, B. Roberts, E. Adam, D. W. Eaton, J. Wu, and M. H. Salisbury, 2000, Development of seismic exploration technology for deep nickel-copper deposits - A case history from the Sudbury basin, Canada: Geophysics, **65**, 1890–1189.

Musgrave, M. J. P., 1959, The propagation of elastic waves in crystals and other anisotropic media: Reports on progress in physics, **22**, no. 1, 74.

Nafe, J. E., and C. L. Drake, 1963, Physical properties of marine sediments: in Hill, M. N., ed., The sea: Interscience publishers, **3**, 794–815.

Nedimovic, M. R., and G. F. West, 2003, Crooked-line 2D seismic reflection imaging in crystalline terrains: Part 1, Data Processing: Geophysics, **68**, 274–285.

ODriscoll, E. S. T., 1986, Observations of the lineament–ore relation: in Reading, H. G., J. Watterson, and S. H. White, ed., Major crustal lineaments and their

influence on the geological history of the continental lithosphere, Royal Society of London. Philosophical Transactions, **317**, 195–218.

Olsen, S., 2010, The Hillside Discovery: A new frontier of IOCG discoveries on the Yorke Peninsula: AUSIMM Melbourne Branch News Letter.

Okan, E. O., A. Kepic, M. Urosevic, and S. Ziramov, 2015, A for Regional Seismic Surveys in the Gawler Craton, South Australia: ASEG Extended Abstract, 2015.

Oreskes, N., and M. T. Einaudi, 1990, Origin of rare earth element-enriched hematite breccias at the Olympic Dam Cu-U-Au-Ag deposit, Roxby Downs, South Australia: Economic Geology and the Bulletin of the Society of Economic Geologists, **85**, 1–28, doi:10.2113/gsecongeo.85.1.1.

Orville, 1963, Alkali ion exchange between vapour and feldspar phases: American Journal of Science, **261**, 201–237.

Page, R.W., and Sun, 1998, Aspects of geochronology and crustal evolution in the Eastern fold belt, Mt Isa inlier: Australian Journal of Earth Sciences, **45**, 343–361.

Parker, A. J., 1990, Precambrian provinces of South Australia; tectonic setting: in Hughes, F. E., ed., Geology of the mineral deposits of Australia and Papua New Guinea, **2**, Monograph Series - Australasian Institute of Mining and Metallurgy, Australasian Institute of Mining and Metallurgy, Melbourne, Victoria, Australia, 985-–-990.

Parker, A. J., S. J. Daly, D. J. Flint, R. B. Flint, W. V. Preiss, and G. S. Teale, 1993, Paleoproterozoic: in: J.F. Drexel, W.V. Preiss and A.J. Parker (Editors), the geology of South Australia, **1**, The Precambrian, Bulletin Geological Survey of South Australia. Geological Survey of South Australia, Adelaide, South Australia, Australia, 50–105.

Partington, G. A., and P. J. Williams, 2000, Proterozoic lode gold and (iron)-copper-gold deposits: A comparison of Australian and global examples: Reviews of Society of Economic Geologists, **13**, 69–101.

Pawlowski, Robert S. (1995). Prefential Continuation for Potential-Field anomaly enhancement. Geophysics. Vol. 60, Issues 2: Pages 390-398

Primary Industries and Regions SA (PIRSA), 2003, Gawler Craton Geological Excursion and Map Release.

Primary Industries and Regions SA (PIRSA), 2013, Reports on Hillside copper mine proposal management plan, found at

http://www.pir.sa.gov.au/minerals/public_notices, sections 5/68–71 and 6/13–15.

Pollard, P. J., and McNaughton, N. J., 1997, U/Pb geochronology and Sm/Nd isotope characterization of Proterozoic intrusive rocks in the Cloncurry district, Mount Isa inlier, Australia: Australian Mineral Industry Research Association (AMIRA), Cloncurry Base Metals and Gold Final Report P438, section 4, 19.

Pollard P. J., 2001, Sodic (-calcic) alteration in Fe-oxide-Cu–Au districts: an origin via unmixing of magmatic H2O-CO2-NaCl ±CaCl2-KCl fluids; Mineralium Deposita, **36**, 93–100.

Pollard, P. J., 2006, An intrusion-related origin for Cu-Au mineralisation in iron oxide-copper-gold (IOCG) provinces: Mineralium Deposita, **41**, 179–187.

Porter, T. M., ed., 2000, Hydrothermal Iron Oxide Copper-Gold and Related Deposits. A Global Perspective: Adelaide, Australia, Australian Mineral Foundation, **1**, 330,

Porter, T. M., ed., 2013, IOCG Deposits Description: Adelaide Workshop, hosted by DMITRE Minerals, South Australian Government.

Preiss, W.V., 1987, The Adelaide Geosyncline: Late Proterozoic stratigraphy, sedimentation, palaeontology and tectonics: South Australia Geological Survey Bulletin, **53**, 384–389.

Preiss, W.V., 1993, Neoproterozoic: in Drexel, J. F., W. V. Preiss, and A. J. Parker, ed., The geology of South Australia, **1**, The Precambrian, South Australia Geological Survey Bulletin, **54**, 171–197.

Pretorius, C. C., W. F. Trewick, A. Fourie, and C. Irons, 2000, Application of 3D seismic to mine planning at Vaal Reef's gold mine, number 10 shaft, Republic of South Africa: Geophysics, **65**, 1862–1870.

Pretorius, C., W. F. Trewick, and C. Irons, 1997, Application of 3D Seismic to Mine Planning at Vaal Reefs Gold Mine.

Pretorius, C. C., A. Jamison, C. Irons, 1989, Seismic exploration in the Witwatersrand Basin, Republic of South Africa: in Garland G. D., ed., Proceeding of Exploration'87, Ontario Geological Survey, Special Volume, **3**, 241−253.

Rattigan, J. H., R. W. Gersteling, and D. G. Tonkin, 1977, Exploration geochemistry of the Stuart Shelf, South Australia: Journal of Geochemical Exploration, **8**, 203–217.

Reeve, J. S., K. C. Cross, R. N. Smith, and N. Oreskes, 1990, Olympic Dam copper-uranium-gold-silver deposit, in Hughes, F. E., ed., Geology of the mineral deposits of Australia and Papua New Guinea: Melbourne, Australia, Australian Institute of Mining and Metallurgy, 1009–1035.

Fessenden, R., 1914, Ref. Weatherbay, B. B., Paper, **1**, Geophysical case histories, 1948, Nettleton, L. L., ed.

Rex Minerals, 2009, 2010, 2013, Annual reports on Hillside Copper-Gold deposit, www.rexminerals.com.au.

Requia, K., H. Stein, L. Fontboté, and M. Chiaradia, 2003, Re-Os and Pb-Pb geochronology in the Archean Salobo iron oxide copper-gold deposit, Carajás mineral province, northern Brazil: Mineralium Deposita, **38**, 727–738.

Reynolds, L. J., 2000, Geology of the Olympic Dam Cu-U-Au-Ag-REE deposit: in Porter, T. M., ed., Hydrothermal iron oxide copper-gold and related deposits: A global perspective: Adelaide, Australian Mineral Foundation, 93–104.

Roberts, D. E., and G. R. T. Hudson, 1983, The Olympic Dam copper-uranium-gold deposit, Roxby Downs, South-Australia: Economic Geology and the Bulletin of the Society of Economic Geologists, **78**, 799–822, doi:10.2113/gsecongeo.78.5.799.

Robertsson, J. O. A., B. Bednar, J. Blanch, C. Kostov, and D. van Manen, 2007. Introduction to the supplement on seismic modelling with applications to acquisition, processing, and interpretation. Geophysics, **72**, no. 5, SM1–SM4.

Saether, O., 2013, Seismic Forward Modelling of Deltaic Sequences: Master of Science Thesis, Department of Petroleum Engineering and Applied Geophysics, Norwegian University of Science and Technology.

Salisbury, M. H., B. Milkereit, and W. Bleeker, 1996, Seismic imaging of massive sulphide deposits; Part I, Rock properties, Economic Geology, **91**, no. 5, 821–828.

Salisbury, M. H., B. Milkereit, G. Ascough, R. Adair, D. Schmidt, and L. W. Matthews, 1997, Physical Properties and Seismic Imaging of Massive Sulphides: Exploration 97, Toronto, Canada.

Salisbury, M. H., and R. Iuliucci, 1999, Geological Survey of Canada/ Dalhousie University rock properties database: http://gsca.nrcan.gc.ca/pubprod/rockproperties/ index_e.php.

Salisbury, M. H., B. Milkereit, G. Ascough, R. Adair, L. Matthews, D. R. Schmitt, and J. Wu, 2000, Physical properties and seismic imaging of massive sulphides, Geophysics, ***65***, no. 6, 1882–1889.

Salisbury, M. H., C. W. Harvey, and L. Matthews, 2003, The acoustic properties of ores and host rocks in Hardrock terranes: Hardrock seismic exploration, SEG, 9–19.

Salisbury, M. H., and D. Snyder, 2007, Application of seismic methods to mineral exploration, in W. D. Goodfellow, ed., Mineral deposits of Canada: A synthesis of major deposit types, district metallogeny, the evolution of geological provinces, and exploration methods: Geological Association of Canada, Mineral Deposits Division, Special Publication, **5**, 971–982.

Schmitt, D. R., C. J. Mwenifumbo, K. A. Pflug, and I. L. Meglis, 2003, Geophysical logging for elastic properties in hard rock: a tutorial: Hardrock seismic exploration: Eaton, D. W., B. Milkereit, and M. H. Salisbury, ed., Society of Exploration Geophysicists, Tulsa, Okla., 20–42.

Schwarz, M. P., M. J. Sheard, G. M. Ferris, G. M. Fairclough, S. J. Daly, and M. B. Davies, 2006, Gawler Craton: in Cooper, B. J., and M. A. McGeough, ed., South Australia mineral explorers guide, Second edition, South Australia, Department of Primary Industries and Resources Mineral Exploration Data Package 11, Ch. 4.

Schön, J. H., 1996, Physical properties of Rocks: Fundamentals and principle of petrophysics: in Klaus, H., and T. Sven, ed., Handbook of Geophysical Exploration, **18**, Pergamon Press, London, 583.

Schonharting, G., and N. Abrahamsen, 1984, Magnetic investigations on cores from the Lopra-1 drill-hole, Faeroe Islands: in Berthelsen, O., A. Noe-Nygaard, and J. Rasmussen, ed., The Deep Drilling Project 1980–81 in the Faeroe Islands, Annales Societatis Scientiarum Faeroensis, Supplementum IX, 109–114.

Sheriff, R. E., and L. P. Geldart, 1982, Exploration seismology: history, theory, and data acquisition, **1**.

Sheriff, R. E., 2004, Encyclopaedic dictionary of exploration geophysics: Society of Exploration Geophysicists.

Shuel, R. T., 1985, A simplification of the Zoeppritz equations: Geophysics, **50**, 609–614.

Skirrow, R. G., P. M. Ashley, K. Suzuki, and N. J. McNaughton, 2000,Time–space framework of Cu–Au(–Mo) and regional alteration systems in the Curnamona Province: AGSO Record, 2000, **10**, 83–86.

Skirrow, R., 2004, Iron oxide Cu-Au deposits: An Australian perspective on their unifying characteristics: in: McPhie, J., and McGoldrick, P. (ed.), 2004, Dynamic Earth: Past, Present and Future, Abstracts of the 17th Australian Geological Convention, Hobart, Tasmania, February 8–13, Geological Society of Australia, Abstracts, no. 73, 121.

Skirrow, R., 2014, The Olympic IOCG Province (Gawler Craton): Lithospheric-to district-scale controls on ore formation, and targeting of IOCG mineral systems: Geoconferences, IOCG workshop, Perth WA.

Skirrow, R., 2015, Iron Oxide Copper (IOCG) Deposits: Settings, Origins and Exploration Targeting, PACRIM, 2015.

Smith, J. B., 2010, Seismic reflection as a direct detection of Gold Mineralisation in the Carlin District: B.Sc. Thesis submitted to the Department of Exploration Geophysics, Curtin University.

Smith, M., and W. Chengyu, 2000, The geology and genesis of the Bayan Obo Fe-REE-Nb deposit: A review, in Porter, T. M., ed., Hydrothermal Iron Oxide Copper-Gold and Related Deposit: A Global Perspective, Adelaide, PGC Publishing, **1**, 271-282.

Stefani, J. P., 1995, Turning-ray tomography: Geophysics, **60**, no. 6, 1917–1929

Stewart, K., and J. Foden, 2003, Mesoproterozoic Granites of South Australia: Department of Primary Industries and Resources Report Book, 2003, **15**, 142.

Stuart, G., and S. Jolley, 1999, Structural and stratigraphic analysis of 3D seismic attributes applied to mine planning: Target gold deposit, South Africa: in 1999 SEG Annual Meeting, Society of Exploration Geophysicists.

Stuart, G. W., S. J. Jolley, L. G. Polome, and R. F. Tucker, 2000, Application of 3D seismic attributes analysis to mine planning: Target gold deposit, South Africa: The Leading Edge, **19**, no. 7, 736–742.

Subrahmanyam, D., P. H. and Rao, 2008, Seismic Attributes- A Review: 7th International Conference & Exposition on Petroleum Geophysics.

Tasman Resources Limited, 2009, 2010, 2011, 2012, 2013 and 2014, Reports on Vulcan IOCGU, www.tasmanresources.com.au.

Tertyshnikov, K., 2014, Seismic imaging in hard rock environments: PhD, Curtin University, Western Australia School of Mines, Department of Exploration Geophysics.

Theys, P., 1997, Accuracy – Essential information for a log measurement, SPWLA, 38th Annual Logging Symposium.

Theys, P., 1999, Log data acquisition and quality control: 2nd edition, Technip, 453, Worthington, P. E., 1985, The evolution of shaly-sand concepts in reservoir evaluation, The Log Analyst, Jan-Feb.

Thomas B. M., and D. N. Smith, 1976, Carnarvon Basin. In: Economic Geology of Australia and Papua New Guinea: Petroleum, **3**, Leslie R. B., Evans H. J. and Knight C. L., ed., Australasian Institute of Mining & Metallurgy, Monograph, **7**, 127–155.

Tonkin D. G., R. A. Creelman, 1990, Mount Gunson Copper deposits: in Hughes F. E. ed., 1990, Geology of the Mineral Deposits of Australia & Papua New Guinea, The AusIMM, Melbourne, Mono 14, **2**, 1037–1043.

Urosevic, M., E. Stoltz, and S. Massey, 2005, Seismic Exploration for Gold in a Hard Rock Environment Yilgarn Cration, Western Australia: Presented at EAGE 67th Meeting.

Urosevic, M., Kepic, A., Stolz, E., and Juhlin, C., 2007, Seismic exploration of mineral deposits in Yilgarn Craton, Western Australia: Proceedings of Exploration'07, Toronto, Canada.

Urosevic, M., D. Sherlock, A. Kepic, and S. Nakanishi, 2008, Time lapse VSP program for Otway Basin CO2 sequestration pilot project: in 70th EAGE Conference & Exhibition.

Urosevic, M., G. Bhat, and M. H. Grochau, 2012, Targeting nickel sulphide deposits from 3D seismic reflection data at Kambalda, Australia: Geophysics, **77**, no. 5, WC123–WC132.

Urosevic, M., 2017, personal communications.

Vassallo, J. J., and C. J. L. Wilson, 2002, Paleoproterozoic regional-scale non-coaxial deformation; an example from eastern Eyre Peninsula, South Australia: Journal of Structural Geology, 24, 1–24.

Virieux, J., 1986, P-SV wave propagation in heterogeneous media: Velocity-stress finite-difference method: Geophysics, **51**, no. 4, 889–901.

Weatherby, B. B., 1940, The history and development of seismic prospecting: Geophysics, **5**, no. 3, 215–230.

White, D., D. Secord, and M. Malinowski, 2012, 3D seismic imaging of volcanogenic massive sulphide deposits in the Flin Flon mining camp, Canada: Part 1—Seismic results: Geophysics, **77**, no. 5, WC47–WC58.

Whitely, R. J., 1994, Seismic refraction testing-a tutorial. Geophysical Characterization of Sites, **10**, 45–47.

Williams, G. E., and D. G. Tonkin, 1985, Periglacial structures and palaeoclimatic significance of a late Precambrian block field in the Cattle Grid copper mine, Mount Gunson, South Australia: Australian Journal of Earth Science, **32**, 287–300.

Williams and Blake, 1993, Alteration in the Cloncurry District; Roles of recognition and interpretation in exploration for Cu-Au and Pb-Zn-Ag deposits: Economic Geology Research Unit, Contribution 49, James Cook University of North Queensland.

Williams, P. J., 1999, Fluid inclusion geochemistry of Cloncurry (Fe)-CuAu Deposits, in Stanley, C. J., ed., Mineral Deposits: Processes to Processing, 1, Rotterdam, A. A., and Balkema P., 111–114.

Williams, P. J., and R. G. Skirrow, 2000, Overview of iron oxide-copper-gold deposits in the Curnamona Province and Cloncurry District (Eastern Mount Isa Block), Australia: in Porter, T. M., ed., Hydrothermal iron oxide copper-gold and related deposits: A global perspective, PGC Publishing, Adelaide, **1**, 105–122.

Williams, P. J., and P. J. Pollard, 2003, Australian Proterozoic iron oxide-Cu-Au deposits: An overview with new metallogenic and exploration data from the Cloncurry district, northwest Queensland: Exploration and Mining Geology, **10**, 191–213

Williams, P. J., M. D. Barton, D. A. Johnson, L. Fontboté, A. De Haller, G. Mark, N. H. Oliver, and R. Marschik, 2005, Iron oxide copper-gold deposits: geology, space-time distribution, and possible modes of origin: Economic Geology, 371–405

Willman, C. E., R. J. Korsch, D. H. Moore, R. A. Cayley, V. A. Lisitsin, T. J.Rawling, V. J. Morand, and P. J. O'Shea, 2010, Crustal-scale fluid path-ways and source rocks in the Victorian Gold Province, Australia: Insight from deep seismic reflection profiles: Economic Geology, **105**, 895–915.

Wright, P. M., 1981, Seismic methods in mineral exploration, Economic Geology, 863–870.

Yilmaz, O., 2001, Seismic Data Analysis Volumes 1 and 2, Society of Exploration Geophysicists, Tulsa, USA, **1** and **2**, 2nd Ed.

Zoeppritz, K., 1919, Erdbebenwellen VII. Nachrichten von der Gesellschaft der Wissenschaften zu Göttingen, Mathematisch- Physikalische Klasse, 1919: 57–65.